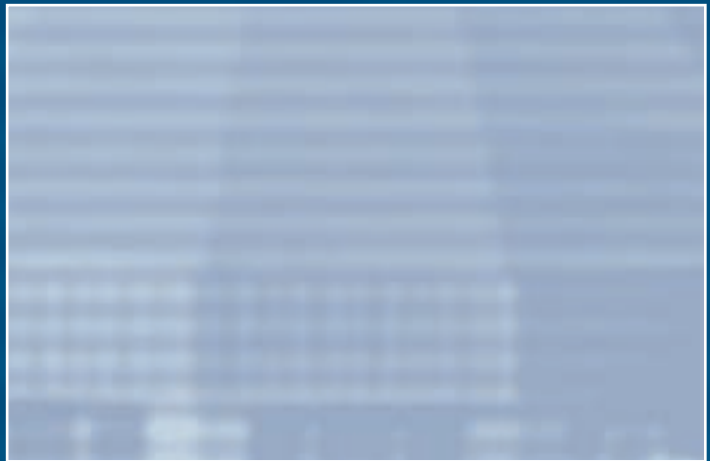


# ADVANCED LIGHT SOURCE

ACTIVITY REPORT 2002



JUNE 2003

#### **EDITORS:**

Theresa Duque  
Annette Greiner  
Elizabeth Moxon  
Arthur L. Robinson  
Lori Tamura

#### **DESIGN, LAYOUT, PHOTOGRAPHY:**

Berkeley Lab's Technical and Electronic Information Department  
(TEID) Creative Services

*The editors gratefully acknowledge the ALS users and staff for their contributions, advice, and patience.*

#### **DISCLAIMER**

This document was prepared as an account of work sponsored by the United States Government. While this document is believed to contain correct information, neither the United States Government nor any agency thereof, nor The Regents of the University of California, nor any of their employees, makes any warranty, express or implied, or assumes any legal responsibility for the accuracy, completeness, or usefulness of any information, apparatus, product, or process disclosed, or represents that its use would not infringe privately owned rights. Reference herein to any specific commercial product, process, or service by its trade name, trademark, manufacturer, or otherwise, does not necessarily constitute or imply its endorsement, recommendation, or favoring by the United States Government or any agency thereof, or The Regents of the University of California. The views and opinions of authors expressed herein do not necessarily state or reflect those of the United States Government or any agency thereof, or The Regents of the University of California.

Available to DOE and DOE Contractors from the Office of Scientific and Technical Communication, P.O. Box 62, Oak Ridge, TN 37831. Prices available from (615) 576-8401.

Available to the public from the National Technical Information Service, U.S. Department of Commerce, 5285 Port Royal Road, Springfield, VA 22161.

Ernest Orlando Lawrence Berkeley National Laboratory is an equal opportunity employer.

# ADVANCED LIGHT SOURCE ACTIVITY REPORT 2002

JUNE 2003

Ernest Orlando Lawrence Berkeley National Laboratory  
University of California, Berkeley, California 94720-8235  
LBNL-52972

This work was supported by the Director, Office of Science,  
Office of Basic Energy Sciences, Materials Sciences  
Division, of the U.S. Department of Energy under Contract  
No. DE-AC03-76SF00098.





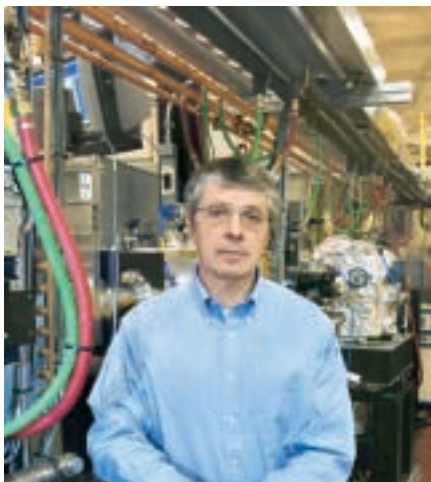
# CONTENTS

<b>Introduction</b> .....	v
<b>Note from the UEC Chair</b> .....	vi
<b>Science Highlights</b> .....	1
Overview .....	3
Feature: The ALS Takes the Plunge: Diving into Water's Hydrogen-Bond Structure .....	5
Condensed Matter Physics .....	11
Materials Science .....	21
Polymers and Bioscience .....	32
Environmental and Earth Science .....	35
Structural Biology .....	41
Atomic and Molecular Science .....	50
Accelerator Physics .....	60
<b>Facility Report</b> .....	63
Feature: Structural Biology Hits High Gear: New Beamlines Double Crystallography Opportunities .....	65
Operations .....	71
Accelerator Physics .....	73
Experimental Systems .....	79
Scientific Support .....	86
User Services .....	94
<b>Special Events</b> .....	99
<b>ALS Advisory Panels</b> .....	112
<b>ALS Staff</b> .....	114
<b>Facts and Figures</b> .....	117
<b>2002 Publications</b> .....	121



# INTRODUCTION

*Daniel Chemla, ALS Director*



In preparing for an important review in February 2002, I challenged my management team to formulate a succinct statement of the mission of the Advanced Light Source. The result was “Support users in doing outstanding science.” I thoroughly endorse this statement and expect every member of the ALS staff to relate their activities to this overriding goal. The expression “outstanding science” is self-explanatory; the scientific highlights offered in

this volume represent a sampling of the excellent work that is going on at the ALS. The expression “supporting users” is more elastic, and I distinguish between supporting users in the present and supporting users in the future.

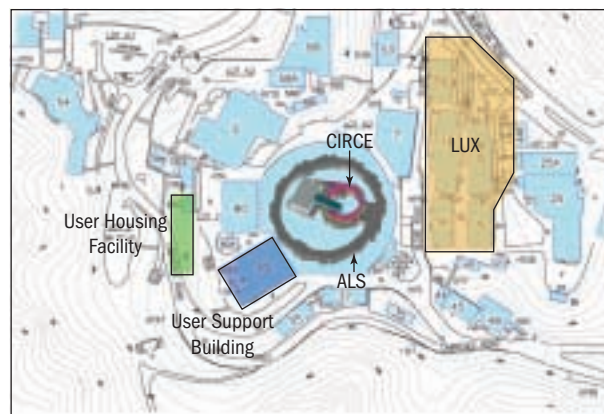
The most fundamental support that we offer users in the present is to supply regular, reliable, and stable beam. We then strive to ensure that our users have a favorable experience when they get here, that they receive the help they need in setting up their experiments, and that they get assistance, if needed, with the execution of their experiments. We also assist our users in publicizing their work. It is not sufficient merely to do outstanding science. The rest of the world must be told about it.

Supporting users in the future presents a major challenge. In 2003, we will be entering our second decade of operation. Are we sufficiently equipped to sustain the cutting-edge position that we presently enjoy? Do we have a strategy to continue into a third and possibly a fourth decade? We are at a pivotal point in our history in that all the available straight sections in our storage ring have been built out or spoken for. We are proposing that we now enter a phase of upgrade and renewal.

First, we would like to increase the brightness by going to “top-up” injection, upgrading the rf system, and reducing the vertical beam size. We would then like to start retiring our older undulators and replacing them with the more

advanced designs that have emerged over the last ten years: elliptically polarizing undulators, in-vacuum small-gap devices, and superconducting devices. Finally, we would like to build out a full complement of beamlines. The philosophy here would be to continue our move away from multipurpose beamlines and to come out of the upgrade with an array of application-specific beamlines, each of which is optimized to do one thing and to do it superbly. With these upgrades, we are confident that the ALS can sustain its international cutting-edge position into the foreseeable future. In the coming year, I intend to engage our advisory committees, in particular the Users’ Executive Committee and the Scientific Advisory Committee, to flesh out the details and present me with a vision of what the ideal suite of insertion devices and beamlines should look like ten years from now.

Besides upgrading the existing facilities, we would like to add a small ring, CIRCE (Coherent InfraRed Center), dedicated to the production of coherent infrared and terahertz radiation. Such a source could revolutionize studies of ultrafast dynamic properties of materials, molecular vibrations and rotations, low-frequency protein motions, phonons, superconductor band gaps, electron scattering, and collective excitations. There is also a study under way at Berkeley Lab for a large-scale Linac-based Ultrafast X-ray source (LUX) to address the growing national and international need for femtosecond pulses of both soft and hard x rays. A favored site for LUX would be immediately adjacent to the ALS (see the layout below). In this long-range vision, the ALS, CIRCE, and LUX would become parts of a light-source cluster sharing a common infrastructure, including a new user building and user housing facility. I look forward to participating in the challenges ahead to convert these proposals into reality.



# NOTE FROM THE UEC CHAIR

*Roger Falcone, UEC Chair for 2002*



I was very pleased to serve the users of the ALS as Chair of the Users' Executive Committee (UEC) during 2002. Thanks to the users, to the ALS staff, and to ALS and DOE management, it was a very productive year for both scientific achievement and long-term planning to ensure the continued importance and success of the ALS. Key issues, such as housing for visiting scientists, scheduling, and new modes of interaction between users and the facility, were significantly addressed this year. However,

these issues require constant attention, as we seek to continually improve the way we operate.

Users of the ALS range from scientists and engineers whose daily research activities are exclusively conducted at the ALS, to those who might occasionally carry in a sample for sophisticated material analysis, to those who explore

novel ways of manipulating the magical machine behind the wall to explore temporal, spatial, and spectral domains that weren't even envisioned when the ALS was built. What unifies us is a common concern for making the ALS work better in carrying out the highest quality science. Whether the needs of the users are for housing, technical assistance on the floor, beam time, funding for facility improvement, or day-to-day experimental expenses, we know that we can call Daniel, Ben, Neville, Gary, Howard, Zahid, or any of the other great people associated with the ALS to get help and resolve issues.

It is very clear that the resources given to users in support of their science are both enormous and never enough, and that we receive funds in a competition with similarly legitimate calls on society's resources. The UEC can function best when it helps coordinate and articulate the needs of the outstanding scientists it represents. I urge all users to continue to engage the UEC in this job in the coming year, as we explain both our successes and our vision to the public and to our representatives and funders in Washington.



# SCIENCE HIGHLIGHTS



As a national user facility, the Advanced Light Source generates light for cutting-edge scientific and technological research. Users come from industry, academia, and government laboratories around the world to take advantage of the bright synchrotron light (primarily x rays) generated by accelerated electrons circulating in the ALS storage ring. The light is directed along specialized beamlines to deliver the desired range of wavelengths to a precise spot on a sample in an experiment endstation. The types of samples and techniques for collecting data span a tremendous range, enabling a broad spectrum of research and applications, from protein folding to atomic physics. Competition for time on a beamline ("beam time") is keen, and prospective users earn the opportunity through a peer-review process, either as general users or by joining an approved program or participating research team. These highlights represent a selection from that already elite group. A fuller accounting of the year's experiments is nestled inside the back cover of this volume—the Compendium of User Abstracts on CD.



# OVERVIEW

*Neville Smith, Division Deputy for Science*



Neville Smith introduced the concept of approved programs at the 2002 ALS Users' Meeting.

The mission of the ALS is "Support users in doing outstanding science." Some of the outstanding science published in 2002 is offered in the highlights presented below. To keep this volume within reasonable bounds, we restrict the selection to about 20–25 items distributed over the full range of scientific activities. It is therefore very much the tip of the iceberg.

Following the practice started last year, we lead off with a feature article, or "highlight of highlights," that takes a broader view than possible with the single-publication focus of our science highlights. This year we have chosen the topic of water's hydrogen-bond structure as revealed by x-ray spectroscopy. It is remarkable that at this late date a substance as basic as water is still not fully understood. Noting the several independent studies that came to fruition at about the same time, we are pleased to see that the ALS is becoming a place for outstanding research related to water.

To ensure that the science that gets done is as truly outstanding as possible, access to the ALS is through peer review. Responsibility for approving and evaluating the performance of participating research teams (PRTs) resides with the Scientific Advisory Committee (SAC). General user (GU) proposals are evaluated by one of our two Proposal Study Panels (PSPs), either the Protein Crystallography PSP, which operates on a two-month cycle, or the General Sciences PSP, which meets every six months. We are indebted to the members of the PSPs for their generosity with their time, thereby ensuring that the process works.

Over the last year we have formalized a new mode of access that we call "approved programs" (APs). An AP is an investigator or group of investigators that gets a regular allocation of beam time (typically 10%) for an extended period (typically three years) in order to carry out a program of research. The initial complement of APs was created through the reorganization of some PRTs following their most recent SAC-mandated reviews. It is anticipated that responsibility for review and evaluation of proposals for AP status will pass to the General Sciences PSP. The details are being finalized in consultation with our various advisory bodies, and we expect to publish the process on our Web site ([www-als.lbl.gov](http://www-als.lbl.gov)) very soon. Our Users' Executive Committee (UEC) has urged that the access procedures be fair, clear, and transparent. We agree.

We encourage you to share your perspective, insights, and questions regarding the ALS scientific program, including its portrayal in the Activity Report and the peer-review process. Contact information for ALS management and the UEC is on our Web site ([www-als.lbl.gov/als/contacts.html](http://www-als.lbl.gov/als/contacts.html)).

## THE ALS TAKES THE

# PLUNGE

## DIVING INTO WATER'S HYDROGEN-BOND STRUCTURE



Life on earth depends on the unusual structure and anomalous nature of liquid water. The hydrogen-bond (H-bond) structure between water molecules is responsible for much of water's weirdness and its consequences, such as the ability of cell membranes to keep the cell contents in and the environment out. H-bonds are not completely understood in water, in part because they have not been accessible to direct investigation. In 2002, four papers from researchers working at the ALS showed that local H-bonding can be effectively probed via x-ray spectroscopy of the electronic structure of water.

Water molecules are polar with a weak positive charge on each of the hydrogen atoms and negative charges on the oxygen. The attraction between the charges on neighboring water molecules results in an H-bonded network (see Where the Atoms Are in Water) with a locally tetrahedral structure comprising a central molecule surrounded by four others (Figure 1). H-bonds are weak and easily broken, but they are constantly reformed. When all the hydrogen bonds are intact, a configuration denoted SYM, the H-bond length in liquid water exhibits small deviations from the 2.7-Å distance known for ice.

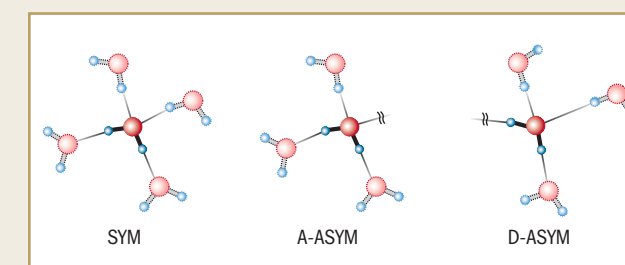


**FIGURE 1** Locally tetrahedral configuration of H-bonded water molecules consisting of a central molecule with four H-bonds between it and neighboring molecules, two between the central oxygen and neighbor hydrogen atoms, and two between the central hydrogens and the neighbor oxygen atoms (SYM). Broken bonds give rise to other configurations, including A-ASYM and D-ASYM.

## Where the Atoms are in Water

Water consists of a flexible, three-dimensional network consisting of rings of water molecules bound together via hydrogen bonds (H-bonds). X-ray contributions to understanding this structure began with reports of x-ray scattering in the 1920s for ice and in the 1930s for water. Nowadays, x-ray (sensitive to oxygen) and neutron (sensitive to hydrogen) scattering collectively provide O–O, H–O, and H–H radial distribution functions [ $g(r)$ ], yielding average distances between nearest-neighbor atoms and numbers of atoms in nearest-neighbor shells. The radial distribution functions provide important tests for molecular dynamics simulations of the structure of water based on theoretical interatomic potentials (water models), which must reproduce the measured  $g(r)$  function for each atomic pair, as well as other properties of water.

Despite many years of investigation, the variability from experiment to experiment in  $g(r)$  can be greater than the estimated experimental error. Two years ago, a University of California, Berkeley, group began reporting new “high-quality” x-ray scattering data from ALS Beamline 7.3.3

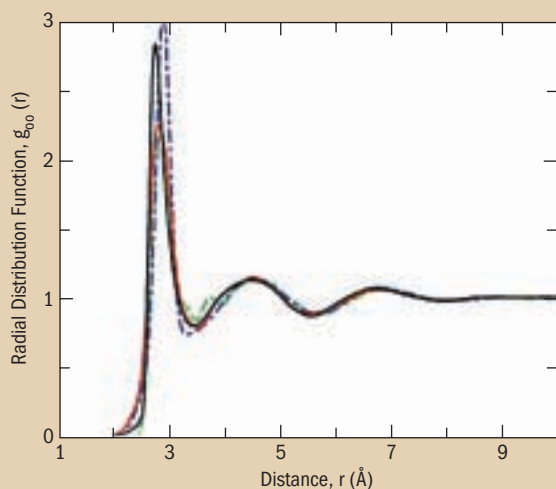


**FIGURE 1** Comparison of new experimental radial distribution function  $g_{O-O}(r)$  with previous results (solid black, ALS data; dashed green, previous x-ray data; dashed blue and solid red, previous neutron-scattering data).

In the liquid phase, a number of different configurations involving broken H-bonds are possible. Two broken-bond configurations of note are those in which (1) one H-bond between the central oxygen and a hydrogen atom from a neighboring molecule is broken (A-ASYM) and (2) one H-bond between a hydrogen atom in the central molecule and a neighboring oxygen is broken (D-ASYM). The A in A-ASYM refers to an H-bond acceptor because the central molecule needs a hydrogen from a neighbor to form the bond, whereas the D in D-ASYM refers to an H-bond donor because the central molecule provides the hydrogen atom for the bond. Interatomic distances shift in different ways, depending on which bonds are broken.

Before the x-ray spectroscopy findings, computer (molecular dynamics) simulations provided the only way to obtain an atomistic view of the H-bond network, but many simulations with different configurations of broken H-bonds were consistent with experimental data, so it was not clear which configuration was correct. The more direct information now obtained from x-ray experiments on liquid water presented some experimental challenges and in some cases required novel instrumentation (see How to Do Spectroscopy of Volatile Liquid Water).

Local H-bonding can be probed via x-ray spectroscopy because the molecular electronic structure is perturbed by the formation of the bonds, and this interaction can be detected by x-ray spectroscopy of the electronic structure. Interpretation of spectral changes depends heavily on the electronic structure calculated for different broken H-bond configurations, so close collaboration between experiment and theory is essential.

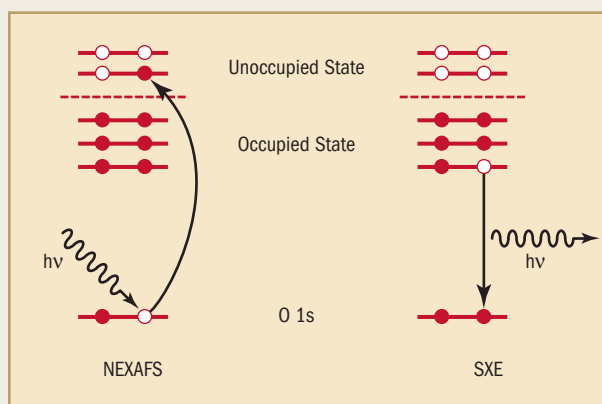


**FIGURE 2** K-edge x-ray absorption and fluorescence in oxygen. In absorption (NEXAFS), the oxygen 1s electron is excited to empty electronic states in the water-molecule conduction band, and the dipole selection rule provides a tool to study locally the oxygen 2p character of these unoccupied (antibonding) molecular orbitals. In emission (SXE), the core vacancy left by the excited 1s electron is filled by a valence-orbital electron, thereby giving direct information about the chemical bonding in which these electrons participate.

Three of the 2002 water research papers, which appeared in the same issue of *Journal of Physics: Condensed Matter*, reported near-edge x-ray absorption fine structure (NEXAFS, also called XANES) measurements made at the oxygen K edge (Figure 2). The fourth paper added soft x-ray emission (SXE) excited at the oxygen K edge to the mix. Because of the femtosecond time scale of the absorption process, the molecular geometry is frozen during these measurements, so there are no effects due to atomic motion.

Myneni et al. reported NEXAFS spectra of liquid water as well as ice and vapor. The researchers compared the measured spectra with those obtained from density functional theory (DFT) calculations for model structures obtained both from molecular dynamics simulations and from small clusters of molecules. Their conclusion was that the differences between the spectra from liquid and those from ice and vapor were due to unsaturated and strongly asymmetric H-bonding; for example, the DFT calculations indicated that the D-ASYM configuration was associated with a strong pre-edge peak below the usual oxygen K edge (Figure 3). They also found that the number (1.2 to 1.6) of broken H-bonds per molecule was larger in the liquid than expected from molecular dynamics simulations.

Guo et al. applied SXE to the same problem. This group relied on Hartree–Fock calculations to provide a picture of molecular orbitals that

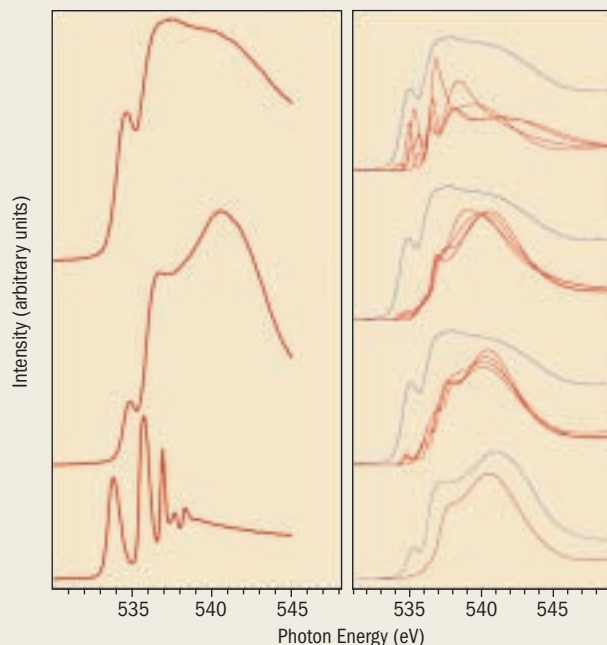


**FIGURE 3** Left, measured NEXAFS spectra for solid, liquid, and vapor phases of water. Right, calculated NEXAFS spectra (red) for ice and three H-bond configurations in liquid water (SYM, D-ASYM, and A-ASYM) and measured spectra (blue). The strong pre-edge feature of liquid water is associated with the D-ASYM configuration, which causes shifts in the antibonding orbitals relative to ice.

based on several experimental improvements and a more comprehensive consideration of the electronic structure of the water molecule than was common in the past [T. Head-Gordon and G. Hura, *Chem. Rev.* **202**, 2651 (2002)]. The group's first published result is an O–O radial distribution function  $g_{O-O}(r)$  with a first peak that is taller and sharper, as compared to earlier experiments, and with other peaks shifted to smaller interatomic distances, suggesting a more “structured” liquid water than had been assumed previously (Figure 1).

Extended x-ray absorption fine structure (EXAFS) is a complementary, element-specific way to obtain interatomic distances in disordered materials. For the last two years, a second group of UCB researchers and their co-workers have been reporting water EXAFS at the ALS. First, they showed that EXAFS from Beamline 9.3.2 taken above the oxygen K edge could detect O–H distances in water vapor [K.R. Wilson et al., *Phys. Rev. Lett.* **85** 4289 (2000)]. With the help of a liquid-microjet technique (see How to Do spectroscopy of Volatile Liquid Water), the same group published EXAFS results from Beamline 8.0.1 for the liquid and the liquid/vapor interface [K.R. Wilson et al., *J. Phys. Chem. B* **105**, 3346 (2001)]. The O–O distance obtained for the liquid agreed with that of bulk water (2.85 Å), and that obtained for the surface was similar to but slightly larger than that of isolated water dimers (2.98 Å). The group's 2002 report of EXAFS measurements expanded the earlier results on water, added liquid methanol to the samples studied, and interpreted results in terms of a broken hydrogen-bond structure, which is quite different in water and methanol [K.R. Wilson et al., *J. Chem. Phys.* **117**, 7738 (2002)].

## How to Do Spectroscopy of Volatile Liquid Water

While x-ray spectroscopy has over the years provided a powerful tool for investigating the electronic structure of a wide variety of sample types, it has not until recently been so successful when applied to volatile liquids, such as water. The pioneering studies of hydrogen bonding in liquid water conducted at the ALS in 2002 (see *The ALS Takes the Plunge*) depended in part on the availability of instrumentation able to deal with the experimental challenges they presented.

X-ray absorption spectroscopy seldom involves measurement of the intensity of the transmitted radiation; instead, it relies on alternative measures of the absorption, notably the total or partial yield of photoelectrons escaping from the surface, the yield of photoions emitted from the surface, and the intensity of x-ray fluorescence. Challenges and opportunities are associated with each of these options for investigating water, which is surrounded by a vapor. For example, electrons and ions cannot readily reach a detector unless they are travelling most of the way through a good vacuum, whereas fluorescent photons can easily reach a detector but their intensity is often low.

For their near-edge x-ray absorption fine structure (NEXAFS) measurements on ALS Beamline 8.0.1, Myneni et al. adopted the x-ray fluorescence approach. In their SXEER (soft x-ray endstation for environmental research) station, a silicon nitride window separated a liquid sample in a polypropylene straw surrounded by 760 torr of helium



**FIGURE 1** Liquid water microjets combined with three-stage differential pumping makes it possible to do x-ray absorption spectroscopy of the water surface by means of electron and ion detection while the surface is in equilibrium with a vapor layer.

could be used to interpret the measured emission spectra. The group's liquid water emission spectra suggested strong involvement of a valence orbital with  $3a_1$  symmetry, which is a mixture of oxygen 2p and hydrogen 1s orbitals, in the H-bonding (Figure 4). The group interpreted this involvement as evidence of electron sharing between water molecules, but an alternative explanation involving charge redistribution within the molecules has also been proposed. Resonant emission spectra excited at the liquid absorption pre-peak and theory also confirmed the strong presence of the D-ASYM configuration of broken H-bonds (Figure 5).

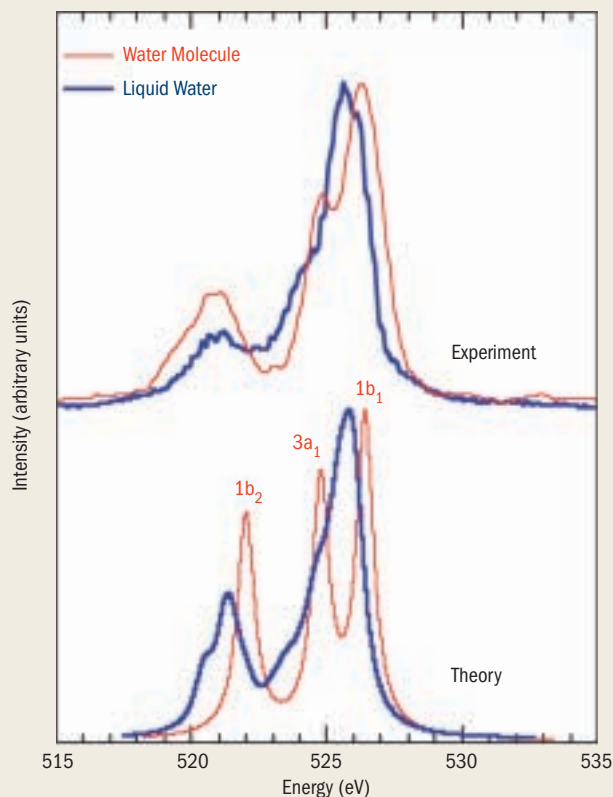


**FIGURE 4** SXE emission of water in the liquid and vapor phases. Comparison of experiment and theory indicates a strong role for the  $3a_1$  orbital in the liquid SXE spectrum.

Wilson et al. extended NEXAFS to the liquid-water surface, where most of the actual interaction of water with other species takes place. They carried out DFT calculations for clusters of water molecules with donor and acceptor broken H-bond configurations deduced from molecular dynamics simulations. Comparison of experiment and theory identified a previously unknown species at the liquid surface, an acceptor-only configuration in which both donor bonds are broken and which is in dynamic equilibrium with the vapor

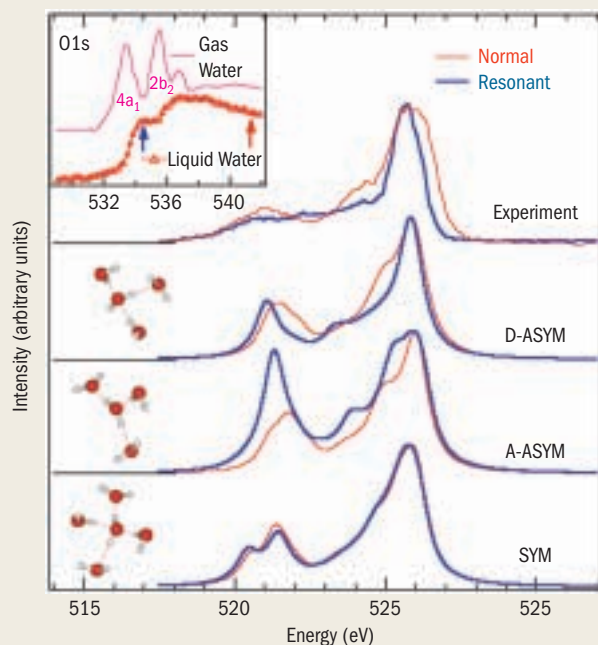


**FIGURE 5** Measured and calculated SXE spectra excited above the oxygen K edge (red, normal) and at the edge (blue, resonant). The resonantly excited spectrum is in good agreement with that predicted for the three-bonded D-ASYM configuration.

(Figure 6). Donor species were found to be more representative of the bulk liquid and the surface of amorphous ice.

Bluhm et al. combined NEXAFS with x-ray photoelectron spectroscopy (XPS) to observe thin layers of liquid on ice. Interpretation of NEXAFS spectra (e.g., emergence of the liquid pre-edge peak) provided evidence for “pre-melting” at the surface of ice at temperatures between  $-20^{\circ}\text{C}$  and  $0^{\circ}\text{C}$ . The group used the pre-edge peak for the liquid to measure the thickness of the layer (Figure 7). Thanks to the XPS spectra of the liquid surface, the cleanliness of the water surface could be ascertained. It was found that submonolayer amounts of oxygen-containing hydrocarbon contaminants can substantially enhance the extent of pre-melting.

It is always hard to predict the impact of a new capability. One view is that presented by an online news article associated with the issue of the *Journal of Physics: Condensed Matter* in which the three NEXAFS papers appeared, which called attention to “...a new era in the all-important field of water research. For the first time the experimentally determined, highly resolved electronic structure of water in the liquid phase must also be taken into consideration when evaluating the accuracy of theoretical models of the liquid.” A good sign is that a growing number of publications in print and in press from groups at other synchrotron sources is adding to what may become a deluge.

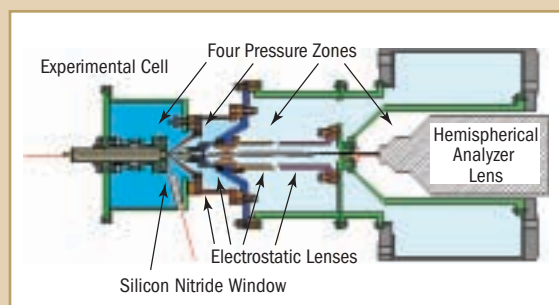


**FIGURE 2** A novel differentially pumped multi-stage electron lens system allows detection and energy analysis of photoelectrons by reducing the distance traveled to reach an aperture into the lens system just above the sample surface.

from the ultrahigh vacuum of the beamline, and a stream of helium removed the water vapor from the sample. In the soft x-ray emission (SXE) measurements conducted by Guo et al. on ALS Beamline 7.0.1, a spectrometer analyzed the x-ray fluorescence from a small volume of liquid sealed in a liquid cell and separated the liquid from the surrounding vacuum by a thin silicon nitride window. The brightness of the ALS was an important factor in generating a large enough fluorescence signal to analyze.

Wilson et al. took on the formidable task of investigating the surface of liquid water, which like most surfaces has a different structure from that in the interior. For their experiments, they adapted to the synchrotron environment an earlier microjet technology in which a pressurized stream of liquid just  $20\ \mu\text{m}$  in diameter is surrounded by a thin vapor blanket (Figure 1). They used total-electron-yield NEXAFS to probe the liquid below the surface of the microjet and total-ion-yield NEXAFS to look at the surface layer. A three-stage differentially pumped sample chamber protected the beamline, and additional pumps kept the pressure in the sample chamber low.

In analogy with SXE, where an x-ray spectrometer rather than a simple detector is required, in photoelectron spectroscopy (XPS) an electron spectrometer analyzes the photoelectron energies. Working at ALS Beamline 9.3.2, Bluhm et al. used a so-called ambient-pressure chamber equipped with a high-pressure transfer lens comprising a four-stage, differentially pumped electron spectrometer with four electrostatic lenses (Figure 2). While a silicon nitride window protects the beamline, the differentially pumped lens allows detection of oxygen Auger KLL electrons for surface sensitivity in NEXAFS and for XPS.

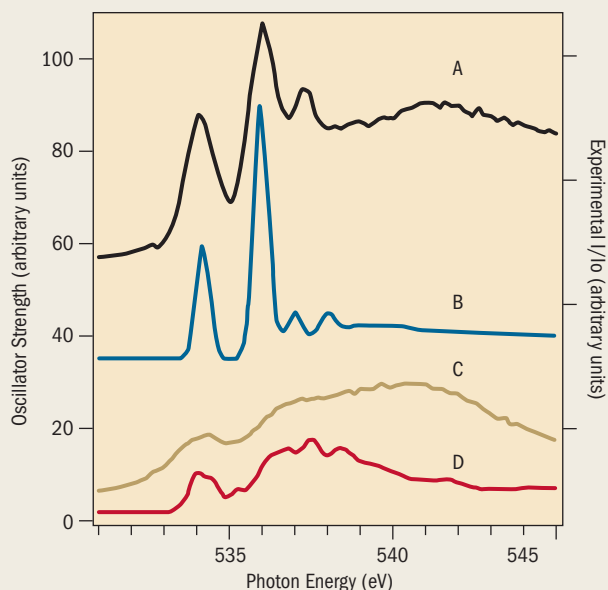


**FIGURE 6** Model NEXAFS spectra computed with density functional theory for two different kinds of surface H-bond configurations obtained from molecular dynamics simulations and measured spectra of the liquid water surface and ice. The spectral features computed for the acceptor-only configuration (B) show a close correspondence to those of the liquid surface spectrum (A). Conversely, the computed single-donor spectrum (D) accounts for the relative intensity in the experimental ice spectrum (C) and is consistent with other structural studies of the ice surface.

## PUBLICATIONS

1. S. Myneni, Y. Luo, L.A. Naslund, L. Ojamae, H. Ogasawara, A. Pelmenshikov, P. Wernet, P. Vaterlain, C. Heske, Z. Hussain, L.G.M. Pettersson, and A. Nilsson, "Spectroscopic probing of local hydrogen-bonding structures in liquid water," *J. Phys.: Condens. Matter* **14**, L213 (2002).
2. J.-H. Guo, Y. Luo, A. Augustsson, J.-E. Rubensson, C. S  the, H.   gren, H. Siegbahn, and J. Nordgren, "X-ray emission spectroscopy of hydrogen bonding and electronic structure of liquid water," *Phys. Rev. Lett.* **89**, 137402 (2002).
3. K.R. Wilson, M. Cavalleri, B.S. Rude, R.D. Schaller, A. Nilsson, L.G. Pettersson, N. Goldman, R. Catalano, J.D. Bozek, and R.J. Saykally, "Characterization of hydrogen bond acceptor molecules at the water surface using near-edge x-ray absorption fine structure spectroscopy and density functional theory," *J. Phys.: Condens. Matter* **14**, L221 (2002).
4. H. Bluhm, D.F. Ogletree, C.S. Fadley, Z. Hussain, and M. Salmeron, "The premelting of ice studied with photoelectron spectroscopy," *J. Phys. Condens. Matter* **14**, L227 (2002).

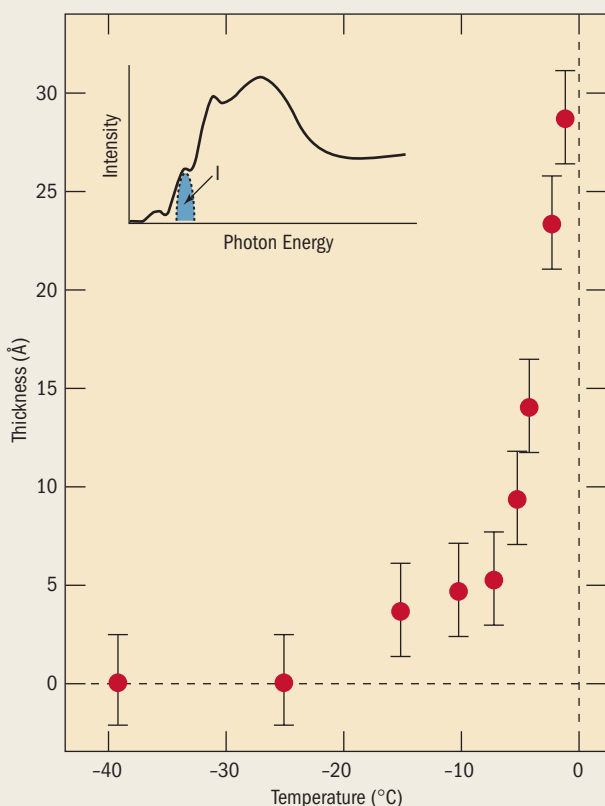


**FIGURE 7** Thickness of the liquid-like layer as a function of temperature, as determined from the intensity (*I*) of the pre-edge peak (*blue*).

# CONDENSED MATTER PHYSICS

## Putting a New Spin on Surface Electronic Structure

*One of the great themes of modern solid-state physics is that one can make a metal or some other material behave in an unusual way by making it very small. Magnets are a case in point with the potential to affect the life of everyone who uses computers of any kind. For example, computer disks have larger storage capacities, work faster, and cost less each year, in part because the magnetic area that represents a piece of data has been getting progressively smaller. If the trend continues, these magnets eventually will consist of only a few atoms. With the help of an x-ray technique, Hochstrasser et al. have confirmed an earlier, surprising conjecture that electrons in thin surface regions only a few atoms thick on otherwise nonmagnetic metals behave in a way similar to electrons in magnets. This finding will now have to be folded into the interpretation of experiments aimed at studying magnetism in small structures.*

To everyone's great benefit, magnetic storage devices have gotten progressively smaller, faster, and cheaper in the last few years. Based on past trends, the future is expected to bring ever smaller magnetic elements until at last the atomic scale is achieved. To that end, scientists today are exploring the fundamentals of magnetism in model systems with at least one dimension only a few atoms wide, such as surfaces. Surprisingly, experiments have suggested not only that electrons confined to the surfaces of some nonmagnetic metals exhibit a spin ordering somewhat similar to the momentum-dependent spin order in magnets, but that adsorbed atoms can enhance the ordering. Our spin-resolved photoemission measurements have now directly confirmed the previously controversial interpretation of momentum-dependent spin ordering on some nonmagnetic metallic surfaces.

In nonmagnetic metals, electrons in a given state, or band, have an energy uniquely determined by their momenta, irrespective of their spins. But as the earlier experiments demonstrated, even without long-range magnetic order, the local environment around an electron at the surface of a

metal can cause an energy splitting in a surface state that can be detected with spectroscopy. Since the earlier experiments were not sensitive to the electrons' spins, some effect other than the proposed momentum-dependent spin ordering might have been responsible for the splitting. Therefore, we sought to directly confirm the effect with spin-resolved measurements. Because the electron throughput is so reduced for photoemission with both spin and angular resolution, our measurements needed to be done at a third-generation synchrotron source.

Our group—a collaboration between scientists from the Lawrence Livermore National Laboratory, the University of Oregon, and the ALS—performed its experiments at Beamline 7.0.1 of the ALS. We studied a monolayer of hydrogen on tungsten. The physics behind the results are illustrated in Figure 1. As electrons traverse the surface plane of the solid, they feel the surface electric field as a magnetic field in their reference frame. Since by symmetry the electric field is normal to the surface, the induced magnetic field must be in the plane. The energy of the electrons therefore depends on how their spins are aligned relative to the field, so we expect to find that the surface state's energy is split into two bands. The purpose of the hydrogen is to make the effect stronger by increasing the surface

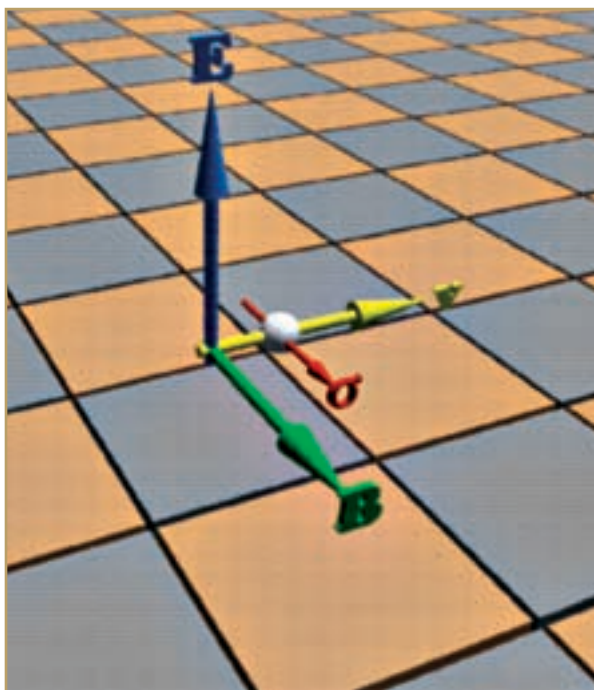


**FIGURE 1** The relationship for an electron traveling in the surface plane between the surface electric field,  $E$ ; the electron velocity,  $v$  (related to slope of the electron energy–momentum curve); the surface magnetic field,  $B$  (in the electron's rest frame); and the electron spin,  $\sigma$ .

electric field and by redistributing the surface charge closer to the strong-field region.

Figure 2 shows in-plane, spin-resolved, valence-band spectra for a particular momentum. Two peaks near the Fermi level (zero binding energy) are due to surface-confined electron states. The inset shows the energy–momentum (angle) bands for these two peaks measured without spin resolution. The issue is whether or not the splitting between the bands is due to spin ordering. If it is, the two peaks should appear only in the opposite spin channels. The data show that this is indeed the case. We see that the other peaks in the spectra, which are dominated by bulk states, do not show the effect in any way, while the surface peaks show the effect for in-plane spin-polarization but not for out-of-plane spin directions. Therefore the hypothesis of momentum-dependent spin ordering is proven.

This effect is important because it shows that the surface structure can impose a spin ordering regardless of magnetization (which may also be present) and must be taken into account when interpreting similar experiments at magnetic surfaces. It also may play a technological role in spin-based electronic (“spintronic”) devices at the nanometer scale. For example, by suitable arrangement of apertures, a 100 percent spin-polarized electron beam could be generated by photoemission.

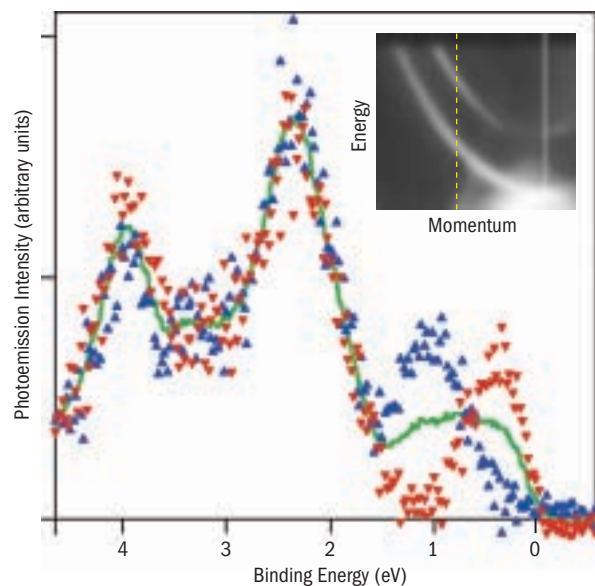


**FIGURE 2** Spin-resolved photoemission spectra for a particular electron momentum indicated by the dashed yellow line in the angle-resolved band map (*inset*). Two peaks are observed near the Fermi energy (zero binding energy) for surface electrons, corresponding to whether the electron spin is aligned or anti-aligned with the surface magnetic field. *Red and blue triangles*, in-plane spin-polarization; *green line*, out-of-plane spin directions.

## INVESTIGATORS

M. Hochstrasser and J.G. Tobin (Lawrence Livermore National Laboratory); E. Rotenberg (ALS); and S.D. Kevan (University of Oregon).

## FUNDING

U.S. Department of Energy, Office of Basic Energy Sciences.

## PUBLICATION

1. M. Hochstrasser, J.G. Tobin, E. Rotenberg, and S.D. Kevan, “Spin-resolved photoemission of surface states of  $W(110)-(1\times 1)H$ ,” *Phys. Rev. Lett.* **89**, 216802 (2002).

## Auger Resonant Raman Scattering in Itinerant Electron Systems

*In an atom, electrons orbit around the nucleus. Everyone knows that. But what happens when two or more atoms join to form a molecule? It turns out that some electrons stay localized around one nucleus, while others wander more freely around the entire molecule. In a chunk of metal, effectively a huge molecule, these itinerant electrons roam everywhere. Collectively, the details of these electron behaviors make up the electronic structure of the molecule, a structure that determines many of the day-to-day properties of matter. Scientists use forms of x-ray spectroscopy (e.g., absorption, fluorescence, and electron emission) to study the electronic structure. A particularly useful form of x-ray spectroscopy that applies equally to atoms, molecules, and solids is resonant photoemission based on a process called Auger resonant Raman scattering. It had been thought that localized electrons were required in order to observe this process. However, Föhlisch et al. have now shown that a scattering description also holds for only weakly localized electrons, thereby making it a general feature of resonant photoemission.*

Resonant photoemission in the vicinity of a core-level threshold is a powerful technique for investigating the electronic structure of matter, both in basic atomic and molecular physics and in applied materials science. The basis of resonant photoemission is the opening of an Auger resonant Raman scattering channel at the core-level threshold, so that the same final state is reached via direct photoemission and Auger resonant Raman scattering (excitation and decay of a core resonance with the energy released in the emission of an Auger electron).

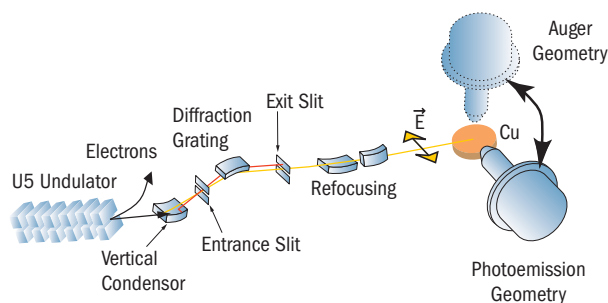


**FIGURE 3** Schematic diagram of Beamline 8.0.1 and the two detection geometries used in the experiments.

In Auger resonant Raman scattering, the core-excitation/decay sequence must be considered a single process (a one-step or coherent process). Experimentally, scattering into a localized intermediate state is manifested through a linear dispersion of spectral features with photon energy. In contrast, normal Auger decay is commonly seen as a two-step or incoherent process, where the emission of the Auger electron is independent from the initial absorption, thus leading to emission at constant kinetic energy for all photon energies above the threshold sufficient to excite an electron into the continuum.

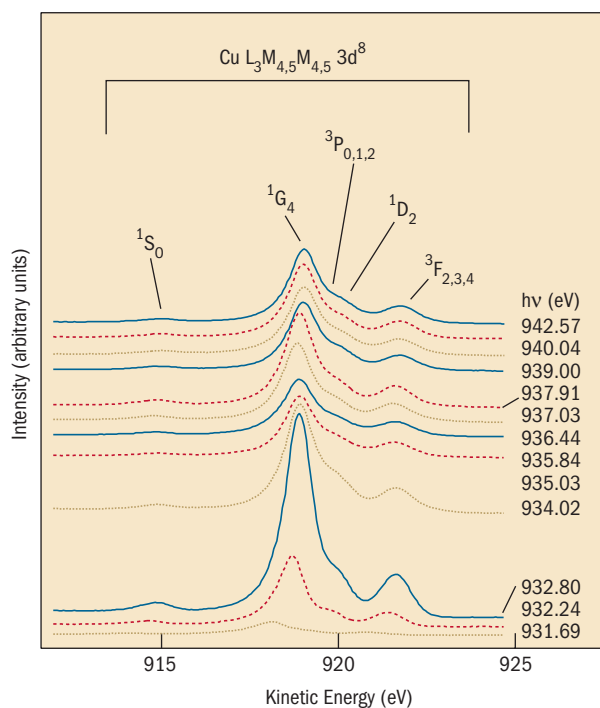


**FIGURE 4** Spectra obtained in the photoemission geometry over a range of exciting photon energies near and above the copper  $L_3$  edge. Above threshold, the kinetic energies of the peaks in the spectra show departures from the kinetic-energy-independent peaks expected for normal Auger emission for excitation into the continuum.

Whether Auger resonant Raman scattering requires localized absorption resonances and to what degree the occurrence of Auger resonant Raman scattering can be taken as an experimental measure of electron localization have been controversial issues. Our approach to investigating the connection between the degree of electron localization in an extended system and the occurrence of coherent scattering in resonant photoemission was to conduct polarization-dependent photoemission at the Cu L edges.

Our polarization-dependent photoemission measurements in copper now show that significant Auger resonant Raman scattering can also occur via itinerant continuum states. This finding makes Auger resonant Raman scattering a general feature taking place both in localized and rather delocalized electron systems.

The experiment was performed at ALS Beamline 8.0.1. Two detection geometries were used, as indicated in Figure 3. In the photoemission geometry, the electric field vector of the synchrotron radiation is parallel to the direction of detection. In the Auger geometry, the electric field vector lies perpendicular to the direction of detection.

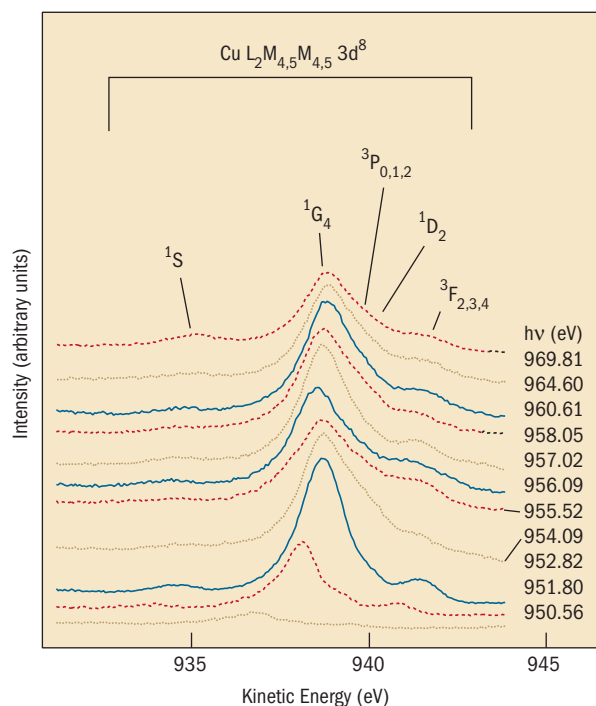


**FIGURE 5** Spectra obtained in the photoemission geometry over a range of exciting photon energies near and above the copper  $L_2$  edge. Above threshold, the kinetic energies of the peaks in the spectra show departures from the kinetic-energy-independent peaks expected for normal Auger emission for excitation into the continuum.

Figures 4 and 5 show spectra taken in the photoemission geometry for a photon-energy range from just below the thresholds for copper  $L_3$  and  $L_2$  excitation to the continuum. While the Cu  $L_3M_{4,5}M_{4,5}$  and  $L_2M_{4,5}M_{4,5}$  normal Auger lines with continuum excitation would have a constant kinetic energy, the spectra show deviations from this behavior at 4.2 eV and 7.7 eV above the respective  $L_3$  and  $L_2$  thresholds. This evolution is summarized for peak position and peak intensity of the  $3d^8\ ^1G_4$  spin-orbit component, as measured in both the photoemission and Auger detection geometries above the  $L_3$  edge (Figure 6).

Most notably, we observe characteristic deviations from the constant kinetic energy 4.2 eV and 7.7 eV above the  $L_3$  edge. Furthermore, we observe a significant variation of these deviations above the  $L_3$  and  $L_2$  edges, and the weak polarization anisotropy directly indicates dominant Auger resonant Raman scattering and weak direct photoemission for the  $3d^8$  final states. These deviations, which occur at critical points at the  $L_1$  and  $X_1$  points in the first Brillouin zone of fcc copper where the density of states varies, can be fully described by a simple energy-conserving numerical model of the scattering process (Figure 7) using the different  $L_3$  and  $L_2$  core-hole lifetimes.

In a nutshell, our findings directly point toward Auger resonant Raman scattering as a general feature of photoemission, independent of the degree of electron localization.

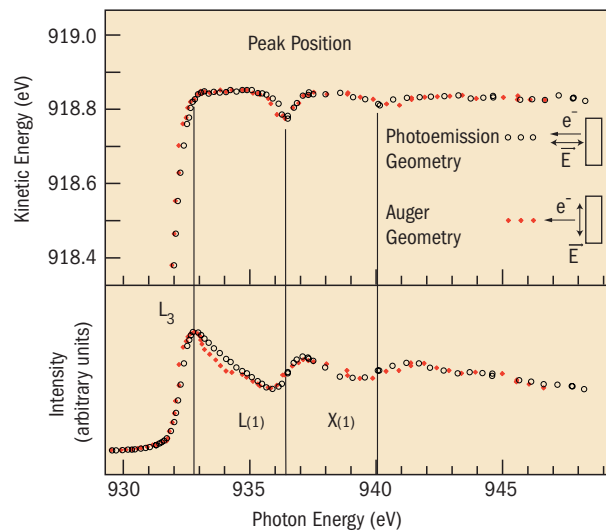


**FIGURE 6** Photon-energy dependence of the  $L_3M_{4,5}M_{4,5}3d^8\ ^1G_4$  final state. *Top*, the kinetic energies of the peaks in photoemission geometry (open circles) and the Auger geometry (red dots) for different exciting photon energies shows that the deviations from constant kinetic energy occur 4.2 eV and 7.7 eV above the  $L_3$  threshold. *Bottom*, intensities of the peaks.

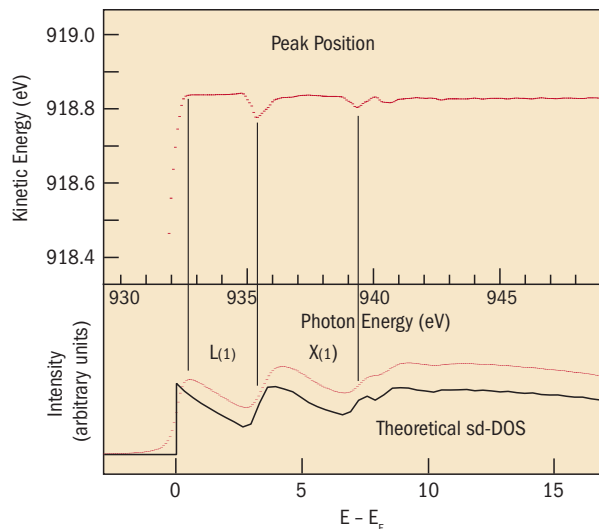


**FIGURE 7** Auger resonant Raman numerical simulation of the photon-energy dependence of the  $L_3M_{4,5}M_{4,5}3d^8\ ^1G_4$  final state. *Top*,  $3d^8\ ^1G_4$  peak energy. *Bottom*,  $3d^8\ ^1G_4$  peak intensity and theoretical Cu sd density of states (courtesy of O. Eriksson and B. Johansson) used in the calculation.

#### INVESTIGATORS

A. Föhlisch (Uppsala University and Universität Hamburg), O. Karis and J. Hasselström (Uppsala University and Asea Brown Boveri), M. Weinelt (Uppsala University and Universität Erlangen-Nürnberg), A. Nilsson (Stockholm University and Stanford Synchrotron Radiation Laboratory), and N. Mårtensson (Uppsala University and MAX-lab)

#### FUNDING

Swedish Natural Science Research Council (NFR) and the Göran Gustavsson Foundation for Research in Natural Sciences and Medicine.

#### PUBLICATION

1. A. Föhlisch et al., “Auger resonant Raman scattering in itinerant electron systems: Continuum excitations in Cu,” *Phys. Rev. Lett.* **88**, 027601 (2002).

## RIXS Technique Measures Hubbard Interaction

*With their repulsive negative electric charges, electrons would just as soon avoid each other, but crammed together in a solid material, they must find a way to get along. In many materials, such as metals and semiconductors, electrons are able to dance smoothly together without a second thought. But in certain “strongly correlated” materials, the mutual repulsion between electrons overshadows the interaction with positively charged atomic nuclei that otherwise smooths*

the way. The theory of strongly correlated materials is so tough that theorists are still struggling with ways to describe the unsociable electrons. In the Hubbard model, named for the British theorist who devised it, some electrons split into two groups called Hubbard bands. Zhang et al. have used x rays to measure the energy difference between the Hubbard bands in a material (sodium vanadate) for which they were also able to calculate the energy difference. The close match they found between the measured and calculated values lends confidence in the experimental and theoretical tools for probing strongly correlated materials.

The Hubbard interaction term,  $U$ , is a measure of the strength of the repulsion between electrons in certain solids, but direct measurements of its value have been difficult. Our group from the University of Tennessee, Knoxville, and the Oak Ridge National Laboratory has used the technique of resonant inelastic x-ray scattering (RIXS) at the Advanced Light Source to make a particularly clean measurement of  $U$  in sodium vanadate ( $\text{NaV}_2\text{O}_5$ ). We were able to compare measured RIXS spectra to spectra calculated with the  $U$  of the Hubbard model as a variable. For a particular value of  $U$ , theory and experiment turn out to be in good agreement, thereby suggesting that RIXS provides useful information for solids with strong electron–electron interactions.

Multielement oxide compounds containing transition metals variously known as complex materials or strongly correlated materials are at the forefront of today's solid-state science. On the level of fundamental understanding, they have for many decades defied theorists' efforts to model them accurately, owing to the large electron–electron interaction that casts into doubt the applicability of the conventional energy-band models of solids (both conventional one-electron and more sophisticated quasiparticle varieties). At the same time, these materials exhibit a wondrous variety of phenomena signaled by phase transitions and collective or many-body effects of various types, some of which potentially have commercial overtones, such as the high-temperature superconductivity and colossal magnetoresistance that result by doping the parent compounds with small concentrations of additional elements.

In thinking about strongly correlated materials, theorists frequently start from the Hubbard model, a simplified scheme that contains a single parameter, the Hubbard interaction term,  $U$ , to characterize electron–electron repulsion. When  $U$  is large, a partially occupied band straddling the Fermi energy can split into two Hubbard bands, producing an energy gap that converts what was a metal into a Mott insulator. In real Mott insulators, the many energy bands traceable to electrons originating from the different atomic

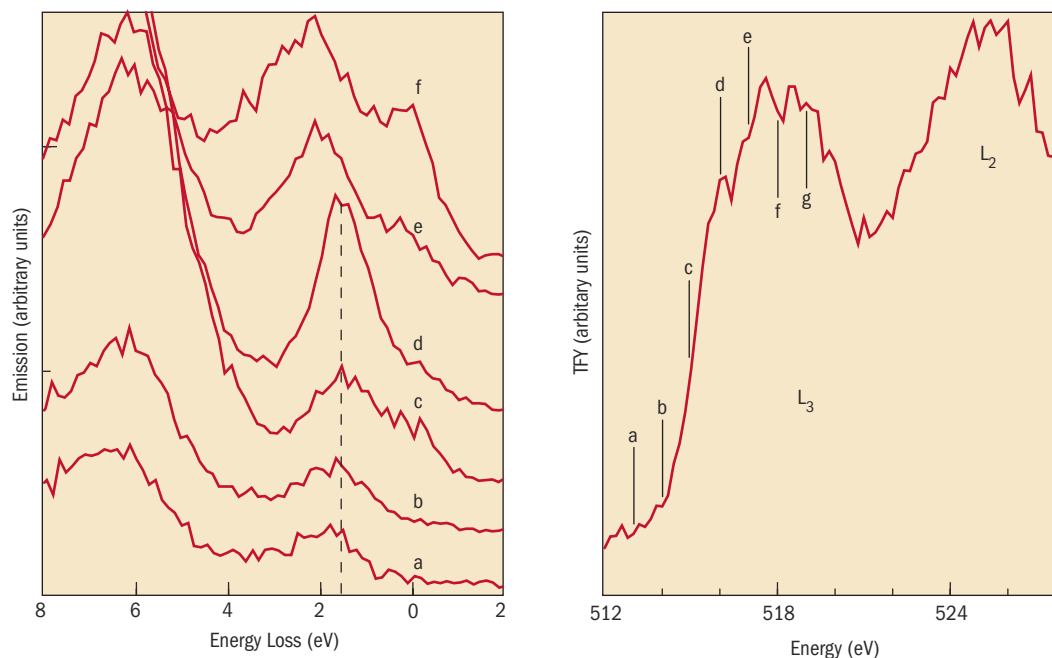


**FIGURE 8** In inelastic x-ray scattering (left), researchers measure the intensity of the emitted x rays as a function of the energy loss (difference between the energies of the absorbed and emitted x rays) for several excitation energies (indicated by the lower-case letters in the total fluorescent yield spectrum, right). The emission peak (dotted line) that is independent of excitation energy is due to resonant inelastic scattering (RIXS).

shells (s, p, d, etc.) can overlap, so that extracting the splitting between the Hubbard bands is not so easy.

Study of sodium vanadate overcomes this problem because there is a single narrow band at the Fermi level before the strong electron–electron interaction is taken into account. But it introduces a new complication for optical absorption spectroscopy of the Hubbard bands, because quantum-mechanical selection rules prohibit transitions excited by absorption of a single photon between electron states with the same angular momentum. Our collaboration attacked the selection-rule problem with RIXS, which is a two-photon soft x-ray technique in which the first photon can excite an electron from a core state to the upper Hubbard band and the second photon is that emitted when an electron in the lower Hubbard band falls into the hole (missing electron) in the core state.

In measurements at ALS Beamline 8.0.1, our group excited electrons from vanadium 2p core states (vanadium L edges). The resulting x-ray emission spectra contained two prominent features over a small photon-energy range that could be distinguished by watching how peak positions changed with excitation energy (Figure 8). In this way, we isolated the emission peak due to excitation into the upper Hubbard band followed by recombination from the lower

band. Both bands derive from vanadium d states (or more specifically,  $d_{xy}$  states). From the energy difference between the inelastic and elastic (emitted photon energy is the same as the excitation energy) peaks, we derived the energy splitting between the bands. A calculation, based on a simple cluster model of sodium vanadate with the Hubbard interaction term,  $U$ , as a variable parameter, yielded good agreement between experimental and theoretical energy splittings for a particular value of  $U$  equal to 3.0 eV (Figure 9).

### INVESTIGATORS

G.P. Zhang (University of Tennessee, Knoxville, and State University of New York, College at Buffalo); T.A. Callcott, G.T. Woods, and L. Lin (University of Tennessee, Knoxville); and B. Sales, D. Mandrus, and J. He (Oak Ridge National Laboratory).

### FUNDING

National Science Foundation and U. S. Department of Energy, Office of Basic Energy Sciences.

### PUBLICATION

1. G.P. Zhang et al., “Electron correlation effects in resonant inelastic x-ray scattering of  $\text{NaV}_2\text{O}_5$ ,” *Phys. Rev. Lett.* **88**, 077401 (2002).

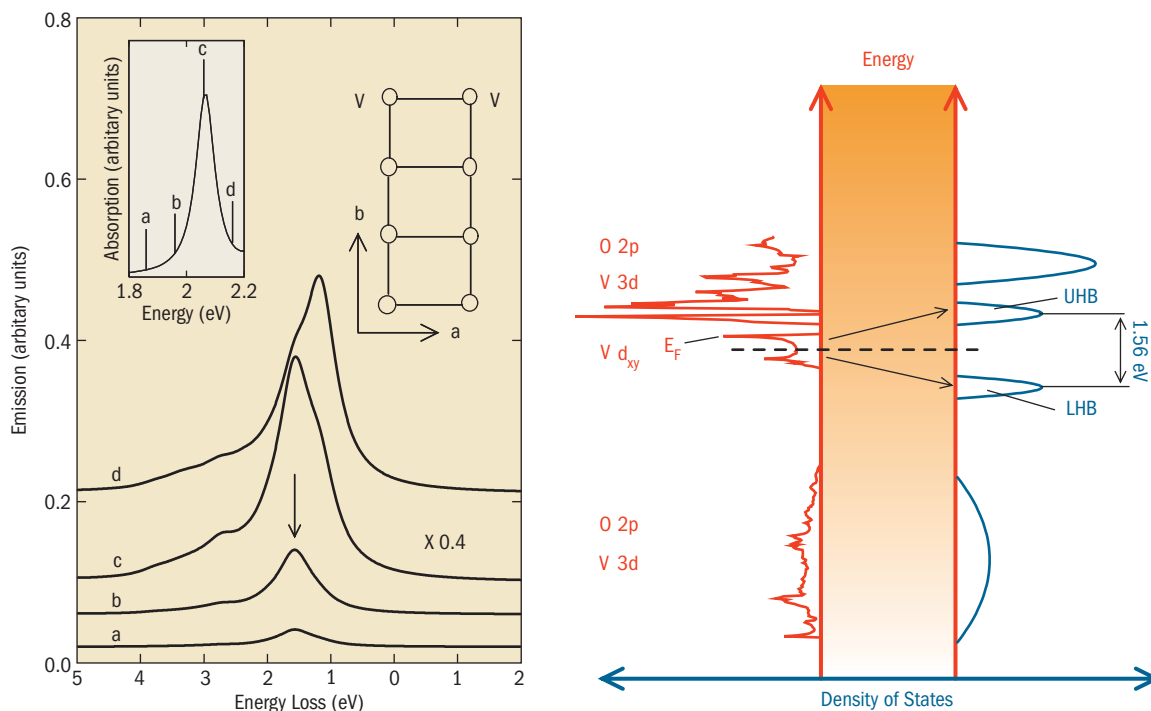


**FIGURE 9** Comparison of the experimental emission spectra and those calculated for a simple model of sodium vanadate (*left*) identifies the RIXS peak as due to excitation to and recombination from the upper and lower Hubbard bands that arise from electron correlation (*right*). Letters indicate the excitation photon energy. A value of 3.0 eV for the Hubbard interaction term,  $U$ , was also obtained.

## Electronic Structure of $\text{MgB}_2$ from X-Ray Emission and Absorption

For many decades, all the known superconductors (materials that conduct electricity with no resistance when cooled to frigid temperatures within a few degrees Kelvin of absolute zero) were predominantly metals and metal alloys and compounds whose behavior was well explained by the Bardeen-Cooper-Schrieffer (BCS) theory. In 1986, a revolutionary new class of “high-temperature” superconductors comprising families of copper-oxide ceramics was discovered, some of which retained their superconductivity above 100 degrees Kelvin. There is no adequate theory as yet for these superconductors. Two years ago, researchers were excited yet again when a possible third category of superconductors entered the scene with the discovery of superconductivity in a metal compound, magnesium diboride, that remained superconducting at a much higher temperature than expected from the BCS theory but not so high as the high-temperature materials. Kurmaev et al. have performed x-ray spectroscopy experiments on magnesium diboride that explore the behavior of electrons in this material with an eye toward understanding what makes it tick.

The recent discovery of superconductivity in magnesium diboride ( $\text{MgB}_2$ ) with a transition temperature  $T_c$  close to 40 K was unexpected. Not only is this value of  $T_c$  the highest reported for any binary compound, it is much higher than previously expected within the context of the standard BCS theory of superconductivity and thus raises the possibility of a whole new class of superconductors. Amid the experimental and theoretical activity stimulated by this discovery, our group—a collaboration of Russian, German, Canadian, and Japanese researchers—measured boron and magnesium x-ray emission and absorption spectra (XES and XAS, respectively) in  $\text{MgB}_2$  and the related compounds graphite and  $\text{AlB}_2$ . Our results support one interpretation of the origin of the superconductivity.

X-ray spectroscopy is a powerful element-specific probe of the electronic structure of solids. The accessible core states are localized states, which allows interpreting the experimental spectra in terms of unoccupied states for absorption and occupied states for emission. Since dipole selection rules govern the transitions to or from the core level, it is actually the angular-momentum-resolved density of states (DOS) that is measured. Accordingly, we compared our results obtained with first-principles calculations of the partial density of states.

The boron K emission and absorption spectra were studied at Beamline 8.0.1 of the Advanced Light Source with the soft x-ray fluorescence endstation. The measurements of the magnesium L-emission spectra were performed using an ultrasoft x-ray grating spectrometer with electron excitation. The magnesium 2p absorption spectra were measured at Beamline BL-12A at the Photon Factory (KEK, Tsukuba). The calculations were made using the full-potential LAPW code WIEN97.

Theoretical and measured boron K emission and absorption spectra of  $\text{MgB}_2$ , which probe boron 2p occupied and unoccupied states, respectively, are presented in Figures 10 and 11. In order to determine the position of the Fermi level and convert experimental spectra to the binding-energy scale used in the calculation, we made x-ray photoemission (XPS) measurements of the boron 1s and magnesium 2p core levels. The calculated spectra, which show that emission and absorption follow the boron 2p partial density of states very closely, are in good agreement with the experimental spectra.

Calculated and measured magnesium L emission and absorption spectra, which probe occupied and unoccupied Mg 3s states, are shown in Figures 12 and 13. The calculated emission differs somewhat from the magnesium 3s partial DOS because the contribution to the x-ray intensity is larger for states near the Fermi level than it is for those at the bottom of the valence band, in accordance with the energy dependence of the radial dipole matrix elements. We found reasonable agreement between calculated and experimental spectra, thus suggesting that electron–electron

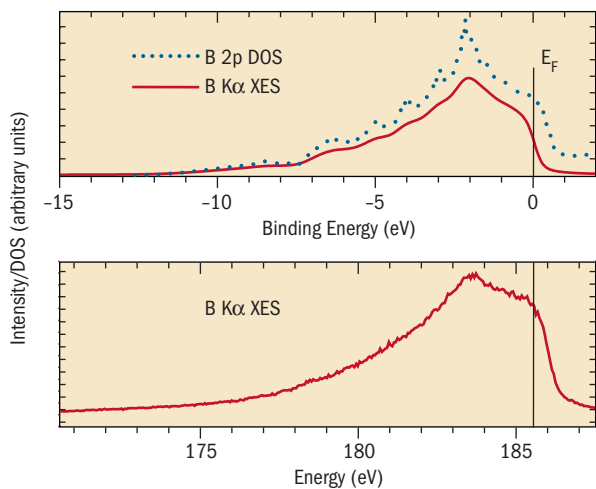


**FIGURE 10** Calculated (*top*) and measured (*bottom*) boron K emission spectra of  $\text{MgB}_2$ . The spectra closely follow the calculated density of unoccupied boron 2p states.

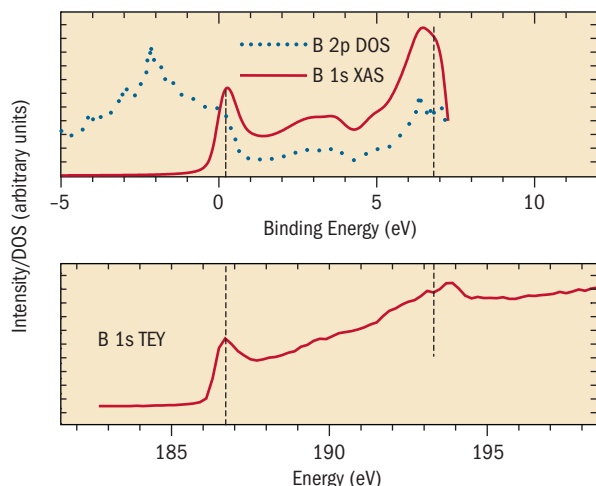


**FIGURE 11** Calculated (*top*) and measured (*bottom*) boron K absorption spectra of  $\text{MgB}_2$ . The spectra closely follow the calculated density of occupied boron 2p states.

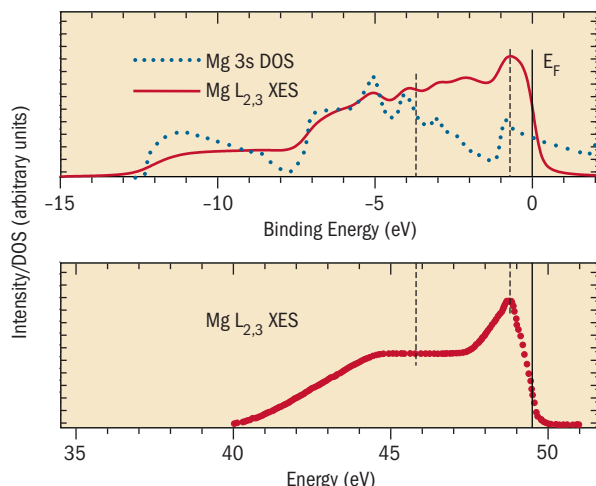


**FIGURE 12** Calculated (*top*) and measured (*bottom*) magnesium L emission spectra of  $\text{MgB}_2$ . The spectra near the Fermi energy show some departure from the calculated density of unoccupied magnesium 3s states.

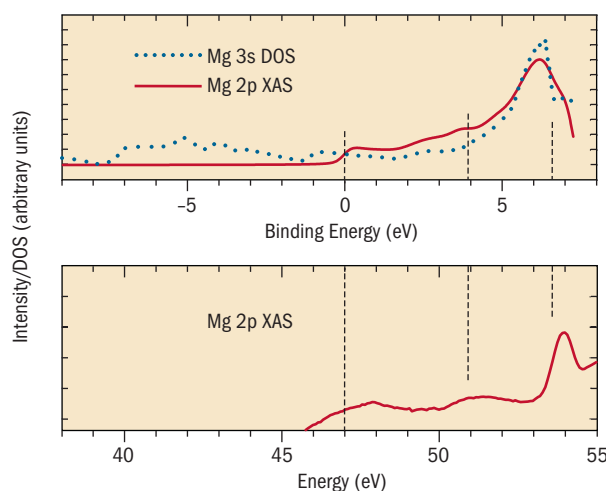


**FIGURE 13** Calculated (*top*) and measured (*bottom*) magnesium L absorption spectra of  $\text{MgB}_2$ . The reasonable agreement between theory and experiment for all boron and magnesium XES and XAS spectra suggests that electron–electron interactions are not important in this material.

interactions are not important in the case of  $\text{MgB}_2$ , so that it behaves like a conventional metal well described by band theory.

A negative chemical shift of about 0.5 eV is found in the magnesium  $L_{2,3}$  XES with respect to that of pure magnesium, which we consider evidence for charge transfer from magnesium to boron atoms in this compound. This is an important effect because it lowers the  $\pi$  ( $p_z$ ) bands relative to the bonding  $\sigma$  ( $sp^2$ ) bands. This lowering causes  $\sigma \rightarrow \pi$  charge transfer and  $\sigma$ -band hole doping and is said to drive the superconductivity in  $\text{MgB}_2$ .

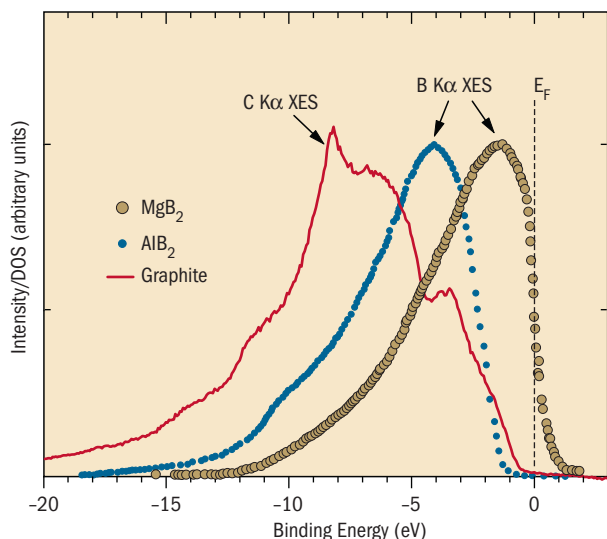


**FIGURE 14** Comparison of x-ray K emission spectra of hexagonal graphite,  $\text{AlB}_2$ , and  $\text{MgB}_2$  on the binding-energy scale. The maximum originating from  $\sigma$  states is shifted in  $\text{MgB}_2$  toward the Fermi level with respect to that of graphite, while the maximum in  $\text{AlB}_2$  occupies an intermediate position.

In order to investigate this interpretation further, we compared the  $K\alpha$  XES for graphite,  $\text{AlB}_2$ , and  $\text{MgB}_2$  by alignment of the Fermi levels as determined from XPS measurements (Figure 14). The maximum originating from  $\sigma$  states is shifted in  $\text{MgB}_2$  toward the Fermi level with respect to that of graphite.  $\text{AlB}_2$  occupies an intermediate position, which results in filling of the  $\sigma$  bands, decreasing the density of states at the Fermi level,  $N(E_F)$  and finally destroying superconductivity.

#### INVESTIGATORS

E.Z. Kurmaev (Institute of Metal Physics, Yekaterinburg);

I.I. Lyakhovskaya (St. Petersburg University); J. Kortus (Max-Planck-Institut für Festkörperforschung, Stuttgart); A. Moewes (University of Saskatchewan); M. Demeter and M. Neumann (University of Osnabrueck); N. Miyata, M. Yanagihara, and M. Watanabe (Tohoku University, Sendai); and T. Muranaka and J. Akimitsu (Aoyama-Gakuin University, Tokyo).

### FUNDING

The Russian State Program on Superconductivity; Russian Foundation for Basic Research; NATO Collaborative Linkage Grant; Schloëßmann Foundation; University of Saskatchewan; and U.S. Department of Energy, Office of Basic Energy Sciences.

### PUBLICATION

1. E.Z. Kurmaev et al., “Electronic structure of  $\text{MgB}_2$ : X-ray emission and absorption studies,” *Phys. Rev. B* **65**, 134509 (2002).

## Hot Spots Turn Cold in the Overdoped Regime of Cuprate Superconductors

*The origin of superconductivity (resistanceless flow of electricity) in “high-temperature” superconductors has remained a mystery since the discovery of the first of these ceramic compounds in 1986, despite a mountain of experimental data and reams of calculations by theorists. A key requirement of any model of superconductivity is to explain how electron pairing occurs. When the electrons pair up, the usual causes of electrical resistance become inoperative until there is enough energy available to break up the pairs. In most superconductors, pairing is mediated by vibrations of the atoms around their nominal positions (an electron–phonon interaction, in the scientific jargon). Scientists have made many proposals for alternative pairing mechanisms in high-temperature superconductors, but the evidence for any of them is as yet unconfirmed. By irradiating a sample with x rays and making careful photoemission measurements of the energy and number of electrons emitted in various directions, Bogdanov et al. have now produced strong evidence against one of the proposed pairing mechanisms.*

Over the last decade, angle-resolved photoemission spectroscopy (ARPES) has served as a powerful tool to uncover some of the main aspects of the physics of high-temperature superconductors (cuprates). In particular, one can directly

extract information about the dynamics of quasiparticles in solids, such as the quasiparticle energy–momentum (dispersion) relation and the lifetime. In this way, it is possible to probe the fundamental scattering process in the material. Our ARPES measurements of the electron scattering rate in lead-doped  $\text{Bi}_2\text{Sr}_2\text{CaCu}_2\text{O}_8$  (Pb-Bi2212), one among several families of cuprates, show that a postulated magnetic resonance (spin scattering) mode cannot be the dominant scattering mechanism that drives electron pairing in these materials.

By studying the lineshapes of photoemission energy distribution curves (EDCs), in particular the width of spectral peaks, one can extract a quantity proportional to the quasiparticle lifetime, which is a very sensitive test of the scattering processes in cuprates. The continuing improvement of the angular resolution in photoemission spectroscopy has made it possible to use ARPES to search for anisotropic scattering by studying the variation of the linewidth with momentum direction (direction in  $k$  space).

The observation of broader photoemission spectra in the anti-nodal direction  $(\pi, 0)$  with respect to those in other momentum regions has been attributed to spin scattering centered around the scattering vector  $Q=(\pi, \pi)$ . This vector connects the Fermi surface “hot spot” at the  $(\pi, 0)$  point of

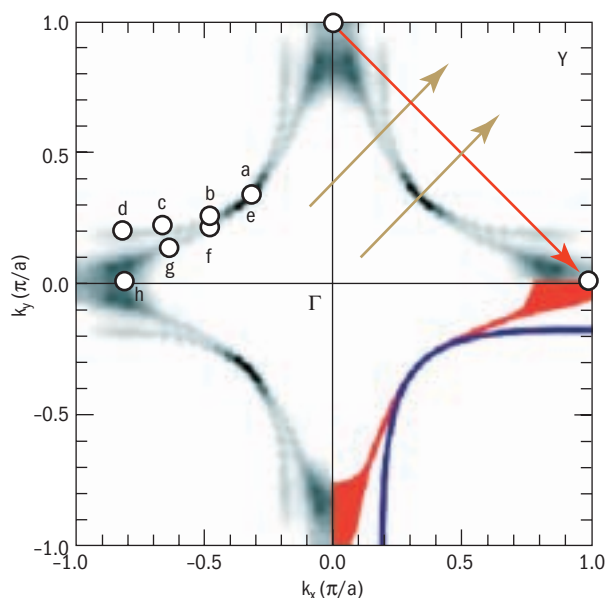


**FIGURE 15** Fermi surface mapping of overdoped Pb-Bi2212 single crystal. The lower right quadrant of the Brillouin zone identifies the bonding band Fermi surface (blue) and the anti-bonding band Fermi surface (red). The yellow arrows indicate the direction along which the data were collected. The red arrow represents the  $Q=(\pi, \pi)$  vector, as determined in neutron scattering experiments, connecting the two  $(\pi, 0)$  hot spots of the Fermi surface.

the Brillouin zone to the  $(0, \pi)$  hot spot (Figure 15), resulting in a broadening of the photoemission spectra by the simultaneous excitation of collective modes near this region.

From this finding, an anisotropy in which the peak width increases toward  $(\pi, 0)$  can be considered as a sign of the presence of antiferromagnetic interactions in the electron dynamics. However, the recent report of a momentum-dependent splitting between bonding and antibonding energy bands (bilayer splitting) in the superconductor Bi2212 raises the question whether a second, unresolved bilayer splitting may be the actual source of the observed broadening at  $(\pi, 0)$ . The fundamental importance of this question to identifying the main scattering mechanism for superconductivity motivated our investigation.

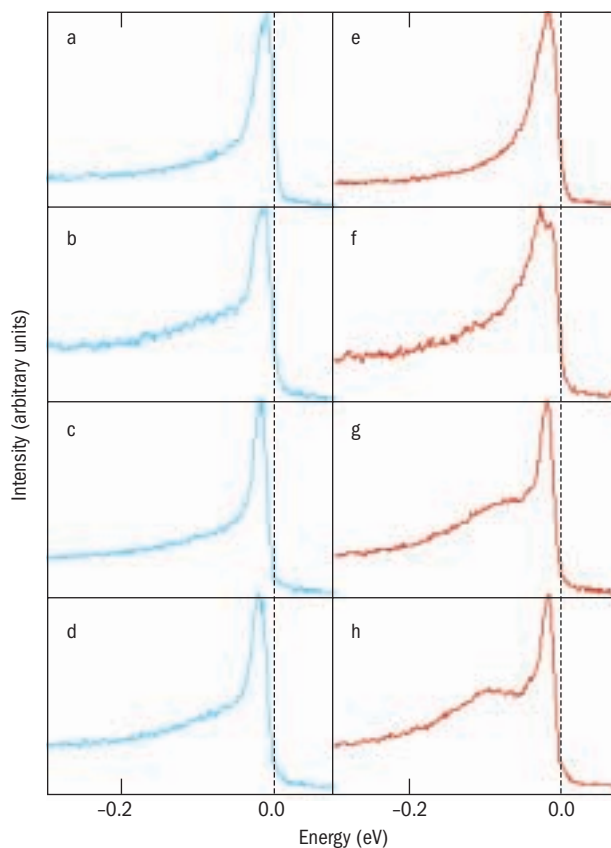


**FIGURE 16** Energy distribution curves (EDCs) along the two bonding and antibonding sheets of the Fermi surface taken at the points indicated in Figure 15. The blue EDCs are for the bonding band and the red are for the antibonding band at the Fermi surface. Analysis shows that the peak width (scattering rate) does not change significantly near the hot spots.

Our approach was to focus on the lead-doped material Pb-Bi2212 in the overdoped regime ( $T_c=70$  K), where a “superstructure band” that arises from the lattice mismatch of the BiO with the  $\text{CuO}_2$  planes is suppressed by the introduction of lead. In addition, in this doping range, the bonding and antibonding bands can be well resolved, making it possible to study in detail the momentum evolution of the quasiparticle scattering rate. We recorded our spectra at ALS Beamline 10.0.1 with 22-eV photons on single crystals in both the superconducting and normal states.

We carefully studied the evolution of the widths of the quasiparticle peaks along the two resolved Fermi surface pieces. In particular, as can be seen in Figure 16, one sees that along the bonding Fermi surface the spectra do not change significantly, and the width of the peak appears almost constant, hinting at an isotropic scattering rate. A similar conclusion can be drawn for the lineshapes along the antibonding Fermi surface, despite the more complex structure of the lineshapes, which consist of two features: a peak at the Fermi level and a feature that disperses to higher binding energy. We adopted different analysis procedures to extract the width of the EDCs and have unambiguously shown that the scattering rate does not increase towards  $(\pi, 0)$ .

This result contradicts what is expected from the  $Q=(\pi, \pi)$  scattering, indicating that the hot spot has turned cold at this doping level and therefore promotes another kind of mechanism. This finding puts a very strong constraint on any theory of high-temperature superconductivity, and in particular it shows that the magnetic resonance mode cannot be the driving force for electron pairing.

#### INVESTIGATORS

A. Lanzara (Stanford University, ALS, and University of California, Berkeley); P.V. Bogdanov, X.J. Zhou, H. Eisaki, and Z.X. Shen (Stanford University and Stanford Synchrotron Radiation Laboratory); and W.L. Yang and Z. Hussain (ALS).

#### FUNDING

U.S. Department of Energy, Office of Basic Energy Sciences; National Science Foundation.

#### PUBLICATION

1. P.V. Bogdanov et al., “Anomalous momentum dependence of the quasiparticle scattering rate in overdoped  $\text{Bi}_2\text{Sr}_2\text{CaCu}_2\text{O}_8$ ,” *Phys. Rev. Lett.* **89**, 167002 (2002).

# MATERIALS SCIENCE

## Standing Waves Probe Nanowedge Interfaces

Magnetic nanostructures comprising multiple layers of magnetic and nonmagnetic materials each only a few atoms thick are the foundation of modern magnetic data storage and memory devices. But because most of the action takes place out of sight in the comparatively few atoms that reside at or near the boundaries (interfaces) between the layers, some details are hard to study. Yang et al. have attacked this problem for the interface between iron and chromium by creating a so-called x-ray standing wave that penetrates vertically through the sample so that the maximum x-ray intensity, which will generate most of the signal to be measured, occurs at a particular depth below the surface. By scanning a focused x-ray beam across the surface of a wedge-shaped sample in which the position of the interfaces changes with thickness, they were able to map the changes in chemical and magnetic behavior at and around the interface. Researchers in other areas of nanostructure science should also find this technique valuable.

Structures with nanometer-scale dimensions are ever more important in science and technology. Integrated circuits are the most familiar example, but nanostructures of a different type are also commercialized in magnetic read heads for high-density data storage and may soon appear in magnetic memory chips. With the increased importance in such nanostructures of atoms residing at buried solid/solid interfaces, characterizing buried interfaces becomes a crucial step in understanding mechanisms and developing new devices based on these state-of-the-art materials. For example, new methods to nondestructively study buried interfaces would help to clarify the nature of both the giant magnetoresistance effect and exchange biasing, two key phenomena that make magnetic nanostructures useful.

To this end, our group of researchers from Berkeley Lab and the University of California, Davis, has combined the technique of generating standing waves of circularly polarized soft x rays with the growth of wedge-shaped samples. In this way, we demonstrated the ability to map both composition and magnetization across an iron/chromium interface by means of core-level photoelectron spectroscopy, magnetic circular dichroism, and parallel mathematical modeling.

In order to study buried interfaces in this way, we first realized that soft x-ray standing waves generated via Bragg reflection from a multilayer mirror should make it possible to spectroscopically study buried interfaces nondestructively, provided that there is a way to vary the position of the standing-wave intensity maximum around the interface. We also knew that wedge-shaped samples can be used to investigate the thickness dependence of many types of phenomena. In a combined approach, we grew the sample to be studied on top of the mirror in a wedge shape, and then simply by translating the sample horizontally in front of a focused x-ray beam, the standing wave could be scanned vertically through the buried interface.

In the experiments, which were carried out at ALS Beamline 4.0.2, strong standing waves with a period of 4.0 nm and an approximately 3:1 ratio between the maximum and minimum intensities were created by a synthetic multilayer mirror fabricated at Berkeley Lab's Center for X-Ray Optics. The mirror consisted of 40 periods of  $B_4C$  and tungsten:  $[B_4C/W]_{40}$ . A wedge-shaped bilayer of chromium (variable thickness) and iron (1.6 nm thick) was grown on top of the multilayer (Figure 1). By analyzing various core-level photoelectron intensities as a function of both x-ray incidence angle and beam position, we could derive layer thicknesses and measure the interface mixing/roughness due to migration of atoms across the interface to form a mixture of iron and chromium.

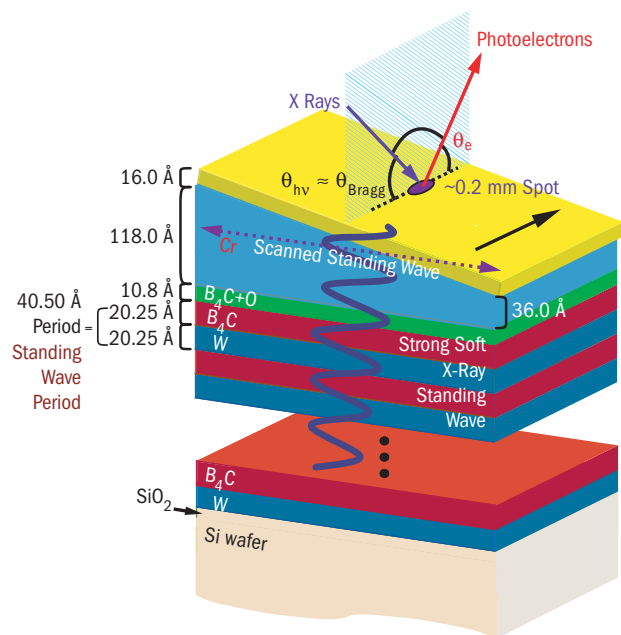


**FIGURE 1** Wedge-shaped sample. Scanning the sample in the direction of the wedge moves the intensity maximum of the standing wave from one side of the iron/chromium interface to the other.

In addition, magnetic circular dichroism in photoemission from the 2p and 3p levels of iron and chromium (Figure 2) resulted in identification of regions with decreased (increased) ferromagnetic alignment for iron (chromium) and a quantitative determination of the positions and widths of these regions (Figure 3). The magnetically altered regions in both metals were only one to two atomic layers in thickness. From these results, our group concluded that (1) normally antiferromagnetic chromium becomes ferromagnetic just below the center of the interface but with antiparallel alignment with respect to iron, and (2) the equal-concentration region in the center of the interface strongly inhibits magnetic alignment for both species along the direction of net magnetization that was probed (also the direction of light incidence). Multiplet-split spectra from the 3s levels of iron and chromium further indicated that the local spin moments on both atoms do not change on crossing the interface.

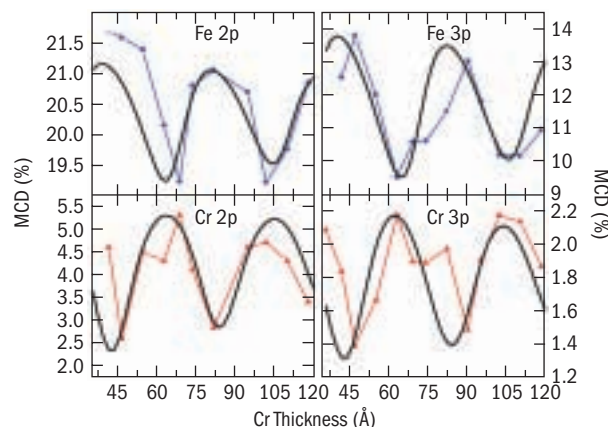


**FIGURE 2** Magnetic circular dichroism in iron and chromium core photoemission as a function of standing-wave position. The black lines are simulations for the best-fit values of the depth and width of the regions with decreased (increased) ferromagnetic alignment for iron (chromium).

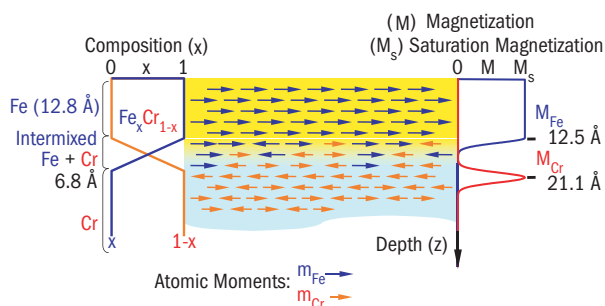


**FIGURE 3** Analysis of the core-level photoemission and magnetic circular dichroism as the standing wave moves through the interface yields composition and magnetization profiles across the interface, including a region of intermixed iron and chromium in which the atomic magnetic moments change orientation.

We expect that the standing-wave-plus-wedge method will not be limited to magnetic nanolayers but should apply equally well to the characterization of other types of nanostructures and their interfaces. Expanding the signal detected to include soft x-ray fluorescence, valence-band photoemission, or the spin of the photoelectrons will also extend the range of applications.

#### INVESTIGATORS

S.-H. Yang, J.B. Kortright, J. Underwood, and F. Salmasi (Berkeley Lab); B.S. Mun, N. Mannella, and M.A. Van Hove (Berkeley Lab and University of California, Davis); S.-K. Kim (Seoul National University, Korea); E. Arenholz, A. Young, and Z. Hussain (ALS); and C.S. Fadley (Berkeley Lab, University of California, Davis, and University of Hawaii).

#### FUNDING

U.S. Department of Energy, Office of Basic Energy Sciences, and Korea Science and Engineering Foundation.

#### PUBLICATION

1. S.-H. Yang et al., "Probing buried interfaces with soft x-ray standing wave spectroscopy: Application to the Fe/Cr interface," *J. Phys.: Condens. Matter* **14**, L407 (2002).

## Electromigration in Advanced Integrated Circuits

*In state-of-the-art computer chips, more than 100 million transistors have to be connected by metal lines buried in an insulator (dielectric). The metal interconnects in advanced microelectronic devices are only about 1000 atoms wide and operate at high current densities at least a hundred times higher than in common metal wires. As a result, one of the major failure mechanisms is electromigration, i.e., the transport of atoms in an interconnect along the direction of electron flow. The transport of many atoms can result in voids in the wire, leading to open circuits, as well as hillocks that extrude from the original interconnect, causing short circuits. Schneider et al. have used an x-ray microscope to study the pathways by which copper atoms move by observing directly the transport of matter in interconnects during electromigration. Correlation of these real-time measurements with post-mortem electron-microscope images shows that the nucleation and subsequent motion of voids in copper occurs at boundaries between crystalline regions (grain boundaries), an observation that any cure for electromigration will have to take into account.*

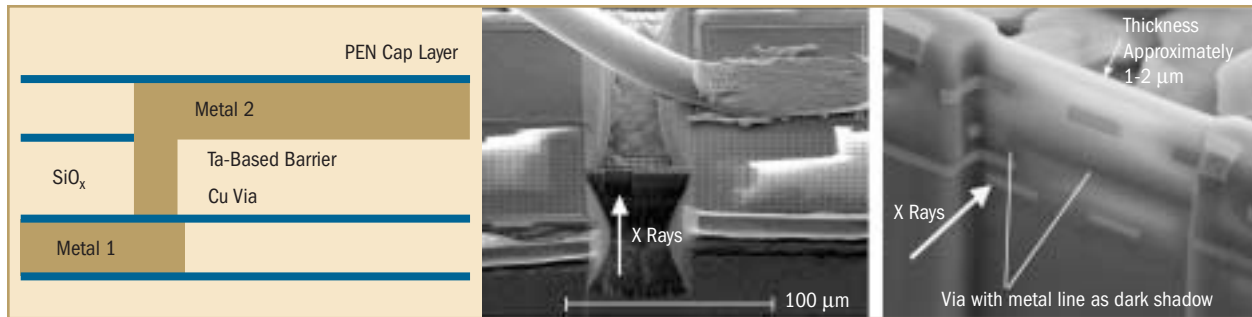


**FIGURE 4** Left, schematic diagram of the cross-section of the electromigration test sample with copper via (interconnect) structures. Center, SEM micrograph of a fully prepared test sample. Right, SEM micrograph of the cross-section of copper metallization thinned locally with a focused ion beam.

Electromigration-induced atomic transport in the metal lines connecting transistors in integrated circuits (ICs) is best studied in situ in an intact IC, so that a technique capable of high spatial resolution when penetrating through several microns of dielectrics is needed. Since x rays have the penetrating power and they are element specific, our collaboration comprising Berkeley Lab and German researchers used x-ray microscopy to image copper interconnect lines embedded within  $\text{SiO}_2$  while electromigration was occurring. In this way, we were able to study the dynamics of void development in passivated copper structures comprising interconnect lines in different layers and the vias that link them.

The challenge in designing advanced ICs is to ensure reliability while the number of devices increases. As both transistor and interconnect dimensions decrease, the overall performance of microprocessors is increasingly determined by interconnect design and materials. While aluminum-based interconnects are being replaced by inlaid copper with a higher conductivity and improved electromigration performance, electromigration phenomena nevertheless remain severe reliability concerns. Among the issues associated with electromigration in an IC, the mass flow in an interconnect due to electromigration is constrained by encapsulation. The resulting high mechanical stress in the interconnect influences the material transport significantly.

To investigate this behavior, we used the full-field x-ray microscope, XM-1, at ALS Beamline 6.1.2, which is operated by Berkeley Lab's Center for X-Ray Optics. The interconnect structures used for our electromigration experiments are located within the scribe lines of production wafers. Figure 4 (left panel) shows a schematic cross-section of our test structures with a two-level copper interconnect. A focused ion beam (FIB) was used to thin the IC at the region of interest to a thickness of about 2  $\mu\text{m}$  (see middle and right of Figure 4). Material was removed from both sides of the

copper structures under test, so that all neighboring metal lines were removed from the XM-1 field of view. A 50- $\mu\text{m}$ -wide trench leading to the area of interest was cut. The x-ray beam penetrated the sample through this trench (see Figure 4, middle).

Figure 5 (parts a–e) shows a sequence of in-situ x-ray micrographs of the copper via/line interconnect structure that were captured with XM-1 at a 1.8-keV photon energy. The electron flow was from left to right in the image, and upwards through the via. Figure 5a shows the initial state of the interconnect structure without any voids. During the experiment, void formation (Figure 5b), movement (Figure 5c–d) and agglomeration (Figure 5e) were seen in the via.

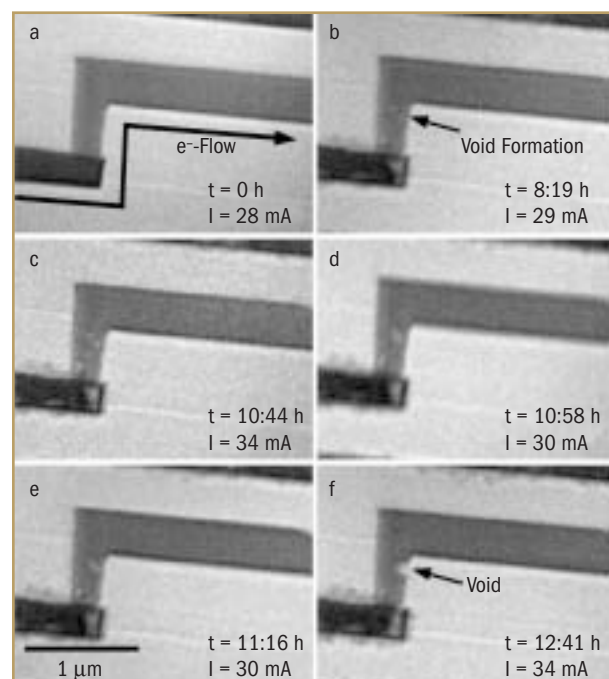


**FIGURE 5** Selected images (a–f) from a sequence of x-ray micrographs taken at successive times showing void formation, movement, and agglomeration inside the passivated copper via.

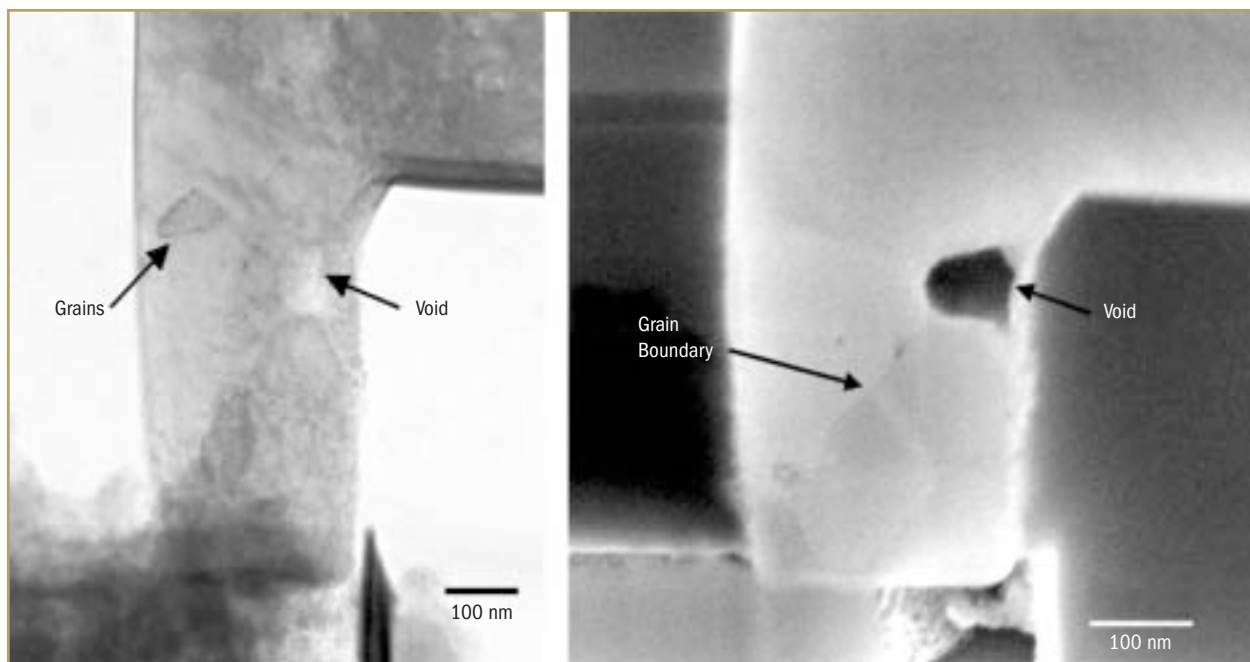


**FIGURE 6** High-voltage transmission electron microscopy bright-field image (*left*) and SEM micrograph (*right*) showing the copper line/via structure after the electromigration test. Grain boundaries that appear consistent with the path of the void as it migrated can be seen. The void that was formed during the electromigration experiment is also clearly visible.

The image sequence indicates that initial voids are formed in the copper bulk structure, probably at grain boundaries or grain boundary triple points.

To obtain detailed structural information of the via after the electromigration experiment, the JEOL Atomic Resolution Microscope operating at an accelerating voltage of 800 kV at Berkeley Lab's National Center for Electron Microscopy was used to image the stressed sample. There seems to be a significant mass transport along grain boundaries to the copper/tantalum interface at the via sidewall, where voids grow and agglomerate (see Figure 6). Figure 6 also shows a scanning electron microscopy (SEM) image of an FIB-thinned cross-section of the test sample, which shows a grain boundary leading to the large void. Small voids are visible along this grain boundary, giving evidence for the grain boundary diffusion mechanism.

By correlating the information showing the transport of matter with the copper microstructure obtained from x-ray micrographs, the dominant copper diffusion pathways can

be identified. Visualizing the exact location (bulk or interface) of voids in interconnects during electromigration by means of real-time x-ray tomography and its correlation with electron micrographs might help to design faster microprocessors.

#### INVESTIGATORS

G. Schneider, G. Denbeaux, E.H. Anderson, B. Bates, A. Pearson, and E.A. Stach (Berkeley Lab); M.A. Meyer and E. Zschech (AMD Dresden, Germany); and D. Hambach (University of Göttingen, Germany).

#### FUNDING

Deutsche Forschungsgemeinschaft; U.S. Department of Energy, Office of Basic Energy Sciences; and the DARPA Advanced Lithography Program.

#### PUBLICATION

1. G. Schneider et al., "Dynamical x-ray microscopy investigation of electromigration in passivated inlaid Cu interconnect structures," *Appl. Phys. Lett.* **81**, 2535 (2002).

## Resolving Nanometer-Scale Magnetic and Chemical Structure in Magnetic Recording Media Films

*The usual way to look at something very small is to examine it through a microscope. As the size shrinks below the microscopic, x-ray and electron microscopes become the tools of choice. But what is the researcher to do when even these instruments cannot resolve the details of interest? At this point, scattering rather than imaging may come to the rescue. Scattering measures the angular variation of the intensity of the radiation (whether light waves, x-ray beams, or electrons) that is deflected (scattered) on passing through a sample. From the intensities of scattered radiation and the angles at which they occur, one can work backwards to deduce something about the sizes of the objects within the sample responsible for the scattering and about the composition and other properties of the objects. Drawing on the sensitivity of x rays to magnetic atoms, Kortright et al. took this tack in their x-ray scattering investigation of the composition and magnetic properties of the tiny particles that hold the bits of information in computer disks.*

Current magnetic recording media alloy films consist of chemically segregated, polycrystalline grains whose centers are ferromagnetic and whose boundaries are nominally nonmagnetic. Our Berkeley Lab-IBM group has used the high sensitivity of resonant soft x-ray scattering to make the first direct measurements of magnetic correlation lengths in advanced recording media, to obtain estimates of the chemical compositions of the segregated phases, and to follow the evolution of this correlation length with alloy composition on media films grown on a common buffer layer structure similar to that used in current technology.

The chemically and magnetically heterogeneous microstructure of magnetic recording media has evolved through an increasingly complex set of alloys from CoCr to CoPtCr to CoPtCrB. Chemical segregation in these films can be resolved with high-resolution transmission electron microscopy (TEM), as seen in Figure 7. However, to directly measure the magnetic correlation length giving the distance over which grain-to-grain magnetism is correlated has remained difficult because the length scales are too small to resolve with microscopies (e.g., magnetic force and Lorentz transmission electron microscopy), and the scattering contrast is too weak for polarized neutron-scattering measurements. The high sensitivity of resonant soft x-ray

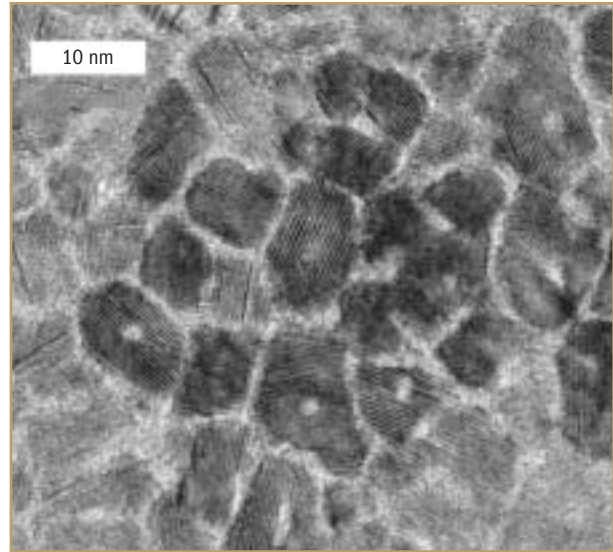


**FIGURE 7** This plan-view high-resolution TEM image shows the polycrystalline grain structure in a CoPtCrB recording media film. Analytical techniques can reveal that chromium and boron segregate to the grain-boundary areas that are lighter in color and believed to be nonmagnetic. The darker grain centers are rich in cobalt and platinum and are magnetic. Until now it has remained difficult to measure the magnetic-correlation length that gives the distance over which the grain-to-grain magnetization is strongly coupled. Short magnetic-correlation lengths are desired for recording media alloys, since this length sets a limit on how sharp the magnetic transition between memory bits can be. (Photo courtesy Kai Tang, IBM)

scattering to elemental, magnetic, and charge scattering has allowed us to resolve and follow magnetic correlation lengths in recording media films.

The strong resonant sensitivity of soft x-rays is illustrated in Figure 8, which shows intensity as a function of scattering vector  $q$  and photon energy  $h\nu$  near the cobalt  $L_3$  edge from a  $\text{Co}_{69}\text{Pt}_3\text{Cr}_{22}$  granular media film. Of the two peaks observed, the one at larger  $q$  clearly results from the chemically segregated grain structure, since  $2\pi/q = 11$  nm corresponds to the chemical grain size known from TEM. The origin of the low- $q$  peak is unambiguously determined by modeling its energy spectrum; only a model assuming pure magnetic scattering can reproduce the shape. Modeling also confirms the chemical origin of the high- $q$  peak and yields a good estimate of the compositions of the grain boundary and center phases. For CoPtCr media, the magnetic correlation length is several times the chemical grain size, indicating that exchange coupling between adjacent grains limits its recording density.

The effect of alloy composition on magnetic and chemical length scales was also studied (Figure 9). These data were collected at x-ray energies near the chromium and cobalt  $L_3$

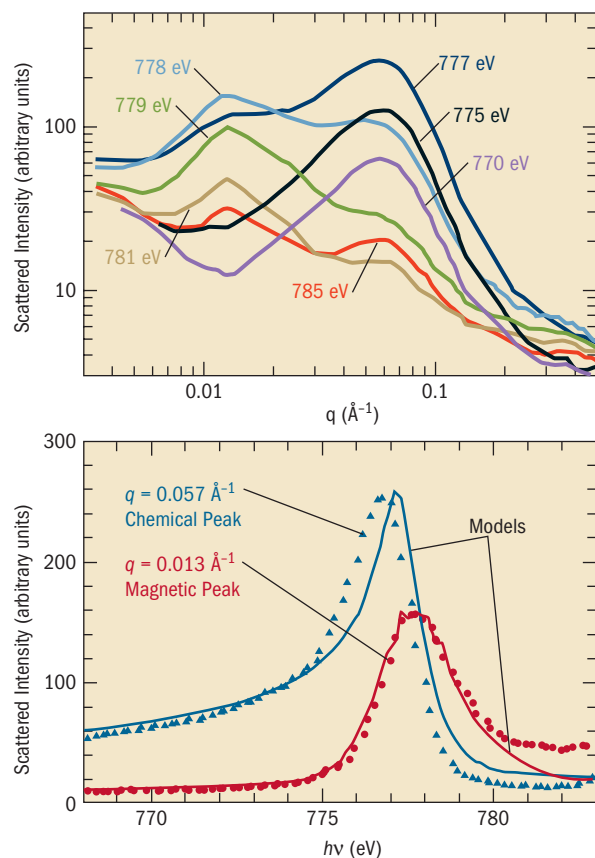


**FIGURE 8** *Top*, resonant small-angle scattering from a  $\text{Co}_{69}\text{Pt}_9\text{Cr}_{22}$  in-plane recording media film reveals two peaks in  $q$  space that disperse differently with photon energy near the cobalt  $L_3$  edge at 778 eV. *Bottom*, energy spectra (symbols) measured at these two peaks are modeled using measured resonant charge and magnetic scattering factors for cobalt and tabulated values for platinum and chromium. The models (lines) confirm the magnetic origin of the low- $q$  peak and the chemical origin of the high- $q$  peak and further provide a measure of the chemical compositions of the segregated grain-center and grain-boundary phases. The large magnetic-correlation length indicates that some fraction of individual grains remain magnetically coupled by intergranular exchange.

core resonances. At the chromium edge, all samples have a single peak at the high- $q$  position of the chemical grain size peak, which changes little between the three alloys. The absence of magnetic peaks at lower  $q$  is expected, since the chromium in these films is *not* magnetic. At the cobalt edge, the magnetic low- $q$  peaks are prominent for the CoCr and CoPtCr films but not for CoPtCrB. The difference between the cobalt and chromium resonant scans results from cobalt magnetic–magnetic and magnetic–charge correlations, the former dominating the low- $q$  peak and the latter contributing progressively with increasing  $q$ . In the progression of alloy compositions, the magnetic correlation length remains unchanged between CoCr and CoPtCr but moves much closer to the polycrystalline grain size peak for

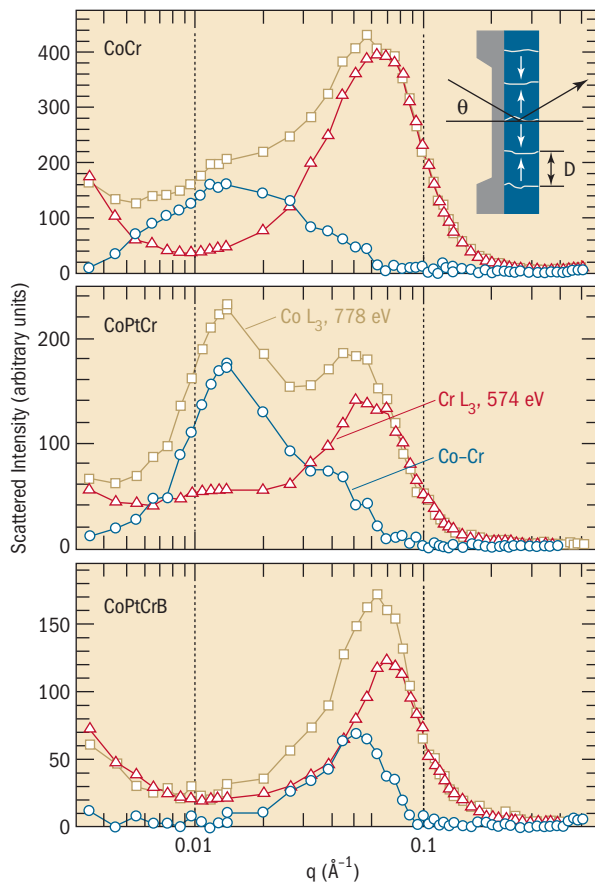


**FIGURE 9** Resonant x-ray scattering from CoCr (*top*), CoPtCr (*center*), and CoPtCrB (*bottom*) media measured at the cobalt (brown squares) and chromium (red triangles)  $L_3$  lines and the difference between the spectra (scaled to match at high  $q$ ) (blue circles). The inset shows the scattering geometry and the media layer with magnetic grains (diameter  $D$  and the in-plane magnetization direction represented by the arrows) and nonmagnetic grain boundaries. Intensity peaks result from interference between the scattering of well-defined neighboring scattering centers. The high- $q$  peaks in the chromium-edge data give the average chemical grain size of about 10 nm. The low- $q$  peaks in the difference data approximate the magnetic interference and show how the magnetic correlation length changes with alloy composition.

the boron-containing sample. Boron addition is thus highly effective in reducing magnetic correlation lengths, explaining why B is the segregant of choice in current recording media.

Systematic studies of the effects of composition, growth, and processing on magnetic and chemical properties of films of potential interest in future generations of magnetic storage media are already under way. As the recording industry moves toward perpendicular recording, resonant soft x-ray scattering is particularly well suited to characterize the new recording media that will be needed. The same resonant scattering techniques will also provide valuable new information on a broad range of nanostructured magnetic materials.

## INVESTIGATORS

J.B. Kortright (Berkeley Lab) and O. Hellwig, D.T. Marguiles, B. Lengfield, and E.E. Fullerton (IBM Almaden Research Center, now Hitachi Global Storage Technology, San Jose Research Center).

## FUNDING

U.S. Department of Energy, Office of Basic Energy Sciences; IBM; and Deutsche Forschungsgemeinschaft.

## PUBLICATIONS

1. J.B. Kortright, O. Hellwig, D.T. Marguiles, and E.E. Fullerton, "Resolving magnetic and chemical correlations in CoPtCr films using soft x-ray resonant scattering," *J. Magn. and Magn. Mater.* **240**, 325 (2002).
2. O. Hellwig, D.T. Marguiles, B. Lengsfeld, E.E. Fullerton, and J.B. Kortright, "Role of B on grain sizes and magnetic correlation lengths in recording media as determined by soft x-ray scattering," *Appl. Phys. Lett.* **80**, 1234 (2002).

## Electromigration-Induced Plastic Deformation

*Anybody who has contemplated a boulder-strewn beach after a big storm implicitly understands the power of large numbers of little things (the water molecules) acting in concert to push around much bigger things (the boulders). The same phenomenon plagues the metal conductors that connect the hundreds of millions of transistors on a state-of-the-art computer chip. In the connectors, nowadays only a fraction of a micrometer wide and much thinner than that, the raging electrons dislodge the atoms and carry them away. It is easy to imagine that over time, such atomic transport can lead to breaks in a connector and, hence, failure of the chip to operate correctly. The first step to solving this increasingly urgent problem, known as electromigration, is understanding exactly how it occurs. At the ALS, researchers have developed and now put to use an x-ray technique (microdiffraction) that is able to look with submicroscopic resolution at local stresses in metal conducting lines on test microchips, thereby catching the early stages of electromigration in the act.*

X-ray microdiffraction is joining x-ray imaging and spectroscopy in the arsenal of spatially resolved techniques at synchrotron radiation sources. At the ALS, our collaboration comprising researchers from Stanford University, the ALS, Bell Laboratories (Lucent Technologies), and the Intel

Corporation has focused on mapping with submicron spatial resolution the local crystalline orientation and strain/stress distributions in polycrystalline thin films. With this capability, we have made the first observation of plastic (permanent) deformation induced by electromigration in metal interconnects in computer microchips.

Electromigration refers to the motion of atoms induced by the flow of electric current. It increasingly affects the reliability of integrated circuits as the dimensions of the metal lines that connect the transistors on a chip become ever smaller with each new technology generation, so that the current density in these interconnects can be enormous (around a million amperes per square centimeter). The resulting atomic transport leads to the formation of voids or metal extrusions and, eventually, circuit failure due to breaks in the lines or short circuits with neighboring metal areas. Insight into the details of electromigration has awaited techniques able to measure local stresses with micron spatial resolution.

Enter x-ray microbeam techniques and microdiffraction in particular. X rays make an ideal probe because they can be focused to submicron spot sizes to probe individual grains within the patterned polycrystalline metal films that represent interconnect lines on a silicon chip. X rays can also penetrate through passivating layers, such as silicon dioxide, that overlie the metal lines. The ALS has been one of the centers of microdiffraction activity with the development of Beamline 7.3.3, a bend-magnet beamline that provides a

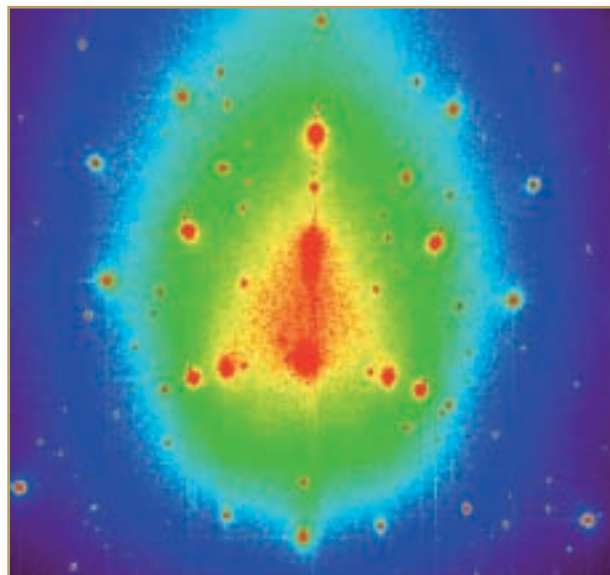


**FIGURE 10** Laue diffraction pattern of grains in an aluminum line on a silicon substrate.

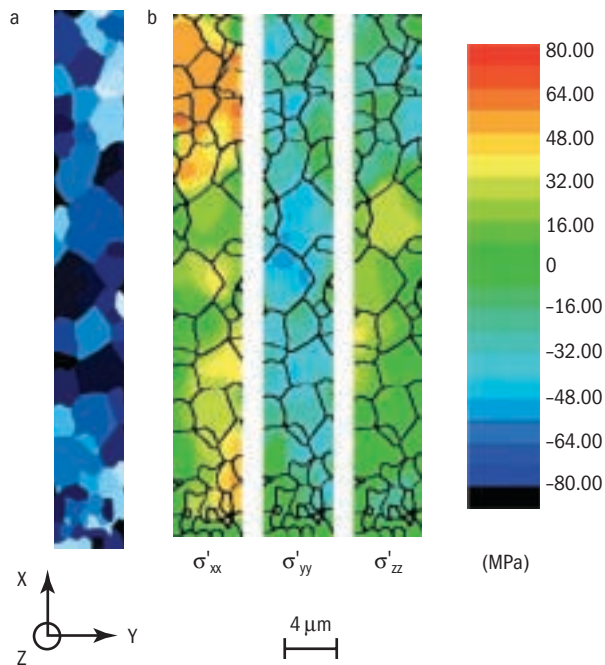


**FIGURE 11** Microdiffraction of a 4.1- $\mu\text{m}$ -wide, 30- $\mu\text{m}$ -long aluminum (0.5-weight-percent copper) sputtered test line passivated with a 0.7- $\mu\text{m}$ -thick layer of silicon dioxide. *a*, grain map shows the orientation of the grains in the polycrystalline line. *b*, local *x*, *y*, and *z* components of the distortional (deviatoric) stress tensor map the inhomogeneous distribution of stress in the line even before any current is passed.

white-light beam spanning the photon-energy range from 6 to 14 keV for Laue diffraction measurements (Figure 10). A Kirkpatrick–Baez pair of bendable elliptical mirrors focuses the beam to a spot 0.8  $\mu\text{m}$  by 0.8  $\mu\text{m}$ , and a CCD area detector records the diffraction patterns.

In our electromigration experiments, we studied a test line consisting of an aluminum (plus 0.5-weight-percent

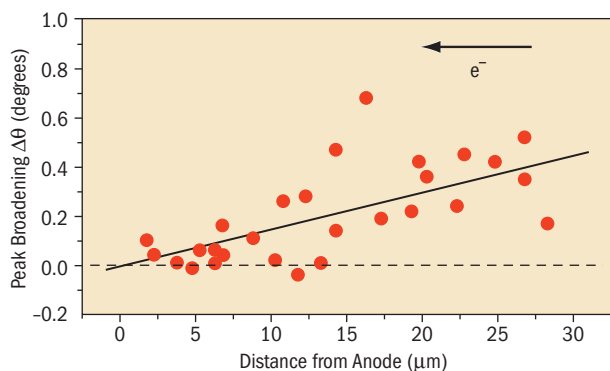


**FIGURE 12** Effects of passing a 30-mA current through the metal test line for 24 hours. Broadening of the diffraction peaks from the grains along the length of the line suggests a gradient in the plastic deformation along the line with the maximum at the cathode end.

copper) strip 30  $\mu\text{m}$  long by 4.1  $\mu\text{m}$  wide by 0.75  $\mu\text{m}$  thick that was sputtered onto a silicon substrate and covered by a 0.7- $\mu\text{m}$ -thick passivation layer of silicon dioxide. The first set of measurements made with no current applied yielded a map showing the orientation of each of the grains in the aluminum line and the diagonal components (i.e., along the length, across the width, and through the thickness) of the distortional (deviatoric) stress tensor for each of the grains. The changing values of these components from grain to grain demonstrated that the stress state was far from homogeneous and that appreciable local stress gradients existed even without an applied current (Figure 11).

Next, we increased the current to 30 mA in steps of 10 mA; after 24 hours, we turned off the current for 12 hours; then we reversed the current to  $-30$  mA for 18 more hours. At the 30-hour point, we observed gradients from the anode to the cathode in both the width of the diffraction peaks and the changing angular positions of the diffraction peaks (Figures 12 and 13). During the 54-hour experiment, we saw that the distortional stress components averaged over all the grains increased while the current was on, relaxed when it was off, and increased again when the current was reversed (Figure 14). Taken together, these findings demonstrate the existence of electromigration-induced plasticity, most likely due to local shear stresses as metal is removed from the cathode end and deposited at the anode end. Such plastic deformation, which results in rotation and concave bowing of the grains, occurs before formation of failure-causing voids or hillocks.

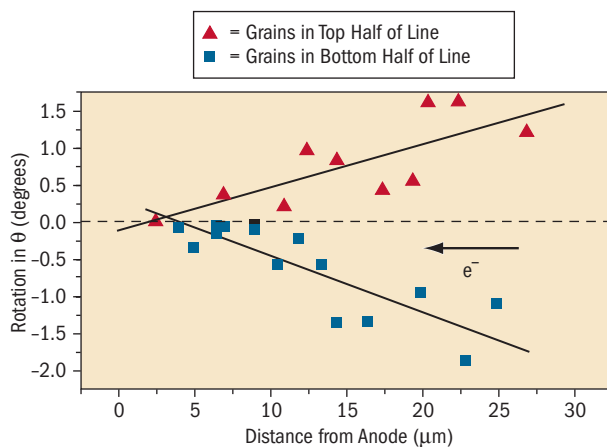


**FIGURE 13** Further effects of passing a 30-mA current through the metal test line for 24 hours. Rotation of individual grains on the top and bottom halves of the test line demonstrates a similar gradient in a concave bowing across the width of the line due to removal of material from the cathode and deposition at the anode.

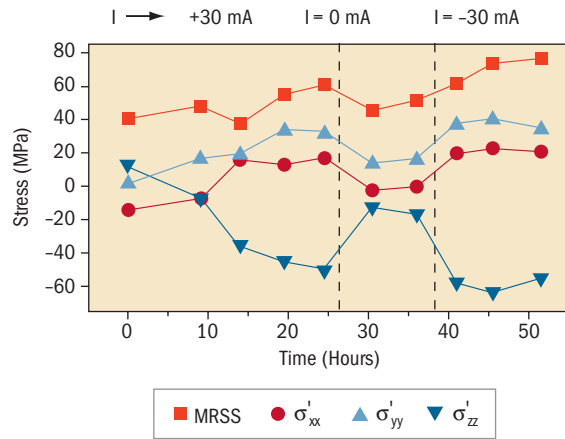


**FIGURE 14** Evolution of the average (over all grains) maximum resolved shear stress (MRSS) and the average distortional (deviatoric) stress components with time as current is reversed from +30 mA to -30 mA. The in-situ measured stresses increase with time until the current is removed and they relax; then their growth resumes when the current is reversed.

#### INVESTIGATORS

B.C. Valek and J.C. Bravman (Stanford University); N. Tamura, A.A. MacDowell, R.S. Celestre, and H.A. Padmore (ALS); R. Spolenak and W.L. Brown (Lucent Technologies); T. Marieb and H. Fujimoto (Intel Corporation); and B.W. Batterman and J.R. Patel (ALS and Stanford Synchrotron Radiation Laboratory).

#### FUNDING

U.S. Department of Energy, Office of Basic Energy Sciences, and Intel Corporation.

#### PUBLICATIONS

1. N. Tamura et al., "High spatial resolution grain orientation and strain mapping in thin films using polychromatic submicron x-ray diffraction," *Appl. Phys. Lett.* **80**, 3724 (2002)

2. B.C. Valek et al., "Electromigration-induced plastic deformation in passivated metal lines," *Appl. Phys. Lett.* **81**, 4168 (2002).

## A Sharper View of Atoms

A guiding maxim for those studying solid materials and the devices made from them is that structure determines function. Therefore deciphering the structure—where the atoms are—is an activity of some importance in understanding why a material behaves the way it does. The corollary is that knowing how to put the atoms, or other structural units, where you want them will enable you to construct materials with the properties you want, everything from mechanical strength to magnetic and electrical behavior. Today's frontier in imaging and manipulating atomic positions lies in the realm of the ultrasmall, the region of nanostructures, where the atoms on a surface play an important and sometimes dominating role. Omori et al. have devised a method that is especially effective at obtaining accurate positions of atoms on or near the surfaces of samples. Their method, called differential photoelectron holography, is based on the same principle as the holography familiar to all of us, but it operates at the level of atoms. Hence, its sensitivity to atomic positions.

Directly seeing atoms has been a long-sought goal, one with increasing relevance in nanoscale materials, but true three-dimensional imaging at the atomic scale has been elusive. In particular, the quality and precision of the atomic images obtained to date via electron holography have been limited by the complexity of the scattering properties of these particles in matter. Now we have developed a new technique (we are calling it differential photoelectron holography) that makes it possible to greatly improve the atomic images obtained with holography at surfaces, which are both ubiquitous and of growing importance in nanostructures.

Partial success in imaging atomic positions has been achieved with electron microscopy (especially in periodic crystal lattices) and with electron holography and scanning tunneling microscopy (particularly at surfaces of solids). Our new technique is an extension of photoelectron diffraction, in which x-rays eject core-level electrons from near-surface atoms. These photoelectrons then scatter from other atoms as they escape through the surface so as to form an interference (or diffraction) pattern that contains all the desired information about atomic positions. Up to now, the challenge has been to extract that information and directly produce a sharp three-dimensional image of the atoms.

The differential method is based on a simple and powerful idea: although the scattering properties of electrons are complex (thus causing the poor prior images), they only

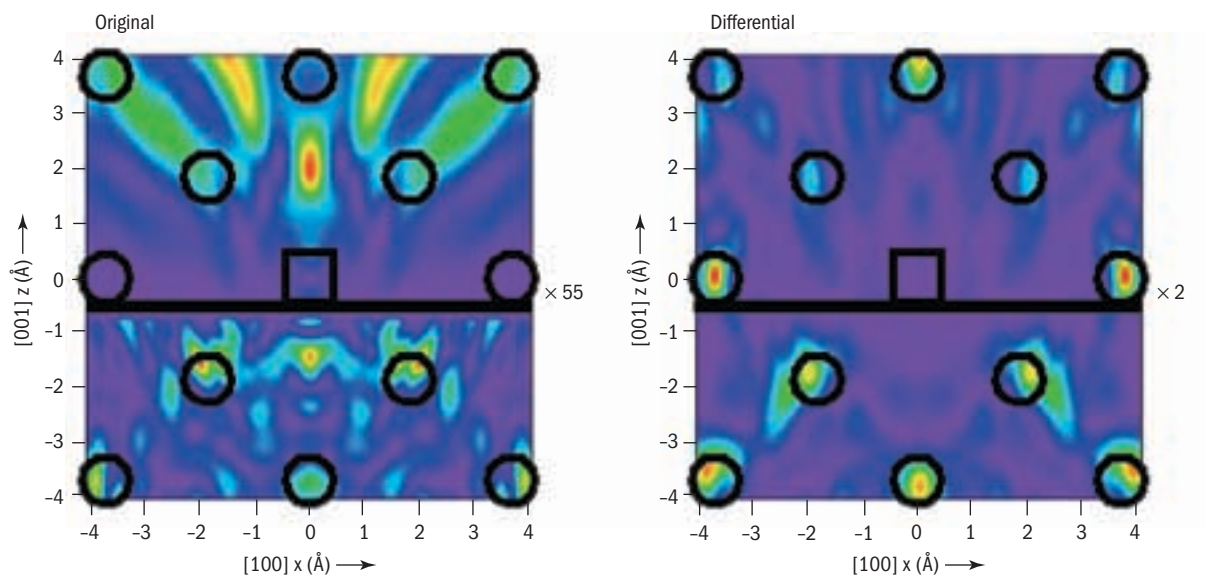


**FIGURE 15** Two atomic images of the same cross-section of a copper (001) surface with the bulk crystal at the bottom and vacuum at the top. The left image results from a typical previous holographic method (the Barton approach), while the right image results from our new differential photoelectron holography. Realistic calculated, rather than measured, holograms are used as the “experimental data” in these images. Squares and circles represent known atomic positions, while non-blue colors indicate where holography images atoms. (The image intensity is magnified by the indicated factors below and above the thick horizontal line.)

change slowly with the kinetic energy of the scattering electrons. At the same time, the diffraction that gives relative atomic positions changes rapidly with this energy. Thus, if

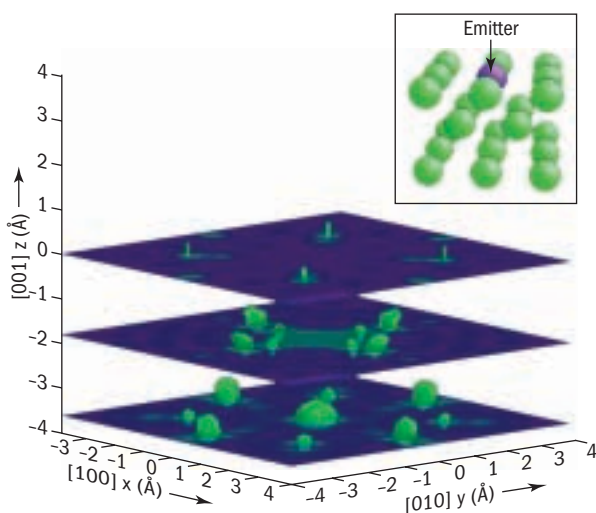


**FIGURE 16** Three-dimensional image composed of three two-dimensional cross-sections parallel to the same copper (001) surface as in Figure 15 with actual experimental data measured at the ALS. The green features are images of the green atoms drawn in the inset (the photoemitting atom, always at the origin, is not imaged). The image splittings and nonalignments reflect the limited experimental data ranges and residual nonideal scattering effects and could be improved in future experiments.

we measure two diffraction patterns at nearby energies and take the difference between them, the resulting differential hologram eliminates most of the disturbing scattering properties. This procedure allows a much cleaner conversion from diffraction pattern to atomic image.

Figure 15 shows the improved atomic images that we achieved with differential photoelectron holography at a simple surface of crystalline copper, as compared to previous holographic methods. The black square and circles indicate the known positions of atoms in a cross-section through the surface (the solid crystal lies toward the bottom of the images). The non-blue regions show where this kind of experiment “sees” the atoms. Success in imaging is achieved when the non-blue regions coincide with the black circles. Clearly, the prior methods performed poorly, especially for the surface atoms (seen in the upper part of the images above a deeper emitting atom located at the black square).

The new differential photoelectron holography method greatly improves both the location and the sharpness of the atomic images, particularly near the surface where this detailed information is usually lacking. Figure 16, which gives a three-dimensional view (composed of two-dimensional slices) of the same surface obtained from actual experimental data measured at the ALS, likewise

clearly locates the various atoms close to their known positions, as shown in the inset.

Differential photoelectron holography thus promises to more sharply image the near-surface atoms that play such important roles in the physical and chemical properties of nanostructured materials. Images of surface-atom positions, which might even include time-dependent measurements of changing geometries in the future, should expose the functionality of these atoms more directly.

The differential approach has also been fruitfully used in two related forms of holography that we have developed. In spin-polarized photoelectron holography, the slight difference in scattering properties between spin-up and spin-down electrons is exploited to provide images of the local magnetic order within the surface of a magnetic material. And in resonant x-ray fluorescence holography (in which x rays rather than electrons scatter), the atom-specific anomalous resonant scattering of x rays is used to image the local chemical order of a material. Both of these types of atomic imaging should be useful in future studies of complex, multicomponent materials.

### INVESTIGATORS

S. Omori (University of Tokyo and Berkeley Lab), Y. Nihei (University of Tokyo), E. Rotenberg and J.D. Denlinger (ALS), S. Marchesini (Berkeley Lab), S.D. Kevan (University of Oregon), B.P. Tonner (University of Central Florida), M.A. Van Hove (Berkeley Lab, ALS, and University of California, Davis), and C.S. Fadley (Berkeley Lab, University of California, Davis, and University of Hawaii, Honolulu).

### FUNDING

U.S. Department of Energy, Office of Basic Energy Sciences; Japan Society for the Promotion of Science.

### PUBLICATIONS

1. S. Omori et al, "Differential photoelectron holography: A new approach for three-dimensional atomic imaging," *Phys. Rev. Lett.* **88**, 055504 (2002).
2. S. Omori, L. Zhao, S. Marchesini, M. A. Van Hove, and C.S. Fadley, "Resonant x-ray fluorescence holography: Three-dimensional atomic imaging in true color," *Phys. Rev. B* **65**, 014106 (2002).

# POLYMERS AND BIOSCIENCE

## Segregation in Mixed Polymer Brushes

How water behaves on a surface is a big deal to some of us, so we buy dishwasher detergents and rinses that promise to leave dishes without water spots and the like. But how about a way to make a “smart” surface that adapts to its environment? Such an adaptive behavior would be just the ticket in medicine and biological science for designing surfaces that mimic the permeability of living cell membranes or that selectively recognize and stick to cells or their constituents, as well as in applications such as self-cleaning clothes. Toward this end, Minko et al. started by binding different polymers (long chain molecules) to a solid surface (substrate) to form a polymer “brush.” Then they exposed the brush to chemical solvents that caused the film structure to adopt the particular desired property, such as being hydrophobic (on which water forms droplets) or hydrophilic (on which it spreads out). They used x-ray microscopy at the ALS to image the chemical changes in the brush films induced by the solvents.

The chemical separation of mixed polymers into microphases represents a powerful and inexpensive tool for the fabrication of nanostructures. Our international team comprising researchers from Germany and the ALS has explored the changing surface chemical structure of mixed polymer brushes exposed to different solvents. A brush consists of polymer chains chemically attached to the substrate. Our observations, made with the PEEM2 photoemission electron microscope at the ALS and an atomic force microscope (AFM), provide guidance for

creating novel materials that adapt to their environment by changing their surface properties.

Polymers make perfect building blocks for manufacturing nanostructures because of their variable chemical functionality and the size of the polymer molecules. Moreover, the morphology and other important properties of polymers, such as wetting, adhesion, or biocompatibility, can be externally modified, e.g., by solvents. Such an adaptive behavior is very promising for the engineering of smart surfaces for biomedical applications and nanodevices. For example, a mixed brush of hydrophilic and hydrophobic homopolymers that is exposed to a hydrophilic solvent should chemically segregate and the hydrophilic component will accumulate at the surface, a process called perpendicular segregation. Although the reversible switching from hydrophilic to hydrophobic character has been observed, the detailed local chemical structure has remained unknown.

Photoemission electron microscopy based on near-edge x-ray absorption fine structure (NEXAFS) provides a way to identify differences in local chemical structure. By combining NEXAFS, which has been very successfully used for years in spectroscopic studies of polymer materials, with the high surface sensitivity and the high nanometer spatial resolution (<50 nm) of the PEEM2 on ALS Beamline 7.3.1.1, we were able to image the chemical structure at the surface of a mixed polymer brush, including the lateral and perpendicular segregation predicted by self-consistent-field (SCF) calculations. We were also able to correlate the chemical morphology of the sample with its topography, as detected by atomic force microscopy.

The samples, a mixed brush whose two components were polymethylmethacrylate (PMMA) and a random copolymer of styrene and pentafluorostyrene (PSF), were fabricated at the Institute for Polymer Research in Dresden, Germany.

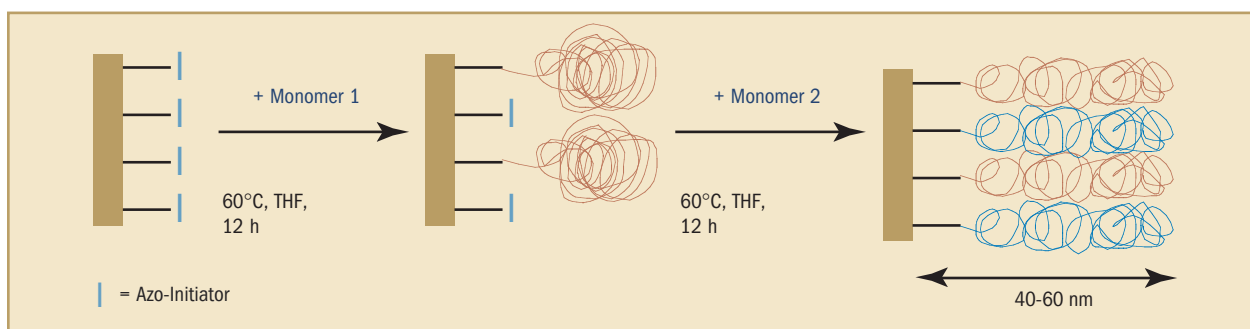


**FIGURE 1** Synthesis of a mixed polymer brush comprising hydrophobic and hydrophilic homopolymers (PSF and PMMA, respectively) via a two-step surface-initiated radical polymerization.

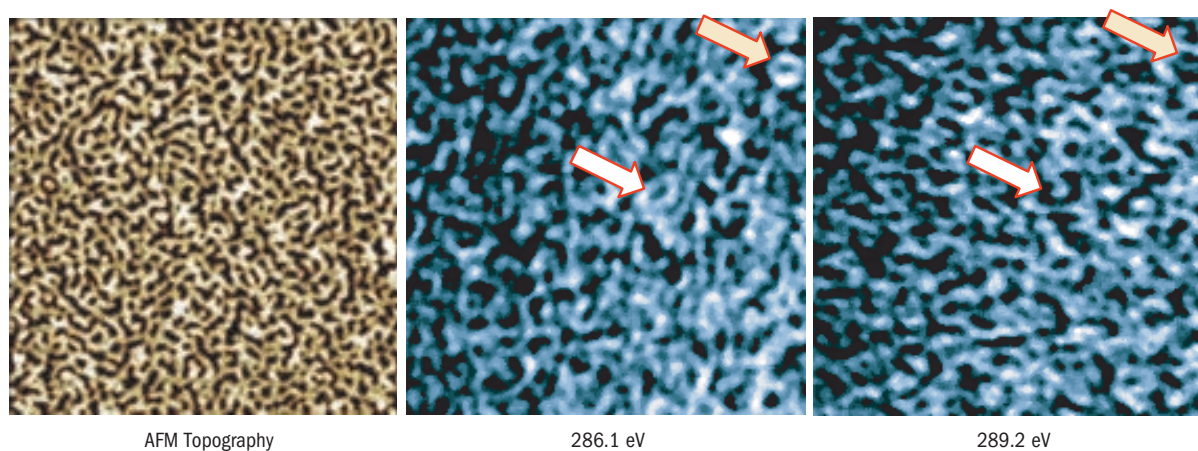


**FIGURE 2** Left, an AFM image of a PSF/PMMA brush after treatment with toluene shows that exposure to toluene creates a “ripple phase.” The PEEM images show inverted contrast (arrows) at x-ray energies specific for PSF (center) and PMMA (right).

There a sophisticated technique of grafting the two incompatible polymers randomly on the surface of a silicon wafer was used. This prevents macroscopic phase separation of the incompatible components, the hydrophobic PSF and hydrophilic PMMA (Figure 1).

Utilizing the chemical sensitivity of PEEM, we observed that, after exposure to the nonselective solvent toluene, the components of the mixed polymer brush created a laterally segregated “ripple” phase comprising worm-like domains, 150 to 160 nm in width (Figure 2). This lateral segregation showed up as a reversal in contrast in PEEM images, which were acquired at two specific x-ray energies corresponding to characteristic absorption peaks for the two polymers at the carbon absorption edge. This observation was corroborated by AFM images, which showed the same ripple phase in the topography of the sample. The

observed lateral segregation was predicted by the SCF calculations, which considered among other parameters the length of the polymer chains, the repulsion between the chains, and the selectivity of the solvent.

When the polymer was exposed to the selective solvent acetone, a hydrophilic solvent that preferentially dissolves the PMMA component, we observed a new microscopically segregated phase that could be described as a “dimple phase,” with both lateral and perpendicular segregation (Figure 3). The segregation of the two polymer components perpendicular to the surface resulted in an enhancement of the PMMA at the top of the brush (Figure 4). This segregation appeared in the PEEM images as a strong reduction in contrast, owing to the prevalence of one polymer component at the surface. Calculations were again able to explain the formation of this new polymer phase.

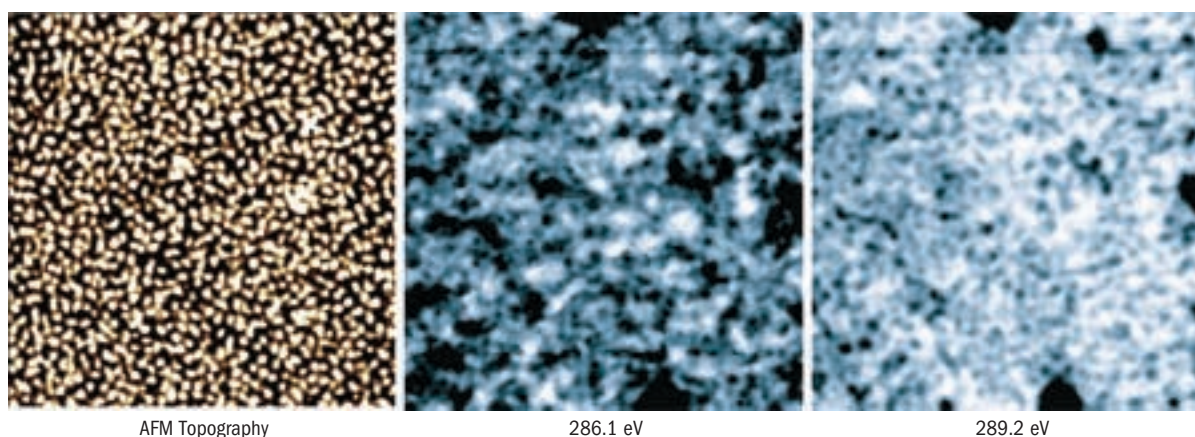


**FIGURE 3** Left, an AFM image of a PSF/PMMA brush after treatment with acetone shows that exposure to acetone creates a “dimple phase.” The surface is dominantly PMMA, and PEEM images (center, right) show no indication of contrast reversal.

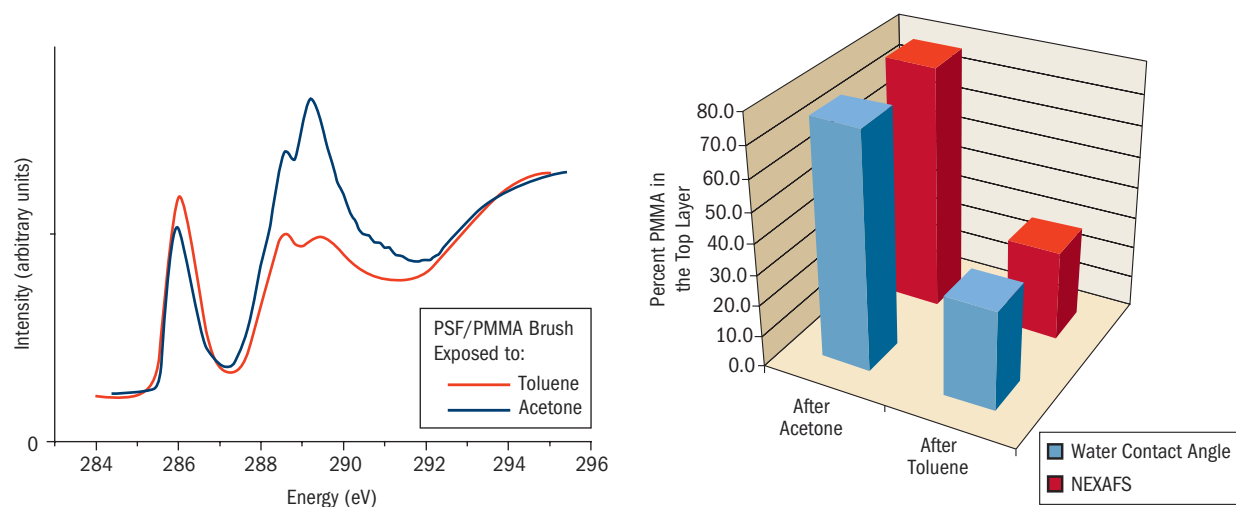


**FIGURE 4** Left, differences in x-ray absorption spectra after exposure of the brushed polymer to the solvents toluene and acetone suggest a changing surface chemistry. Right, quantitative analysis of the x-ray absorption spectra indicates accumulation of PMMA at the surface after exposure to acetone, a finding in agreement with measurement of the PMMA content from the water contact angle.

#### INVESTIGATORS

S. Minko, D. Usov, C. Froeck, and M. Stamm (Institut für Polymerforschung Dresden); M. Müller (Johannes Gutenberg Universität, Mainz); and A. Scholl (Berkeley Lab).

#### FUNDING

German Federal Ministry for Education and Research (BMBF), German Research Foundation (DFG), and U.S. Department of Energy, Office of Basic Energy Sciences.

#### PUBLICATION

1. S. Minko et al., "Lateral versus perpendicular segregation in mixed polymer brushes," *Phys. Rev. Lett.* **88**, 035502 (2002).

# ENVIRONMENTAL AND EARTH SCIENCE

## Biodegradation of Organic Contaminants Catalyzed by Humic Acid

Contaminants in the environment come in many forms, one of which is that of the toxic organic (carbon-based) chemicals known as polycyclic aromatic hydrocarbons (PAHs). These include more than 100 different chemicals resulting from incomplete burning of coal, oil, gas, garbage, and other organic substances like tobacco or grilled meat. Converting PAHs into nontoxic chemicals removes the hazard, but learning how to do this in an efficient and cost-effective way remains to be accomplished. Remarkably, since bacteria are feared by many people as infectious germs, some species of these microorganisms may provide a solution by, in effect, ingesting the PAHs and during digestion converting them into a less toxic chemical, a process known as biodegradation. Holman et al. made use of an infrared technique to show that the speed of biodegradation can be dramatically increased (almost a hundred times) by adding a soil-derived organic (humic) acid along with the bacteria to a PAH spot on a mineral surface. This finding will influence the development of environmental cleanup strategies based on biodegradation.

The role of humic acid in the biodegradation of toxic polycyclic aromatic hydrocarbons (PAHs) has been the subject of controversy, particularly in unsaturated environments. By utilizing an infrared Fourier transform spectromicroscope and a very bright, nondestructive synchrotron photon source (SR-FTIR spectromicroscopy), we monitored in situ and over time the influence of humic acid on the degradation of pyrene (a model PAH) by a bacterial colony on a magnetite surface. Our results indicate that humic acid dramatically shortens the onset time for PAH biodegradation from 168 to 2 hours. These results will have significant implications for the bioremediation of contaminated soils.

The pyrene-degrading bacterium used for this study is *Mycobacterium* sp. JLS, a gram-positive, rod-shaped bacterium recently isolated from PAH-contaminated soil at the Libby Groundwater Superfund Site in Libby, Montana, USA. Figure 1 summarizes the time series of infrared spectra

obtained from the same location on each pyrene-coated sample over more than a month.

Abiotic (no bacteria present) results show that almost all of the pyrene remains on the mineral surface, owing to slow removal mechanisms. After introduction of *M. sp. JLS* in the absence of humic acid, it took the bacteria about 168 hours to produce sufficient glycolipids to solubilize pyrene. At this point, biodegradation could proceed, resulting in a rapid decrease of pyrene and a rapid increase of biomass within the next 35 hours. After the pyrene was depleted, the biomass signal significantly decreased, presumably as the *M. sp. JLS* bacteria transformed themselves into ultramicrocells, a starvation-survival strategy commonly observed among bacteria in waters that are relatively low in accumulated nutrients and high in dissolved oxygen (oligotrophic environments).

In the presence of humic acid (specifically Elliot soil humic acid, or ESHA), pyrene biodegradation began within an hour, and the pyrene was depleted by the end of the fourth hour, with a concurrent increase of biomass. Both the degradation of pyrene and the increase of biomass corroborate the effectiveness of ESHA in radically accelerating biodegradation of pyrene. It is likely that the water-insoluble pyrene is solubilized into the cores of humic acid pseudo-micelles and therefore becomes directly available for bacterial uptake and consumption.

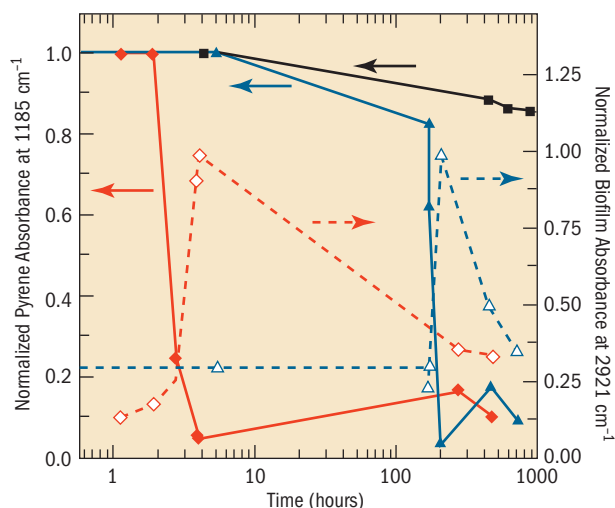


**FIGURE 1** Summary of IR results showing that pyrene degradation occurs much faster when humic acid is present (note the log scale on the time axis). The color scheme is black for abiotic, blue for biotic without humic acid, and red for biotic with humic acid. The solid lines show the pyrene amount (left axis) as a function of time for each experiment. The dotted lines show a subsequent increase in *Mycobacterium* sp. JLS biomass (right axis) after pyrene degradation.

Over longer times, infrared absorption bands of pyrene on magnetite surfaces first showed a slight increase and subsequently a decrease. The increase is probably due to diffusion of pyrene trapped in micropores ( $\leq 0.5 \mu\text{m}$  in

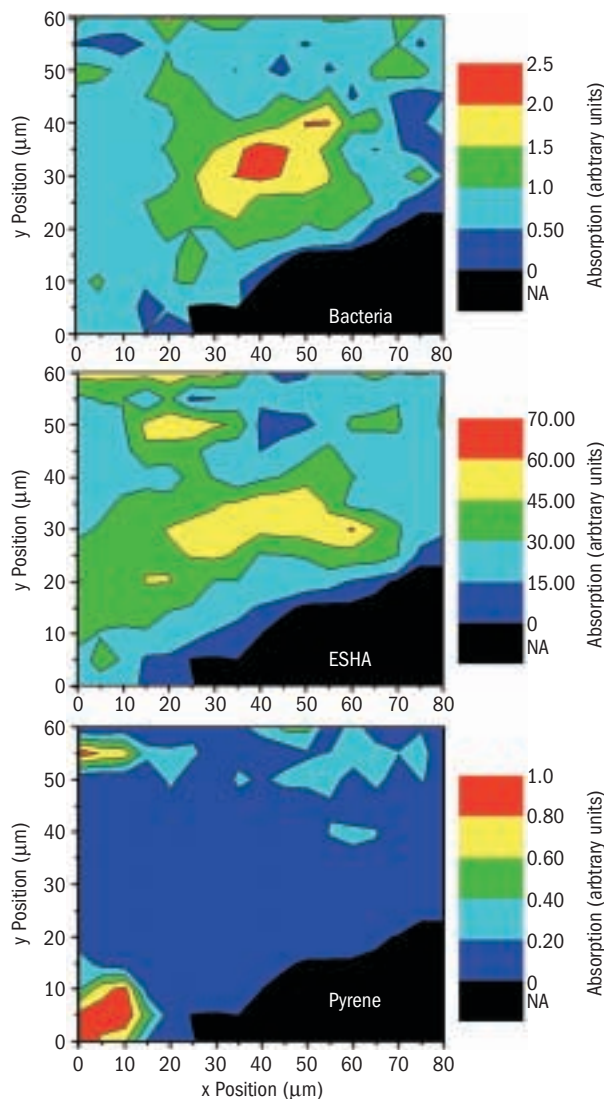


**FIGURE 2** Contour diagrams from infrared mapping obtained at the end of the experiment showing the spatial distribution of the infrared absorption peaks corresponding to (top) *Mycobacterium* sp. JLS bacteria, (center) humic acid, and (bottom) pyrene. Appropriate spectral regions were integrated for each point on the maps. The color scales for each contour plot use red for high integrated IR peak area (high concentration of the corresponding component) and blue for low peak area (low concentration); black marks an out-of-focus region of the sample. The center of the map shows a region with high density of bacteria and high concentration of ESHA, where pyrene has been completely degraded.

diameter) of the magnetite and/or neighboring surfaces of higher pyrene concentration after the first wave of rapid depletion of pyrene by *M. sp. JLS* set up a diffusion gradient from the pyrene-containing micropores toward the bacterial colony. For the surface containing humic acid, the biomass remained almost constant over a period of more than 200 hours, indicating that the flux of pyrene from the micropores was sufficient to maintain the bacterial colony. For the surface free of humic acid, there is little evidence of the presence of a quasi-steady-state biomass.

At the end of the time-resolved experiment (about 460 hours), spatial distributions of pyrene, *M. sp. JLS*, and ESHA were measured by acquiring infrared spectra at  $5\text{-}\mu\text{m}$  intervals across the center of the bacterial colony with humic acid. Figure 2 shows contour maps of the spatial distribution of measured infrared absorbances corresponding to *M. sp. JLS*, humic acid, and pyrene. The central region of the maps has a high population density of *M. sp. JLS* and a high concentration of humic acid, but the pyrene in this region was completely biodegraded. Where pyrene is present without *M. sp. JLS*, there is no significant degradation.

We conclude that SR-FTIR spectromicroscopy can assess real-time interactions between multiple constituents in contaminated soils. Combined with conventional mineralization measurements, which monitor respiration through carbon dioxide production, SR-FTIR spectromicroscopy is thus a powerful tool for evaluating bioremediation options and designing bioremediation strategies for contaminated vadose zone environments.

#### INVESTIGATORS

H.-Y.N. Holman (Berkeley Lab); K. Nieman, D.L. Sorenson, C.D. Miller, and R.C. Sims (Utah State University); M.C. Martin and W.R. McKinney (ALS); and T. Borch (Montana State University).

#### FUNDING

U.S. Department of Energy, Office of Basic Energy Sciences.

#### PUBLICATIONS

1. H.-Y.N. Holman et al., "Catalysis of PAH biodegradation by humic acid shown in synchrotron infrared studies," *Environmental Science and Technology* **36**, 1276 (2002).

## An X-Ray View of the Microworld of Trace Metals in Soils and Sediments

Heavy metals are components of hazardous waste at many industrial and government sites. They can exist in combination with other species in water-soluble and insoluble forms and, unfortunately, cannot be completely broken down. As a rule, the less soluble a chemical species, the less mobile and less toxic; the more soluble it is, the more mobile and more toxic. Manceau et al. focused on nickel because certain nickel sulfates, sulfides, and oxides are suspected carcinogens. In soils, nickel often ends up bound (sequestered) in compressed aggregates or nodules that are rich in iron and manganese. By using three x-ray techniques in combination, the researchers were able to determine at the molecular scale where and how nickel naturally hides itself in soils, leading to the eventual ability to (1) predict with greater

accuracy the evolution of metal chemistry in a contaminated environment and (2) modify and control the metal's form in order to maintain soil quality and to frame effective, site-specific strategies for waste cleanup (remediation).

In the last two years, our international team comprising researchers from France and the ALS has developed new analytical capabilities that allow them to noninvasively peer into the heterogeneous world of soils and sediments and identify and quantify heavy-metal contaminants at micrometer scales of resolution. The synergistic use of three powerful x-ray techniques—x-ray fluorescence (SXRF), diffraction (XRD), and absorption (XAFS)—allowed us to identify the molecular nature of the host mineral species and the trace metal's speciation, distribution, and coordination chemistry with micrometer spatial resolution.

One of the difficulties in assessing the state of these metals is that the earth's surface and subsurface are extremely heterogeneous and become even more so at

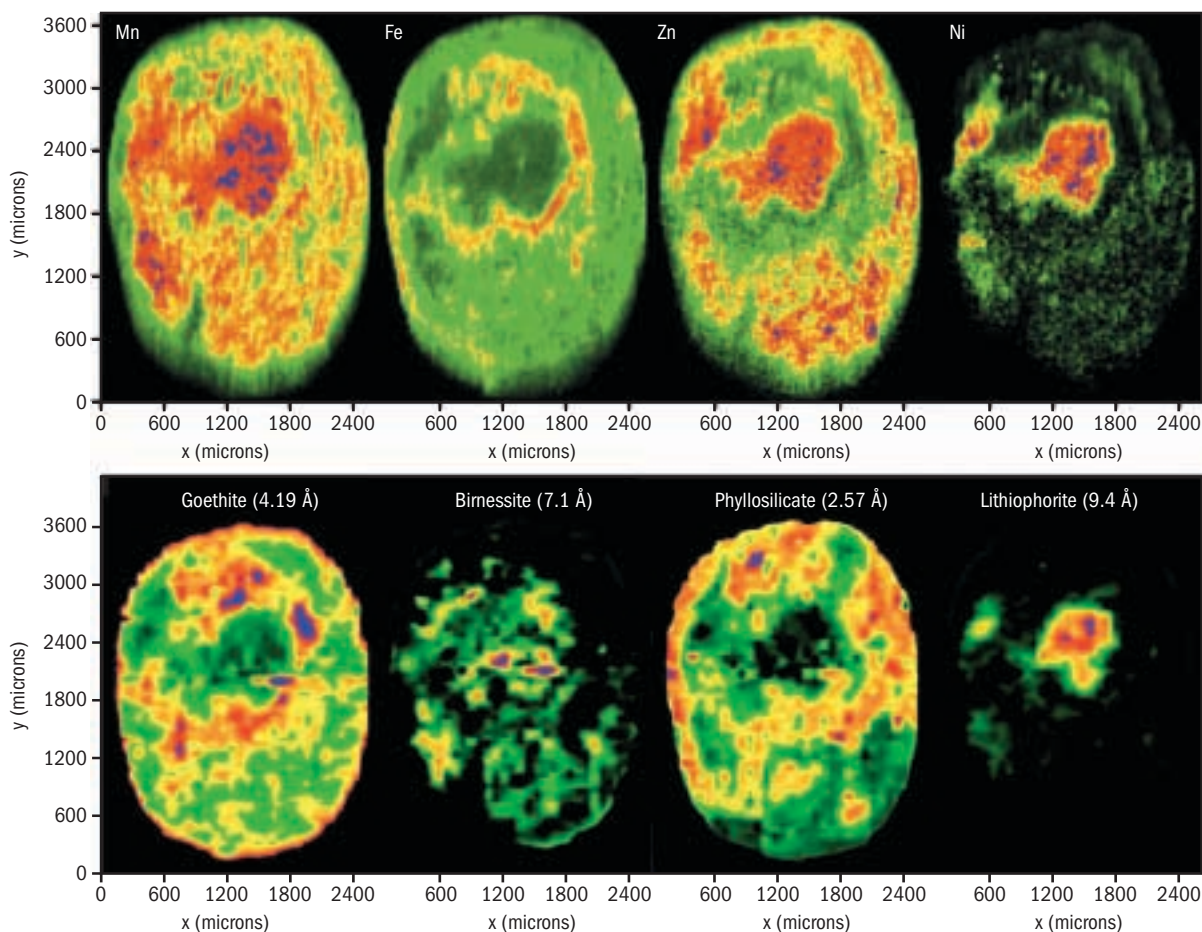


**FIGURE 3** Combined  $\mu$ SXRF- $\mu$ SXRD measurements recorded on a soil iron-manganese nodule. The four images on the top are elemental maps obtained by  $\mu$ SXRF, and the four images on the bottom are mineral species maps obtained by rastering the sample in an x-y pattern and analyzing the diffraction patterns.

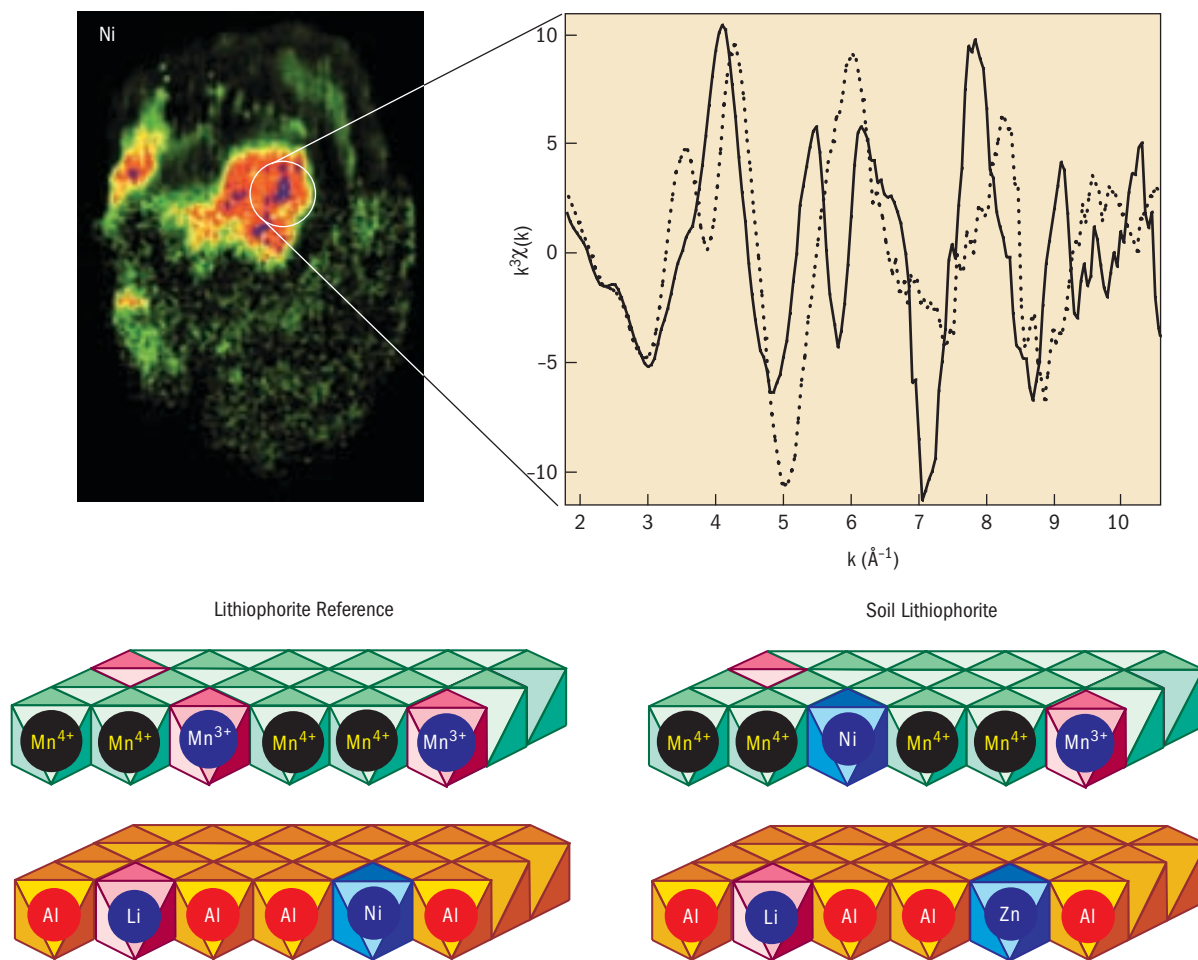


**FIGURE 4** A  $\mu$ EXAFS examination of the sequestration mechanism of nickel in a soil ferromanganese nodule, showing a nickel K-edge  $\mu$ EXAFS spectrum from a nickel “hot spot” of the core of the nodule seen in the  $\mu$ SAXRF image (*solid line*), as compared to a spectrum from the literature for a nickel-containing lithiophorite reference (*dotted line*). In the reference, nickel substitutes for lithium in the  $\text{Al}(\text{OH})_3$  layer, and in the soil lithiophorite, nickel substitutes for  $\text{Mn}^{3+}$  in the  $\text{MnO}_2$  layer.

these scales, where heavy metals can exist as trace and major elements in mineral hosts. We were able to successfully apply the three-pronged approach to the speciation of nickel and zinc in a soil ferromanganese nodule at the ALS using the microfoc capabilities of Beamlines 7.3.3 and 10.3.2.

The exquisite sensitivity of scanning x-ray microfluorescence ( $\mu$ SAXRF) to trace elements makes  $\mu$ SAXRF an ideal tool to map trace element distribution within a heterogeneous matrix. After  $\mu$ SAXRF has identified the location of trace and major elements within a matrix, the new technique of scanning x-ray microdiffraction ( $\mu$ SAXRD) identifies and images the distribution of mineral species in the nanoscale particles that are the most reactive toward the trace metals. Then, the nature of minerals hosting a particular trace element within the heterogeneous matrix is

deduced from the comparison of elemental and mineral species maps (from  $\mu$ SAXRF and  $\mu$ SAXRD, respectively). Finally, with micro-extended x-ray absorption fine structure ( $\mu$ EXAFS) spectroscopy, the structural relationship between metal and mineral host is examined. Specifically, the coordination chemistry of the metal is determined, and hence its incorporation mechanism within the mineral host is identified.

The  $\mu$ SAXRF elemental maps of the nodule show that iron, manganese, nickel, and zinc are unevenly distributed at the micrometer scale (Figure 3). Iron and manganese have no detectable correlation, and nickel and zinc are both strongly correlated with manganese and not with iron. Highest zinc and nickel amounts are observed in the manganese-rich core; the outer regions also contain significant amounts of manganese and zinc but are depleted in nickel. The partial

nickel–manganese association suggests that manganese is present in at least two forms, only one containing nickel. The comparison of  $\mu$ SXRF and  $\mu$ SXRD maps clearly shows that nickel and the mineral lithiophorite have the same distribution, therefore indicating that nickel is exclusively bound to this particular manganese phase (Figure 4). The goethite map does not match the zinc and iron elemental maps, which means that this constituent is devoid of zinc.

The sequestration mechanism of nickel inferred from  $\mu$ SXRF and  $\mu$ SXRD was confirmed by nickel K-edge  $\mu$ EXAFS measurements from selected regions of interest in this nodule and others from the same soil and from various soils from different countries across several continents.

Unlike nickel, the zinc map does not resemble any of the mineral species maps obtained from  $\mu$ SXRD, nor can it be reconstructed by a combination of several. Therefore, the

nature and proportion of the zinc host phases were determined by analyses of five  $\mu$ EXAFS spectra recorded in different spots chosen to vary the proportions of component species (principal component analysis and least-squares fitting analysis), which indicated the presence of three predominant species, lithiophorite, birnessite, and poorly crystallized iron oxide (e.g., ferrihydrite) (Figure 5). Finally, bulk EXAFS spectra were recorded in order to verify that these assessments truly represent all of what is found in the entire sample.

### INVESTIGATORS

A. Manceau (Université Joseph Fourier and CNRS, France, and ALS); N. Tamura, M.A. Marcus, A.A. MacDowell, R.S. Celestre, R.E. Sublett, and H.A. Padmore (ALS); and G. Sposito (Berkeley Lab).

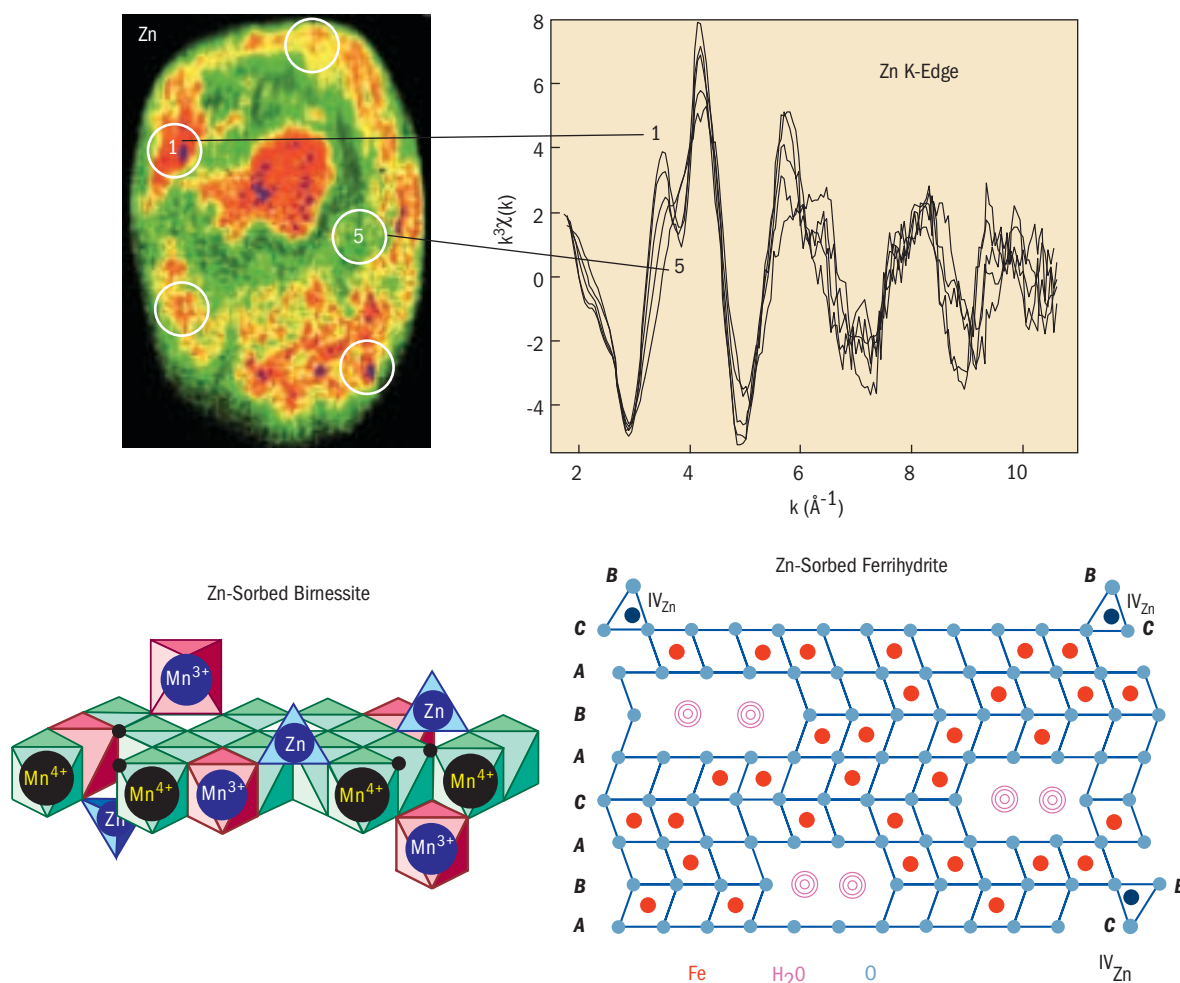


**FIGURE 5** A  $\mu$ EXAFS examination of zinc sequestration in a soil ferromanganese nodule, showing zinc K-edge  $\mu$ EXAFS spectra collected from five points of interest having variable manganese/iron ratios, as indicated in the  $\mu$ SXRF image. Zinc is bound to three minerals: lithiophorite, birnessite, and poorly crystalline iron oxide. (Ferrihydrite is used as a proxy for the general class of defective iron oxides.)

**FUNDING**

U.S. Department of Energy, Office of Basic Energy Sciences, and Berkeley Lab Laboratory Directed Research and Development.

**PUBLICATIONS**

1. A. Manceau et al., "Deciphering nickel sequestration in soil ferromanganese nodules by combining x-ray fluorescence, absorption and diffraction at micrometer scales of resolution," *American Mineralogist* **87**, 1494 (2002).

# STRUCTURAL BIOLOGY

## Structural Basis for Recognition of Acidic-Cluster Dileucine by GGA1

*For each of the 10 trillion or so cells in the human body, the cell nucleus with its strands of DNA is just the beginning of the story. Outside the nucleus is a tangle of organelles tasked to manufacture biomolecules (proteins) according to the instructions encoded in the DNA, fine tune them for their myriad jobs within the cell, and direct them to their working sites. One of these organelles is the Golgi body, a network of flattened sacs stacked loosely on one another that serves as a packaging and distribution center. For example, the final touches are added here to make certain proteins (glycoproteins) that are headed for duty elsewhere. Once completed, the mature proteins must be sorted and transported via mobile sacs (vesicles) to their correct destinations. Sorting and transport require the molecules involved to recognize each other. Shiba et al. have obtained the atomic structure of a portion (a domain) of a protein called GGA1 that recognizes the region in a receptor that signals that a glycoprotein should be transported, thereby revealing the recognition mechanism.*

Structural features of certain proteins are key players in sorting newly processed proteins and transporting them to the cell sites where they will perform their respective functions. In order to investigate the structural basis for the specific interactions involved in transporting lysosomal hydrolases (digestive enzymes that will become the contents of the vesicles known as lysosomes), we have determined to a resolution of 2.0 Å the x-ray crystal structures of the VHS domain of the GGA1 protein that facilitates the transport. We obtained two structures of the domain, including one in complex with a peptide [a 13-residue acidic-cluster dileucine (ACLL) sequence] that is the sorting signal to be recognized. Our structure provides insight into the transport mechanism. It also is in agreement with the structure of the VHS domain of a GGA3 protein, recently determined by another group.

Many eukaryotic proteins are glycosylated (chemically linked to carbohydrate residues) after translation to

become mature glycoproteins. Essential for the cell's function, efficient sorting of glycosylated proteins is achieved by vesicle transport in two stages. First, mannose 6-phosphate receptors (MPRs) recognize the mannose 6-phosphate groups on lysosomal hydrolases in the trans-Golgi network (TGN). In the second step, an adaptor protein called AP-1 was traditionally thought to recognize the cargo-loaded MPRs and transport them from the TGN to the endosome, or early lysosome (i.e., a lysosome not yet filled with its complement of enzymes), with the help of still another protein complex involving clathrins. In 2000, a new family of transport proteins, GGAs, was identified, and later in 2001 it was shown that GGAs facilitate this second step.

All GGAs in the family have a common domain organization. At the N-terminus, they have a VHS (Vps27p/Hrs/STAM) domain, which is conserved in various proteins involved in endocytic processes (those in which the cell surrounds an external object) and signal transduction. Following this domain, there is a highly conserved region in the GGA family, referred to as the GAT domain, which binds small G-protein ARF (ADP-ribosylation factor) and is responsible for the family's TGN membrane association. At the C-terminus, GGAs have a domain called GAE which is homologous to the ear domain of the  $\gamma$ -adaptin subunit of AP-1 and interacts with various accessory proteins. The GAT and GAE domains are connected by a hinge region that binds clathrin.

The N-terminal VHS domain recognizes the ACLL sequence, a sorting signal in the cytoplasmic domain of MPRs. In order to investigate the structural basis for the specific interactions between the GGA VHS domains and the ACLL sequences, we determined the x-ray crystal structures of GGA1-VHS domain, in the apo form and in complex with a 13-residue ACLL peptide from MPR (Figure 1). The high brightness of ALS Beamline 5.0.2 was essential for solving the structure of the complex at the 2.0-Å resolution.

The GGA1-VHS domain forms a right-handed superhelix with eight  $\alpha$ -helices. The hydrophobic core in the center stabilizes the superhelix, and there is only slight conformational change in the overall structure upon binding of the ACLL peptide. The crystal structure shows that the helices  $\alpha 6$  and  $\alpha 8$  and the loop immediately after  $\alpha 6$  form a recognition site for the ACLL sequence by a combination of shape and both electrostatic and hydrophobic interactions (Figures 2 and 3). This was confirmed by a mutant analysis.

The binding of the ACLL peptide to the GGA1-VHS domain changes the surface properties of the protein significantly

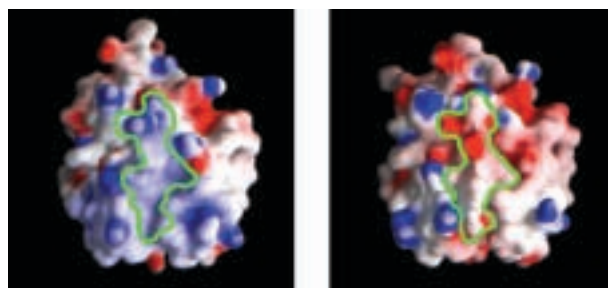


**FIGURE 1** The GGA1-VHS domain with and without the ACLL peptide. The surfaces are colored according to the electrostatic surface potential (*blue*, positive; *red*, negative). *Left*, the VHS domain (in complex form) without the peptide. The green line outlines the location of the bound peptide. *Right*, the same view of the VHS domain with the peptide.

(Figure 1). This change might provide a signal to other events of membrane traffic, for instance, the interaction between the GGA-GAT domain and membrane-bound ARF1, recruitment of clathrin molecules, or interaction with accessory proteins that all play important roles in the highly selective transport processes. Incidentally, a very similar result was reported for the GGA3-VHS domain by Misra et al. [*Nature* **415**, 933 (2002)].

#### INVESTIGATORS

T. Shiba (KEK Photon Factory and Foundation for Advancement of International Science, Tsukuba); H. Takatsu (University of Tsukuba and RIKEN); T. Nog $\acute{e}$ , N. Matsugaki, M. Kawasaki, N. Igarashi, M. Suzuki, R. Kato, and S. Wakatsuki (KEK Photon Factory); T. Earnest (Berkeley Lab); and K. Nakayama (University of Tsukuba and Kanazawa University).

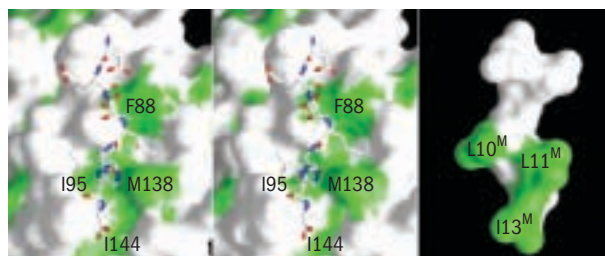


**FIGURE 3** Close-up of the GGA1-VHS domain interacting with the ACLL peptide. The surfaces are colored according to the hydrophobicity (*green*), and the basic residues interacting with the peptide are labeled. *Left*, stereo diagram showing the peptide bound to the VHS domain (same view as in Figure 2). *Right*, the side of the peptide facing the protein (same view as in Figure 2).

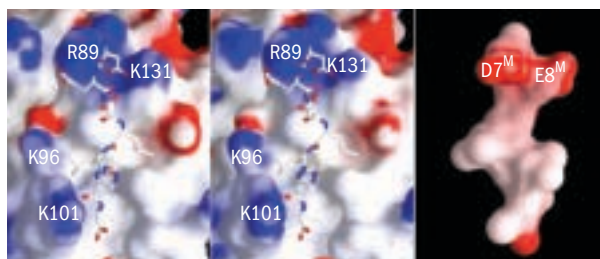


**FIGURE 2** Close-up of the GGA1-VHS domain interacting with the ACLL peptide. The surfaces are colored according to the electrostatic surface potential (*blue*, positive; *red*, negative), and the basic residues interacting with the peptide are labeled. *Left*, stereo diagram of the peptide bound to the VHS domain. The peptide is shown as a stick structure. *Right*, the side of the peptide facing the GGA1-VHS domain.

#### FUNDING

Ministry of Education, Culture, Sports, Science, and Technology of Japan; Japan Society for Promotion of Science; and University of Tsukuba Research Projects.

#### PUBLICATIONS

1. T. Shiba et al., "Structural basis for recognition of acidic-cluster dileucine sequence by GGA1," *Nature*, **415**, 937 (2002).

## Aquaporin Structure Elucidates Water Transport

*The transport of water through the human body is essential to our existence. For example, kidney function depends on the transport of water into and out of cells, reclaiming an amazing 150 liters a day. Our nerves, digestion, reproduction, body temperature, and even vision can be adversely affected by water transport problems. Water transport is so important to the business of a cell that biochemists often model a cell as nothing more than a bag of water. But the bag itself (the cell membrane) must reliably allow the right sort of molecule in the right amount to move in the right direction. And not only must a cell get all that right, it must adapt to changes in its environment. Aquaporin-1 is one of the membrane proteins that control water transport, giving the theoretical bag its amazing properties. Sui et al. have obtained the atomic-level structure of this protein with the goal of understanding what magic these proteins possess and ultimately how to restore function when the magic is lost.*

From aqueducts to osmosis, water transport is crucial to life. Yet, precisely how life manages the transport of water across membranes has remained a mystery for eons—until now. Our team of researchers from the Berkeley Lab Life Sciences Division has solved the structure of aquaporin-1 (AQP1), a membrane protein that selectively controls the movement of water molecules into and out of mammalian cells. It is a member of the aquaporin superfamily, whose members include those that transport water, glycerol, or urea. The new structure offers a resolution of 2.2 Å, allowing us to deduce just how the protein does its job.

After preliminary work at the National Synchrotron Light Source and the Stanford Synchrotron Radiation Laboratory, our team turned to the Berkeley Center for Structural Biology and ALS Beamline 5.0.2. We began by studying thallium-derivatized crystals of AQP1 from bovine red blood cells by multiwavelength anomalous diffraction (MAD). We then refined the resulting data set to 2.2 Å by using crystals grown in the presence of gold cyanide. The high-resolution structure shows atomic-level details of the protein and water molecules captured in transit.

The overall structure of AQP1 is that of a tetramer, the four parts (monomers) of which each define a single pore (Figure 4). These monomers are arranged side by side in a tight cluster, with the pores running parallel. Each monomer in turn comprises six membrane-spanning helices that partially surround two shorter helices (Figure 5). The short

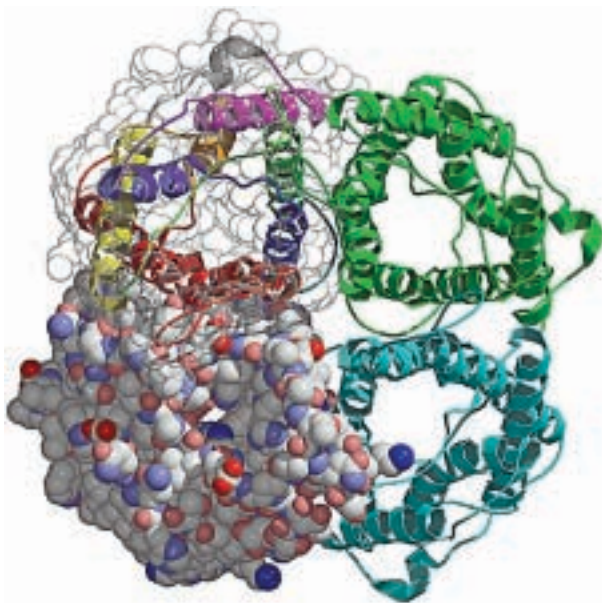


**FIGURE 4** The AQP1 tetramer viewed looking down the pores from the cytoplasmic side, normal to the membrane. One monomer of the four is represented as a solid space-filling model.

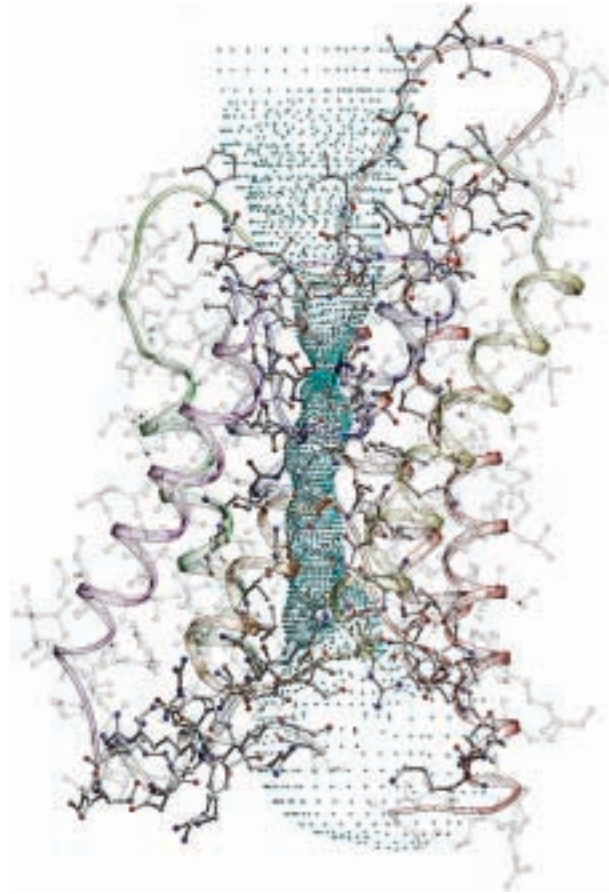


**FIGURE 5** Side view of AQP1 showing the pore profile (turquoise dots) and the residues that line the pore (opaque ball-and-stick structures). The extracellular vestibule is above; cytoplasmic, below. The pinched-in area with the highest concentration of turquoise dots is the constriction region.

non-membrane-spanning helices make up the major portion of the pore. Each pore has a dumbbell-like shape. One broad end is the cytoplasmic vestibule; the other is the extracellular vestibule. The bar of the dumbbell is the selectivity filter, which narrows to a constriction region on the extracellular end.

In the new structure, the key elements of the constriction region can be discerned (Figure 6). A series of carbonyl oxygens forms a hydrophilic path across the region and through the rest of the selectivity filter. One of these oxygens, along with a histidine residue and an arginine residue, forms the hydrophilic face of the constriction region. Opposite this face is a hydrophobic face formed by a phenylalanine residue. Three of the four residues that form the constriction region (the arginine, histidine, and phenylalanine residues) are conserved in all known water-specific aquaporins. This observation suggests that the presence of these residues can be used as a marker for identifying other water-specific aquaporins.

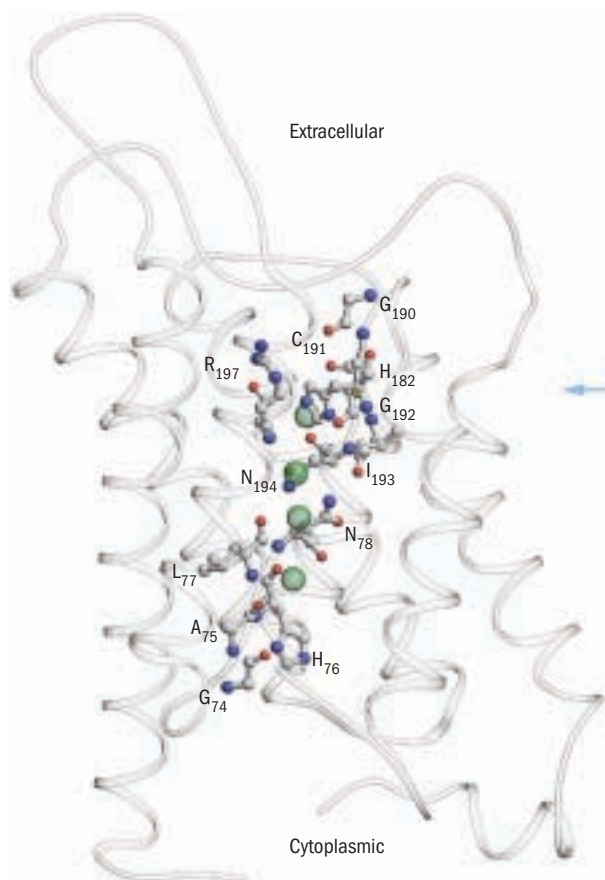


**FIGURE 6** The hydrophilic path across the selectivity filter, highlighted by ball-and-stick structures of the side chains involved. The green spheres are the water molecules observed in transit. The constriction region is indicated by the blue arrow.

An earlier study by a different group—also done at the ALS—revealed the structure of a closely related bacterial channel, the *Escherichia coli* glycerol facilitator (GlpF), which selectively transports glycerol. The structure found for GlpF differs from that of AQP1 in that its constriction region is about 1 Å wider and slightly less polar. The resulting decreases in steric hindrance (physical blocking) and hydrophilicity favor glycerol transport at the expense of rapid water throughput. Despite the functional difference, the GlpF constriction region is strikingly similar to its AQP1 counterpart. It differs only in the replacement of a histidine by a glycine and a cysteine by a phenylalanine. As both the cysteine and the phenylalanine provide carbonyl oxygens to shape the constriction region, the difference in functionality turns out to depend primarily upon the residue found in the location of the histidine (H182) in AQP1. This residue thus appears to be a key in defining selectivity throughout the aquaporin superfamily.

#### INVESTIGATORS

H. Sui, B.-G. Han, J.K. Lee, P. Walian, and B.K. Jap (Berkeley Lab).

#### FUNDING

National Institutes of Health; U.S. Department of Energy, Office of Biological and Environmental Research.

#### PUBLICATION

H. Sui, B.-G. Han, J.K. Lee, P. Walian, and B.K. Jap, “Structural basis of water-specific transport through the AQP1 water channel,” *Nature* **414**, 872 (2001).

## Mechanism for Proton Exclusion by Water-Conducting Aquaglyceroporin GlpF

*Who goes there, friend or foe? For the cells in our bodies, the sentries that lie at the entry ports or channels in the membranes that surround our cells are critical. Aquaporins are channels that control water flow into cells in all life forms. Water, of course, is hydrogen and oxygen in the combination  $H_2O$ . In the water molecule, hydrogen nuclei (protons) carry a positive electrical charge and thus potentially can carry an electric current. This would be a disaster for cell function, which depends on the maintenance of an electrochemical potential (like a voltage) across the cell membrane, because it would short-circuit the potential. So how does an aquaporin let water pass while at the same time blocking the passage of protons? Tajkhorshid et al. combined an atomic-level structure of an aquaporin with mathematical simulations of the motions of molecules within the structure to find the answer. The key is the nonuniform orientation of the water molecules, which prevents proton transfer along the single-file line of water molecules in the channel.*

Aquaporins are transmembrane channels found in cell membranes of all life forms. These channels have the apparently paradoxical property of facilitating efficient water permeation through the membrane while excluding protons, a property that is of critical importance in preserving the electrochemical potential across the membrane. To understand how the channel performs this function, we determined the structure of the integral membrane protein *E. coli* aquaglyceroporin GlpF with bound water and the structure of a double mutant form of this glycerol facilitator with two key residues replaced in the center of the water channel. Extensive molecular dynamics simulations shed

critical additional information on the water-conduction mechanism.

Our multiwavelength anomalous dispersion (MAD) x-ray diffraction measurements were carried out at ALS Beamlines 5.0.2 and 8.3.1. We chose the ALS for this work because of the very favorable characteristics of the endstations and operations and because of the efficient tunability of the beam.

First, we determined to a resolution of 2.7 Å the structure of the *E. coli* aquaglyceroporin GlpF with bound water by difference mapping against a 2.2-Å structure with glycerol that we had obtained previously [D. Fu et al., *Science* **290**, 481 (2000)]. The gene-duplicated sequence has a structural counterpart in a pseudo-twofold symmetry within the monomeric channel protein seen in Figure 7. We also carried out extensive molecular dynamics simulations (over 12 ns using NAMD) that defined the spatial and temporal probability distribution and orientation of water molecules inside the channel. The results reveal that the channel favors a single file of seven to nine water molecules that are hydrogen bonded with channel-lining carbonyl groups and with each other.

Then we made a double mutant (W48F/F200T), replacing two of the key residues in the center of the channel with residues seen in the water channels that do not conduct glycerol, and determined its structure at 2.1 Å (atomic

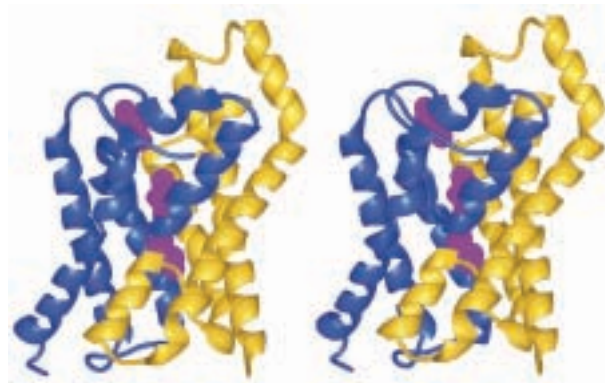


**FIGURE 7** Water conduction in *E. coli* aquaglyceroporin GlpF. Stereo images of the monomer of GlpF viewed down the quasi-twofold symmetry axis with the cytoplasmic side down. The two gene-duplicated segments (*blue and yellow*), are related by a quasi-twofold symmetry axis that passes through the center of the molecule. The two segments are separated by a linker region on the periplasmic side that is quite variable between AQPs. The pseudo-twofold symmetry within the monomeric channel favors a single file of seven to nine water molecules (*purple*) that are hydrogen bonded with channel-lining carbonyl groups and with each other.

resolution. We were particularly interested in how these channels absolutely prevent conduction of protons through the line of hydrogen-bonded waters. We carried out additional 12-ns molecular dynamics simulations and compared them directly with the crystal structures.

Two conserved asparagines force a central water molecule to serve strictly as a hydrogen-bond donor to its neighboring water molecules. Assisted by the electrostatic potential generated by two half-membrane-spanning loops, this property dictates opposite orientations of water molecules in the two halves of the channel and thus prevents the formation of a “proton wire” while permitting rapid water diffusion. Both simulations and observations revealed an increased water permeability for the W48F/F200T mutant. We also measured the conductance of our mutant channel for glycerol, getting results very close to that predicted by our molecular mechanics calculations. This in turn predicted the probability of finding the water molecules in the channel, very much as we see them to be positioned.

The results explain precisely how the channel freely passes water molecules near the diffusion limit and remains absolutely insulating to the passage of protons, even though a line of single-file water molecules moves freely through the channel. The remarkable synergy of the x-ray experiment is a first in terms of understanding membrane-channel conductances. The molecular mechanics allowed us to separate the contributions of each of the different components to the polarization of the central water, which then polarizes all the remaining line of waters oppositely out to the membrane surface, producing an effect almost as if two electric diodes of opposite sense are wired in series for protons, while freely conducting a line of water.

#### INVESTIGATORS

P. Nollert, L.J.W. Miercke, and R.M. Stroud (University of California, San Francisco); E. Tajkhorshid and K. Schulten (University of Illinois, Urbana-Champaign); and M.Ø. Jensen (University of Illinois, Urbana-Champaign, and University of California, San Francisco).

#### FUNDING

The National Institutes of Health and the Human Frontier Science Program Organization.

#### PUBLICATIONS

1. E. Tajkhorshid, P. Nollert, M.Ø. Jensen, L.J.W. Miercke, J. O’Connell, R.M. Stroud, and K. Schulten, “Control of the selectivity of the aquaporin water channel family by global orientational tuning,” *Science* **296**, 525 (2002).

2. P. Nollert, W.E.C. Harris, D. Fu, L.J.W. Miercke, and R.M. Stroud, "Atomic structure of a glycerol channel and implications for substrate permeation in aqua(glycero)-porins," *FEBS Letters* **504**, 112 (2001).

## Unraveling the Regulation of the Hypoxia-Inducible Transcription Factor (HIF)

*The panicky feeling that arises when trying to hold one's breath too long is first-hand evidence that the body forcefully reacts to a shortage of oxygen. Even under less extreme circumstances, cells have to make adjustments when the oxygen level available to them changes by producing more or fewer of various biomolecules (proteins) as appropriate. Since production of proteins begins with the instructions coded in the cell's DNA, regulation takes place at the point where the instructions are decoded (transcribed). As it happens, the cellular response to a low oxygen level influences certain deadly diseases like heart attacks and some types of cancer. One would like to stimulate the response in the first case, for example to promote the formation of blood vessels (vascularization) in injured tissue but decrease it in tumors to stop their growth. Learning how to artificially regulate this response via drugs is the motivation for the work of Dann et al., who determined the atomic-level structure of an important protein called factor-inhibiting HIF, or FIH-1, that regulates the transcription process.*

Cellular responses to oxygen levels in mammals are mediated primarily through the action of a family of transcription factors known as hypoxia-inducible factors (HIFs). Activation of the hypoxic (low-oxygen) response by HIF transcription factors ultimately leads to the production of a diverse array of proteins designed to help deliver oxygen to cells both in the short term through increase in red blood cell production and in the long term via the generation of new blood vessels (vascularization).

During the last two years, experiments have identified hydroxylation of a specific HIF residue as a key process in the regulation of its activity. Generating inhibitors or activators for specific hydroxylation enzymes (hydroxylases) and identifying potential sites for interaction with other components of the hypoxic response pathway may lead to pharmaceuticals able to treat diseases affected by cellular oxygen levels. To this end, our research has focused on the

crystallographic structure of the HIF-regulating hydroxylases. Here we report our structure for one of these enzymes, factor-inhibiting HIF (FIH-1).

Like many transcription factors, HIFs act as heterodimers to regulate transcription. Under hypoxic conditions, the steady-state level of the HIF  $\alpha$ -subunit increases, the protein translocates to the nucleus where it heterodimerizes with a constitutive  $\beta$ -subunit, and HIF gene targets are transcribed. Many studies have shown that, under normoxic (normal-oxygen) conditions, the HIF  $\alpha$ -subunit is regulated at the level of protein stability and transcriptional activation. The exact biochemical mechanism by which HIF regulation is coupled to oxygen levels remained elusive until the last two years, when experiments identified hydroxylation as a post-translational modification responsible for regulation of HIF (Figure 8). Under normoxic conditions, hydroxylases modify specific proline and asparagine residues leading to degradation of HIF  $\alpha$ -subunits via the proteasome and to decreased interaction of HIF with coactivators required to initiate transcription.

Hypoxia sensing by HIF has roles in the progression of many high-mortality conditions including stroke, myocardial infarction (cardiac arrest), and peripheral vascular disease, a common symptom of diabetes. Activation of HIF under normoxic conditions via the inhibition of regulatory hydroxylases leads to vascularization and increased oxygen delivery to tissues, and it may therefore be an effective treatment for these ischemic conditions. Conversely, activation of the HIF hypoxic response pathway has been noted in several cancer types and may promote cell survival in the tumor. Reduction of HIF through activation of inhibitory hydroxylases may provide a useful mode of treatment for these cancer types. However, the only available drugs that

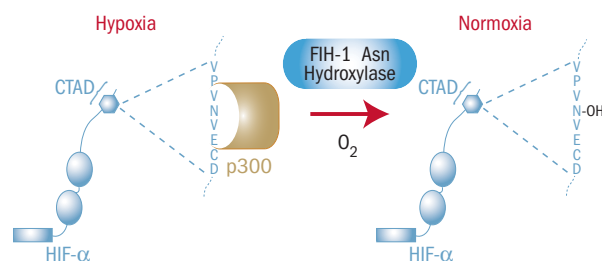


**FIGURE 8** Under normoxic (normal-oxygen) conditions, factor-inhibiting HIF (FIH-1) reduces the transcriptional activity of HIF- $\alpha$  through hydroxylation of a specific asparagine (Asn) residue in the carboxy-terminal activation domain (CTAD). Under hypoxic (low-oxygen) conditions, the asparagine on HIF- $\alpha$  is not hydroxylated and p300, a transcriptional coactivator, can bind HIF- $\alpha$ , allowing full transcriptional activation.

modulate hydroxylase activity are relatively nonspecific inhibitors that act by chelating the active site Fe(II).

Our research has focused on discerning the crystallographic structure of these hydroxylases. The hope is that structural studies on hydroxylases including FIH-1 can lead to development of specific drugs that modulate hypoxic responses in a therapeutically useful manner and can provide information on the interactions and regulation of these enzymes.

The enzymes responsible for the hydroxylation on HIF belong to a larger class of oxygenases dependent on Fe(II) and 2-oxoglutarate (2-OG). This class of hydroxylase requires Fe(II), 2-OG, and molecular oxygen to effect a modification on HIF, thereby providing an intriguing link between HIF regulation and oxygen levels. Three hydroxylases have been identified in humans that act as HIF prolyl hydroxylases (HPH-1, HPH-2, and HPH-3), while only a single HIF asparaginyl hydroxylase, factor-inhibiting HIF (FIH-1), has been identified. FIH-1 down regulates the transcriptional activity of HIF, since hydroxylation of a specific asparagine residue in HIF abrogates its interaction with the p300 protein, a general transcriptional coactivator (Figure 8).

The structure of the asparaginyl hydroxylase FIH-1 in complex with both Fe(II) and 2-OG was determined by x-ray crystallography to 2.4 Å (Figure 9). The structure has verified the residues predicted to bind Fe(II) and elucidated the residues responsible for 2-OG binding. The active site architecture differs from structurally known hydroxylases, particularly in the residues mediating 2-OG binding, allowing hope for the

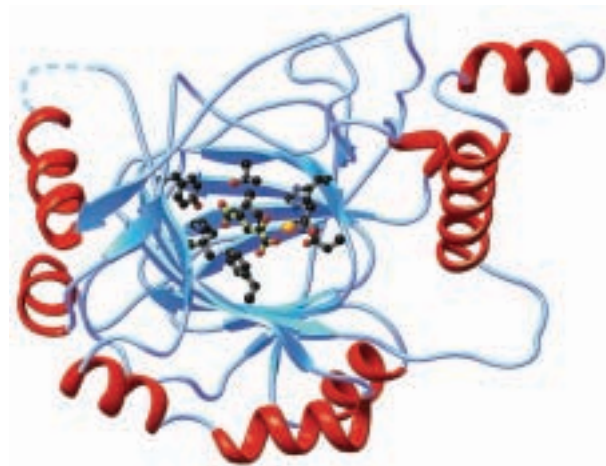


**FIGURE 9** Structure of FIH-1 in complex with Fe(II) (gold sphere) and 2-oxoglutarate (2-OG, yellow ball-and-stick structure). The side chains of residues responsible for Fe(II) coordination and in close proximity to 2-OG are shown (gray ball-and-stick structures).

development of drugs specific to FIH-1. In addition, the structure reveals that FIH-1 forms a homodimer mediated by its two C-terminal helices. Subsequent functional studies have shown that dimer formation is required for FIH-1 activity.

#### INVESTIGATORS

C.E. Dann III and J. Deisenhofer (University of Texas Southwestern Medical Center and Howard Hughes Medical Institute) and R. K. Bruick (University of Texas Southwestern Medical Center).

#### FUNDING

Burroughs Wellcome Fund.

#### PUBLICATION

1. C.E. Dann III, R.K. Bruick, and J. Deisenhofer, "Structure of factor-inhibiting hypoxia-inducible factor 1: An asparaginyl hydroxylase involved in the hypoxic response pathway," *Proceedings of the National Academy of Science USA* **99**, 15351 (2002).

## Structure of the Extracellular Portion of the Human LDL Receptor at Acidic pH

*Most people these days are aware that a high blood cholesterol level can clog arteries and increase the risks of stroke and heart attack. For most people, a healthy, low-animal-fat diet along with moderate exercise goes a long way toward reducing these risks. However, about one in 500 people are affected by familial hypercholesterolemia (FH), an inherited genetic condition marked by elevated LDL cholesterol levels beginning at birth and resulting in heart attacks at an early age. It is known that FH is caused by genetic mutations that disrupt the body's ability to metabolize cholesterol, but how exactly do these mutations interfere with the mechanics of the process? The mechanism proposed by Rudenko et al. adds one more piece to the puzzle and brings us one step closer to new treatments and drug discovery. As Brown and Goldstein, two of this work's Nobel-laureate authors, wrote, "it may one day be possible for many people to have their steak and live to enjoy it too."*

Cholesterol, especially in the "bad" form attached to low-density lipoprotein (LDL) particles, has been maligned as the culprit behind increased risk of atherosclerosis and heart disease. The truth, however, is that cholesterol is an essential component of cell membranes and provides the raw material for the synthesis of hormones, including

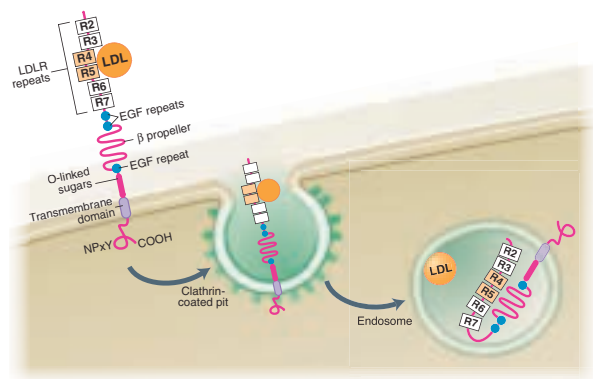


**FIGURE 10** Capture and release of LDL. Spherical LDL particles attach to LDLR anchored to the cell membrane. The cell membrane folds inwards and pinches off into a cavity within the cell (vesicle). Fusion of several vesicles gives rise to an endosome, an acidic “compartment” where the LDL particle is released. The LDLR is then recycled to the cell surface. Reprinted with permission from T. Innerarity, *Science* **298**, 2337 (2002). Illustration: K. Sutliff. Copyright 2002 American Association for the Advancement of Science.

estrogen and testosterone. A healthy level of cholesterol is regulated in part by a protein called the LDL receptor (LDLR). Anchored to the cell surface, LDLR captures LDL particles from the bloodstream and draws them inside the cell, where a shift to more acidic pH triggers LDL release (Figure 10). Our team of researchers examined the structure of LDLR at protein crystallography beamlines at the ALS and the Advanced Photon Source (APS). The LDLR crystals, painstakingly prepared to reflect the conditions for LDL release within the cell (pH less than 6), yielded the structure of a key portion of LDLR, providing clues as to how the LDL release mechanism works. Such “working” knowledge is essential to understanding how breakdowns in the system lead to cholesterol-related disease.

Human LDLR is a chain of 839 amino acids organized into several modular domains. The “ligand-binding domain,” crucial to binding LDL, consists of seven repeated amino-acid sequences (repeats R1 to R7). Next is a section referred to as the “epidermal growth factor (EGF) precursor homology domain,” because it is analogous to a precursor protein that stimulates cell growth. The EGF precursor homology domain in LDLR includes the EGF-like domains A, B, and C as well as a distinctive protein structure called a “ $\beta$  propeller.” The remainder of the protein contains a highly sugar-linked region, a membrane-spanning region, and a cytoplasmic domain. In this study, we focused on a fragment of LDLR that contains the ligand-binding and EGF precursor homology domains. We wanted to determine the organization of and interactions between the domains and

shed light on the mechanism by which LDLR releases its ligand when the pH changes from 7.5 (extracellular) to less than 6 (in endosomes inside the cell, where the LDL is released).

Crystals of the human LDLR fragment were grown at pH 5.3. They diffracted x rays very weakly with a best resolution of 7.5 Å, obtained with intense sources such as ALS Beamlines 5.0.2 and 8.2.1 and APS Beamline 19-ID. Tungsten clusters soaked into the crystals of a mutant LDLR dramatically increased the resolution to 3.7 Å and also provided anomalous scatterers for the multiwavelength anomalous diffraction experiments that were used to solve the phase problem. Using known high-resolution structures of smaller fragments of the LDLR, we were able to interpret electron density maps. The resulting model of human LDLR at pH 5.3 (Figure 11) shows that, while repeat R1 is disordered in the crystal, repeats R2 to R7 are arranged in an arch covering one side of the EGF precursor homology domain; in this domain, modules A, B, C, and the  $\beta$  propeller (Figure 12) form an apparently rigid entity. Repeats R4 and R5 interact extensively with the  $\beta$  propeller; this interaction would preclude the binding of a ligand such as LDL.

The structure offers a plausible hypothesis for the mechanism of ligand release upon a change in pH. While at neutral pH, the LDLR probably adopts a flexible, extended conformation and can bind ligands; at low pH, it develops a binding site for the central part of its own ligand-binding domain. This new binding site can compete with the ligand, which is then released. This hypothesis can explain why

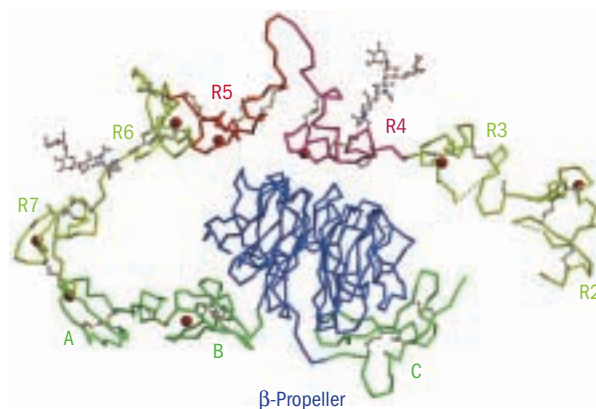


**FIGURE 11** Model of human LDLR at 3.7 Å. The cysteine-rich repeats R2, R3, R4, R5, R6, and R7 are found in the ligand-binding domain. The EGF-like repeats A, B, and C as well as the  $\beta$  propeller form the EGF-precursor homology domain. Repeats R4 and R5 (critical for LDL binding) interact extensively with the  $\beta$  propeller.



**FIGURE 12** Model of LDLR  $\beta$  propeller as described in T.A. Springer, *J. Mol. Biol.* **283**, 837 (1998), and further verified by H. Jeon et al., *Nat. Struct. Biol.* **8**, 499 (2001). As described by Rudenko et al., the propeller plays a key role in displacing LDL and promoting its release within cells. Illustration rendered by PyMOL ([www.pymol.org](http://www.pymol.org)).

LDLR mutants that lack the  $\beta$  propeller can bind, but not release, ligands. The model can also serve as a basis for explaining the effects of many mutations in LDLR that cause familial hypercholesterolemia, one of the most common single human gene disorders.

#### INVESTIGATORS

G. Rudenko, K. Ichtchenko, M.S. Brown, and J.L. Goldstein (University of Texas Southwestern Medical Center); K. Henderson (Berkeley Lab); and L. Henry and J. Deisenhofer (University of Texas Southwestern Medical Center and Howard Hughes Medical Institute).

#### FUNDING

Howard Hughes Medical Institute, National Institutes of Health, and Perot Family Foundation.

#### PUBLICATION

1. G. Rudenko et al., "Structure of the LDL receptor extracellular domain at endosomal pH," *Science* **298**, 2353 (2002).

# ATOMIC AND MOLECULAR SCIENCE

## Circular Dichroism in K-Shell Ionization of Fixed-in-Space CO and N<sub>2</sub> Molecules

Look at yourself in the mirror: what is the difference between you and the mirror image? For one thing, your left hand looks like a right hand. A special kind of light called circularly polarized is another example of mirror images. One can visualize the light as tracing out a spiral as it moves forward. In left-handed and right-handed circularly polarized light, the spirals rotate in the opposite directions (the mirror images). As it happens, scientists studying how x rays interact with molecules and atoms find circular polarization to be a useful tool, but it poses challenges for the theorists. To obtain data from relatively simple molecules for which good theories are available, Jahnke et al. have used a remarkable apparatus that records the directions of the electrons and molecular fragments as they fly apart after a molecule is torn apart by absorbing circularly polarized x rays. They found large differences between the effects of left- and right-handed polarizations for carbon monoxide and nitrogen molecules. Calculated results provided a good but not perfect match to experiment, suggesting more challenges for the theorists.

In atomic and molecular photoionization, the use of circularly polarized x rays gives direct access to phase differences inside the photoelectron wave-function, quantities completely hidden otherwise. It therefore provides a benchmark test for today's state-of-the-art theoretical models of electron emission. We have applied the COLTRIMS technique to the photoionization of carbon monoxide and nitrogen molecules in the gas phase by circularly polarized synchrotron radiation. Our results show that theory reproduces the main features, but not all the details of the measurements.

The electric field of a light wave oscillates in a plane perpendicular to the direction the light is moving. This oscillation axis may be fixed, in which case the light is termed linearly polarized. If the electric field vector of the light rotates clockwise or counterclockwise as the light moves away from the observer, the light is said to have a right circular or left circular polarization, respectively. When such

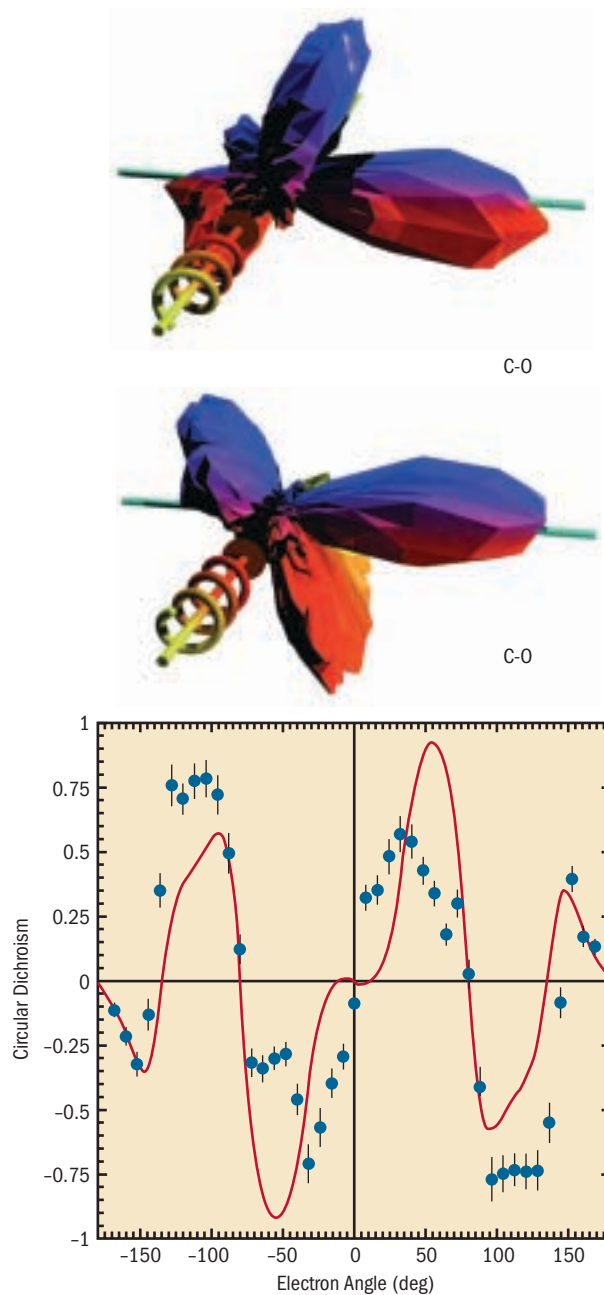


**FIGURE 1** Measured angular distributions and circular dichroism of the photoelectron (with 10 eV final kinetic energy) in the molecular frame, ejected from the carbon K shell of carbon monoxide. *Top*, the distribution for left-handed circularly polarized light. The spiral indicates the direction and the polarization property of the photon; the molecular axis is shown by the turquoise bar with the carbon atom at left. *Center*, the same distribution for right-handed polarization. *Bottom*, circular dichroism (in the plane of polarization) calculated from the distributions. *Dots*, experiment; *line*, multiple-scattering theory using nonspherical potentials (MSNSP).

photons ionize a molecule, the electron angular distributions with respect to the molecular axis may be different for the two polarizations. This circular dichroism is calculated by subtracting the angular distribution originating from photoionization with left from that obtained with right circularly polarized light.

How are the angular distributions for a gas measured? After a photon removes an inner-shell electron from a diatomic molecule, an electron from an outer shell drops into the vacant place, giving its energy to a second outer-shell electron, which is released from the molecule. The initial photoionization and subsequent Auger electron emission leave behind two singly charged ions that repel each other so strongly that often the doubly charged molecule dissociates rapidly in a “Coulomb explosion.” In most cases, the molecular axis at the instant of the photoionization can be determined by measuring the directions in which the two ionic fragments move.

Our experiment took advantage of the outstanding circular polarization properties of ALS Beamline 4.0.2. For each single molecule ionized from the gas phase, the momentum vector of the photoelectron and two ionic fragments are measured simultaneously. This multi-coincidence imaging technique termed COLTRIMS (COLd Target Recoil Ion Momentum Spectroscopy) uses electric and magnetic fields to guide electrons and ions toward two large-area, position-sensitive detectors. From the measured times of flight and positions of impact for each particle (the photoelectron and the two ions), their trajectories can be reconstructed. The technique provides multidimensional images of the fragmentation process similar to those obtained from cloud chambers or bubble chambers in nuclear and particle physics.

The measured photoelectron angular distributions in the molecular frame of CO are shown in Figure 1 for left- and right-handed circularly polarized x rays. The narrow lobes and deep minima of the distribution are a consequence of the wavelike character of the outgoing photoelectron. It is scattered in the potential of the CO molecule, leading to interference patterns that cause clearly visible minima and maxima at certain angles of emission. As the polarization of the photon is switched, the distribution is mirrored exactly as expected. The circular dichroism can now be determined from the distributions and compared to theoretical models.

Figure 2 depicts the angular distribution for an  $N_2$  molecule. In  $N_2$ , the two ends of the molecule are indistinguishable, and furthermore it is not obvious from which of

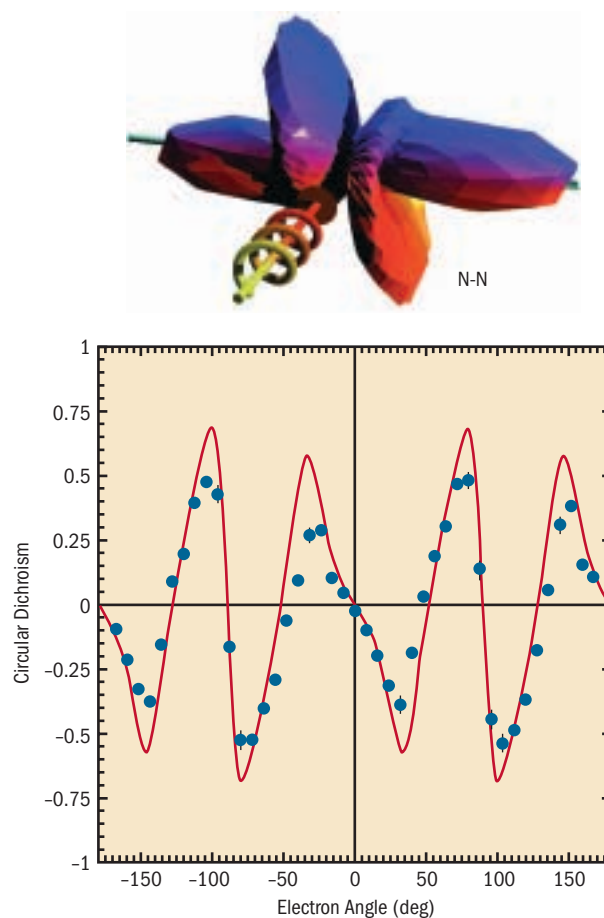


**FIGURE 2** Top, angular distribution and, bottom, circular dichroism for  $N_2$  K photoelectrons 10 eV above threshold. Dots, experiment; line, relaxed-core Hartree-Fock RPA theory. The agreement between theory and experiment is not as good for electron energies closer to threshold.

the two nitrogen K shells the photoelectron is ejected. Thus the distribution must be symmetric with respect to the center of the molecule. Still the left- or right-handed torque of the ionizing photon is important, so circular dichroism occurs for  $N_2$  as well.

In sum, current theory can reproduce many of the observations, but not all. The points of disagreement are driving theorists to make improvements in their approaches. The results will be a better understanding of the dynamics of photoemission from core-ionized molecules and perhaps predictions of new phenomena as yet to be observed.

#### INVESTIGATORS

T. Jahnke, Th. Weber, A. Knapp, S. Schöblier, J. Nickles, S. Kammer, O. Jagutzki, L. Schmidt, A. Czasch, H. Schmidt-Böcking, and R. Dörner (Institut für Kernphysik, University of Frankfurt, Germany); A.L. Landers (Western Michigan

University); T. Osipov and C.L. Cocke (Kansas State University); E. Arenholz, A.T. Young, and D. Rolles (ALS); F.J. Garcia de Abajo, J. Rösch, and M.H. Prior (Berkeley Lab); R. Díez Muiño (Berkeley Lab and Donostia International Physics Center, San Sebastian, Spain); C.S. Fadley and M.A. Van Hove (Berkeley Lab and University of California, Davis); and S.K. Semenov and N.A. Cherepkov (State University of Aerospace Instrumentation, St. Petersburg, Russia).

#### FUNDING

Bundesministerium für Bildung und Forschung; Deutsche Forschungsgemeinschaft; and U. S. Department of Energy, Office of Basic Energy Sciences.

#### PUBLICATION

1. T. Jahnke et al., "Circular dichroism in K-shell ionization from fixed-in-space CO and N<sub>2</sub> molecules," *Phys. Rev. Lett.* **88**, 073002 (2002).

## Large Nondipole Effects in the Angular Distributions of K-Shell Photoelectrons from N<sub>2</sub>

Absorption of an x ray by an atom or molecule often results in the emission of an electron. In photoelectron spectroscopy, scientists measure the spectrum of kinetic energies of the photoemitted electrons and thereby are able to probe the orbitals in which the electrons normally reside. The goal is a description of the "electronic structure" of the atom or molecule. But electrons also emerge in a variety of directions. Measuring their spatial distributions provides a more complete picture of the electronic structure, assuming that the theoretical framework is in place to interpret the results. For this reason, angle-resolved photoelectron spectroscopy has been used for many years to provide stringent tests of our understanding of the interaction of x rays with matter and as a tool to probe physical and chemical structure. Hemmers et al. have discovered that, for even simple molecules comprised of only two atoms, the angular distributions differ significantly from those expected from the standard theory called the dipole approximation. The deviations appear to depend on distances between the atoms (bond lengths), suggesting they may be a universal feature.

Photoelectron spectroscopy is a powerful technique to directly probe electronic structure in gaseous and condensed matter. It is even more powerful in an angle-resolved mode,

where photoelectrons also are distinguished by their direction of emission. Electron ejection probabilities as a function of angle are excellent probes of quantum-mechanical photoemission channels, because they are sensitive to phase differences among these channels. One of the basic approaches to interpreting angle-resolved photoemission spectra is the "dipole approximation," which predicts electron ejection patterns as a function of angle. Our work on molecular nitrogen performed at the ALS has found large anisotropies in electron photoemission based on bond-length-dependent terms that are indicative of a potentially universal behavior in molecular photoionization.

A mainstay of angle-resolved photoemission is the (electric-) dipole approximation, which includes only the electric-dipole interaction and ignores all higher-order photon interactions, such as electric quadrupole (E2) and magnetic dipole (M1) effects. In the dipole approximation, the differential cross-section predicts simple electron ejection patterns as a function of angle, and a single parameter,  $\beta$ , completely describes electron angular distributions as a function of the angle  $\theta$  relative to the linear polarization vector,  $\mathbf{E}$ , of the ionizing radiation (Figure 3).

In the first step beyond the dipole approximation, higher-order photon interactions (E2 and M1) lead to additional

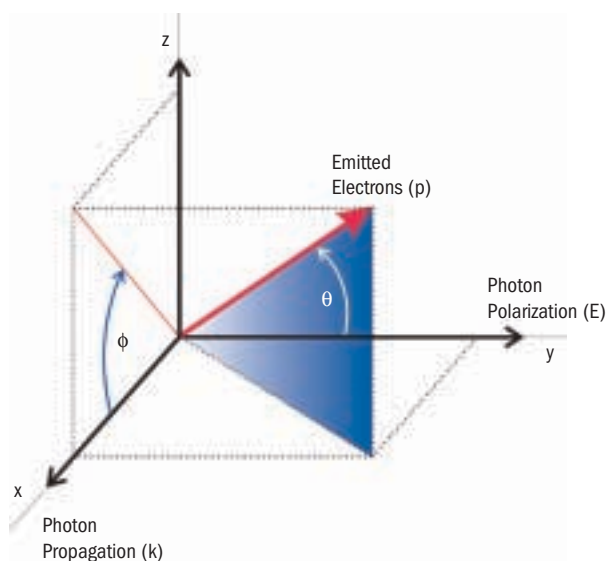


**FIGURE 3** In the dipole approximation, a single term describes electron angular distributions as a function of the angle  $\theta$  relative to the linear polarization vector,  $\mathbf{E}$ , of the radiation. Higher-order photon interactions lead to nondipole effects, which in the experiments reported here can be described by two new parameters and a second angle,  $\phi$ , relative to the propagation direction,  $\mathbf{k}$ , of the radiation.

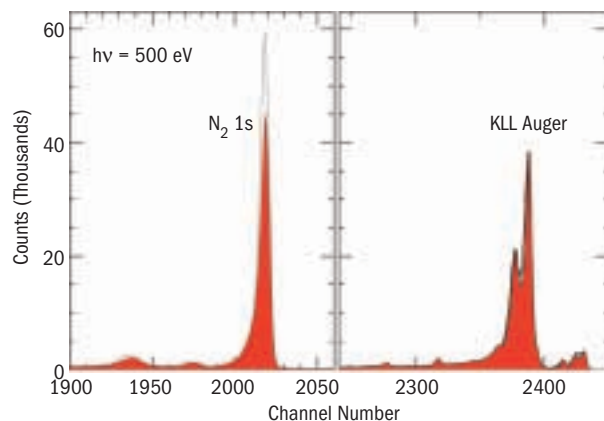


**FIGURE 4** Superimposed molecular nitrogen photoemission spectra taken with “magic-angle” analyzers, one in the  $y$ - $z$  plane (red), and the other in the  $x$ - $y$  plane. The spectra were scaled to each other by using nitrogen KLL Auger lines, and argon calibration spectra. The intensity differences between the  $N_2$  1s photoemission peaks are due to nondipole effects.

electron angular distributions, also known as nondipole effects, commonly described by three new parameters,  $\delta$ ,  $\gamma$ , and  $\zeta = \gamma + 3\delta$ . A second angle,  $\phi$ , relative to the propagation direction,  $\mathbf{k}$ , of the ionizing radiation (Figure 3), also comes into play, permitting forward–backward asymmetry of photoemission along  $\mathbf{k}$ .

To probe the limits of the dipole approximation, soft x-ray photoemission measurements on molecular nitrogen were made at Beamline 8.0.1. Two-bunch operation was necessary because electron kinetic energies were determined via time of flight (TOF), an efficient technique in which nearly

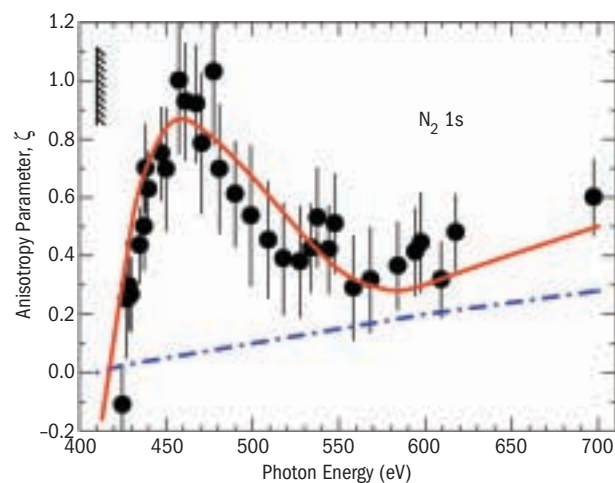


**FIGURE 5** Experimental (data points) and theoretical (solid line, molecular nitrogen; dot-dash line, atomic nitrogen) values of the first-order correction term  $\zeta = \gamma + 3\delta$  for molecular nitrogen photoemission determined in the “magic-angle” geometry.

all kinetic energies can be measured simultaneously. Two analyzers, placed at the “magic angle” ( $\theta = 54.7^\circ$ ), where  $\beta$  has no influence, but at different angles  $\phi$  ( $0^\circ$  and  $90^\circ$ ) to be sensitive to forward–backward asymmetries, sufficed to measure nondipole effects (expressed as the asymmetry parameter,  $\zeta$ ) as a function of photon energy.

In Figure 4, two nitrogen photoemission spectra taken with the “magic-angle” analyzers, one in the  $y$ - $z$  plane and the other in the  $x$ - $y$  plane, are superimposed. The spectra are scaled to each other by using nitrogen KLL Auger lines, which almost always have isotropic angular distributions ( $\beta = \delta = \gamma = 0$ ), as well as argon calibration spectra with known values for  $\beta$ ,  $\delta$ , and  $\gamma$ . Obvious intensity differences between the 1s photoemission peaks are due to nondipole effects.

Figure 5 shows the experimental results over a wide range of photon energies as well as theoretical data for molecular nitrogen and for atomic nitrogen. The agreement between the experimental and theoretical molecular results is excellent, and the deviation from the atomic theory shows that the large nondipole effects observed are due to the molecular field. Electrons emitted from  $N_2$  can rescatter in the molecular field, which introduces a bond-length dependence (distance between the two nitrogen atoms in  $N_2$ ) that causes a change from the pure atomic behavior for the photoelectron angular distributions. The theory for molecular nitrogen agrees with the theory for atomic nitrogen when the bond-length is set to zero.

More significantly, measurements on other atoms and molecules demonstrate that “low-energy” breakdown of the dipole approximation is a general phenomenon. It is likely that many applications of angle-resolved photoemission (e.g., most studies of atoms and molecules, band mapping in solids, photoelectron diffraction and holography, orientational studies of adsorbates, etc.) need to include nondipole effects in their analyses. More work to determine the range of validity of the dipole approximation is under way.

#### INVESTIGATORS

O. Hemmers and D.W. Lindle (University of Nevada, Las Vegas); H. Wang (MAX-Lab, Lund University, Sweden); P. Focke and I.A. Sellin (University of Tennessee, Knoxville); J.C. Arce (Universidad del Valle, Cali, Colombia); J.A. Sheehy (Air Force Research Laboratory, Edwards); and P.W. Langhoff (University of California, San Diego).

#### FUNDING

National Research Council, US Air Force Office of Scientific Research, and National Science Foundation.

## PUBLICATIONS

1. O. Hemmers et al., "Large nondipole effects in the angular distributions of K-shell photoelectrons from molecular nitrogen," *Phys. Rev. Lett.* **87**, 273003 (2001).
2. J.C. Arce et al., "On the angular distributions of molecular photoelectrons: Dipole cross sections for fixed-in-space and randomly oriented molecules," *Chem. Phys. Lett.* **346**, 341 (2001); Erratum 349, 349 (2001).
3. R. Guillemin et al., "Non-dipolar electron angular distributions from fixed-in-space molecules," *Phys. Rev. Lett.* **89**, 022002 (2002).

## Dynamic Jahn–Teller Effect in Buckyball Cations

*Stability in nature is associated with the lowest possible energy. The arrangement of atoms in a molecule is a prime example; the atoms assume a configuration with the lowest energy, and then they stay put except for the slight quiver of molecular vibrations. Quantum mechanics, which governs motion on the atomic level, adds a subtlety. When the nominally lowest energy configuration is highly symmetric, like cubes or pyramids, interactions between the molecule's electrons and the atomic vibrations make it possible to lower the energy still further by a slight distortion to a less symmetric configuration. Canton et al. have identified for the first time in positively charged ions of the soccer-ball-shaped carbon clusters ( $C_{60}$ ) familiarly known as buckyballs a particular example of a distortion known as the "dynamic Jahn–Teller effect." Though the effect occurs on the tiny scale of atoms and molecules, its results can be big. Such refinements can work important results in our macroscopic world, from superconductivity (resistanceless flow of electricity) to infrared absorption of molecules in outer space.*

High symmetry is not always the attribute preferred by nature when it comes to the geometry of atoms in molecules and solids, where structural distortions can in certain circumstances lower the overall energy and make for a more stable, if less symmetric, configuration. The latest example comes from our multinational team from the United States, Finland, and Brazil, which has uncovered the first experimental evidence for a dynamic Jahn–Teller effect in isolated cations of  $C_{60}^+$ . With an origin in a strong coupling between electronic and vibrational states, the Jahn–Teller effect results in a lowering of the icosahedral

symmetry of the neutral cluster. From the valence photoelectron spectrum, our group was able to unambiguously identify the relaxed geometry of the ionic ground state and determine that it was different from that believed to hold in matrix-isolated ions.

If some of the glamour of carbon-based nanostructures has passed to carbon nanotubes,  $C_{60}$  clusters (buckminsterfullerene, or even more familiarly, buckyballs) retain considerable allure in many areas of science. Cations ( $C_{60}^+$ ) are of particular interest. In astrophysics, the infrared bands due to molecular vibrations in these cations have recently been implicated in the long-standing problem of diffuse interstellar infrared bands. In condensed matter, it appears that some of the properties of solids comprising clusters weakly bonded by van der Waals forces are connected to the electronic structure of the isolated cations. For example, superconductivity may be mediated by an electron–phonon interaction that is strengthened by the Jahn–Teller effect in the cations.

The Jahn–Teller effect in buckyball cations is associated with the breakdown of the widely used Born–Oppenheimer approximation, which allows theorists to calculate the electronic and vibrational states separately with any interaction between the two systems treated as a small perturbation. In highly symmetric molecules or solids, where otherwise distinct electron states may be degenerate (have the same energy), the Born–Oppenheimer approximation is not necessarily valid, because the electronic and vibrational systems can then interact strongly to form coupled vibronic states. In the Jahn–Teller effect, this interaction results in structural distortion that lowers the symmetry while enabling the atoms to assume a relaxed geometry. A splitting of the degenerate electronic states and a lower energy is another consequence.

At the ALS, our group investigated free  $C_{60}^+$  ions produced by ionizing with synchrotron radiation a beam of neutral particles from a heated oven. We conducted valence photoelectron spectroscopy measurements at a photon energy of 50 eV in this crossed-beam configuration, and we found that the first band in the photoionization spectrum, which is due to excitation from the highest occupied molecular orbitals, consisted of three components (Figure 6). Curve fitting with three asymmetric Gaussian peaks and a simplified cation potential well enabled us to reproduce the measured spectrum and determine the symmetry and energy of each component (Figure 7).

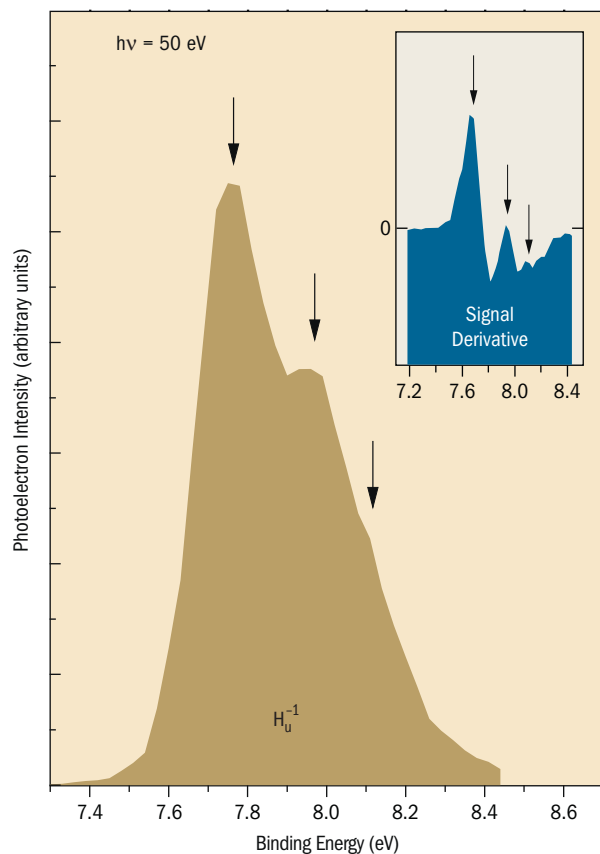


**FIGURE 6** The structural distortion that accompanies the Jahn–Teller effect is reflected in the photoionization spectrum. The measured spectrum for buckyball cations exhibits three features (the two peaks and the shoulder marked by arrows). The differential spectrum (*inset*) obtained from the signal derivative clearly defines the positions of these features.

Interpreting these findings, we concluded that the three components were due to vibronic states that tunnel between energetically equivalent potential wells in the distorted geometry, which has the overall symmetry  $D_{3d}$ . Tunneling is what makes this Jahn–Teller effect dynamic, as opposed to a static effect in which nuclear states are confined to one well. The observed peak with three bands with relative intensities appropriate to this symmetry appears to rule out an alternative static Jahn–Teller  $D_{5d}$  geometry suggested by previous experiments by other groups with optical and infrared spectroscopy of  $C_{60}^+$  ions trapped in glassy or rare-gas matrices. Earlier photoionization measurements also ruled out the possibility that the three peaks were due to individual vibrational states.

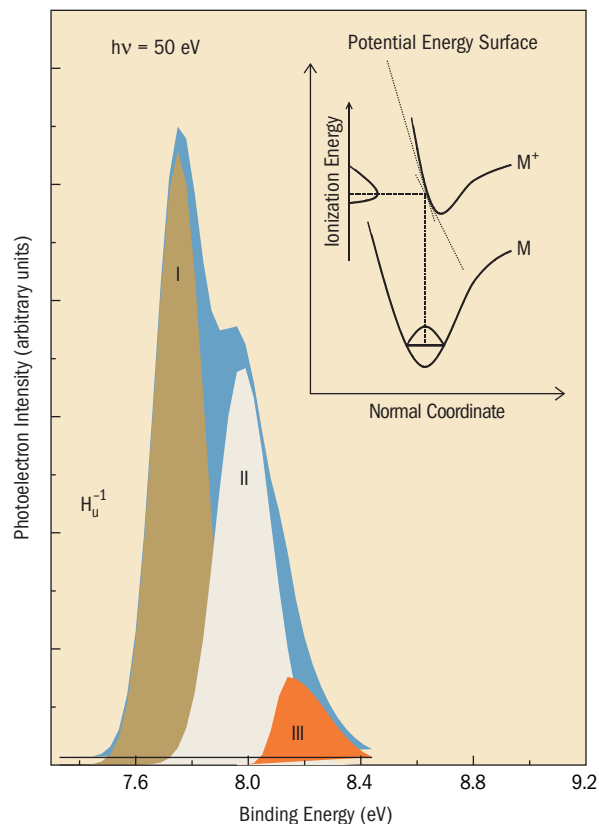


**FIGURE 7** The photoionization spectrum, when curve-fitted with three asymmetric Gaussian peaks and a simplified cation potential (*inset*), reproduces the measured spectrum and provides the symmetry and energy of each peak.

#### INVESTIGATORS

S.E. Canton (Western Michigan University and ALS), A.J. Yench (State University of New York at Albany), E. Kukk (Oulu University, Finland), J.D. Bozek (ALS), M.C.A. Lopes (Universidade Federal de Juiz de Fora, Brazil), and G. Snell and N. Berrah (Western Michigan University).

#### FUNDING

U.S. Department of Energy, Office of Basic Energy Sciences, and CNPq (Brazil).

#### PUBLICATION

1. S.E. Canton et al., “Experimental evidence of a dynamic Jahn–Teller effect in  $C_{60}^+$ ” *Phys. Rev. Lett.* **89**, 045502 (2002).

## Toward the Goal of Quantum Mechanically Complete Experiments

*At the level of individual atoms, quantum mechanics controls the action. In recent years, the trend among practitioners of atomic physics is to move from being a passive observer to an active controller of quantum phenomena. Accomplishing this goal has important ramifications for varied technologies, from the emerging quantum computing and cryptography to the long-standing problem of controlling chemical reactions. Full control of quantum processes requires complete information about the quantum system. Experiments that measure all information allowed by quantum mechanics are called “quantum mechanically complete experiments.” For complex quantum phenomena, quantum mechanically complete experiments fully test the theory and avoid the pitfalls of determining certain quantities (technically, a subset of cross-sections) where a match between the theory and experiment may be fortuitous. McLaughlin et al. have developed a new method that takes scientists a step closer to this goal, and they have tested it on argon vapor.*

For pure states, the maximum knowledge about a quantum process is obtained when one determines the wave function of the system rather than a set of cross-sections. The experimental determination of wave functions, up to an overall phase, for atomic and molecular systems has been elusive. Atomic photoionization is one example of complex quantum phenomena where some progress has been made in performing quantum mechanically complete experiments. The wavefunction of the photoelectron can be written as a superposition of spherical harmonics that are related to the orbital angular momentum content of the photoelectron and hence its angular distribution. The coefficients of this expansion are called the partial-wave amplitudes. The absolute squares of these partial-wave amplitudes are the probabilities of measuring a particular partial wave with a well-defined total angular momentum.

In atomic photoionization, a quantum mechanically complete experiment involves the determination of partial-wave probabilities of the photoelectron and the phases between these partial waves. Conservation of angular momentum and parity restricts these partial waves to a maximum of three. Thus, one experimentally needs to determine five parameters: the three partial-wave probabilities and the two independent phases between these partial waves.

We have developed a new method to determine all of the partial-wave probabilities of the photoelectron from the linear and circular polarization measurements of the ionic fluorescent radiation. The intensity and polarizations of the fluorescent radiation reflect the angular-momentum content of the excited residual ionic state. In turn, the angular-momentum content of the quantum state of the excited residual ion is intimately related to the quantum state of the photoelectron through conservation laws and coupling rules. This intimate coupling between the residual excited ion and the photoelectron allows us to determine the properties of the photoelectron without any direct measurement on the electron.

In the experiment, we photoionize argon atoms with circularly polarized vacuum-ultraviolet photons. The circularly polarized photons are produced from the linearly polarized radiation from the undulator of ALS Beamline 10.0.1 by means of a unique phase retarder based on quadruple reflections. With this device, one can obtain radiation with high circular polarization (of the order of unity) over an extended range of photon energies from 10 to 60 eV. Around 36 eV, the transmission efficiency is about 0.01 (1%), and the degree of circular polarization is better than 99.7%. The experimental setup is schematically shown in Figure 8. The 476.5-nm fluorescence is produced during decay of an excited argon ion ( $\text{Ar}^+$ )<sup>\*</sup> from the  $\text{Ar}\{3p^6\ ^1\text{S}_0\} + h\nu \rightarrow \text{Ar}^+\{3p^4\ [^3\text{P}]\ 4p\ ^2\text{P}^0_{3/2}\} + e$  photoionization channel. In

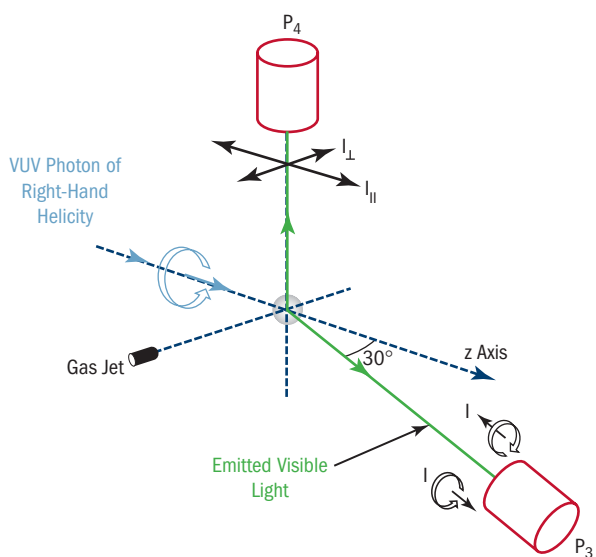


**FIGURE 8** Experimental setup to determine all three partial-wave probabilities of the photoelectron for the  $\text{Ar}\{3p^6\ ^1\text{S}_0\} + h\nu \rightarrow \text{Ar}^+\{3p^4\ [^3\text{P}]\ 4p\ ^2\text{P}^0_{3/2}\} + e$  photoionization channel.

order to obtain the maximum information about the angular momentum content of the excited ionic state, we measure the degree of circular polarization in the forward direction at an angle of  $30^\circ$  with respect to the beam direction and the degree of linear polarization in a direction perpendicular to the beam.

Figure 9 shows the partial-wave probabilities  $s_{1/2}$ ,  $d_{3/2}$ , and  $d_{5/2}$  of the photoelectron as a function of photon energy. It is quite informative to observe that the partial-wave content varies for different resonances. It should be noted the resonance profiles for different partial waves vary with angular momentum, indicating that the phase difference between a resonance and the continuum depends on the partial wave. Finally, the  $d_{3/2}$  and  $d_{5/2}$  partial wave ratio is dramatically different from the constant value of 1.5 predicted by neglecting spin-dependent relativistic interactions, by an order of magnitude or more.

In summary, we have developed an experimental method to directly measure for the first time all three partial-wave probabilities of photoelectrons produced by multielectron processes over an extended range of energies. This capability brings us a step closer to carrying out quantum mechanically complete photoionization experiments.

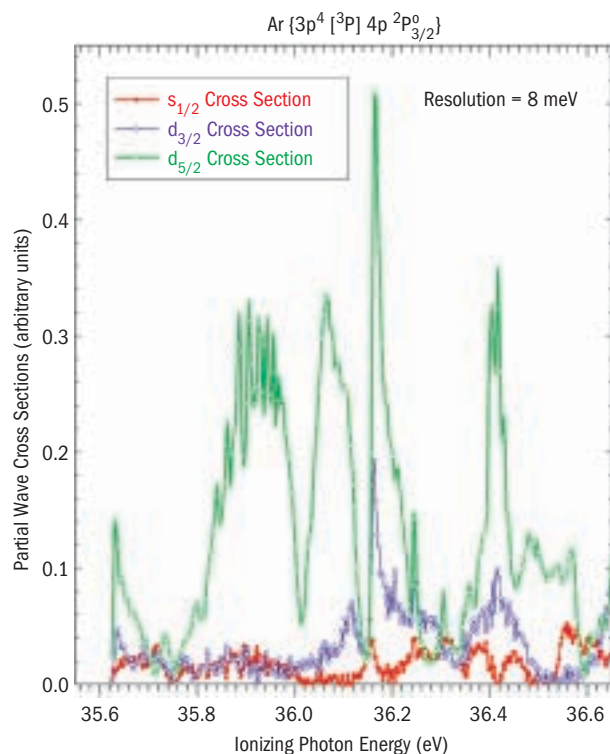


**FIGURE 9** All three partial-wave cross-sections of the photoelectron for the  $\text{Ar}\{3p^5\ ^1S_0\} + h\nu \rightarrow \text{Ar}^+\{3p^4\ [^3P] 4p\ ^2P_{3/2}^0\} + e$  photoionization channel.

## INVESTIGATORS

K.W. McLaughlin (Loras College); D.H. Jaecks, O. Yenen, T.J. Gay, B. Thaden-Jordan (University of Nebraska–Lincoln); M.M. Sant’Anna (ALS); and D. Calabrese (Sierra Community College).

## FUNDING

National Science Foundation.

## PUBLICATION

1. K.W. McLaughlin et al, “Effect of relativistic many-electron interactions on photoelectron partial wave probabilities,” *Phys. Rev. Lett.* **88**, 123003 (2002).

## An Application of Detailed Balance in a Unique Atomic System

*Much as we’d sometimes like to make time run backwards, we know that it won’t happen. On the atomic level, however, a kind of time reversal is built into the quantum mechanics that governs processes within atoms. This principle of microscopic time reversal, in which the probability of a physical process and its inverse are the same, is called detailed balance. Theorists not only use detailed balance widely, but they depend on it as a way to make a connection between inverse processes. For example, an atom can absorb an x ray and emit a photoelectron (photoionization), and an ion can attract an electron and return to the initial state by emitting an x ray (photorecombination). Each process is characterized by a “cross-section” that measures the probability for its occurrence. Schippers et al. made a novel use of detailed balance and the comparison of experimental photoionization and photorecombination results obtained by two very distinct techniques to determine cross-sections for both processes in scandium ions (i.e., photoionization of doubly ionized scandium and photorecombination of triply ionized scandium).*

The experimental determination of photoionization cross-sections of atomic ions, which are, for example, relevant for the detailed understanding of both astrophysical and artificial plasmas, is challenging because the target densities in an ion beam are limited by space-charge effects to values of the order of  $10^6\ \text{cm}^{-3}$  (to be compared with  $\sim 10^{13}\ \text{cm}^{-3}$  in an effusive beam of neutral atoms). Moreover, unknown fractions of metastable states in the ion beam often prevent the derivation of *absolute* cross-sections. We report a novel method for the experimental determination

of the fractional abundances of the  $3p^6 3d^2 D_{3/2}$  ground state as well as of the  $3p^6 3d^2 D_{5/2}$  and  $3p^6 4s^2 S_{1/2}$  metastable states in an  $Sc^{2+}$  ion beam.

Our method consists of comparing experimental  $Sc^{2+}$  photoionization cross-sections, obtained at the ion-photon beam (IPB) endstation of ALS Beamline 10.0.1, with the previously measured  $Sc^{3+}$  photorecombination cross-section from the heavy-ion storage ring TSR of the Max-Planck-Institute for Nuclear Physics in Heidelberg, Germany. The method relies on the fact that photoionization and photorecombination are linked on a state-to-state level by the principle of detailed balance.

The measured  $Sc^{2+}$  photoionization and  $Sc^{3+}$  photorecombination cross-sections are shown in Figure 10 (top and bottom panels, respectively). Because of the high resolving power of the ALS IPB endstation (up to  $E/\Delta E = 35,000$ ), we were able to obtain detailed spectroscopic information about numerous photoionization resonances. In the photon energy range of the top panel of Figure 10, these resonances are mainly due to  $3p \rightarrow 3d$  excitations.

Apart from the lower energy resolution of the photorecombination experiment, there are obvious similarities with

respect to relative resonance positions and strengths in the cross-sections. The resonance at  $h\nu = 41.8$  eV in the photoionization spectrum appears in the photorecombination spectrum at 20.2 eV, an energy higher by about 3.1 eV after allowing for the ionization potential (24.757 eV) of the  $Sc^{2+}$  ground state. This shift corresponds to the  $3d \rightarrow 4s$  excitation energy and is therefore a clear indication for the presence of metastable  $Sc^{2+}(3p^6 4s)$  ions in the photoionization experiment. In contrast, in the ion-storage-ring photorecombination experiment, we could be sure that the stored  $Sc^{3+}$  ions were in the ground state by simply waiting long enough in between the filling of the storage ring and the data taking.

Having determined which photoionization resonances are to be attributed to metastable  $Sc^{2+}$  ions, we fit the weighted sum of the partial photoionization cross-sections to the measured photorecombination spectrum, where the weights correspond to the fractional abundances of the  $3p^6 3d^2 D_{3/2}$  ( $0.207 \pm 0.030$ ),  $3p^6 3d^2 D_{5/2}$  ( $0.546 \pm 0.043$ ), and  $3p^6 4s^2 S_{1/2}$  ( $0.247 \pm 0.013$ )  $Sc^{2+}$  states. Notably, the fit results in a nonstatistical distribution. The fit implicitly assumed that the radiative decay paths of the  $3p^5 3d^2$  and  $3p^5 3d 4s$  photorecombination resonance states into the  $3p^6 3d$

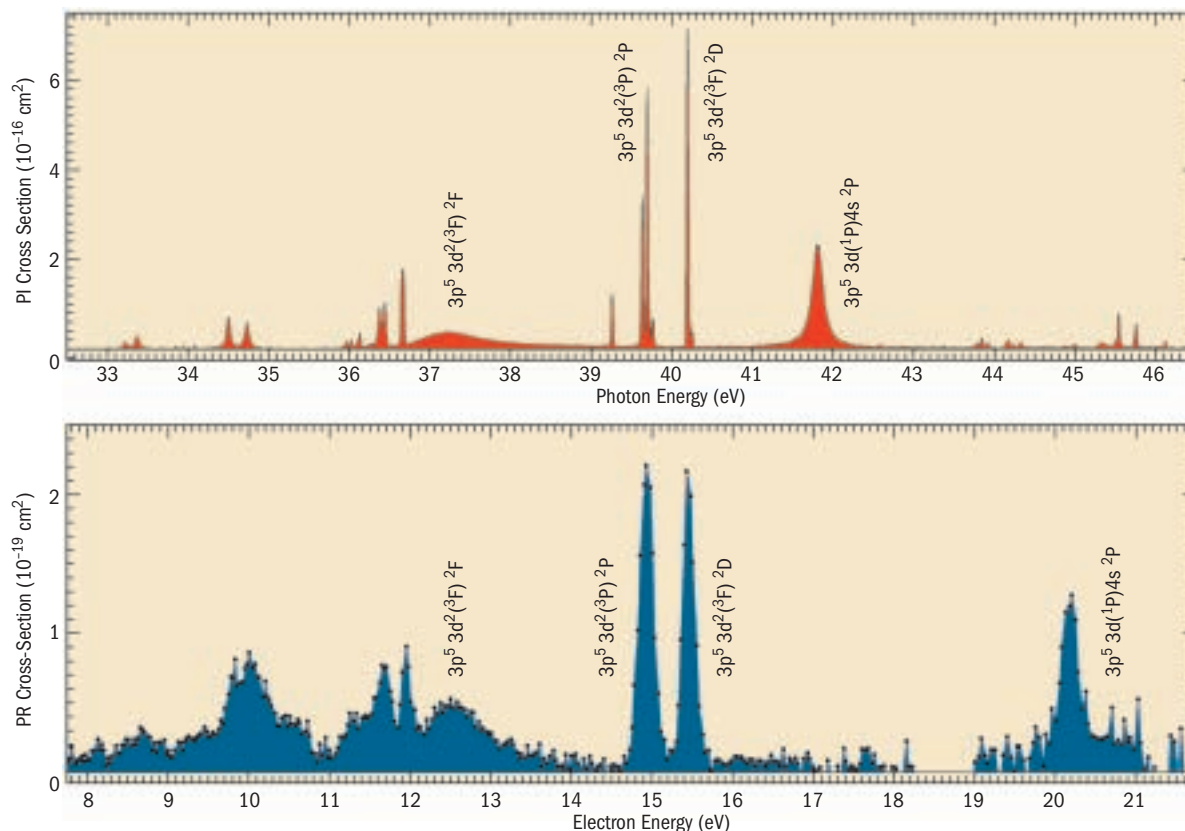


**FIGURE 10** Photoionization of  $Sc^{2+}$  (top) and photorecombination of  $Sc^{3+}$  (bottom). The electron energy scale in the bottom panel has been shifted with respect to the photon energy scale by the ionization potential (24.757 eV) of the  $Sc^{2+}$  ground state, so that the photoionization and photorecombination spectra can easily be compared.

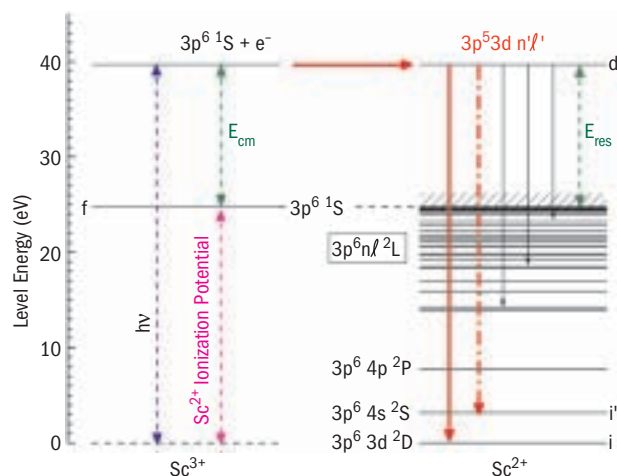


**FIGURE 11** Energy level diagram for the dielectronic (resonant) recombination of  $\text{Sc}^{3+}$  ions. Initially, the ion in the  $3p^6\ ^1S$  ground state ( $f$ ) collides with a free electron with energy  $E_{\text{cm}}$  above the first  $\text{Sc}^{2+}$  ionization threshold. If  $E_{\text{cm}} \approx E_{\text{res}}$ , an  $\text{Sc}^{2+}(3p^5\ 3d\ n'l')$  doubly excited state ( $d$ ) may be formed by dielectronic capture (inverse autoionization) with nonzero probability (*horizontal red arrow*). The recombination event is completed by a subsequent radiative transition to a bound state below the  $\text{Sc}^{2+}$  ionization threshold (*vertical arrows*). For  $3p^5\ 3d^2$  and  $3p^5\ 3d\ 4s$  doubly excited intermediate states, the radiative decay paths to the photoionization initial states  $3p^6\ 3d$  ( $i$ , *red vertical arrow*) and  $3p^6\ 4s$  ( $i'$ , *dash-dotted red vertical arrow*), respectively, are unique, i.e., the multitude of other energetically allowed transitions (*vertical black arrows*) can be neglected. On the scale of the figure, fine-structure level splittings are not resolved.

and  $3p^6\ 4s$  photoionization initial states are unique. As explained in Figure 11, this is a very special feature of the atomic system under study.

The strongest photoionization resonance at  $h\nu = 41.8\ \text{eV}$  is due to a  $3p \rightarrow 3d$  excitation of the  $3p\ 4s\ ^2S_{1/2}$  metastable state. As a result of the photoionization–photorecombination comparison outlined above, its oscillator strength was obtained as  $2.1 \pm 0.4$ . This value agrees with that for the same transition in iso-electronic  $\text{Ca}^+$  ions. This coincidence strongly hints that our novel method for the purely experimental derivation of absolute state-selective photoionization cross-sections (i.e., combining the high resolving power of a photoionization experiment at a synchrotron light source with the state selectivity of a heavy-ion storage-ring photorecombination experiment) is valid.

#### INVESTIGATORS

S. Schippers and A. Müller (Justus-Liebig-Universität Giessen, Germany); A. Aguilar, A.M. Covington, M.F. Gharaibeh, and R.A. Phaneuf (University of Nevada, Reno); S. Ricz (Institute of Nuclear Research, Debrecen, Hungary);

M.E. Bannister (Oak Ridge National Laboratory); G.H. Dunn (JILA, University of Colorado, Boulder); J.D. Bozek and A.S. Schlachter (ALS); and G. Hinojosa and C. Cisneros (Universidad Nacional Autónoma de México, México).

#### FUNDING

NATO, U.S. Department of Energy, and Deutsche Forschungsgemeinschaft.

#### PUBLICATIONS

1. S. Schippers et al., “Experimental link of photoionization of  $\text{Sc}^{2+}$  to photorecombination of  $\text{Sc}^{3+}$ : An application of detailed balance in a unique atomic system,” *Phys. Rev. Lett.* **89**, 193002 (2002).
2. S. Schippers et al., “Interference effects in the photorecombination of argonlike  $\text{Sc}^{3+}$  ions: Storage-ring experiment and theory,” *Phys. Rev. A* **65**, 042723 (2002).
3. S. Schippers et al., “Photoionization of  $\text{Sc}^{2+}$  ions by synchrotron radiation: Measurements and absolute cross sections in the photon energy range 23–68 eV,” *Phys. Rev. A* **67**, 032702 (2003).

# ACCELERATOR PHYSICS

## Self-Amplified Spontaneous Coherent THz Synchrotron Radiation at the ALS

The Advanced Light Source was built to produce synchrotron radiation from a high-energy electron beam. The beam is not continuous but consists of a few hundred bunches into which the electrons are grouped. Ordinarily, each electron emits independently, and the total power radiated is proportional to the number of electrons. However, when the wavelength of the emitted radiation is comparable to the length of an electron bunch, the electrons emit in unison rather than as individuals. This coherent emission results in a dramatic increase in the power emitted (proportional to the square of the number of electrons, thereby also causing a wave of enthusiasm among scientists who are potential users of coherent synchrotron radiation (CSR), which occurs primarily at very long wavelengths in the far-infrared portion of the spectrum. Byrd et al. have used the ALS to observe and explain an instability in the electron beam that potentially prevents the generation of CSR, thereby contributing to the ability to design future electron accelerators (storage rings) optimized to produce it.

When the wavelength of synchrotron radiation is comparable to the length of an electron bunch in the storage ring, or the length of any structure on the bunch, the radiation from multiple electrons is in phase, resulting in a quadratic rather than the usual linear dependence of the power emitted on the number of electrons. Because the number of electrons participating in the coherence can be large (more than 1 million), the potential power enhancement is very large, making coherent synchrotron radiation (CSR) a subject of great interest to both synchrotron users and accelerator designers. However, the electromagnetic field associated with CSR can influence the motion of the electrons in the bunch, resulting in a self-amplified instability. This instability increases the electron bunch length and energy spread and represents a fundamental limitation in the performance of an electron storage ring. In our studies at the ALS, we have been able to observe and, for the first time, explain this instability.

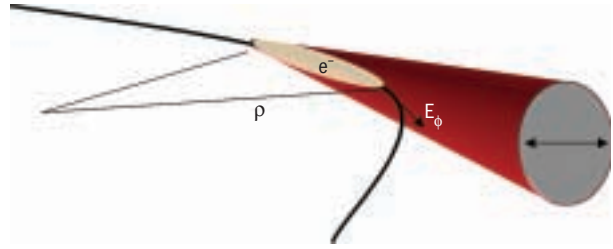


**FIGURE 1** Schematic view of the interaction of an electron bunch with its own synchrotron radiation. The curvature of the electron orbit allows the radiation field to accelerate or decelerate the electron.

The interaction of an electron bunch and its synchrotron radiation is shown schematically in Figure 1. The electron bunch bends through a magnetic field and emits a cone of synchrotron radiation that has a transverse electromagnetic field. Because of its bent trajectory, an electron in the front of the bunch senses a longitudinal component of the radiation field that can either accelerate or decelerate the electron, depending on its position. The interaction can give rise to a self-amplified instability starting from a small modulation in the bunch profile. This modulation radiates coherently, causing the bunch modulation to increase. Counteracting this effect is the natural energy spread within the bunch, which tends to cause any modulation to smear out. An instability occurs when the runaway amplification beats out the damping effect of the energy spread.

The microbunching instability is illustrated by the computer simulation shown in Figure 2. Above the instability threshold, a ripple in the energy distribution is evident, along with a small ripple in the bunch profile. As the instability

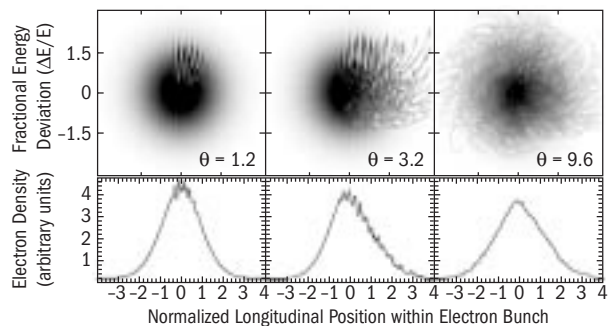


**FIGURE 2** Evolution of a microbunching instability illustrated via a computer simulation. *Top row*, electron density in coordinates of relative position along the bunch and fractional energy offset; *bottom row*, projection of the top row on the longitudinal charge density. An initial small modulation in the density (*left*) is amplified until the instability reaches saturation (*right*).

progresses, the disruption in the bunch increases, giving a larger modulation in the bunch profile. Finally, the instability reaches saturation and the bunch profile smooths over, albeit with an increased length. After radiation damping returns the bunch distribution to its original shape, the instability repeats.

During the instability, the microbunching results in bursts of CSR at the wavelength of the bunch modulation, which for ALS parameters ranges from a few millimeters down to half a millimeter (far infrared or terahertz). To observe these bursts experimentally, we installed detectors, such as bolometers and heterodyne receivers, at ALS infrared Beamline 1.4.3. Examples of the signals detected with one of the bolometers are shown in Figure 3. Above a threshold single-bunch current, the bursts appear. As the bunch current increases, the burst rate and amplitude increase and eventually saturate the detector. At the highest bunch currents

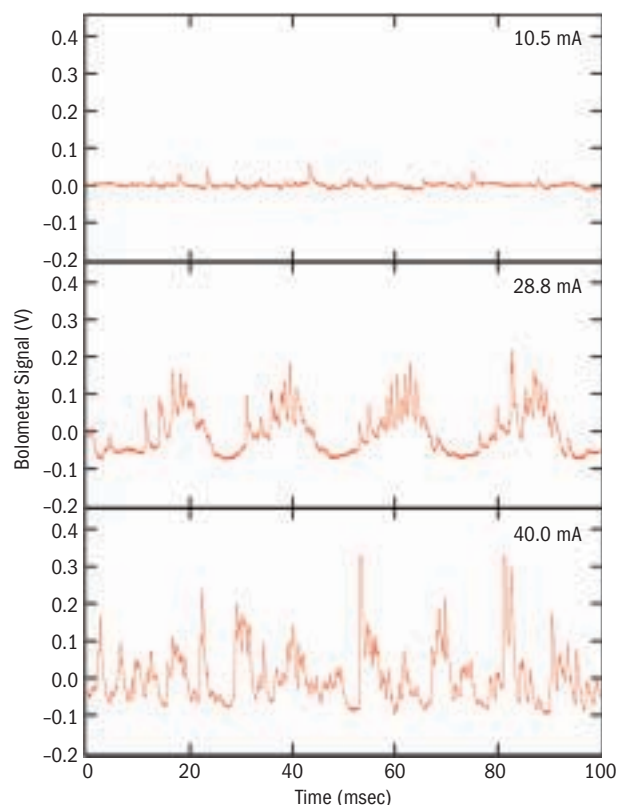


**FIGURE 3** Examples of bursts of far-infrared synchrotron radiation measured with a bolometer. Each of the bursts is associated with a microbunching of the electron beam caused by interaction with the synchrotron radiation. At larger bunch currents, the burst rate and amplitude increased.

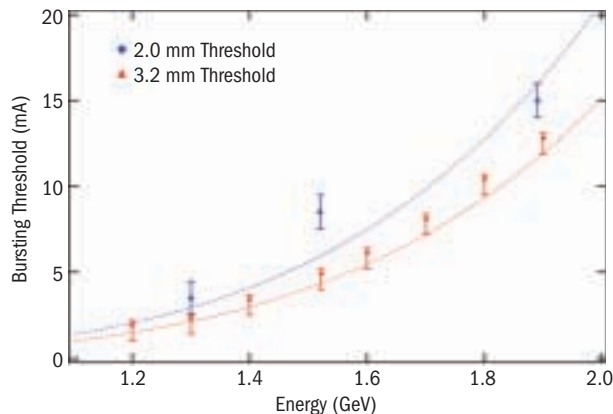


**FIGURE 4** Comparison of the measured microbunching instability threshold as a function of electron beam energy with that predicted by a model (lines) for wavelengths of 2.0 and 3.2 mm. The comparison shows good agreement between the two.

achievable in the ALS, we measured a 700-fold enhancement in the power of the CSR emission over the normal incoherent radiation. However, the bursting nature of the signal presents a challenge for its use as a source of CSR.

To compare our results with a model recently developed elsewhere, we measured the bursting threshold as a function of electron beam energy. The results are shown in Figure 4. The points with error bars indicate the experimental data, while the lines show the theoretical threshold calculated for nominal ALS parameters. The data show good agreement with the model. We believe we have a good understanding of this instability and can use the model to predict the performance of future storage rings, particularly sources of CSR.

#### INVESTIGATORS

J.M. Byrd (ALS and University of California, Davis); W.P. Leemans and B. Marcelis (Berkeley Lab); A. Loftsdottir (Berkeley Lab and University of California, Davis); and M.C. Martin, W.R. McKinney, F. Sannibale, T. Scarvie, and C. Steier (ALS).

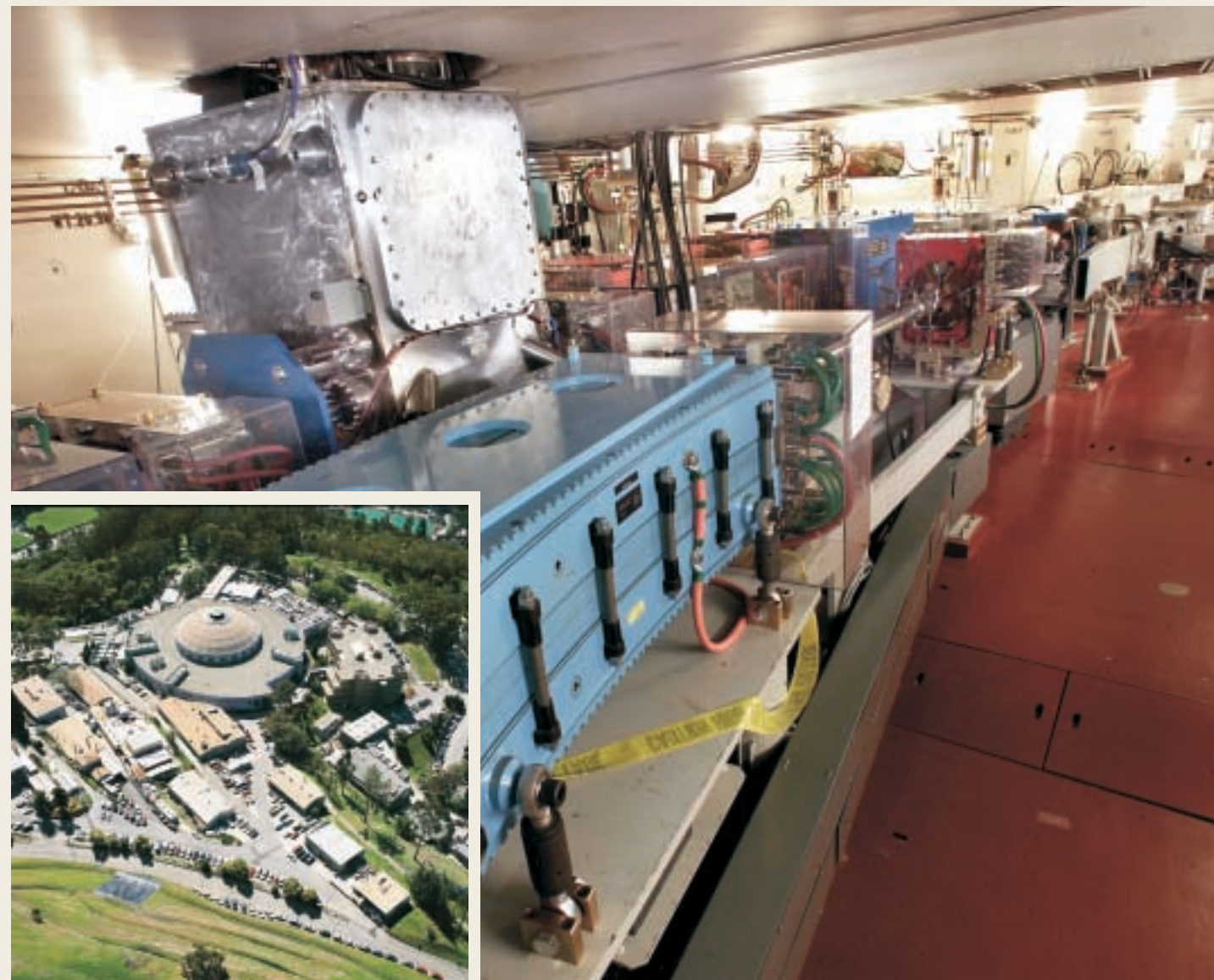
#### FUNDING

U.S. Department of Energy, Office of Basic Energy Science, and Berkeley Lab Laboratory Directed Research and Development.

#### PUBLICATIONS

1. J.M. Byrd et al., "Observation of broadband self-amplified spontaneous coherent terahertz synchrotron radiation in a storage ring," *Phys. Rev. Lett.* **89**, 224801 (2002).

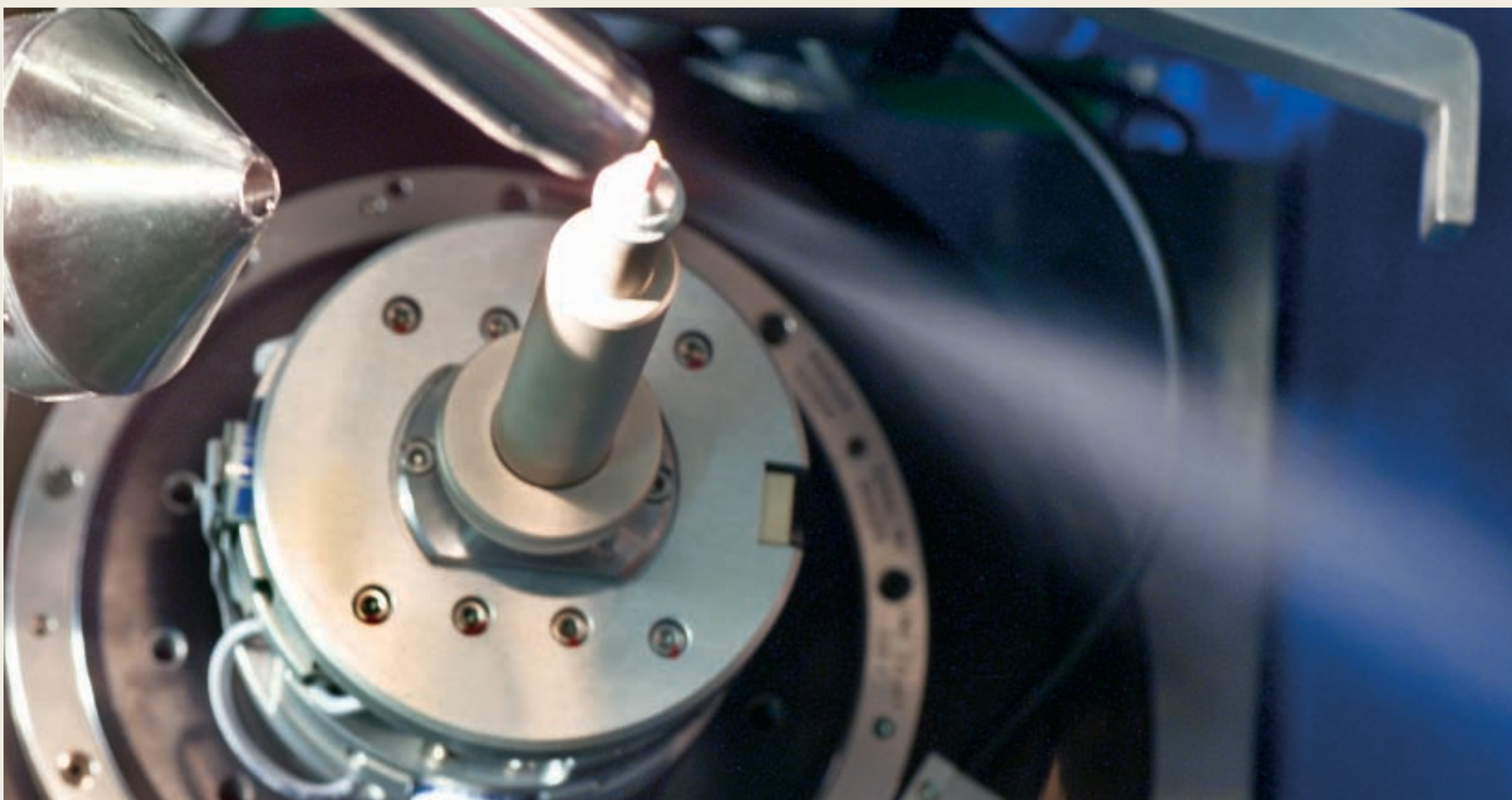
# FACILITY REPORT



Keeping the Advanced Light Source running smoothly requires the efforts of many minds and many hands. In this section, the leaders of the various teams responsible for making the facility available to its users discuss the year's work. The largest of these, Operations, is responsible for day-to-day running and optimization of the accelerators, while the Accelerator Physics Group works to develop the accelerator systems in order to meet the changing needs of the user community. The Experimental Systems Group engages in the design and construction of new beamlines and advocacy for new projects. The Scientific Support Group helps researchers using ALS beamlines through scientific and technical collaboration and outreach. All of these groups work closely with ALS engineering, whose work is so integral to their efforts that a separate engineering report would be redundant. The User Services Group supports the users through administrative services, logistics, and technical information.

# STRUCTURAL BIOLOGY HITS HIGH GEAR

NEW BEAMLINES DOUBLE CRYSTALLOGRAPHY OPPORTUNITIES

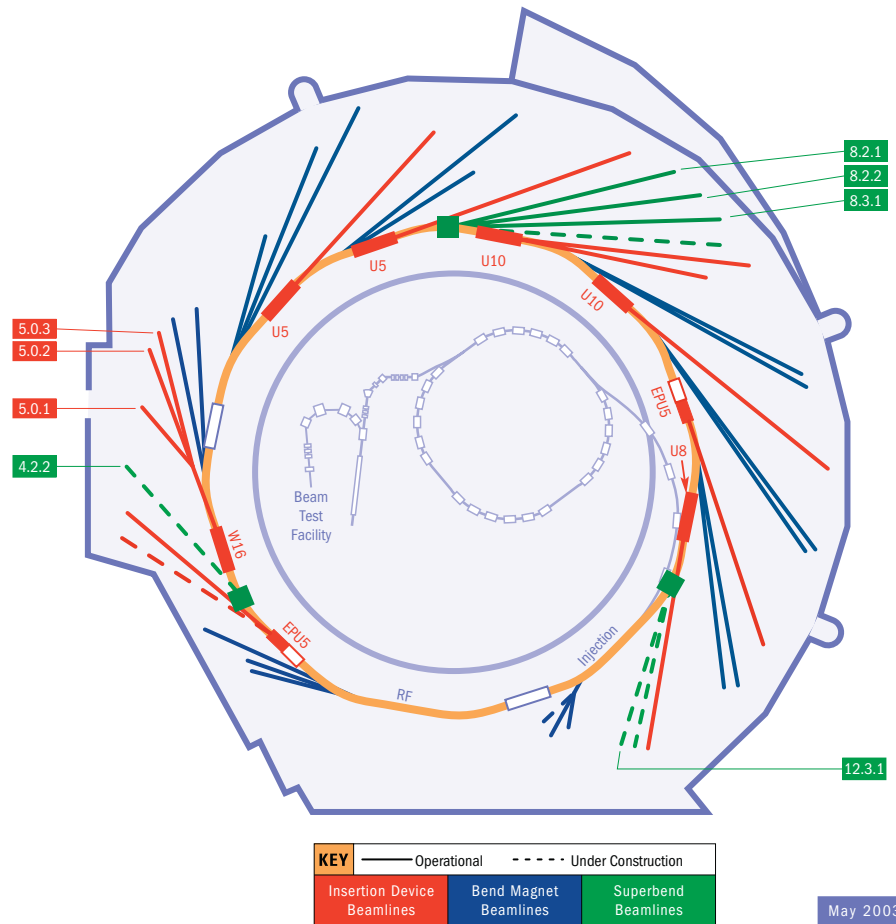


Question: What's a better way to grow a user community than starting up a new beamline? Answer: Starting up three new beamlines. The end of 2001 and the beginning of 2002 saw the Berkeley Center for Structural Biology (BCSB) and the ALS Experimental Systems Group (ESG) work together with the ALS engineering groups to pull off that very hat trick, doubling the number of beamlines available for protein crystallography studies at the ALS. Even before the first of the three new superbend beamlines became operational, crystallographers accounted for nearly a quarter of the ALS user community. In 2002, that fraction jumped to more than one third. As the new beamlines get up to speed, the numbers of scientists using the light source to determine crystal structures are likely to go through the ALS's famous domed roof, and two more beamlines are on the way.

The BCSB is currently responsible for the user programs on six operating ALS beamlines. The first three beamlines were constructed in Sector 5 to take advantage of the hard x-ray light from the ALS's wiggler. Beamlines 5.0.1 and 5.0.3 enable monochromatic crystallography studies, while Beamline 5.0.2 is optimized for multiwavelength anomalous diffraction (MAD) phasing. Endstations in Sector 5 are all equipped with robotic automounters to speed sample throughput.

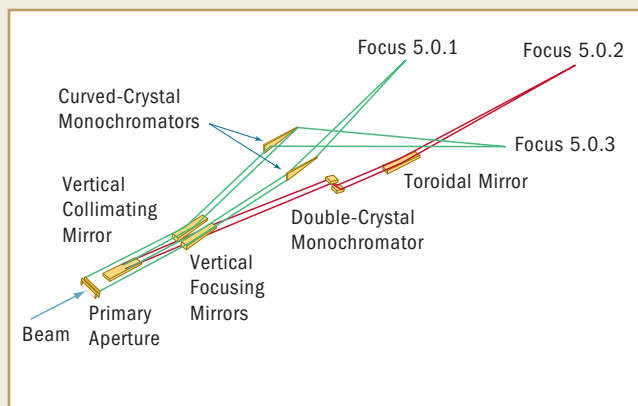
With the addition of superbends to the ALS magnet lattice (a challenge whose history is featured in the 2001 ALS Activity Report), a group of new crystallography beamlines has sprouted up in Sector 8. The superbends have proven to be an excellent source of hard x-rays for both MAD and monochromatic work. The Sector-8 lines are also distinctive in that their endstations are ensconced in "minihutches." These narrow enclosures allow easy sample mounting through a large sliding window. Beamlines 8.2.1 and 8.2.2 were built by the ALS for the Howard Hughes Medical Institute, and Beamline 8.3.1, for a collaboration between UC Berkeley, UC San Francisco, Plexikon, the Alberta Synchrotron Institute, and the M.D. Anderson Cancer Research Center.

On the horizon are two more superbend beamlines, one in Sector 12 and the other in Sector 4. Beamline 12.3.1, created for the SIBYLS (Structurally Integrated Biology for Life Sciences) project, will be optimized for small-molecule biological

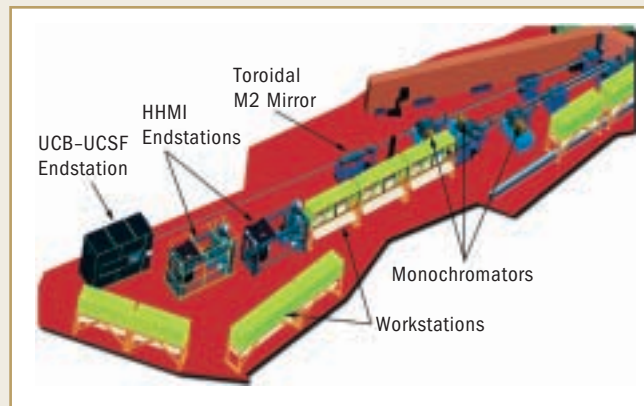


## PROTEIN CRYSTALLOGRAPHY BEAMLINES AND AVAILABLE TECHNIQUES

BEAMLINE	MONOCHROMATIC PROTEIN CRYSTALLOGRAPHY	MULTIPLE-WAVELENGTH ANOMALOUS DIFFRACTION (MAD)	SMALL-ANGLE X-RAY SCATTERING (SAXS)
4.2.2	✓	✓	
5.0.1	✓		
5.0.2	✓	✓	
5.0.3	✓		
8.2.1	✓	✓	
8.2.2	✓	✓	
8.3.1	✓	✓	
12.3.1	✓	✓	✓



Optical layout of Sector-5 beamlines.



Overall layout of Sectors 8.2 and 8.3 showing the three new protein crystallography beamlines and their corresponding endstations.

crystallography. The goal of its collaborators, headed by John Tainer of the Scripps Research Institute and Priscilla Cooper of the Berkeley Lab Life Sciences Division, is insight into DNA repair mechanisms and genome integrity. This beamline's capabilities include single-crystal diffraction with MAD phasing and small-angle x-ray scattering (SAXS). Beamline 4.2.2 will specialize in MAD and monochromatic protein crystallography. The primary research team for the latter beamline is the Molecular Biology Consortium, a group of crystallographers from 16 academic institutions across the United States. Both new beamlines are expected to begin operation in the summer of 2003.

The idea of doing crystallography at the ALS began to solidify in late 1993, when Thomas Earnest, now head of the BCSB, and Howard Padmore, head of ESG, put heads together. Their collaboration led to a white paper that convinced Laboratory Director Charles Shank to contribute \$500,000 in University of California Directed Research and Development funding to build a wiggler. This success, in addition to funding from the Department of Energy's Office of Biological and Environmental Research (OBER) for biological support facilities, provided the momentum needed to fund crystallography beamlines. In response to a 1994 proposal, OBER provided \$4 million for the design and construction of Beamline 5.0.2. Industrial partners and other academic institutions, ultimately including Roche Bioscience, UC Berkeley, Amgen, Syrrx, and the Genomics Institute of the Novartis Research Foundation (GNF), soon began funding the rest of Sector 5, which became known as the Macromolecular Crystallography Facility. Both the wiggler and the support facilities were in place by the end of 1996, and Beamline 5.0.2 began serving users in 1997.



The minihutch endstation on Beamline 8.2.2 is easily accessible through a sliding window.

## Cranking Out Crystal Structures

“Crystals in, structures out.” That’s how BCSB Head Thomas Earnest envisions the future of crystallography at the ALS. Once all its beamlines are built, BCSB will rely primarily on improvements in automation for increases in throughput. Earnest hopes to tap into the possibilities of robotics, advanced software, and artificial intelligence to make crystallography faster and more straightforward.

BCSB’s most recent foray into the world of robotics is represented by the High-Throughput Nanovolume Crystallization Robot, developed in conjunction with Scripps Research Institute, GNF, the University of Illinois at Chicago, and Syrrx, Inc. This robot speeds the most time-consuming and difficult step in preparing a sample for structure determination—crystallization. Its ability to automate and vastly accelerate the process won it a 2002 R&D 100 Award.

Another significant robotic development was the “robohutch,” the automounting system now employed on all three Sector-5 beamlines. It was developed as a collaboration between BCSB, Berkeley Lab’s Bioinstrumentation Group, Syrrx, and GNF, with additional funding from the National



The Structural Biology Support Facilities, which overlook the ALS experiment hall, include this electron paramagnetic resonance spectrometer.

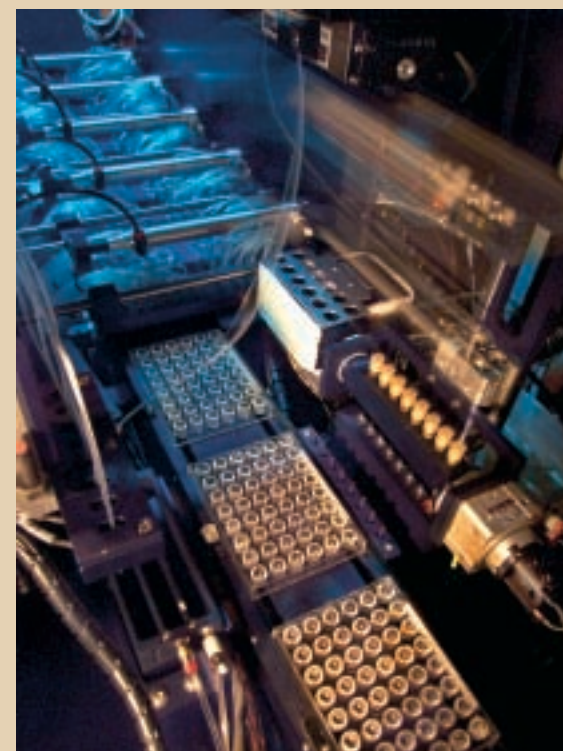
The MCF quickly became oversubscribed as crystallographers realized that the ALS’s stability and very low emittance were ideal for high-energy-resolution multiwavelength studies. Earnest says that he expected much more interest than anyone else, but even he was surprised by the reality. Growth in the crystallography field itself further fueled the influx, as the biotech literature reported more and more structures, more and more of which were obtained at synchrotrons.

To address the clear need for more crystallography facilities, the Experimental Systems Group began studying the feasibility of using superbends as sources for protein crystallography. Working with the research groups of Tom Alber, James Berger, and Robert Glaeser of UC Berkeley, they set up a temporary crystallography endstation on Beamline 7.3.3 to study the capabilities of bend-magnet sources. By solving a few initial structures on a regular bend magnet, measuring radiation damage, and modeling the probable outcomes with a superbend, they showed that the superbend sources would provide at least as much useful flux as a wiggler. Thus, it was no accident that the first research team to commit to a superbend beamline at the ALS (The UC Berkeley structural biology group at Beamline 8.3.1) consisted of crystallographers.

Padmore recalls how hard the ESG scientists and engineers worked to come up with a new brightness-preserving design for Beamline 8.3.1. Their

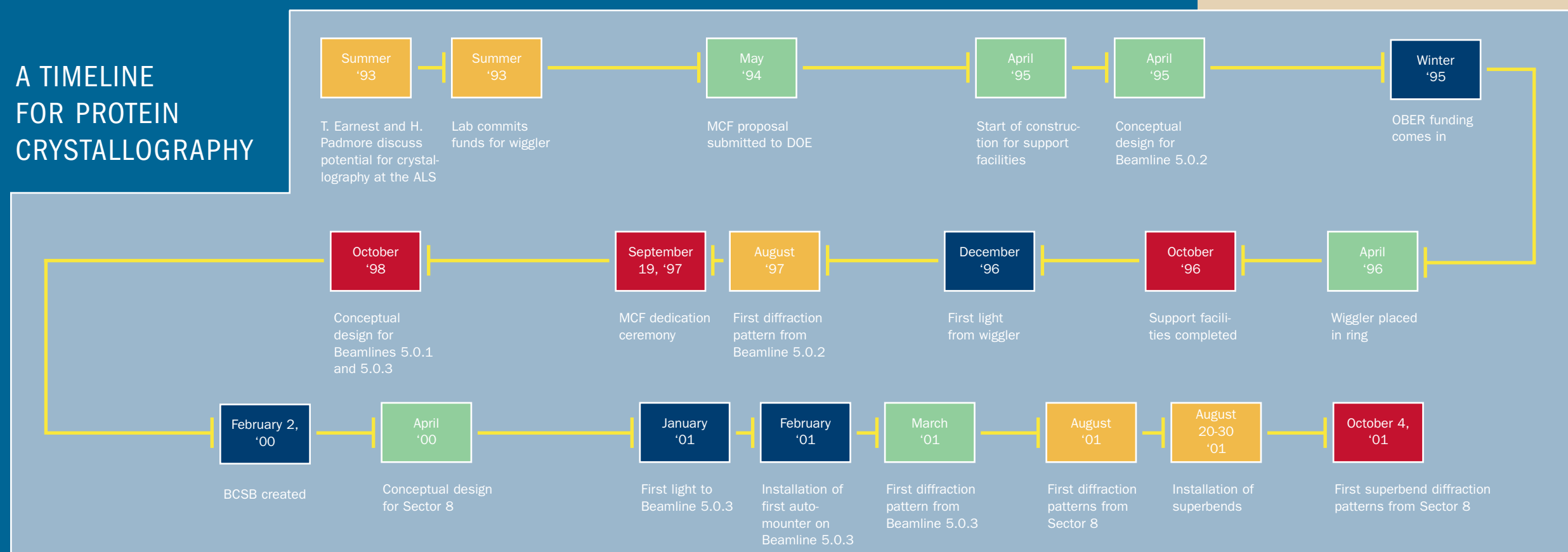
Institute of General Medical Sciences. The robohutches have reduced the ten to twenty minutes normally spent mounting and aligning a sample to about ten seconds. BCSB is now helping researchers at the National Synchrotron Light Source and the Cornell High-Energy Synchrotron Source install similar devices.

The automounter system will eventually become much more powerful, as it is coupled with advanced software being developed by another PBD group, the Computational Crystallography Initiative (CCI). In collaboration with scientists at the University of Cambridge, Los Alamos National Laboratory, and Texas A&M University, CCI is working to create the next generation of crystallography software, known as PHENIX (Python-based Hierarchical Environment for Integrated Xtallography). Current crystallography software analyzes a set of crystals and gives a strategy for taking data. PHENIX will take crystallography software into the realm of artificial intelligence. Besides strategizing, it will evaluate crystallographic data while it is being collected, adjust the experimental setup as needed, and eventually decide when it has enough data to calculate the structure. The scientist will no longer be burdened with the technicalities of taking data and will be better able to focus on the science the data reveals.



The protein crystallization robot can screen 480 different crystal growth solutions at once.

## A TIMELINE FOR PROTEIN CRYSTALLOGRAPHY





The wiggler that serves as the photon source for Sector 5 was installed in April 1996.

design sealed the case for the technical feasibility of a superbend-based crystallography beamline. It also served as the prototype for the other beamlines that soon followed.

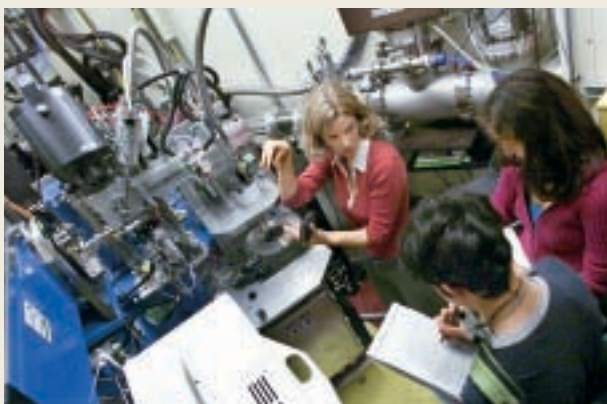
In February 2000, while the superbends were under construction, the BCSB was established within the Berkeley Lab Physical Biosciences Division to take overall responsibility for operation of crystallography beamlines at the ALS. The center handles administration, beamline maintenance, and scientific and technical support for structural biology users. (The proposal submission process is handled by the ALS User Services Office.) Soon after the new center opened, Beamline 5.0.3 came on line. Beamline 5.0.1 followed in April 2001.

With the installation of superbends in late 2001 and the new superbend beamlines getting into gear in 2002, the BCSB and the ALS have been preparing to handle even more growth in the protein crystallography user community. The focus is on smoothing the process of solving a structure. One approach is the use of robotics and advanced software to automate the taking of crystallographic data (see Cranking out Crystal Structures). Another approach is streamlining the proposal process, which now allows bimonthly reviews instead of the traditional twice-or-thrice-a-year cycle of a synchrotron. With the current system, a scientist can be taking data as soon as a month and a half after submitting a proposal.

Once the current crop of new beamlines is up and running, it may seem that the facility's rapid growth will come to an end. Not so, says Earnest. His optimistic eye sees plenty of room to increase throughput via automation and smart management. "We'll put our effort toward making what we have better."



Ribbon-cutting for MCF dedication, September 19, 1997. *Left to right*, researcher Sung-Hou Kim, then-ALS Director Brian Kincaid, Michelle Broido of the DOE office of Biological and Environmental Research, Deputy Berkeley Lab Director Pier Oddone, and then-MCF Director Thomas Earnest.



Researcher Mhairi Donohoe demonstrates the workings of an auto-mounter robot to a tour group.

# OPERATIONS

Ben Feinberg, Division Deputy for Operations

## Operations and Availability

The mission for the ALS is “Support users in doing outstanding science.” The most fundamental support offered to users by the ALS is delivery of high-quality beam. Such beams delivered according to a published schedule along with an efficient, effective safety program allow our researchers to make maximum use of their limited beam time. In 2002, the ALS once again maintained its exemplary operations record while making continuing improvements in beam quality and reliability. In addition, the Operations groups worked with ESG and BCSB staff to construct and install two new superconducting-bend-magnet (superbend) beamlines for protein crystallography to greatly expand the capacity of the program in hard x rays, and one new bend-magnet beamline for small-molecule crystallography.

The research community at the ALS has become accustomed to high operational efficiency and reliability, and it was not disappointed during this period. As shown in Figure 1, the ALS delivered beam to the users about 93% of the time scheduled for user operations in FY02, approximately maintaining the availability of the last several years.

As in years past, we look very carefully at our different systems to determine where to focus our resources to improve reliability. Figure 2 shows our “lost user beam analysis” over the past several years. These figures allow us to pinpoint the most frequent causes of lost user beam time. As a result of the 2002 analysis, we are planning

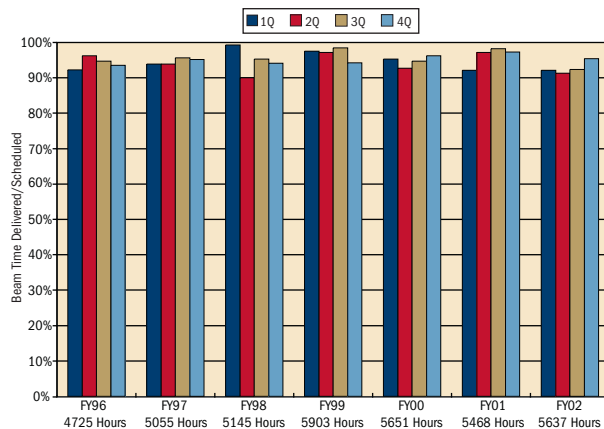


**FIGURE 1** ALS operational availability (percentage of scheduled user beam time actually delivered).

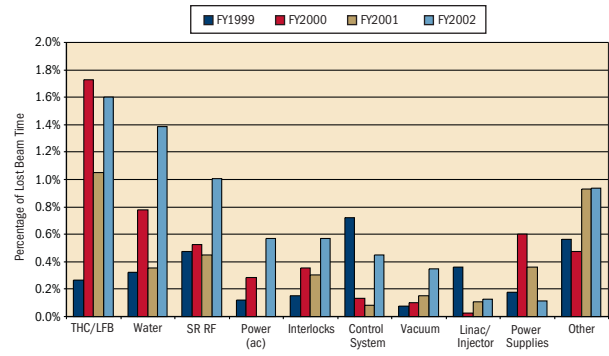


**FIGURE 2** Lost user beam analysis. The bars represent the percentage of user beam time lost over the last four fiscal years, separating out the various machine systems responsible. THC/LBF = third harmonic cavities/longitudinal feedback; SR RF = storage-ring rf power.

improvements in the third-harmonic cavity and water systems to improve reliability. We may also make changes in the storage-ring rf system, to reduce the probability of false beam trips.

## Changes in User and Instrument Hours

The monthly operations schedule continued to include a minimal number of maintenance and installation periods, which has been our practice for the last several years. This has provided the maximum number of hours for user operations while allowing for needed maintenance and installation of new instrumentation. In addition to these monthly periods, this year we had one five-week installation shutdown to install the new undulator and chicane for the Molecular Environmental Sciences (MES) beamline, to install higher-order-mode (HOM) dampers in the main rf

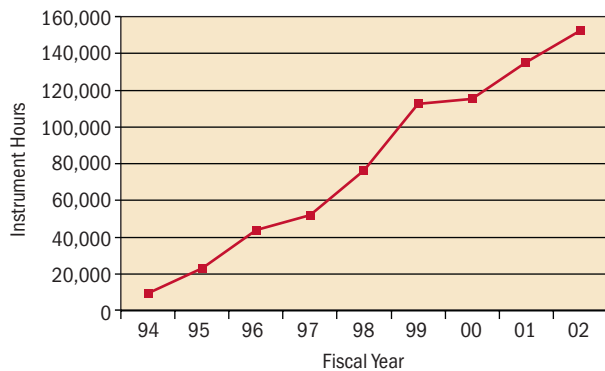


**FIGURE 3** Growth in the number of instrument hours (user hours multiplied by the number of simultaneously running beamlines) from year to year.

cavities, to align the storage ring, and to replace the superbend magnet cryocoolers. The delivered operating hours remained constant in FY02.

With the constant number of operating hours and the installation of new beamlines, we were able to increase the number of instrument hours (user hours multiplied by the number of simultaneous beamlines that can accept beam). We finished the fiscal year with 30 beamlines operating simultaneously, up from 27 at the end of the previous fiscal year. Figure 3 shows the growth of instrument hours since the first full year of ALS operations. The growth this year resulted in the delivery of 152,143 instrument hours, an increase of 12% over FY01.

## Facility Growth

In April, during our one major shutdown for the year, we installed the insertion device for the MES beamline and the chicane magnet that allows us to place a second insertion device in the same straight section. The MES beamline was commissioned just after the end of the fiscal year. In addition, three new crystallography beamlines, two on superbends, were commissioned, as described above. These new beamlines have enhanced our capacity in the hard x-ray region and opened up a major new capability for MES research within the core region of the ALS spectrum.

# ACCELERATOR PHYSICS

David Robin, Accelerator Physics Group Leader

Christoph Steier and John Byrd, Accelerator Physics Group

## Introduction

To achieve the goal of supporting users in doing outstanding science, the ALS Accelerator Physics Group (Figure 1) plays several important roles. The first is to make certain that the ALS provides high-quality beam in a reliable manner to its users. The second is to strive to understand and continually improve the performance of the facility, keeping it at the forefront of synchrotron radiation sources. The third role is to ensure that machine upgrades are implemented smoothly, minimizing any adverse impact to users. The fourth is to study potential upgrades to the facility that will enhance the ALS's capabilities and capacities. In all these roles, the Accelerator Physics Group works very closely with other groups both within the ALS and elsewhere at Berkeley Lab.

In 2001, the ALS storage ring went through a major transition with the installation of the superbends. In 2002, there was no modification as large as that of the superbends, but steady and significant gains were realized in understanding and improving the performance of the ALS



**FIGURE 1** ALS Accelerator Physics Group: left to right, Christoph Steier, Fernando Sannibale, Weishi Wan, Tom Scarvie, Hiroshi Nishimura, Steve Lidia, David Robin, Warren Byrne, and John Byrd.

storage ring. Also, much effort was directed at future projects and upgrades of the facility, particularly for the generation of femtosecond x rays and far-infrared radiation.

With regard to the first of the group's four roles, there was much effort focused on monitoring the performance of the ALS. This was the first full year of operation with the superbends, and we paid particular attention to the impact on accelerator downtime resulting from superbend subsystems. We are pleased to report that in 2002 the downtime resulting from superbend subsystems was a small percentage of the overall downtime.

In 2002, the ALS continued to improve the quality of beam that was delivered to users. In particular there were significant improvements in stability, both in orbit and in beam size. There were three improvements that factored into better orbit stability. The first was the installation of new chicane magnets. The second was the inclusion of additional stable, high-resolution beam-position monitors (BPMs) around the center bend magnets. The third was a set of improvements in the orbit feedback. These efforts are part of a long series of improvements over the years that have resulted in ever increasing orbit stability. We now will elaborate on the impact of the new chicane magnets.

Chicane magnets have several functions. The primary function is to enable two devices to occupy one straight section with independent beamlines by introducing a closed-orbit bump (chicane) into a straight section. This is done with three magnets, as shown in Figure 2. The central chicane bends the beam by about 2.5 mrad. The second function of the chicane magnets is to act as fast horizontal and vertical corrector magnets, compensating for orbit disturbances caused by the insertion devices. Since the effect of the insertion devices on the orbit is very predictable, the correction can be done with a feed-forward algorithm—provided that the correctors have sufficiently small hysteresis.

Long Straight – One 4.5-Meter ID



Chicaned Straight – Two 2-Meter IDs



**FIGURE 2** Comparison of a straight section with one insertion device (top) versus a straight section with two insertion devices and three chicane magnets (in red).

Specifically, the hysteresis of the magnets should be less than 1 Gauss-cm.

The first set of chicane magnets was installed in 1998 in Straight 4, which contains an elliptical polarization undulator (EPU). The chicanes were iron-core magnets, and unfortunately they had larger than acceptable hysteresis. Therefore they could not be used in a feed-forward correction, so the correction was done with other, lower-hysteresis corrector magnets located at the end of the straight section. With this solution, the orbit distortion outside the straight section was acceptably small when the EPU shifted polarization. For the beamlines inside the chicane, however, there were angular variations of up to 10  $\mu$ rad. These angular variations resulted in energy variations in the emitted spectrum.

To solve this problem, a new, low-hysteresis chicane magnet based on a novel design was constructed. The magnet was designed and built by the ALS Magnetics R&D/Analysis unit. Figure 3 shows a drawing of the magnet. Instead of an iron-dominated magnet, the new chicane consists of permanent-magnet cylinders and air-core coils, effectively decoupling the chicane-inducing and orbit-correcting functions of the magnet. The coils can be rotated to gradually adjust the chicane angle from 0 mrad to more than 2.5 mrad. Once in position, the coils provide the fast orbit correction. The result is a magnet with extremely small hysteresis. Now the insertion devices can shift from left to right circular polarization with less than 1  $\mu$ rad angular distortion. This past year, two new chicanes were installed in the two chicaned straight sections (Straights 4 and 11).

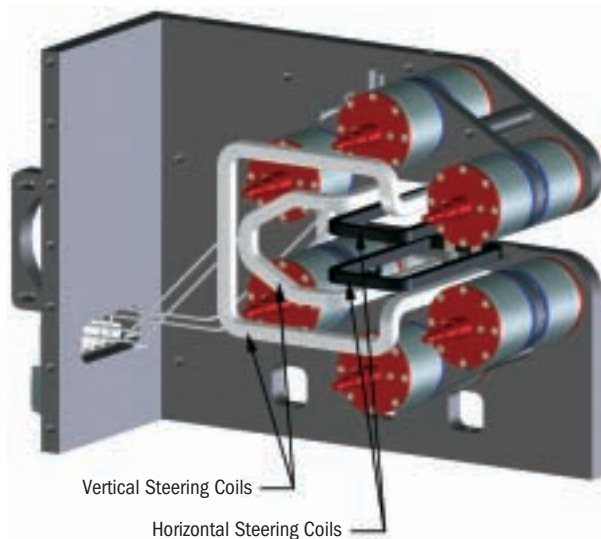


**FIGURE 3** Low-hysteresis chicane magnet for use in straight sections with elliptical polarization undulators.

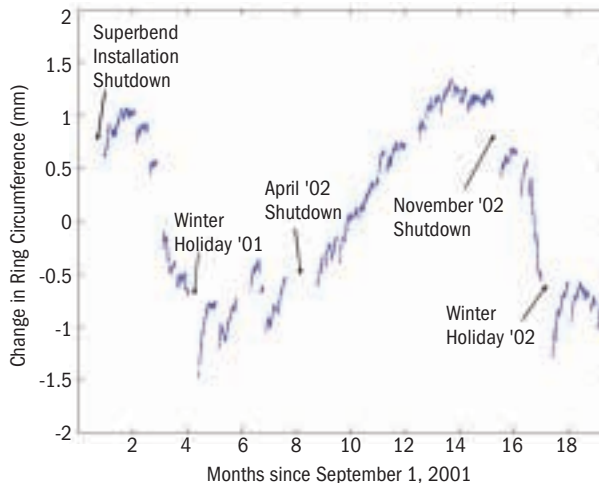


**FIGURE 4** Changes in ring circumference over 19 months from September 2001 to March 2003.

Also, 2002 was the first full year in which rf frequency feedback was routinely included in the orbit feedback program. The orbit feedback now compensates changes in the ring circumference by adjusting the rf frequency. Changes in the ring circumference are determined by monitoring changes in the orbit as measured in BPMs located in regions of dispersion. Then the rf frequency is adjusted to keep the orbit stable.

Figure 4 shows how the ring circumference has changed since rf frequency feedback was implemented in October 2001. What can be seen in the figure is that there are substantial circumference variations. Some of the variations are seasonal and are due to temperature and groundwater levels. These changes correspond to a variation of about 3 millimeters over the year, and the variation appears to be cyclic. For instance, the ALS circumference changes rapidly when the rainy season begins in November (months 3 and 15 in the figure). There are also changes that occur on faster time scales, such as changes in the thermal load corresponding to the three daily fills.

Several other improvements in the orbit stability were realized in 2002. Of particular note was the inclusion of stable, high-resolution BPMs surrounding the central bend magnets in Sectors 7 and 11. The orbit feedback system was then expanded to include these BPMs. The result was a marked improvement in the orbit stability in the beamlines emanating from those bend magnets. This year, there is a plan to include high-resolution BPMs around each center bend magnet.

Another area where the ALS realized significant improvement last year was in vertical beam size control and stability.

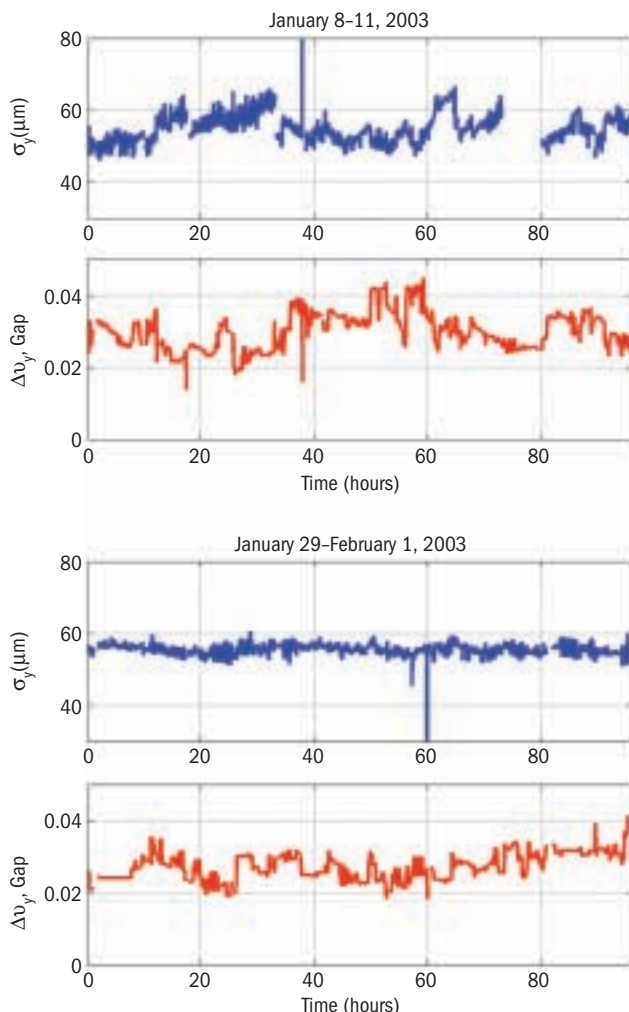


**FIGURE 5** Change in vertical beam size over two run periods of four days each in January 2003. By using a vertical dispersion wave to control the vertical beam size, the sensitivity of the beam size to insertion-device motion was clearly reduced.

Before 2002, the vertical beam size was controlled by a series of skew quadrupoles, all powered by a single power supply to excite the linear coupling resonance. Using this skew quadrupole “family,” we increased the beam size so that the vertical emittance was 2% of the horizontal emittance, thus making the beam lifetime longer. The increase in vertical emittance resulted in the beam decaying from 400 mA to 200 mA in 8 hours. This scheme for controlling the vertical emittance had several undesirable features, however, the first being that exciting the coupling resonance made the vertical beam size very sensitive to changes in the machine conditions. In particular, there was up to 25% variation in the vertical beam size when one of the EUs shifted from left to right circular polarization at minimum gap. The second undesirable effect was that, with only a few “families” of skew quadrupoles, it was not possible to reduce the emittance coupling below 0.5%.

In 2002, new skew quadrupole power supplies were purchased and attached to 18 of the 48 skew quadrupole magnets in the storage ring. These individual skew quadrupole power supplies were installed for several reasons. The first was to locally generate a large vertical dispersion bump in Straight 6 for the femtosecond x-ray R&D effort (discussed below). In addition, these new skew knobs opened the possibility of controlling the vertical emittance in a better way. Using these skew quadrupole families, it was possible to reduce the coupling and vertical dispersion in the ring, allowing the ALS to achieve an emittance coupling as low as 0.1%. It also allows us to increase the vertical emittance by increasing the vertical dispersion while keeping the coupling small. Using vertical dispersion rather than coupling to increase the beam size makes the vertical beam size less sensitive to changes in machine conditions. Figure 5 shows a plot of the vertical beam size for two typical weeks—the first week with the coupling control and the second with the dispersion control. As the comparison shows, there is substantial improvement in the beam size stability with vertical dispersion control.

## The Femtosecond X-Ray R&D Effort: Using an Insertion Device to Generate Bright Femtosecond X-Ray Pulses for Spectroscopy

Based on an idea by Sasha Zholents and Max Zolotarev of the Berkeley Lab Center for Beam Physics, an innovative technique has been developed at the ALS to generate short pulses of x rays with durations of a few hundred femtoseconds. This technique uses the interaction of an electron bunch with a femtosecond laser beam within a wiggler to energy-modulate (slice) a short section of that bunch. By using spatial or angular dispersion downstream of the interaction with the laser, one can then isolate femtosecond x-ray pulses. Over the past years, a scientific case has been developed to make use of this new source of x rays. The proposed experiments make use of time-resolved spectroscopic techniques (x-ray absorption spectroscopy) and require a higher average photon flux than can be delivered by the bending-magnet beamlines on which the slicing technique was pioneered.

To increase the average flux of femtosecond x rays, a new femtosecond x-ray R&D effort has been funded by the Department of Energy, and the x-ray source and beamline

are now in the design phase. They consist of several key components, including two new insertion devices for Straights 5 (modulator) and 6 (radiator), a new undulator beamline (Beamline 6.0.1), a new laser system with a significantly higher repetition rate, and modifications to the storage ring to create the vertical dispersion bump used to spatially separate the sliced electrons and photons. One of the new insertion devices is a new wiggler for Straight 5 (protein crystallography), which will have a shorter period (11.4 cm) than the existing wiggler (16 cm) to allow for optimized, simultaneous use for both protein crystallography and slicing experiments. The second insertion device will be an in-vacuum, permanent-magnet undulator similar to the ones used at SPring8 in Japan, the European Synchrotron Radiation Facility, and the Swiss Light Source.

The accelerator physics efforts to support the femtosecond x-ray R&D effort have been centered on three main areas: generating the vertical dispersion bump to provide the spatial separation to isolate the femtosecond x-ray pulses, minimizing the vertical emittance and unwanted dispersion, and studying insertion-device issues.

Figure 6 shows the vertical dispersion bump, a closed bump with negligible coupling, which is generated by using four skew-quadrupole magnets. The main issue we have studied in connection with the dispersion bump is its

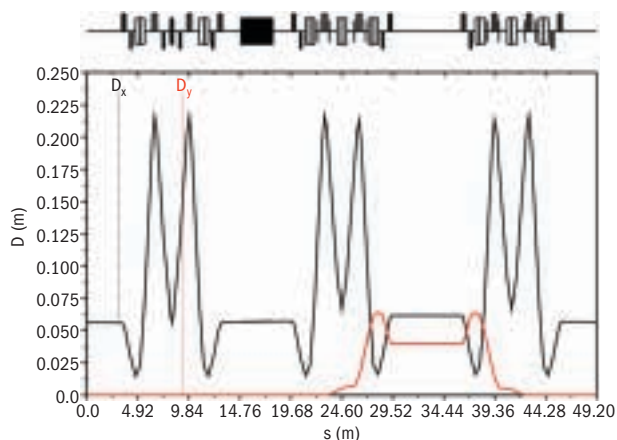


**FIGURE 6** Plot of the horizontal ( $D_x$ ) and vertical ( $D_y$ ) dispersion functions in Sectors 4, 5 and 6 of the ALS. Four skew-quadrupole magnets are used to generate a closed vertical-dispersion bump by transferring horizontal dispersion into the vertical plane.

impact on the nonlinear dynamics of the ALS, particularly injection efficiency and lifetime. A dispersion bump of sufficient amplitude for the femtosecond x-ray R&D effort has been demonstrated experimentally.

Minimizing the vertical emittance and spurious dispersion allows us to maximize the brightness of a synchrotron radiation source. Because the Touschek lifetime (how long electrons survive in the ring before they are lost to intra-bunch scattering) of a low-emittance, low-energy light source like the ALS is very short, reducing the vertical emittance below the current operational value of about 150 pm-rad would reduce the lifetime to unacceptable values (shorter than 8 hours at 400 mA). In the future, this situation will change with the use of top-up operation (essentially continuous injection). The radiator for the femtosecond x-ray R&D effort, on the other hand, will directly create vertical emittance because of the fairly strong insertion device inside the vertical dispersion bump. Therefore, it will be important to minimize the baseline vertical emittance outside the dispersion bump. Using 18 individual skew-quadrupole magnets, whose power supplies were installed last year, we have demonstrated vertical emittances below 10 pm-rad (an improvement of a factor of 15 compared to the current operating condition). This will allow the femtosecond x-ray R&D effort to operate with the vertical dispersion bump at an optimized size, maximizing the femtosecond x-ray signal-to-noise ratio obtainable while still making a high brightness (low vertical emittance) available to all other beamlines.

The issues studied in connection with the two insertion devices include—to name just a few examples—their effect on the nonlinear dynamics (using a new numerical integration technique, a symplectic integrator developed by Ying Wu and Etienne Forest), resistive wall heating effects, impedance issues, and the effects caused by the field imperfections of the devices (coupling, focusing, and orbit errors). Working together with the ALS Magnetics R&D/Analysis unit, we developed a set of specifications and a magnetic design for the new wiggler that minimize all detrimental impacts on the electron beam. This wiggler is now under construction and will be exchanged for the present wiggler in 2004. For the in-vacuum undulator, the studies are in their final phase.

## Installation of Higher-Order-Mode Dampers in the Main rf Cavities

The ALS operates with 400 mA of beam distributed in up to 328 bunches. Coupling of the motion of individual bunches through resonances excited in higher-order modes (HOMs) in the two rf cavities in the ring can lead to beam instabilities, significantly reducing the beam quality. The instabilities are currently controlled by broadband feedback systems. Although the ALS pioneered the use of such feedback systems, the system required continuous adjustment to combat the instabilities driven by higher-order modes in the main rf cavities. To improve the reliability of this system, a team led by Slawomir Kwiatkowski of the ALS Electrical Engineering Group designed and inserted a water-cooled antenna into each of the cavities via an available port to couple to the unwanted modes, reducing their effective strength. The effective damping provided is illustrated in Figure 7, which shows the longitudinal coupling impedance before and after the installation of the dampers. The strongest HOM (TM011) was reduced by 2.5 orders of magnitude, removing the need for careful tuning of the cavity via its temperature to avoid resonances.

Although the procedure was relatively simple, the process required careful engineering and testing because the rf system is so vital to operation of the ALS. Commissioning of this system was successful and has resulted in a marked improvement in beam stability. Experience in the design of the damping antennae has led to the design of similar damping antennae, which will be installed in the third-harmonic rf system in April 2003.

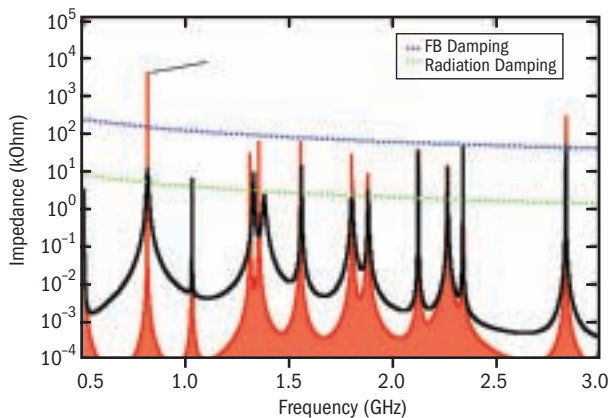


**FIGURE 7** Longitudinal coupling impedance before (red) and after (black) the installation of higher-order-mode dampers in the ALS's main rf cavities. The damping of the longitudinal feedback system and the natural radiation damping are shown for reference.

## CIRCE: a Dedicated Coherent Far-Infrared Ring at the ALS

Synchrotron radiation becomes coherent when the electron bunch length is smaller than the wavelength being emitted. In this regime, the radiating fields of individual electrons add in phase, producing an intensity that scales with the square of the number of electrons instead of linearly, as is the case for the more familiar synchrotron emission. For the last two years, an ALS group led by John Byrd, Michael Martin of the Scientific Support Group, and Fernando Sannibale has been exploring the virtues of a small ring dedicated to the production of coherent far-infrared, or terahertz, radiation. Feasibility studies have demonstrated that such a machine is ready to be constructed. Specifically, the ALS team, in collaboration with researchers from the Thomas Jefferson National Accelerator Facility, has experimentally demonstrated that coherent terahertz emission produces very high powers. In collaboration with researchers from BESSY II, the group has also experimentally verified the regime of stability for coherent emission in a storage ring and performed the first scientific experiment with coherent synchrotron radiation (CSR) in a ring, measuring for the first time the Josephson plasma frequency in the high-temperature superconductor  $\text{Bi}_2\text{Sr}_2\text{CaCu}_2\text{O}_8$ .

The new knowledge of the physics underlying CSR in a storage ring has allowed the design of CIRCE (Coherent

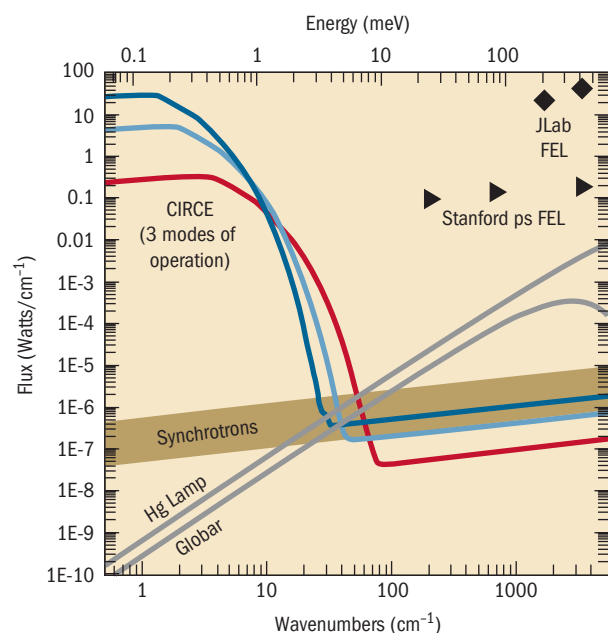


**FIGURE 8** Calculated fluxes expected from the CIRCE infrared ring compared to those from existing sources.

InfraRed Center), a storage ring optimized for terahertz CSR production. We anticipate that CIRCE will be a revolutionary source for a traditionally difficult spectral region at the border between optics and electronics—namely, the “terahertz gap.” The calculated flux for the CIRCE source, compared to those of other sources, is shown in Figure 8. The many-orders-of-magnitude increase in far-IR intensity is the basis of the project and will enable new kinds of science.

The idea of a ring-based CSR source was proposed for the first time by Jim Murphy of Brookhaven National Laboratory about ten years ago, but stable CSR in a ring was observed for the first time only recently, at BESSY II. With a special machine setup incompatible with standard user operation, a gain in flux of about four orders of magnitude was obtained. The ALS CIRCE team recently led collaborative studies with researchers from BESSY II and the Stanford Linear Accelerator Center that have provided a good understanding of the CSR mechanism. The key effect is the interaction of the electron beam with its own radiation. The benefit of this interaction is a self-focusing of the beam, resulting in a stable distortion of the bunch distribution. This distortion gives a sharp edge to the bunch, which emits coherently at significantly shorter wavelengths and shorter pulse lengths than an undistorted Gaussian bunch (see Figure 9). At higher currents, this self-interaction can result in amplification of small modulations in the bunch, causing quasi-chaotic bursts of CSR in a process very similar to that of self-amplified spontaneous emission. As already mentioned, both of these regimes have been experimentally demonstrated, and CIRCE is optimized to exploit the distortion benefits and to produce CSR in the stable region of emission.

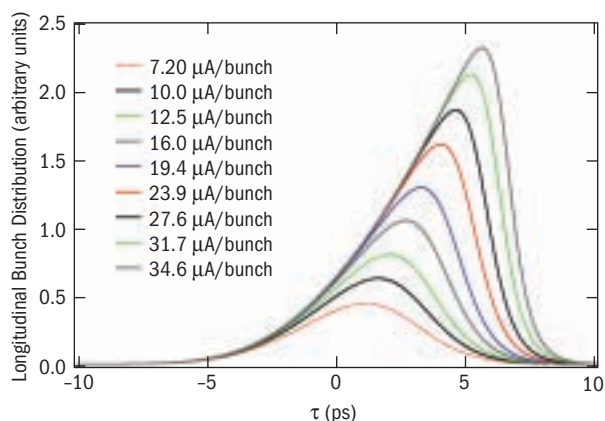


**FIGURE 9** “Distorted” longitudinal bunch distributions as a function of the current per bunch (simulation of the BESSY II case of coherent emission).

Most synchrotron light sources require a large floor space outside the main ring to accommodate long x-ray beamlines. Infrared beamlines, however, require relatively little space and are best located as close to the source as possible. Given the layout of the ALS facility, the ideal location for an IR ring is on top of the booster shielding, as shown in Figure 10. A detailed preliminary design and evaluation have been done, resulting in a 66-meter-circumference ring that fits on the existing booster shielding. Full-energy injection to the ring can be done from the ALS booster without interfering with injection to the main ALS ring, even during continuous top-up operation. The use of the ALS injector as well as existing ALS utilities and general infrastructure has allowed us to design an extremely cost-effective project. The optimized electron-beam energy is 600 MeV with a 1.5-GHz rf system. Nominal bunch lengths of 1–3 ps can be achieved with a combination of high-frequency rf and a modest reduction in the lattice momentum compaction (the relative change in beam energy with changes in rf frequency). The optimization of CIRCE for the terahertz region includes enhanced photon-beam stability and vacuum chambers with very large apertures (140 mrad vertical by 300 mrad horizontal) for the best possible acceptance of the large-divergence coherent terahertz synchrotron radiation.

For additional information about CIRCE, please visit the Web site at [infrared.als.lbl.gov/CIRCE/](http://infrared.als.lbl.gov/CIRCE/).

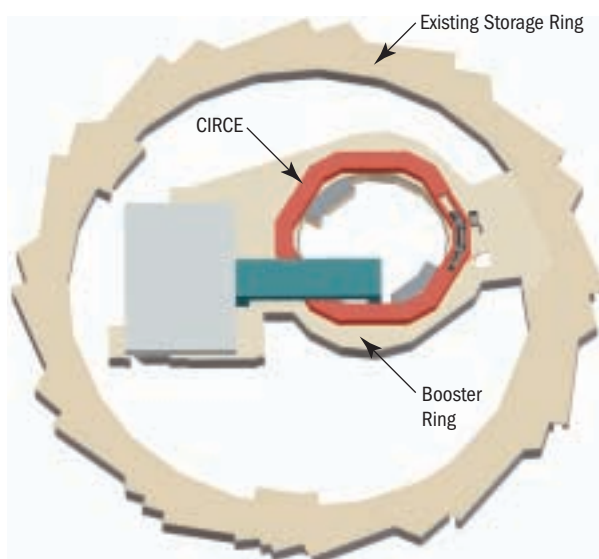


**FIGURE 10** The CIRCE ring, as it will sit atop the ALS booster.

# EXPERIMENTAL SYSTEMS

Howard Padmore, Experimental Systems Group Leader

## Introduction

The roles of the Experimental Systems Group (Figure 1) can be split into several categories: (1) to design and build beamlines and endstations based on the demands of the user program, (2) to conduct forefront research in science and instrumentation that will push the boundaries of the application of synchrotron radiation techniques, and (3) to give support to existing user programs, usually in areas of high technical complexity. Approximately 50% of the group's activity is in this latter area of direct user support. In this short report, I will give several examples of work in the two former areas.



**FIGURE 1** Experimental Systems Group: *left to right*, Jim Patel, James Glossinger, Wayne McKinney, Kathy Opachich, Phil Heimann, Sirine Fakra, Jun Feng, Steve Irick, Jinghua Hao, Alastair MacDowell, Donnacha Lowney, Tony Young, Everett Harvey, Peter Schmid, Malcolm Howells, Rich Celestre, Hendrik Ohldag, Simon Clark, Howard Padmore, Matthew Marcus, Andrew Doran, Sander Caldwell, Hwa Shik Youn, Jamie Nasiatka, Nobumichi Tamura, Andreas Scholl, Ernie Glover, Tony Warwick, Marsha Fenner, and Andrew Franck.

## Photoemission Electron Microscopy (PEEM)

### PEEM2

In 2002, ESG members characterized the resolution of the second-generation photoemission electron microscope (PEEM2) in terms of the image contrast as a function of object spatial frequency. Various test patterns were made to measure contrast, from star patterns of the type shown in Figure 2 to sets of linear arrays with different periodicities. These were made at the Center for X-Ray Optics at Berkeley Lab by Weilun Chao and Erik Anderson with the Nanowriter electron-beam writing machine. The patterns consist of alternating nickel and photoresist lines. The star pattern was used to make gross adjustments of focus and astigmatism, square arrays were used to measure distortion and field curvature, and linear arrays were used to measure the modulation transfer function (MTF). This work was led by Andrew Doran.

Jun Feng calculated the theoretical MTF by starting with a statistical ensemble of electrons occupying position, angle, and energy space; modeling the electrostatic fields in PEEM2; and then tracing the electrons' paths through the potential, taking into account the precise angle–energy filtering action of the objective lens's back-focal-plane

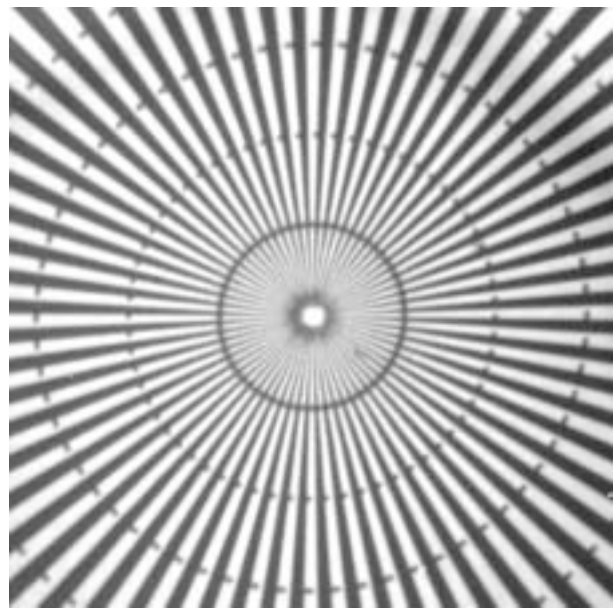


**FIGURE 2** Star test pattern imaged in the PEEM2 photoemission electron microscope. The inner circle encloses 100-nm lines and spaces.

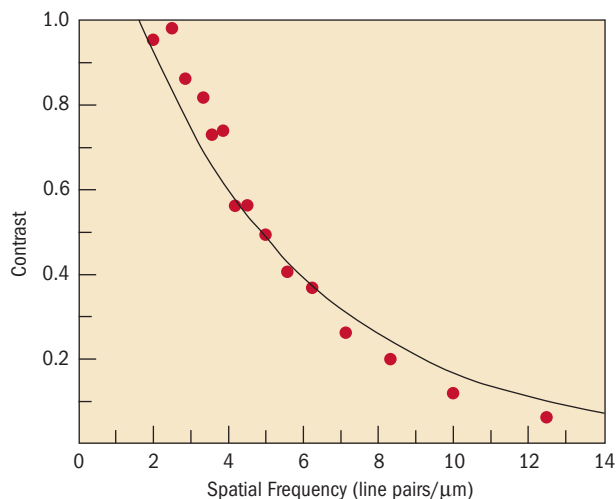


**FIGURE 3** Modulation transfer function for the PEEM2 microscope for a 20-kV extraction field and a 12.5- $\mu\text{m}$ -diameter back-focal-plane aperture. The dots show measurements; the line shows the calculation. The 50% MTF corresponds to a 1/2-period resolution of 100 nm and a Rayleigh-limit resolution of around 45 nm.

aperture. This was done for many combinations of extraction field and back-focal-plane aperture size. The results for one combination are shown in Figure 3, and we can see excellent agreement between theory and measurement. The good agreement means that we can successfully predict the contrast for specific experiments (for example, nanoparticle imaging at a size scale far less than the resolution), we can monitor the performance of the microscope over time, and we have the basis for a good comparison with the future performance of the PEEM3 aberration-corrected microscope. It also means that we can be reasonably assured that the complex modeling involved in this work is on solid ground and can be used for predicting the performance of the microscope in other conditions.

Fundamental magnetization processes occur on a time scale of picoseconds and a length scale of nanometers. While such processes are beyond the scope of what we can study now, a future combination of aberration correction and pulsed sources (such as the proposed LUX facility) should make measurements in this spatial-temporal domain possible. In the meantime, we can still access interesting processes, albeit on a time scale of 100 ps and a spatial scale of 50 nm. While laser-based magnetic microscopy has been used to study picosecond dynamics, the x-ray PEEM technique offers 10 times better spatial resolution with parallel imaging and, through dichroism techniques, the ability to sort out the magnetic state of complex, multielement coupled systems.

In a Laboratory Directed Research and Development-funded program headed by Andreas Scholl, with a team consisting of Sug-Bong Choe, Yves Acremann, Andrew Doran, and Andreas Bauer, a prototype pump-probe magnetization experiment has been successfully carried out. In this experiment, a conductive loop to provide a magnetic field impulse is driven by a pulse of current from a laser-excited GaAs switch. All components sit on the same GaAs substrate. The loop itself is made of a  $\text{Co}_{90}\text{Fe}_{10}$  soft magnetic material. The current pulse leads to an in-plane radial field at the loop of several hundred oersteds and an out-of-plane field at the center of the loop. Figure 4 shows the loop before excitation, at excitation, and more than a nanosecond after excitation. Before excitation, the magnetization state is defined by a ripple structure that results from pixellation in the digitally generated shape of the loop. Under excitation, the magnetization is saturated, leading to an image where the loop is bright at the bottom (because the magnetization and the helicity of the circularly polarized light are parallel) and black at the top (where the magnetization is reversed). Some 1.45 ns later, the magnetization has relaxed to the former ripple state.

Such measurements are done with the ALS operating in single-bunch mode, and images are integrated over millions of shots. It is therefore critical in these experiments that the system return to the magnetic ground state after each shot. Cross-correlation studies show a system time resolution of 150 ps. Although looking at the magnetization dynamics of a simple ferromagnetic system is far from new, we are now in a position for the first time to look at more interesting cases involving coupled magnetic systems that are of fundamental interest and have been completely inaccessible to traditional techniques.

### PEEM3

While PEEM2 has produced a great deal of pioneering science and through the development of time-resolved

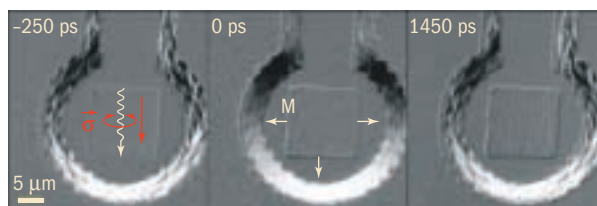


**FIGURE 4** Time-resolved PEEM images of a cobalt microcoil in its unmagnetized state (*left*), fully saturated after a short current pulse (250 ps later), and returned to its magnetic ground state (1.45 ns later).

capabilities is set to continue in this path, the microscope is fundamentally limited in terms of spatial resolution and throughput. In addition, the PEEM2 bend-magnet beamline, 7.3.1.1, is limited in terms of flux density, polarization control, and spectral resolution. The PEEM3 project brings together a state-of-the-art, high-resolution undulator-based beamline and an aberration-corrected photoemission microscope. The beamline is under construction in Sector 11 and is due for commissioning in summer 2004. The beamline project team is led by Tony Warwick.

The undulator will be a now-standard 5-cm-period elliptical polarization undulator (EPU5). Straight 11 is chicaned, with the molecular environmental science (MES) EPU5 in the downstream location. The PEEM3 EPU5 will be in the upstream location. The beamline mechanics will largely be based on those of the MES beamline (Beamline 11.0.2).

The PEEM3 beamline diverges radically from the MES beamline in its optical system. Because dichroism experiments call for extreme spectral stability, we have devised a new optical system based on the Hettrick–Underwood–style converging-beam, variable-line-spacing (VLS) concept. We have added the ability to measure the photon energy in real time by monitoring the spatial position of the zero-order light beam. These measurements can provide extremely accurate values for photon energy, or they can be used as feedback to correct the grating position, maintaining a defined photon energy to sub-meV resolution. The optical system comprises the following components: a horizontally deflecting sagittal cylinder to focus from the source to a vertically defining entrance slit, a converging-beam VLS monochromator, a horizontally deflecting elliptical mirror to provide a large degree of demagnification to the exit slit, an active exit slit that defines the monochromatic beam and monitors zero-order beam, and a refocusing and demagnifying elliptical Kirkpatrick–Baez mirror pair to focus to an image size of  $2 \times 2 \mu\text{m}$ . This matches our field size at high resolution; at lower resolution in the microscope, the Kirkpatrick–Baez pair is defocused to provide a larger field of illumination.

Figure 5 shows the expected flux from this beamline at a resolving power of 3000. In the transition-metal L-edge region, the flux should typically be around  $6 \times 10^{12}$  photons/s. This is more than an order of magnitude higher than the flux from the PEEM2 beamline and will be focused into a field size more than an order of magnitude smaller ( $3 \mu\text{m}$  in diameter). And of course, we will have complete control of the polarization.

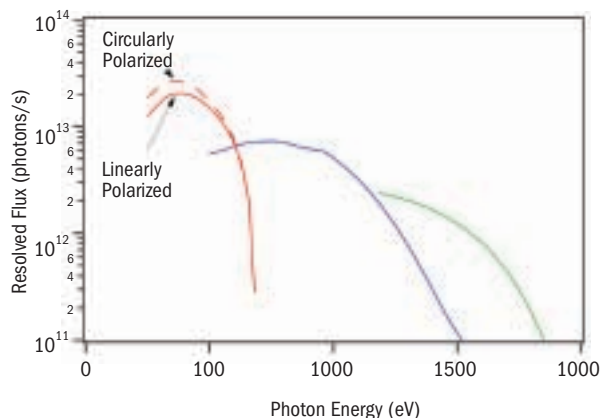


**FIGURE 5** Predicted resolved flux for (left to right) the first, third, and fifth harmonics of the PEEM3 beamline at a resolving power of 3000 for 250-, 500-, and 1000-lines/mm gratings, respectively.

The PEEM3 microscope is based on the successful concepts used in PEEM2 together with elements of the aberration-correction concepts introduced independently by Rempfer in the U.S. and Rose and colleagues in Germany and embodied in the SMART project at BESSY II. The chromatic and spherical aberrations introduced by the accelerating field between the sample and the objective lens and by all the electrostatic lenses together are compensated by the opposite aberrations of an electron mirror. Electrons are directed to and from the electron mirror by a double-focusing, dispersion-free separator magnet. The microscope is highly complex and has been the subject of detailed design over the last several years. The main electron optics simulation is now complete, and we have entered the engineering phase of the project. We expect that the system will enter electron optics commissioning in late summer 2004. We then anticipate an extensive period of adjustment and measurement before the first science experiments are performed.

The electron optics design and simulation is a collaboration between Jun Feng, Peter Schmid, Andreas Scholl, and Matthew Marcus in ESG; Weishi Wan and David Robin in the Accelerator Physics Group; Ross Schlueter in the ALS Magnetics R&D/Analysis unit; Etienne Forest of KEK; and Ying Wu, now at Duke University. The project manager is Alastair MacDowell, and the lead mechanical engineer is Rob Duarte, with support from Dawn Munson, Nicholas Kelez, and Karl Peterman in ALS engineering.

The performance of PEEM3, relative to the existing PEEM2 microscope, is summarized in Figure 6, where the predicted resolution is shown as a function of transmission.

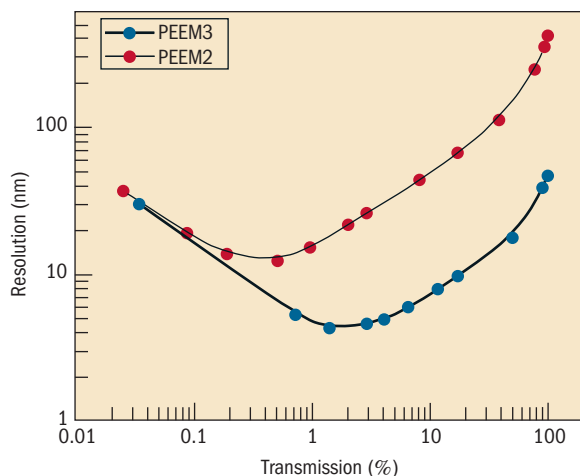


**FIGURE 6** Resolution as a function of throughput for the PEEM3 aberration-corrected photoemission electron microscope and the uncorrected PEEM2.

The latter is controlled by changing the back-focal-plane aperture size. PEEM2 typically operates at 3% transmission. At the resolution attained by PEEM2 with this value, PEEM3 will be 25 times as efficient in detecting electrons. Moreover, at 3% transmission, PEEM3 will be capable of a resolution around six times higher. This, in combination with more than an order of magnitude higher flux, three orders of magnitude higher flux density, and complete polarization control, will give us unprecedented performance for the study of complex magnetic systems.

## Molecular Environmental Science (MES)

The MES project consists of a new EPU5 undulator; an entrance-slitless, collimated-light plane-grating monochromator; a branch mirror; and two branchlines—one for a scanning transmission x-ray microscope (STXM) and one for a suite of spectroscopy endstations. David Shuh (Berkeley Lab Chemical Sciences Division) is the scientific leader of the project, and Tony Warwick is head of the technical implementation. Figure 7 shows a view along the completed beamline.

The monochromator is similar to that pioneered at BESSY II, but the beamline's mechanical system is entirely new. As the function of the beamline is to do soft x-ray spectroscopy and spectromicroscopy, the cleanliness of the optics is of critical concern, as are reproducibility and stability to enable robust user operation. For this reason, we decided to design a new type of mechanical system embodying all of the lessons we have learned on our existing spherical-grating and

plane-grating monochromators. Prime among these was recognition of the need to get cooling water into the monochromator without introducing any strain into the optical or mechanical components. This was achieved by placing the water feeds along the grating and premirror rotation lever arms. Another desired feature was easy and accurate grating changeover, which we accomplished by having the manufacturer ion etch the grating rulings into one substrate and by designing the entire monochromator to translate laterally. We also realized the need to make the whole system truly ultrahigh-vacuum compatible.

The system performs very well, and in initial testing it is meeting all its performance goals in terms of flux, resolution, spot size, stability, etc. Besides being largely cloned for the new PEEM3 beamline, the mechanical aspects of the system have already been adopted at the Canadian Light Source. The new STXM microscope, developed by Tony Warwick and Sirene Fakra at Beamline 7.0.1, has moved to Beamline 11.0.2 and has been recommissioned. With this new microscope, we have pioneered the use of a two-axis differential interferometer to encode the relative motions of the sample and zone plate, thus taking out much of the noise due to vibrations and stage nonlinearity that has plagued STXMs up to this point. The microscope was recommissioned with the help of Tolek Tyliczszak of the MES endstation team within the Berkeley Lab Chemical Sciences Division. The MES system, with new controls developed for the polymer STXM on bend-magnet Beamline 5.3.2, together with the flexibility and power of the EPU, the state-of-the-art beamline, the differential-interferometer-controlled STXM, and new software, defines a new level of performance for this type of instrument worldwide.



**FIGURE 7** The MES beamline (Beamline 11.0.2) is shown from its plane-grating monochromator through the branch mirror to the endstations for STXM (*lower*) and spectroscopy (*upper*). Beamline 10.3.2 is at the top, and beamline 11.3.1 is at the right-hand edge of the photo. The PEEM3 beamline will be located between the MES beamline and Beamline 10.3.2.

## Diffraction Imaging

To go beyond the limits of resolution imposed by x-ray microscopes with lenses, David Sayre (Stony Brook University) proposed many years ago that an image could be constructed from its coherent diffraction pattern alone, i.e., without a lens. This radical suggestion meant that the lost phase information had to be reconstructed in some way, and in later work with John Miao (Stony Brook University, now at Stanford Synchrotron Radiation Laboratory), he showed how this could be done. The trick is that, after assuming initially random phases, one mathematically transforms the diffraction data back and forth between Fourier and real space, applying constraints on the result before beginning each iteration.

This is very much an emerging area in optics, but until recent work at the ALS, it had always been necessary to have a low-resolution image of the object. In recent work led by Malcolm Howells and Heifeng He at the ALS, John Spence and Uwe Weierstall at Arizona State University, and Henry Chapman and Stefano Marchesini at Lawrence Livermore National Laboratory, images at a resolution of 12 nm have been constructed from the diffraction pattern alone with no prior knowledge of the object shape. Figure 8 shows the diffraction pattern from an array of 50-nm gold balls. Figure 9 shows an SEM image and an image constructed from the diffraction pattern. This spectacular work should now allow us to refine the experimental and

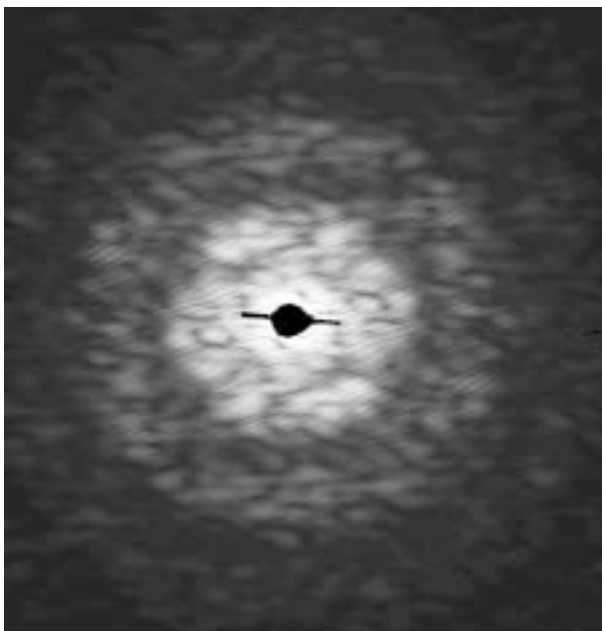


**FIGURE 8** Coherent diffraction pattern from an array of 50-nm gold balls

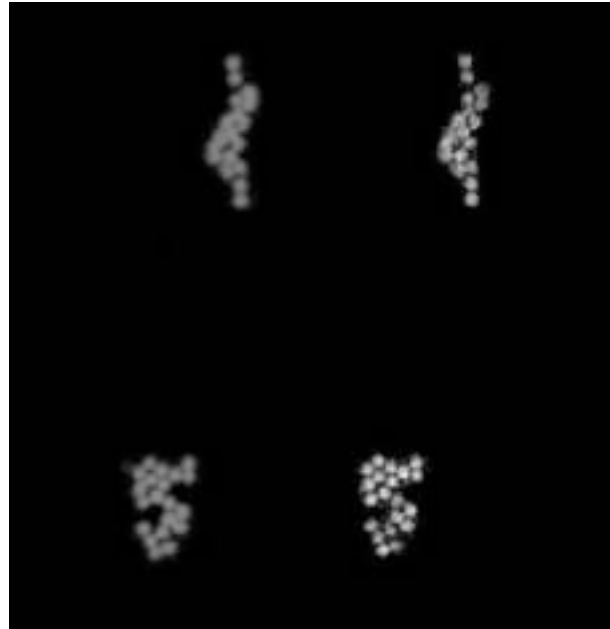


**FIGURE 9** Left, an SEM picture of the object in Figure 8 and, right, image constructed from the coherent diffraction pattern.

computational techniques and to define the limits of resolution imposed by the available coherent flux and radiation damage. It will also lead us to an understanding of the optimum wavelengths for particular experiments and the design of an optimum radiation source, beamline, and endstation.

## Development of the Femtosecond X-Ray Program

The femtosecond bending-magnet beamline, Beamline 5.3.1, has been used for a range of studies during the year using the ALS's normal 80-ps bunch length and streak-camera detection. Several of these are reported in the Compendium of User Abstracts. In the meantime, work has been ongoing to define the conditions required to generate femtosecond x-ray pulses at this beamline with the new femtosecond x-ray R&D effort, a laser slicing source (See Accelerator Physics, p. 83.)

With the current slicing source, the fast (200-fs) modulated x-ray beam is only kicked five standard deviations from the center of the beam on Beamline 5.3.1, and its intensity is less than 1/1000 of the intensity of a single normal x-ray pulse. We must therefore be very careful to ensure that background noise from optical aberrations or scattering is at a minimum. Measurements of mirror scattering have been made at several beamlines and compared to calculations of scattering based on optical measurements of the

mirror surface roughness. Through this work, we hope to be able to close the loop with optical vendors and define more accurate specifications for surface roughness as a function of spatial period. We have R&D contracts with two vendors at present to assess this approach.

Beamline 5.3.1 functions primarily to develop the techniques of subpicosecond spectroscopy and diffraction. In order to carry out a full scientific program, we have always recognized that much higher intensity will be required. Insertion-device Beamline 6.0.1 is being constructed as part of the femtosecond x-ray R&D effort to meet that need. Greater intensity will be gained by using a high-power insertion device, operating as an undulator in the few-keV range and a wiggler above that energy, and by using a higher repetition rate (40 KHz rather than 2 kHz). The latter requires a much higher power laser system.

The overall layout of the beamline is shown in Figure 10. Light from the source is focused inside the shield wall by a toroidal mirror, which directs the light to a high-speed chopper. As the 500-MHz light from the source is only used at the 40-KHz (maximum) repetition rate of the laser, the chopper can prevent a large fraction of the unused light from falling on the optics and on the sample. Immediately after the chopper, there is a space for sample placement and manipulation followed by a large grating spectrograph. The dispersed absorption spectrum can then be detected in the focal plane by an intensified, gated CCD. A miniature collimated-light crystal monochromator can also be translated into the beam between the chopper and the spectrograph

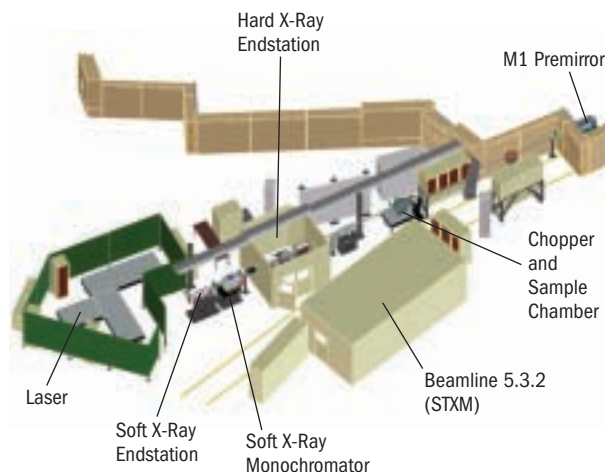


**FIGURE 10** Layout of the femtosecond undulator beamline at Straight 6.

to allow selection of x rays from 2 to 10 keV. In this case, experiments are done in a hutch. Also shown at the end of the beamline is the enclosure for the new high-power laser system. We are now entering the major engineering phase of this program, and we expect first beam in three years.

The scientific leader for this activity is Bob Schoenlein of the Berkeley Lab Materials Sciences Division, the machine aspects are led by Christoph Steier of the ALS Accelerator Physics Group, and the beamline aspects are led by Phil Heimann of ESG, all with support from ALS engineering.

## Other Ongoing Projects

Two beamlines are being built in parallel in superbend Sector 12, one for structural biology (Sibyls, Beamline 12.3.1) and one for high-pressure research (Beamline 12.2.2). These are now in the final stages of completion, with first light expected in summer and fall 2003, respectively. The designs are largely based on the successful Sector-8 protein crystallography systems, with two additions: lower-angle mirrors for the high-pressure beamline for higher-energy operation (to 40 keV) and a small-angle x-ray scattering station for the Sibyls beamline upstream of its protein crystallography station.

The water-cooled premirrors used in the Sector-8 protein crystallography beamlines did not meet specification. As a consequence, although the three beamlines have been highly successful with performances comparable to that of the high-power wiggler beamline (Beamline 5.0.2), the flux through a 0.1-mm collimator, in the normally used angular acceptance of 1.5 mrad, was a factor of 3 lower than expected on the 8.2 beamlines and a factor of 6 lower on Beamline 8.3.1. The premirror has now been replaced on Beamline 8.3.1, with a 3.5-fold increase in flux at the sample at 12.5 keV; we are now less than a factor of two from theory and at a performance level substantially greater than that of Beamline 5.0.2. The other premirrors will be replaced shortly.

Superbend Sector 8 will be full with the imminent completion of the tomography beamline (Beamline 8.3.2). This is a joint enterprise between Lawrence Livermore National Laboratory, UC San Francisco, the Berkeley Lab Earth

Sciences Division, and the ALS. It will have white-light, multilayer-filtered and crystal-filtered imaging capabilities and a 3D resolution down to 1  $\mu\text{m}$  for millimeter-scale objects. It is also designed for imaging centimeter-scale objects at a commensurately larger pixel size.

Following the very successful amalgamation of micro-powder diffraction for mineral phase identification into the microdiffraction station at Beamline 7.3.3, the same capability has been added to the micro-XAS station at Beamline 10.3.2. In each case, enormous gains can be realized by translating the existing beamlines to a super-bend source. We have assessed the complexity and cost

of this task and are working with user groups to raise the necessary funds.

Finally, we are also working closely with the user community in defining the proposed ALS upgrade, which would improve several existing beamlines and add several more through the use of chicaned straight sections. This gives us the opportunity to enhance capability by, for example, exchanging linearly polarized undulators for EPU's on existing beamlines, adding more capacity and offering higher performance by moving programs that now share beamlines onto beamlines specifically designed for them, and by adding entirely new capabilities.

# SCIENTIFIC SUPPORT

*Zahid Hussain, Scientific Support Group Leader*

*John Bozek, Scientific Support Group Deputy Leader*

## Introduction

The primary mission of the Scientific Support Group (SSG, Figure 1) is to support the efforts of researchers at the ALS through scientific and technical collaboration and scientific outreach. Working with the users, SSG plays an important role in developing novel instrumentation that enables cutting-edge science. Depending on the needs of the user, the degree of collaboration can range from technical assistance with the beamline to full partnership in developing new research programs.

## SCIENTIFIC OUTREACH

SSG strives to expand the scientific program of the ALS and broaden its user base through publications and presentations. The group organizes a variety of seminars, including the weekly ALS/CXRO Seminars in X-Ray Science and Technology and a targeted weekly lecture series addressing the Frontier of Synchrotron Radiation Science and Instrumentation. The group also organizes the quarterly ALS Colloquium.

Working together with the Users' Executive Committee, SSG also helps to organize workshops exploring new scientific opportunities and needs for new beamlines or experimental facilities. Six such workshops were held during the 2002 ALS Users' Meeting.

The ALS Doctoral Fellowship in Residence program, established in 2001, has been very popular among doctoral students and has been received with much appreciation. The Doctoral Fellowships enable students to acquire hands-on scientific training and develop professional maturity for independent research. More details are given on the ALS Web site ([www-als.lbl.gov/als/fellowships/](http://www-als.lbl.gov/als/fellowships/)). A selection committee consisting of Roger Falcone (chair, UEC), Zahid Hussain, Steve Kevan (Chair, Scientific Advisory Committee), Neville Smith, and Z.-X. Shen recommended the following recipients for doctoral fellowships in the physical sciences for academic year 2003 (Figure 2):

Alejandro Aguilar (University of Nevada, Reno;  
ion spectroscopy)



**FIGURE 1** Scientific Support Group members, *left to right: front row, Fred Schlachter, Jinghua Guo; second row, Yi-De Chuang (in plaid shirt), Cheryl Hauck, Daniel Rolles, Bill Bates, Zahid Hussain, Bruce Rude, Alexei Fedorov; back row, Glenn Ackerman, Michel Van Hove, Aran Guy, Hoon Koh, Jonathan Denlinger, Elke Arenholz, Gennadi Lebedev, Mike Martin, Edward J. Singley, John Bozek, Eli Rotenberg, Rudy Kimmerling, Joshua Turner.*

Andreas Augustsson (University of Uppsala, Sweden;  
ion spectroscopy)

Henry Chong (UC Berkeley, femtosecond x-ray spectroscopy with a slicing source)

David Edwards (Princeton University, molecular environmental science)

Daniel Rolles (Free University, Germany; atomic, molecular, and optical physics)

Zhe Sun (University of Colorado, angle-resolved photoemission spectroscopy)



**FIGURE 2** ALS Doctoral Fellows: *clockwise from left, David C. Edwards, Henry W. Chong, Daniel Rolles, Alejandro Aguilar, Andreas G. Augustsson, and Zhe Sun.*

## SUPPORT

Members of SSG are responsible for the operation, upgrade, and maintenance of most of the facility beamlines and many of the permanent endstations at the ALS. The undulator-based beamlines—4.0.2, 7.0.1, 8.0.1, 10.0.1, and a photoemission branchline on 12.0.1—each have about one to two SSG staff members responsible for their continued operation. SSG is also playing an active role in fixing some of the problems in the operation of the chemical dynamics complex (Beamline 9.0.2), which is operated by the Berkeley Lab Chemical Sciences Division under separate funding from BES. The year 2002 also saw the designing of several new experimental systems. Members of SSG are putting great emphasis on making the development of novel instrumentation more efficient and user friendly.

## MEMBER RESEARCH

Beyond their collaborative roles, staff scientists within SSG are expected to maintain scientific and technical excellence in areas of synchrotron radiation research. Participation in active scientific programs is essential for such development, and all of the SSG scientists are active members of research programs at the ALS.

## Advances in Infrared Research

### EXPERIMENTAL PROGRESS TOWARD A COHERENT SYNCHROTRON SOURCE

Mike Martin of SSG and Wayne McKinney of ESG have been working with accelerator physicists John Byrd and Fernando Sannibale in developing the scientific case and a plan for a high-power coherent synchrotron radiation (CSR) source in the terahertz range. Such a source could enable a number of new scientific research directions, including the study of low-energy phenomena in condensed matter systems; development of direct nondestructive imaging techniques for medical, technological, and security applications; studies of novel nonlinear regimes in materials; and ultrafast time-resolved studies of the dynamic properties of chemical reactions and correlated electron systems.

In October, two CSR workshops were convened by the ALS, one to discuss the scientific opportunities of such a revolutionary source and one to bring together accelerator physicists working to understand the detailed beam physics underlying CSR in storage rings. All of these experimental results are now being used with recently developed

modeling capabilities to determine optimized parameters for achieving stable high-power CSR in a storage-ring source.

In 2002, high-profile experiments brought the goal of a CSR source several steps closer to reality. See *Science Highlights*, p.68, and *Accelerator Physics*, p. 81, for more details about this research.

### SECOND IR MICROSCOPE FOR BEAMLINE 1.4

A second IR microscope and bench have recently been added to the Beamline 1.4 complex as Beamline 1.4.4. The FTIR bench is a Thermo Nicolet Nexus 870, which is capable of both rapid- and step-scan measurements. The IR microscope is a Thermo SpectraTech Continuum that has several new features not found on our Beamline 1.4.3 Nic-Plan instrument. This new microscope has a dichroic element that allows visualization of the sample even while acquiring data. This capability is very convenient, especially with the synchrotron source, because the focused visible-light spot from the synchrotron source can often be observed, indicating exactly where the beam is located on a sample. The optics in this microscope are infinity corrected, which allows the easy addition of several types of optics that can assist in visualizing a sample, including visual and IR polarizers, Nomarski differential interference contrast (DIC) optics, and UV fluorescence with four difference filter cubes. All of these will be available at ALS Beamline 1.4.4. This instrument was purchased through a DOE Office of Biological and Environmental Research grant to develop biological and environmental applications of synchrotron-based infrared spectromicroscopy.

We have conducted initial performance tests on the new microscope by temporarily installing it on the Beamline 1.4.2 photon port. Since the signal-to-noise ratio is a crucial parameter for good FTIR measurements, we measured this ratio for a series of 100% reflection lines on a gold-coated glass sample, comparing the performances of the synchrotron and the internal EverGlo thermal source as a function of aperture size (Figure 3).

Since the focused size of the thermal IR source is approximately  $100 \times 100 \mu\text{m}$ , closing down the aperture below this size simply reduces the total signal in proportion to the area reduction. The noise level becomes significantly worse as the aperture size is decreased, becoming essentially unusable at aperture sizes below  $20 \times 20 \mu\text{m}$ . The focused spot size of the synchrotron source ( $3\text{--}10 \mu\text{m}$  in diameter) is diffraction limited, however, so its

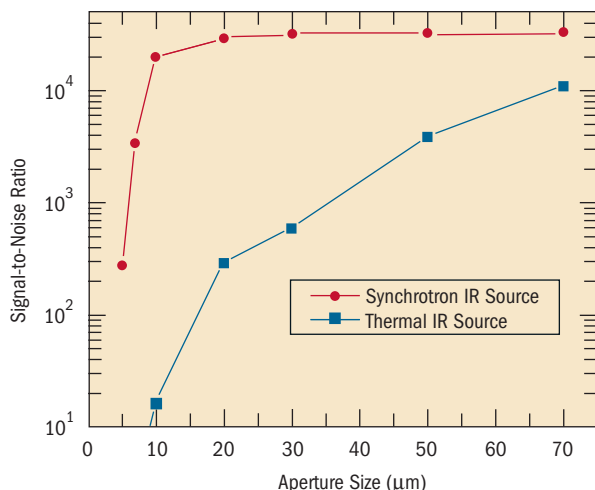


**FIGURE 3** Comparison of the measured signal-to-noise ratio at  $2500\text{ cm}^{-1}$  for the synchrotron and thermal EverGlo IR sources as a function of microscope aperture size. The ratio for the synchrotron source is more than 1000 times better for apertures 10 microns or smaller.

signal-to-noise ratio is only affected at aperture sizes close to the wavelength—smaller than  $10\text{ }\mu\text{m}$ . The synchrotron gives a better signal-to-noise ratio than the thermal IR source at all aperture sizes. For aperture sizes of  $10\text{ }\mu\text{m}$  and smaller, the synchrotron source's signal-to-noise ratio is more than 1000 times better than the thermal source. A usable signal is maintained even at the smallest aperture size available,  $5 \times 5\text{ }\mu\text{m}$ . These results validate the calculated brightness advantage of a synchrotron IR beamline over a conventional thermal IR source for mid-infrared spectromicroscopy.

The Continuum IR microscope and Nexus FTIR bench will be placed permanently on ALS Beamline 1.4.4 with the synchrotron beam cleverly split to feed both IR microscopes simultaneously without any loss of signal. This will be achieved by separately collimating the upstream and downstream ends of the bend-magnet radiation.

## Vector Magnetometry Endstation at Beamline 4.0.2

The newly developed vector magnetometry endstation has been installed at the magnetic spectroscopy and microscopy beamline, Beamline 4.0.2.

The endstation is based on an octupole magnet that surrounds a small vacuum chamber (see Figure 4). The magnet provides magnetic fields up to 0.9 T that can be applied in any direction relative to the incoming x-ray beam. In combination with the variable polarization capabilities of

the beamline (left and right circular as well as linear horizontal to vertical polarization are available), the new system provides a unique facility for magnetic materials research using magnetic dichroism in the soft x-ray range.

As a first demonstration, the magnetic circular and linear dichroism spectra at the iron  $L_{3,2}$  edges of a 40-nm-thick Terfenol film ( $\text{Tb}_{0.3}\text{Dy}_{0.7}\text{Fe}$ ) were measured in a transmission experiment (Figure 5). The magnetic circular dichroism spectrum was obtained with circularly polarized x rays by switching the magnetic field orientation between parallel ( $I_{\parallel}$ ) and antiparallel ( $I_{\perp}$ ) to the incoming x-ray beam for each photon energy. The magnetic linear dichroism spectra were obtained with linearly polarized radiation by switching the applied field from parallel ( $I_{\parallel}$ ) to perpendicular ( $I_{\perp}$ ) to the photon-beam polarization vector. Although the magnetic linear dichroism effect is small, it can be clearly observed with this setup.

With magnetic circular dichroism, the reversal of the magnetization vector can be studied in detail by choosing different angles of light incidence while keeping the relative orientation of the magnetic field and the sample fixed. As an example, the magnetization components  $M_x$ ,  $M_y$ , and  $M_z$  were determined for magnetic fields applied in the sample plane of the Terfenol film (Figure 5).

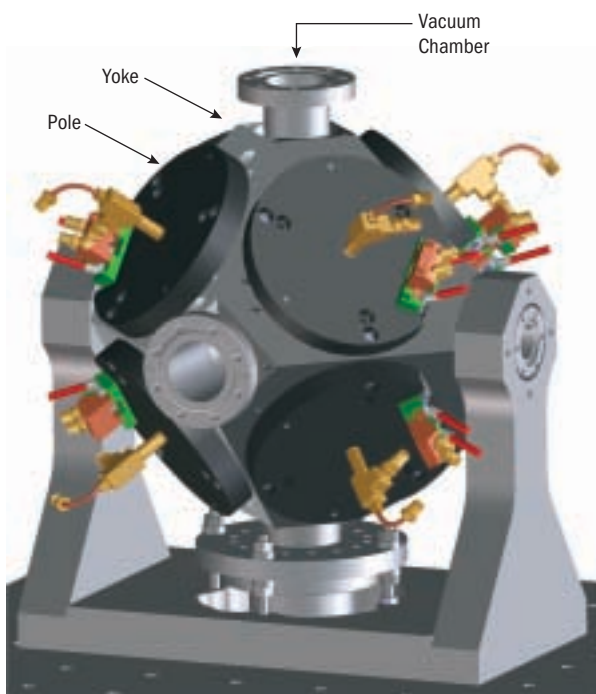


**FIGURE 4** The newly installed vector magnetometry endstation at beamline 4.0.2.

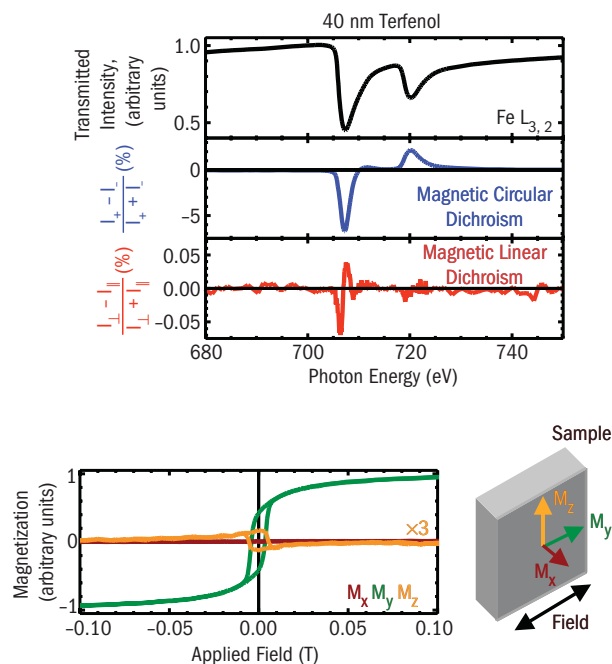


**FIGURE 5** Top, magnetic circular and linear dichroism measurements made at Beamline 4.0.2 for a Terfenol film. Bottom, magnetization components  $M_x$ ,  $M_y$ , and  $M_z$  for magnetic fields applied in the sample plane of the film.

## XPD Out, ESF In

Over the years, the ultrahigh-resolution electron spectroscopy for chemical analysis (UltraESCA) endstation at Beamline 7.0.1.2, also known as the x-ray photoelectron diffraction (XPD) endstation, has evolved from its original design as an angle-resolved core-level instrument into one mostly dedicated to valence-band measurements, with an emphasis on nanostructures grown in situ by molecular beam epitaxy (MBE). In the last year or so, we have brought on line new features to enhance the throughput and quality of experiments (Figure 6). The endstation is now known as the Electronic Structure Factory (ESF).

On the preparation side, we have implemented a new chamber for MBE growth and characterization (via a new low-energy electron diffraction [LEED] and ESCA system) with dedicated pumping and a new sample goniometer. On the analysis side, we implemented a new six-axis ( $x$ ,  $y$ ,  $z$ ,  $\theta$ ,  $\beta$ ,  $\phi$ ), removable sample stage capable of intermittent heating to 2500 K and routine cooling to 16 K (measured at the sample). The lowest temperature is expected to approach 10 K with a future upgrade of the radiation shielding. The  $\beta$  axis is a second polar axis perpendicular to the usual  $\theta$  polar axis. Numerous new scan modes for

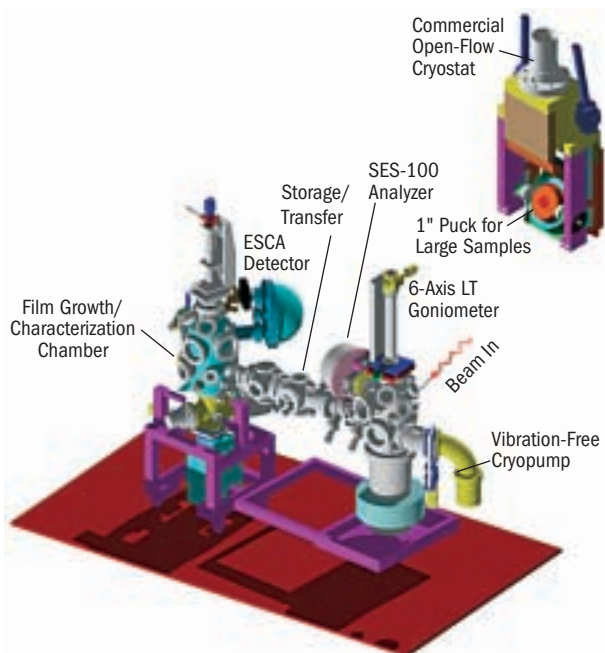


**FIGURE 6** The new Electronic Structure Factory (ESF) endstation configuration at Beamline 7.0.1. The overall system is designed for high-throughput sample growth and characterization without interference with the main analysis chamber. The prep chamber has a new sample goniometer with Mg  $K\alpha$  ESCA, LEED, a crystal monitor, and sputtering. The storage chamber has room for about 10 samples, and the analysis chamber has a cryopump for better base pressure and (upper right) a new six-axis removable sample stage.

polarization dependence are enabled by the goniometer, and the acquisition and analysis software has been revamped to take advantage of the new features.

Figure 7 shows a two-polar-axis scan of the Fermi surface of 1.2 monolayers of indium on silicon (111) ( $\sqrt{7} \times \sqrt{3}$  reconstruction) taken around 40 K; the sharpest features are less than 0.16 degrees wide ( $\sim 0.01 \text{ \AA}^{-1}$  momentum resolution), and the systematic error due to imaging aberrations over a wide angle range is around  $0.02 \text{ \AA}^{-1}$ .

## Nanostructure Characterization Endstation

A new project at Beamline 8.0.1 headed by Franz Himpsel (University of Wisconsin–Madison) is the construction of a new endstation for the characterization of nanostructures by microprobe near-edge x-ray absorption fine structure (NEXAFS) with fluorescence detection. This bulk-sensitive, photon-in–photon-out spectroscopy enables the electronic structure measurement of insulators, dilute species, and buried interfaces. With an efficient microfocus excitation

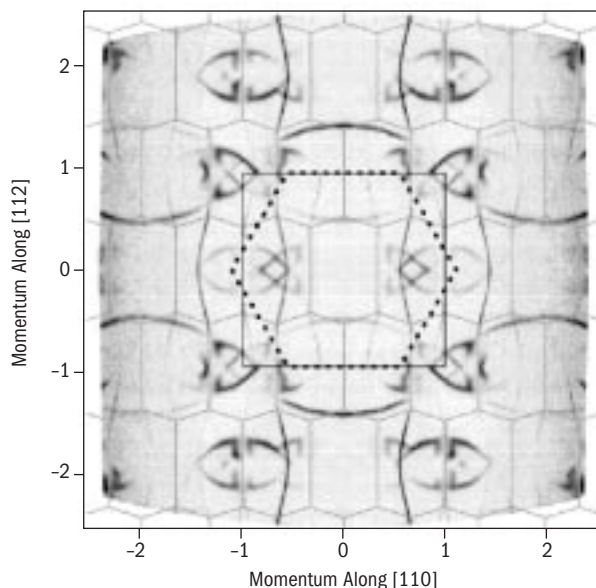


**FIGURE 7** Fermi surface data for 1.2 monolayers of indium on silicon (111) taken around 40 K. The raw data were taken over the range  $k_{x,y} = -0.5$  to  $+2.5 \text{ \AA}^{-1}$ , and the data presented were symmetrized by using mirror symmetry.

probe, Kirkpatrick–Baez refocus optics, and an x–y scanning stage with  $2.5\text{-}\mu\text{m}$  repeatability, the capabilities of the system are extended to include the characterization of small novel samples and a class of “combinatorial materials science” samples, in which a systematic variation of processing parameters is performed across a substrate.

The design of the scanning stage is based on a successful design previously implemented at the micro–x-ray photoelectron spectroscopy (Micro-XPS) endstation at Beamline 7.3.1.2. We are also borrowing from Micro-XPS designs to make sample handling (compatible with up to two-inch wafers) more user friendly. In addition, a new optical layout based on bendable mirrors is being designed to accommodate the new nanostructure characterization endstation (Figure 8), provide the microfocuss capability, and provide more flexible options for rapid switching between this and other Beamline 8.0.1 endstations.

## Heat Shield for Beamline 9.0

The undulator source for Beamline 9.0 is shared between the chemical dynamics group on the 9.0.2 branch, which uses low photon energies (small undulator gap settings), and the coherent science groups on the 9.0.1 branch, which use higher photon energies (larger undulator gaps). When switching between the two branches of the beamline, the users observed large horizontal beam

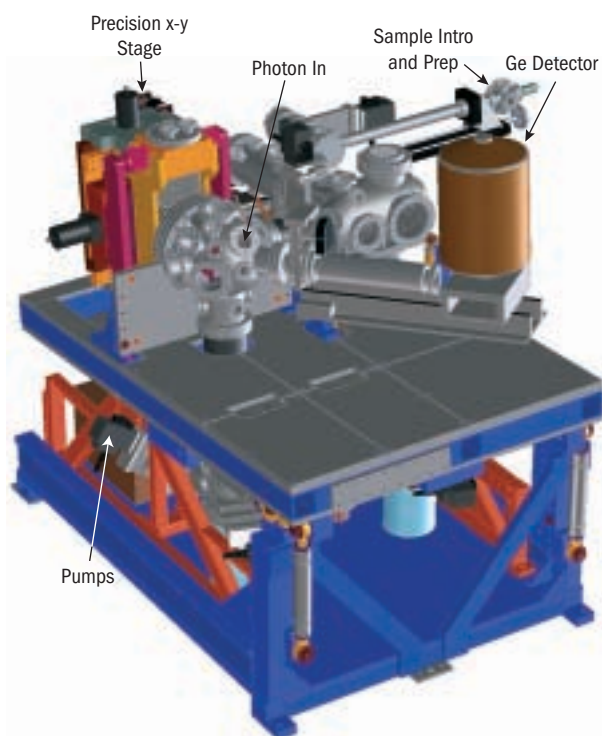


**FIGURE 8** Nanostructure characterization endstation for Beamline 8.0.1. Key features include a sub- $10\text{-}\mu\text{m}$  focus, a scanning stage with sub- $2.5\text{-}\mu\text{m}$  precision, and a fluorescence detector for photon-yield x-ray absorption.

motions over a period of an hour or more. After several attempts to correlate the photon beam displacement with electron beam motion due to large changes in the undulator gap, the problem was found to be caused by heating of the vacuum tank supporting the first mirror (M1), which is shared by both branches of the beamline.

To identify the cause of the heating, we first instrumented the vacuum tank with thermistors in an attempt to monitor the effect of the synchrotron beam power on the cooling water for the mirror. While the water temperature varied by less than  $1^\circ\text{C}$ , the outer surface of the vacuum tank was observed to heat up by as much as  $10^\circ\text{C}$ . The temperature of the vacuum tank followed the incident photon power with some long time constant (Figure 9).

The temperature changes induced a deformation of the vacuum chamber that supports the M1 mirror. The deformation caused the angle of the mirror to change, resulting in the observed movement of the photon beam. Sensitive position measurements of the tank carried out with the assistance of Andrew Franck of the ESG group correlated well with the temperature data and confirmed that the thermal motion of the tank was resulting in the observed beam motion.

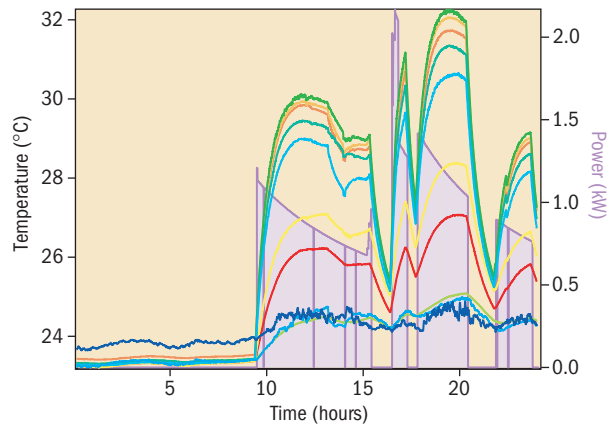


**FIGURE 9** Variations in the temperature of the outside of the vacuum tank that supports Beamline 9.0's M1 mirror, measured at several different locations (multiple colored traces), with variations in the power (filled purple trace) of the applied photon beam.

The transfer of power from the synchrotron beam to the vacuum tank is thought to occur through fluorescence of the materials in the M1 mirror, i.e., copper from the substrate and nickel from the coating. When operating at small gaps, with K values (nondimensional magnetic strengths) up to 8, the 10-cm-period undulator behaves almost like a wiggler, producing an intense beam of high-energy photons. K-shell vacancies created in the mirror substrate by these high-energy photons will decay via fluorescent processes to a large degree. The fluorescent photons re-emitted by the mirror then illuminate the vacuum tank and result in the temperature rise.

To shield the vacuum tank from this fluorescent power, a water-cooled copper shield (Figure 10) was designed by Tony Catalano and installed by Bruce Rude during the spring shutdown. Fitting around the mirror, the 3/8-in.-thick

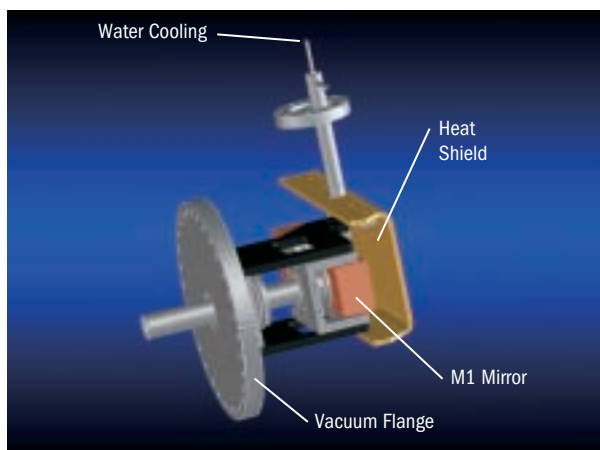


**FIGURE 10** Heat shield for the M1 mirror on Beamline 9.0.

copper shield absorbs most of the fluorescent power and prevents the vacuum tank from heating and deforming. The shield performs as designed, significantly reducing the power incident on the vacuum tank, as measured by the temperature rise (Figure 11).

## Progress on Beamline 10.0.1

### OPTIONS FOR ION SPECTROSCOPY

Spectroscopy of positive and negative ions with the Ion-Photon Beamline (IPB) continues as one of the most active areas of atomic and molecular physics research at ALS Beamline 10.0.1. Three different ion sources are available: an electron cyclotron resonance (ECR) source to produce singly or multiply charged positive ions, a cesium sputtering (SNICS) source to produce negative ions from solid targets, and a rubidium charge-exchange source to produce negative helium and hydrogen ions.

The ECR ion source, developed by Ron Phaneuf's group (University of Nevada, Reno) and in particular ALS Fellow Alejandro Aguilar, serves a large community of users interested in studying singly and multiply charged positive ions. The recent addition of a metal vapor oven to the source has made possible studies of metallic species by Phaneuf's group as well as general users such as Alfred Müller (Giessen) and John West (Daresbury). The multiply charged ion capability of the ECR source has also enabled isoelectronic and isonuclear sequence studies to study the effects of nuclear charge and electronic configuration.

Negative ion spectroscopy with the IPB continued in 2002 with extensive studies of the three-body  $\text{He}^-$  system,

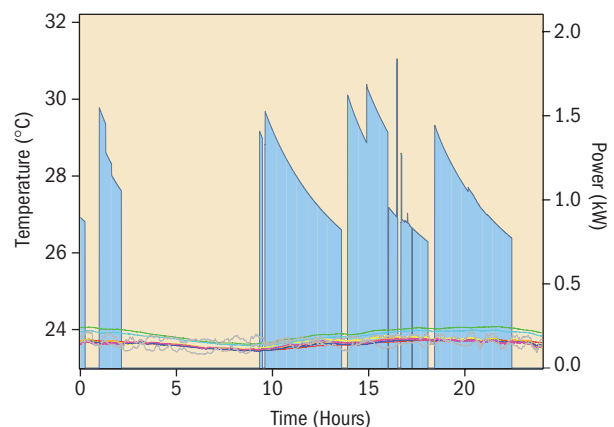


**FIGURE 11** Temperature (multiple colored traces) and power (filled blue trace) variations in the vacuum chamber that supports the M1 mirror, after installation of the copper heat shield.

by Nora Berrah's group (Western Michigan University), as well as other atomic and cluster species. A neutral detector was developed by Glenn Ackerman of SSG and Rene Bilodeau, a postdoctoral researcher from Berrah's group, to study photodetachment (single photoionization) processes in negative ions. Energetic neutrals strike a biased copper scattering plate, generating a shower of secondary electrons. The secondary electrons are electrostatically focused onto a microchannel plate (MCP) detector. The design was complicated by the need to provide an aperture for the photon beam while suppressing background signal from two sources: stray light striking the apparatus and photoionization of background gas.

### A CLUSTER SOURCE FOR PHOTOELECTRON SPECTROSCOPY

John Bozek and Bruce Rude of SSG have developed a continuous cluster source and fitted it to the gas-phase photoelectron spectrometer on Beamline 10.0.1. The source, which is simply a small orifice nozzle with a high backing pressure, is fitted onto an  $x$ - $y$ - $z$  manipulator used to align the orifice with a molecular-beam skimmer fitted into the vacuum chamber. The skimmed beam passes into the main chamber of the spectrometer, where it intersects the photon beam and is ionized. The skimmer chamber is pumped by two 1000-L/s turbo pumps and is allowed to operate in the  $10^{-4}$  Torr range, while the main chamber, which is separated from this region by the 1-mm-aperture skimmer, is in the  $10^{-7}$  Torr range.

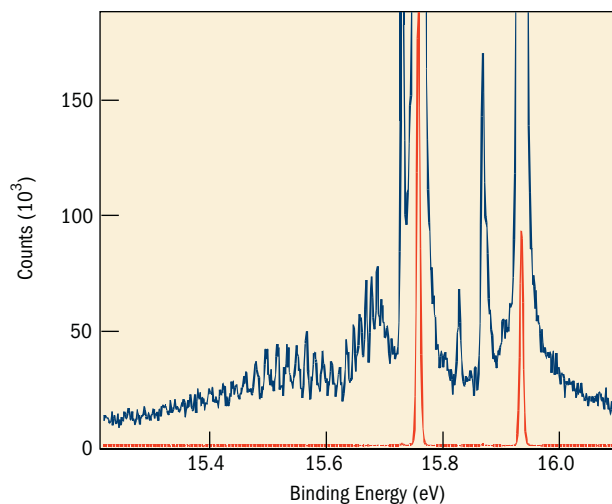


**FIGURE 12** Photoelectron spectrum from a sample consisting of argon monomer and dimer formed in a supersonic expansion. The two curves are the same spectrum, with the intensity scaled up 300 times for the blue curve.

We used this new capability in conjunction with Erwin Poliakoff's group (Louisiana State University) to conduct photoelectron spectroscopy of  $\text{Ar}_2$  dimers. The spectra (Figure 12) exhibited significantly higher resolution than any previously obtained with helium resonance lamps, with the added benefit of the tunability of the synchrotron light source. Further developments of cluster sources for photoelectron spectroscopy of a variety of cluster species will continue over the next year.

### FURTHER IMPROVEMENTS TO HERS

The high-energy-resolution spectrometer (HERS) has been considered one of the world's premier facilities for carrying out angle-resolved photoemission experiments. Further improvements to the experimental capability were made in 2002 by incorporating a new custom-designed Scienta analyzer (SES2002) that has boosted us to the next level in photoemission spectroscopy with ultrahigh angular and energy resolution. The new analyzer, with the use of two different magnification angle modes, offers an angular resolution of either  $\pm 0.05^\circ$  or  $\pm 0.15^\circ$ . Furthermore, it provides energy resolutions as good as 0.9 meV (Figure 13). This improvement in instrumentation is the result of close collaboration between Z.-X. Shen's group from Stanford University and members of the SSG group (primarily Zahid Hussain) with funding from BES and the ALS.

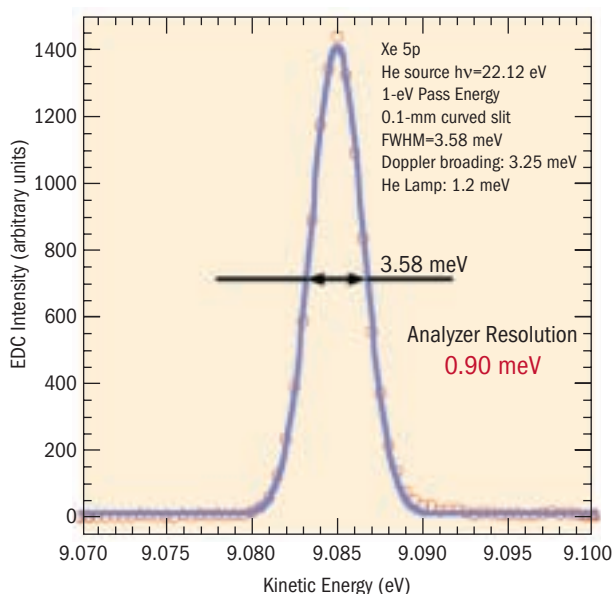


**FIGURE 13** Measurement of the energy resolution of the HERS endstation. With a 22.12-eV helium source and 1-eV pass energy, the xenon 5p peak is seen with 0.90-meV resolution.

## New Angle-Resolved Photoemission Branchline on Beamline 12.0.1

In 2002, the angle-resolved photoemission spectroscopy (ARPES) chamber at Beamline 12.0.1 received a new discharge-driven photon source (offering photon energies of 21.218 eV and 40.8 eV) with a toroidal-grating monochromator. The source delivers  $5 \times 10^{12}$  photons/s and has a line width of  $\sim 1$  meV. The photoemission branch of the beamline was upgraded with a quadruple reflector for converting linearly polarized light from the beamline into circularly polarized light. With these additions, the major construction of the ARPES endstation has been completed and commissioning work has begun. The beamline team was beefed up in a timely manner by hiring an Associate Beamline Scientist, Rudy Kimmerling.

The first runs of the photoelectron spectrometer (SES100) with photons from the beamline have revealed severe aging in its imaging detector, resulting in a rapid loss of detection efficiency and nonuniform sensitivity. The same problem has been reported for other SES spectrometers at the ALS

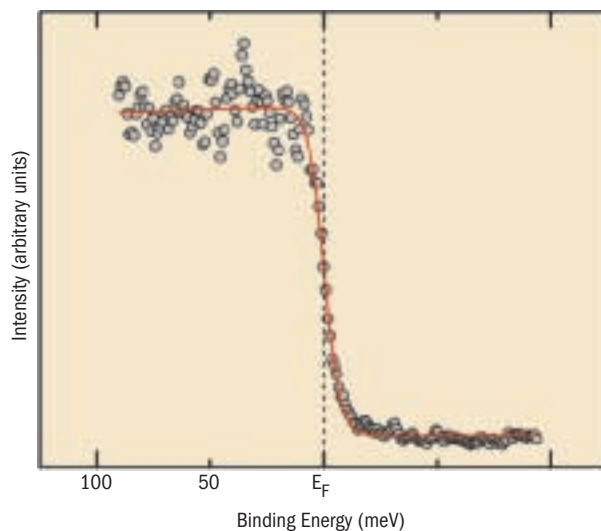


**FIGURE 14** The Fermi edge of gold measured with the ARPES chamber at Beamline 12.0.1 (photon energy, 21.218 eV; pass energy, 5 eV). The fit to the Fermi function convoluted by the Gaussian gives a total resolution of 9 meV.

(at Beamlines 10.0.1 and 7.0.1). Obviously, the standard detectors offered by the manufacturer of the SES electron analyzers (Gammadata-Scienta) are not able to handle the high photon flux of the ALS. As a quick solution, the original MCPs in the detector have been replaced with plates from Hamamatsu. Also, we initiated work to replace the phosphor screen with the more durable and faster scintillating crystals. In spite of the detector problems, the spectrometer demonstrated satisfactory energy and angular resolution. Figure 14 shows data for the Fermi edge of gold demonstrating a total resolution of 9 meV.

The scientific program conducted by the groups of Dan Dessau (University of Colorado, Boulder) and Alessandra Lanzara (UC Berkeley) focused on the studies of cuprate superconductors and carbon nanotubes. Figure 15 shows photoemission data for a single-layer  $\text{Bi}_2\text{Sr}_2\text{CuO}_6$  (Bi2201) sample. A break in the quasiparticle dispersion curve, discovered recently in a double-layer  $\text{Bi}_2\text{Sr}_2\text{CaCu}_2\text{O}_8$  (Bi2212), is also readily seen here about 80 meV below the Fermi energy. Hence, the data give a hint about the universality of the phenomenon in the cuprates. It may indicate the presence of a strong electron-phonon coupling, which could well be a cause of superconductivity in these materials.

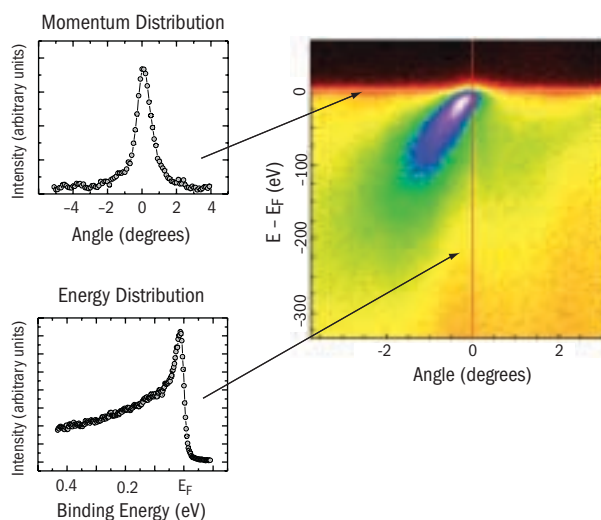


**FIGURE 15** Photoemission data for  $\text{Bi}_2\text{Sr}_2\text{CuO}_6$  (Bi2201), taken at Beamline 12.0.1, show a break in the quasiparticle dispersion about 80 meV below the Fermi level.

# USER SERVICES

Gary Krebs, User Services Group Leader

## Introduction

The User Services Group provides an interface to the ALS for new and continuing users at the ALS. The group is made up of the User Services Administration, Beamline Coordination, and Technical Information Sections. These groups work together to provide the users with a wide range of services. It is our goal to continue to provide these varied services in a friendly and efficient manner.

## User Services Administration

The User Services Office is located on the mezzanine floor of the ALS, down the hall to the left of the reception area as one exits the elevator. The office is staffed from 8:30 to 4:30 by members of the User Services Administration Section (Figure 1), who help new users through the required registration process before they begin work at the ALS. (During off hours, users register at the Control Room.) All users receive an electronic identification card, which allows them access to the ALS experiment floor. About 1400 users had access to the experiment floor in 2002. New users also watch a short safety video that describes some of the potential safety hazards at the facility and outlines the experiment safety checkout process. The Administration Section oversees both badging and safety training. Section members have also worked to enable new users to complete much of the processing before they arrive by pre-registering on the ALS Web site ([www-als.lbl.gov](http://www-als.lbl.gov)). Through its oversight of the registration process, the User Services Administration Section also collects data about user publications and demographics. As a national user facility, the ALS is required to report these statistics annually to the U.S. Department of Energy.

In another of its many functions, the User Services Administration Section coordinates the allocation of beam time through a peer-review process. For all the sciences except protein crystallography, general user requests for beam time are received through the ALS Web site twice annually. Protein crystallography proposals, also submitted over the web, are received and evaluated bimonthly to better serve the needs of this scientific community for rapid access. The proposals for beam time are reviewed by the



**FIGURE 1** ALS User Services Administration Section: *front row, left to right, Zalaysha Lowry, Sharon Fujimura, Barbara Phillips, and Jamila Murray; back row, Gary Krebs, Bernie Dixon, Jeff Troutman, and Jeremy Coyne.*

appropriate Proposal Study Panel (there are separate PSPs for general sciences and protein crystallography), and under the direction of ALS Division Deputy for Science, Neville Smith, beam time is allocated based on principles and guidelines agreed upon by the ALS and the Users' Executive Committee (UEC). These principles and guidelines adhere to those of the International Union of Pure and Applied Physics. The UEC, elected annually by the users, is the voice of that diverse group and represents them at the ALS as an advisory body. Proposal Study Panel members are chosen in consultation with the UEC to cover the wide range of sciences represented at the ALS. The User Services Administration Section provides administrative and logistical support to both the PSPs and the UEC. The proposal submission and beam time allocation process is described in greater detail on the ALS Web site ([www-als.lbl.gov/als/quickguide/independinvest.html](http://www-als.lbl.gov/als/quickguide/independinvest.html)).

The User Services Office can also help out-of-town visitors find a place to stay while working at the ALS. The office manages the ALS apartments (Figure 2), which are located near Berkeley Lab along the route of the main laboratory shuttle bus. The apartments, recently increased to



**FIGURE 2** The ALS apartments serve as home away from home for users on the road.

five in number, are available to all ALS users, and detailed information about costs and other factors can be found on the Web at [www-als.lbl.gov/als/quickguide/housing.html](http://www-als.lbl.gov/als/quickguide/housing.html).

The User Services Administration Section, formerly managed by Bernie Dixon, is now managed by Jeff Troutman and includes Sharon Fujimura, Zalaysha Lowry, Jamila Murray, Barbara Phillips, Adriana Reza, and Barbara Srulovitz (now retired). We are indebted to Bernie Dixon, who contributed in many ways to the efficiency and development of the User Services Office.

## Beamline Coordination

The Beamline Coordination Section serves as a point of contact for users on the experiment floor. Section members act as liaisons between users and ALS and Berkeley Lab resources. They provide shipping and receiving and temporary storage services as well as endstation setup



**FIGURE 3** The User Stock Room keeps needed parts and equipment ready to hand.



**FIGURE 4** The Beamline Coordination Section: *left to right*, Tony Marquez, Gary Giangrasso, Alex Lobodovsky, Ken Winters, Donna Hamamoto, and Todd Anderson.

and safety checkout coordination. Ensuring that all user experiments are checked for safety is a crucial function of this group. Section members work closely with various Berkeley Lab safety specialists in the areas of electrical, mechanical, chemical, radiation, biological, and laser safety, coordinating the process to ensure that all guidelines are met. This process is required in order to assure the safety of all users on the experiment floor. Upon the successful completion of the required safety checks, section members enable the beamline to receive light. The Beamline Coordination Section also maintains a stock room of parts and equipment commonly needed by ALS users and ALS technicians (Figure 3). These supplies are accessible by proximity card 24 hours a day. The Beamline Coordination Section is led by Donna Hamamoto and includes Todd Anderson, Gary Giangrasso, Alex Lobodovsky, Tony Marquez, and Kenneth Winters (Figure 4).

## Technical Information

The Technical Information Section is responsible for this Activity Report as well as the annual Compendium of User Abstracts (a copy of which can be found on the CD inside the back cover of this volume). The group's members also prepare special brochures and create posters and announcements for countless workshops and conferences. They are responsible for the "Science Highlights" shown in the ALS lobby and on the ALS Web site and many of the posters around the experiment floor. In addition, the section maintains

and develops the ALS Web site and writes and edits the electronic newsletter, ALSNews. The section, composed of science writers along with graphics and Web experts, provides the ALS scientific and technical community and government officials as well as the general public with information about the science carried out at the ALS. The group maintains a strong tie to the educational community within the state of California, around the U.S., and even internationally. In conjunction with the User Services Office, this group coordinates tours for the several thousand visitors—often from high schools, universities, and industry—who come to view the ALS annually. The Technical Information section is led by Art Robinson and includes Annette Greiner, Elizabeth Moxon, Lori Tamura, and Greg Vierra (Figure 5).



**FIGURE 5** The Technical Information Section: *left to right*, Art Robinson, Elizabeth Moxon, Lori Tamura, Greg Vierra, and Annette Greiner.



# SPECIAL EVENTS



From introducing young students to career opportunities in synchrotron-related science, to early morning television interviews introducing the Advanced Light Source to the San Francisco Bay Area, ALS staff members continued to enthusiastically participate in a variety of scientific and educational outreach activities. Highlights included participation in Berkeley Lab's Open House, an event that attracted more than 8,000 people; conferences covering a wide range of topics; and visits by distinguished guests from around the world.



The Berkeley Nanoscience Research Center

# MOLECULAR FOUNDRY

## WORKSHOP

April 4-5, 2002



### WHITHER NANOSCIENCE – Beyond Building Blocks to Complex Functional Assemblies

The past few years have seen extraordinary growth in nanoscience research. "Hot" nanosystems, nanotubes, nanowires, and "soft" DNA filaments, polymers, dendrimers, proteins, enzymes and cells have been studied. Single atoms have been manipulated.

Much remains to be done with building blocks: new structures will be found, new phenomena discovered. The future, however, lies in integrating these blocks into multi-component assemblies that perform functions.

Success here will require that investigators have a breadth of facilities available to them. Physicists will need nanofabrication and lithography. All will need theory.

The Berkeley Lab Molecular Foundry will meet these needs: state-of-the-art, multi-disciplinary, staffed by professionals available for assistance and collaboration. It will be a user facility open to researchers from university, industrial, and government laboratories. Scientists with outstanding ideas will exploit its facilities to execute these ideas. Some will make critical components. Others will develop techniques or instruments. Others will conduct long-term collaborations with Foundry scientists.

Workshop sessions will see talks by leaders in the field, exploring challenges and opportunities in assembling nanoscale building blocks into multi-component functional structures and devices.

Session B will involve small group meetings in which attendees will discuss their views of how the Foundry facilities can be designed and operated to be of greatest value to its users.

#### FOUNDRY FACILITIES

- Inorganic Nanostructures Synthesis
- Nanofabrication
- Imaging, Characterization
- Organic Synthesis
- Biopolymer Synthesis
- Plant, Microbial, Mammalian Cell Culture

For more information, go to [foundry.lbl.gov](http://foundry.lbl.gov).

## Molecular Foundry Workshop Berkeley Lab; April 4-5

Over 350 people registered for the first workshop dedicated to creating a roadmap for Berkeley Lab's Molecular Foundry. Slated to open in 2006, the Molecular Foundry is one of five Nanoscale Science Research Centers planned by the Department of Energy's Office of Basic Energy Sciences (BES). Keynote and invited speakers, including Materials Sciences Division Director Paul Alivisatos (*below left*), discussed the concept and design of the facility while others highlighted the exciting future of nanotechnology research to overflow crowds in the plenary sessions (*below right*).



## New Opportunities in Ultrafast Science Using X-Rays

April 14-17, 2002, Napa, CA

**Local Organizing Committee**

Yves Peierls (LBL)	Bob Schuessler (LBL)
Eric Glover (LBL)	Roger Falcone (UC Berkeley)
Phil Herlihy (LBL)	Howard Padmore (LBL)
Jerry Hastings (SLAC)	Andrew Schall (LBL)
John Arthur (SNL)	Swamin Saha (SLAC)

**Program Committee**

R. Abella (ILL)
P. Bakula (SLAC)
P. Coluccia (Maxlab, Institute)
W. Blawieck (Maxlab, Sweden)
R. Falcone (UC Berkeley)
C. Harris (UC Berkeley)
E. Hendriks (Jülich)
G. Holwek (Darmstadt, FAL)
K. Hofner (J. Chicago)
H. Murnane (SLAC, Colorado)
K. F. Nelson (MIT)
C. Shank (UCS / LBNL)
H. Siegrmann (Stanford/SRRL)
J. Stroh (Stanford / SLAC)



## New Opportunities in Ultrafast Science Using X-Rays Napa, California; April 14-17

California's beautiful Napa Valley was the site of an international conference that brought together experts from the research communities of ultrafast optics and ultrafast x-ray sources. Hosted by the ALS, Stanford Synchrotron Radiation Laboratory (SSRL), the Swiss Light Source, BioCARS-NIH, and BES, the workshop focused on cooperation between the two communities to extend experimental capabilities for ultrafast science.

---

## The 7th International Conference on Surface X-Ray and Neutron Scattering (7SNXS) Granlibakken Conference Center, Tahoe City, California; September 23–27

The science of studying surfaces using neutron and x-ray scattering techniques drew researchers from around the world to the shores of Lake Tahoe for this five-day workshop. Of particular interest for this year's attendees was the structure of nanoscale materials.



SXNS meeting participants paused for a group photo between sessions.

---

## Berkeley–Stanford Synchrotron Radiation Summer School Palo Alto, California; July 7–15

This year's jointly organized summer school for the study of synchrotron radiation applications and experimental techniques was held at Stanford University. The 40 students selected for the school were treated to an intensive program of lectures and practical courses designed to showcase the scientific opportunities of synchrotron radiation in the physical and life sciences. Directors of the school were Mike Soltis and Anders Nilsson of Stanford University/SSRL, and John Kuriyan and David Attwood of the University of California, Berkeley/Berkeley Lab.



Synchrotron Radiation Summer School students and organizers at Stanford University.



## ALS Users' Meeting Berkeley Lab; October 10-12

This year's meeting attracted more than 350 ALS users and staff ready to hear about recent research highlights, facility updates, and current user issues. Hot topics included evolving modes of user access, the commissioning of the molecular environmental science beamline, and the success of the superbend magnets. Other meeting highlights were presentations from young researchers, invited speakers, and a busy poster session, vendor exhibits, and an evening awards banquet on the ALS patio. Following the general meeting program, six focused workshops attracted large crowds interested in x-ray microdiffraction in materials and environmental science; applications of infrared radiation; opportunities for chemical physics at the ALS; polarization-dependent x-ray spectroscopy and microscopy; future projects using ultra-high-resolution soft x rays; and atomic, molecular, and materials science.



During the opening session, attendees filled the auditorium to hear ALS Division Deputy for Science Neville Smith present new ideas for user access to the ALS.



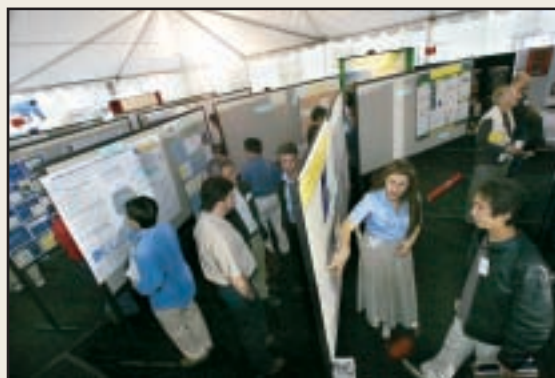
ALS Division Director Daniel Chemla compared notes with Pedro Montano of the BES Division of Materials Science and Engineering during the opening session (*far left*) and listened as BES Deputy Director Iran Thomas posed a question. BES Director of Science for Pat Dehmer looks on.



Keynote speaker Steve Leone of Berkeley Lab's Chemical Sciences Division and the University of California, Berkeley, provided an overview of optical probes of molecular dynamics.



Mary Kaufman of Montana State University and the Idaho National Engineering and Environmental Laboratory discussed her graduate work in microbe–mineral reactions during the always-popular Highlights from Young Researchers session.



The poster session, the student poster competition, vendor exhibits, and the meeting's awards banquet were held in the early evening on the ALS patio.





This year's award winners included, *from left*, Harald Ade, Ximei Qian, Nora Berrah, Charlie Knopf, John Bozek, Roger Falcone (UEC Chair), and Adam Hitchcock (accepting on behalf of Peter Hitchcock).

The 2002 Halbach Award for Innovative Instrumentation at the ALS was presented to Harald Ade (North Carolina State University), Peter Hitchcock (McMaster University, Canada), David Kilcoyne (North Carolina State University), Tolek Tyliszczak (Berkeley Lab), Tony Warwick (ALS), and the STXM Team for the design and implementation of advanced interferometrically controlled scanning transmission x-ray microscopes. The Shirley Award for Outstanding Scientific Achievement was presented jointly to Nora Berrah (Western Michigan University), John Bozek (ALS), Carmen Cisneros (Universidad Nacional Autónoma de México), Aaron Covington (Lake Tahoe Community College), and Ron Phaneuf (University of Nevada, Reno) for their groundbreaking advances in atomic and molecular physics. Ximei Qian (University of California, Davis) won the student poster competition with her submission titled "State-Selected Ion-Molecule Reaction Dynamics at Extremely High Vibrationally Excited States." The Renner User Services Award was split between Charles A. Knopf (Mechanical Engineering Group, retired) and Gerry McDermott (Berkeley Center for Structural Biology).




---

## Workshop on Coherent Synchrotron Radiation in Storage Rings Napa, California; October 28–29

This workshop brought together scientists interested in the possibilities of developing coherent synchrotron radiation (CSR) sources at existing rings or new dedicated rings. Participants (*left*) discussed the theoretical and experimental understanding of stable CSR and CSR-driven instabilities, techniques for configuring lattices for low-momentum-compaction operation, and the planning of future accelerator experiments.

---

## Distinguished Visitors



In February, John Landy, Governor of the State of Victoria, Australia, led a delegation of scientists and advisors from the Australian Synchrotron around the ALS. During their tour of the experiment floor, James Sullivan (*left*), a visiting Australian postdoc currently working in Japan, gave Governor Landy (*fourth from right*) an overview of his research on Beamline 10.0.1.



(*From left*) ALS Division Director Daniel Chemla met with J. Murray Gibson, Associate Laboratory Director for the Advanced Photon Source (APS), and Steven Dierker, Chairman of the National Synchrotron Light Source (NSLS), in early March to discuss how the synchrotron facility directors can work together to provide the best research capabilities possible to the user community.

Neville Smith, ALS Division Deputy for Science, hosted members of the Norwegian Research Council and Department of Medicine and Health as they toured the ALS. The group, comprising ministers in education, research, and health; trade commissioners; and special advisors, was particularly interested in advances on the protein crystallography beamlines and in biotechnology research.



On November 26, U.S. Secretary of Energy Spencer Abraham visited Berkeley Lab as part of a tour of the Department of Energy laboratories in the Bay Area. During his visit to the ALS, Abraham learned about the applications of synchrotron light and presided over an informal ceremony launching the BES-funded Molecular Environmental Science Beamline (Beamline 11.0.2).

Secretary Abraham (*second from right*) and his wife, Jane (*far right*), look at images taken at Beamline 6.1.2 as Carolyn Larabell (*left*) of the Life Sciences Division presents recent advances in 3D tomography of single cells. ALS Division Director Daniel Chemla (*center*) led the tour, which ended after the Secretary addressed more than 200 lab employees on the ALS patio.





On December 17, the ALS welcomed Walter Stevens, new Director of BES's Division of Chemical Sciences, Geosciences, and Biosciences. At the ALS, his division directly supports the Chemical Dynamics Beamline (Beamline 9.0.2), the AMO branches of Beamline 10.0.1, and the new Molecular Environmental Science (MES) Beamline (Beamline 11.0.2). Stevens toured the facility as the guest of Berkeley Lab Division Directors Dan Neumark (Chemical Sciences), Graham Fleming (Physical Biosciences), and Daniel Chemla (ALS). During his tour, Stevens (*center*) was updated on the status of the MES beamline by David Shuh (*right*) of the Chemical Sciences Division as Neumark looked on.

---

## Open House



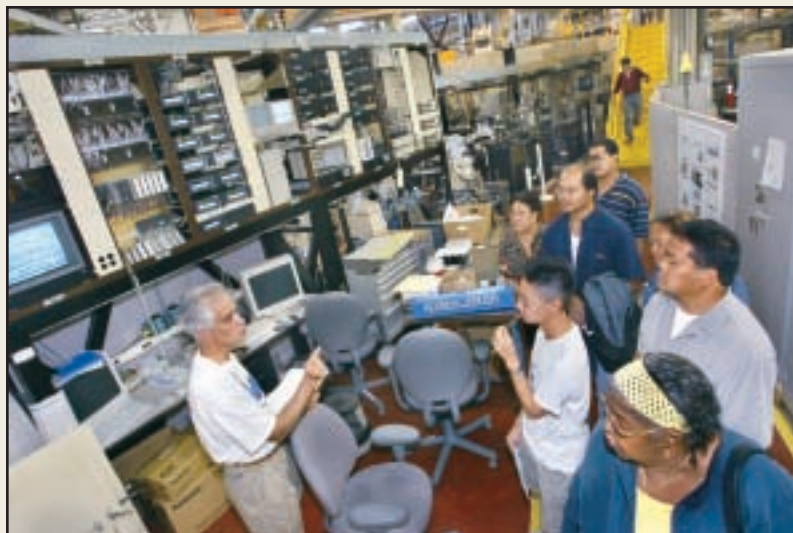
Division Deputy for Science Neville Smith gave early risers an introduction to the ALS and an invitation to attend Berkeley Lab's Open House when he appeared on a local morning television show. Viewers must have been intrigued, as more than 8,000 visitors, the largest crowd ever, attended the October 6 event.

Berkeley Lab Director Charles Shank greeted early arrivals in the Welcome Tent.

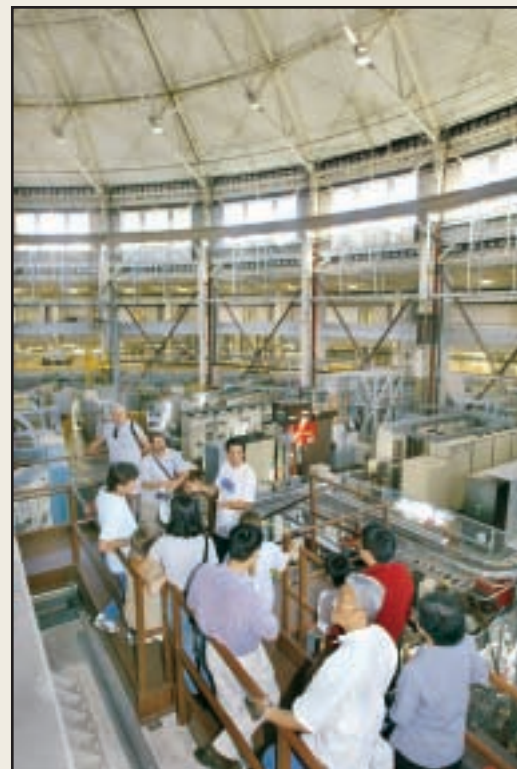


Beamline Coordination Section Leader Donna Hamamoto showed eager and hungry young scientists how liquid nitrogen can make ice cream in a hurry. Donna and ALS postdoc Tobias Funk served more than 1500 happy customers during the day.





Visitors lined up outside the ALS for over an hour to get a tour from staff volunteers. Tours around the experiment floor stopped at different beamlines where guides like Ken Woolfe (*left*) of the Electrical Engineering Group discussed how the ALS works. Visitors were then guided over the shielding for a rare opportunity to view the historic dome.



A visit to Beamline 9.02 was a highlight for younger visitors as Darcy Peterka (*right*), Musa Ahmed (*below, left*), and Christophe Nicholas (*below, background*) of the Chemical Sciences Division invited budding scientists to “push around” electrons using magnets.



---

## Educational Outreach and Diversity

The ALS continues to serve as a teaching resource for local schools and organizations interested in showing students career opportunities in science, engineering, and technology. On an international scale, ALS publications and the educational Web site MicoWorlds provide an introduction to synchrotron science, its applications, and the jobs that make a facility like the ALS run smoothly. To expand their awareness of communicating science effectively to all audiences, ALS editors participated in science communications conferences in Gaithersburg and College Park, Maryland, and in Cape Town, South Africa.



Mhairi Donohoe (*left*) from the Physical Biosciences Division (PBD) welcomed students from Oakland's College Preparatory High School and showed them how to make protein crystals. The experiment was followed by a trip to the protein crystallography endstation where students were shown how a protein is examined with x rays. The students used their experiences at the ALS to create a Web page explaining protein crystallography to their peers.



Berkeley Lab's annual Daughters and Sons to Work Day brought another eager group of young scientists to the ALS. Elizabeth Moxon of the Technical Information Section discusses some of the clues her charges found as they conducted a scientific scavenger hunt around the ALS.



PBD's Gerry McDermott gave a highlight tour for students from Berkeley's Biotechnology Education, Inc. (BBE) as he showed the intrigued students how a protein sample is prepared for crystallography experiments. BBE is a nonprofit organization that trains high-school students for careers in biotechnology and research.

Information Section writers presented posters at the National Institute for Standards and Technology (NIST) Best Practices for Communication of Science and Technology to the Public conference in Gaithersburg, Maryland and at the Materials Education: Opportunities Over a Lifetime meeting in nearby College Park, Maryland. ALS writers also presented a poster (right) and gave a brief talk at the Seventh International Conference on Public Communication of Science and Technology in Cape Town, South Africa.

[www.lbl.gov/MicroWorlds/](http://www.lbl.gov/MicroWorlds/)

### EXPLORING THE STRUCTURE OF MATERIALS

*Science Education for Grades 7-12*

MicroWorlds, an electronic science magazine on the Web, is the corner stone of an extensive educational outreach program at the Advanced Light Source (ALS). Written for students in grades 7-12, their teachers, and the general public, MicroWorlds features information about research at the ALS, a third-generation synchrotron radiation facility at the Lawrence Berkeley National Laboratory (Berkeley Lab) that is used by scientists from academic, industrial, and government laboratories from around the United States and, indeed, the world.

---

### What Makes MicroWorlds Unique?

**Real Science and the People that Make It Happen**

Visitors to MicroWorlds can not only see the various components of a synchrotron, they can also visit the facility online through a virtual-reality tour. In order to understand how a synchrotron works and the unique nature of the light it produces, key science concepts like electromagnetism and light are connected to concepts encountered in everyday life. Links to sources of current research in biology, chemistry, physics and materials science are part of the site. Biographies of scientists, engineers, writers, and technicians give students a look at future career opportunities.

**Interactive Teaching Modules**

Three teaching modules, supported by curriculum materials and hands-on activities, were developed by Berkeley Lab-ALS writers in collaboration with local teachers. The modules explore one a series of questions, their, and activities that challenge students to build on their knowledge.

**Student Participation**

To enhance MicroWorlds' accessibility, high school students spend summers developing stories that they feel would be intriguing to their peers. By following an experiment from start to finish in "the eExperiment EBox" or interviewing ALS scientists, engineers, and technical staff for "The Bright and the Busy," students provide a unique view of the workings of a vibrant research environment. Another unique feature is "Students' Corner," which contains a first-person account about what it's like to be a summer student working with scientists at the ALS.

Robert Miles  
Advanced Light Source, MS 600  
Lawrence Berkeley National Laboratory  
Berkeley, CA 94720  
Tel: 510/486-0200  
E-mail: rmiles@lbl.gov

Arvin Robinson  
Advanced Light Source, MS 608  
Lawrence Berkeley National Laboratory  
Berkeley, CA 94720  
Tel: 510/486-0200  
E-mail: arvin@lbl.gov

*Other Science Education Outreach at the Advanced Light Source*

School Tours



Daughters and Sons to Work Day



Open House



Summer Students and Teachers



# ALS ADVISORY PANELS

## SCIENCE POLICY BOARD

*Advises the Berkeley Lab Director on major policy issues concerning the ALS.*

**William Brinkman**, Lucent Technologies/Bell Laboratories

**John Carruthers**, Intel Corporation

**Chien-Te Chen**, National Synchrotron Radiation Research Center, Taiwan

**Peter Eisenberger**, Columbia Earth Institute

**Paul Fleury**, University of New Mexico

**Franz J. Himpsel**, University of Wisconsin–Madison

**Yuan T. Lee**, Academia Sinica, Taiwan

**Albert Narath**, Lockheed Martin Corporation (retired)

**Yves Petroff**, Lawrence Berkeley National Laboratory/European Synchrotron Radiation Facility

**Stephen D. Kevan** (ex officio), University of Oregon

## SCIENTIFIC ADVISORY COMMITTEE

*Advises Berkeley Lab and ALS management on issues relating to ALS operations, resource allocation, strategic planning, and Participating Research Team proposals and research.*

**Ernst G. Bauer**, Arizona State University

**James Berger**, University of California, Berkeley

**Jeffrey Bokor**, University of California, Berkeley

**John Carruthers**, Intel Corporation

**Wolfgang Eberhardt**, BESSY GmbH, Germany

**Roger Falcone**, University of California, Berkeley

**Yves Idzerda**, Montana State University

**Stephen D. Kevan** (Chair), University of Oregon

**Alain Manceau**, Université Joseph Fourier, France

**Anders Nilsson**, SSRL/Stockholm University, Sweden

**Sunil Sinha**, University of California, San Diego

**Janet L. Smith**, Purdue University

**John Spence**, Arizona State University/Berkeley Lab

**Anthony Starace**, University of Nebraska–Lincoln

**Louis J. Terminello**, Lawrence Livermore National Laboratory

## USERS' EXECUTIVE COMMITTEE

*Elected by the members of the Advanced Light Source Users' Association to act as the official voice of the user community in its interactions with ALS management.*

**Harald Ade** (Past Chair), North Carolina State University

**John Bozek**, Advanced Light Source, Berkeley Lab

**Sophie Canton** (Student), Western Michigan University

**Jennifer A. Doudna** (Vice Chair), Howard Hughes Medical Institute/University of California, Berkeley

**Roger Falcone** (Chair), University of California, Berkeley

**Carolyn A. Larabell**, University of California, San Francisco/  
Life Sciences Division, Berkeley Lab

**Dennis W. Lindle**, University of Nevada, Las Vegas

**Gerry McDermott**, Physical Biosciences Division,  
Berkeley Lab

**Alexander Moewes**, University of Saskatchewan

**Yasuji Muramatsu**, Japan Atomic Research Institute

**Eli Rotenberg**, Advanced Light Source, Berkeley Lab



2002 ALS Users' Executive Committee: *from left*, Eli Rotenberg, Roger Falcone, John Bozek, Dennis Lindle, Alexander Moewes, Sophie Canton, Harald Ade, Gerry McDermott, and Gary Krebs (ALS User Services Group Leader).

# ALS STAFF



*This is a cumulative list of all those who worked at the ALS during the 2002 calendar year. The list includes visitors, students, and staff members from other divisions who were matrixed to the ALS.*

## DIVISION MANAGEMENT

D. Chemla  
B. Feinberg  
J. Krupnick  
Y. Petroff  
N. Smith

## ACCELERATOR PHYSICS

**D. Robin**, Group Leader  
**J. Byrd**, Deputy Leader  
S. Lidia  
L. Nadolski  
H. Nishimura  
F. Sannibale  
T. Scarvie  
C. Steier  
W. Wan

## ADMINISTRATION

B. Dixon  
P. Epps  
M. Fenner  
R. Pepe

A. Reza

L. Senft

## BUDGET

J. Dahlgard  
S. Rossi  
J. Zelver

## CONTROLS

**A. Biocca**, Group Leader  
**C. Timossi**, Deputy Leader  
E. Domning  
K. Fowler  
C. Ikami  
S. Jacobson  
J. McDonald  
A. Robb  
L. Shalz  
J. Spring  
R. Steele  
J. Tunis  
E. Williams

## ENVIRONMENT, HEALTH, AND SAFETY

B. Fairchild  
R. Mueller  
G. Perdue

## ELECTRICAL ENGINEERING

**W. Barry**, Group Leader  
**G. Stover**, Deputy Leader  
B. Bailey  
M. Balagot  
K. Baptiste  
M. Bell  
R. Benjegerdes  
T. Bilstein  
K. Bolin  
R. Candelario  
M. Chin  
R. Cole  
R. Colston  
P. Cull  
A. Detzner  
L. Dominguez

J. Elkins  
M. Estrema  
D. Edwards  
M. Fahmie  
M. Foster  
R. Gassaway  
R. Gervasoni  
A. Geyer  
J. Gregor  
J. Hellmers  
M. Hilburn  
L. Holzer  
L. Jordan  
J. Julian  
T. Kuneli  
S. Kwiatkowski  
E. Lee  
A. Lindner  
P. Molinari  
T. Nhan  
J. Nomura  
F. Ottens  
S. Patterson

A. Ritchie  
 S. Rogoff  
 P. Rosado  
 H. Scheid  
 A. Sippio  
 R. Slater  
 M. Szajbler  
 M. Thomas  
 M. Vinco  
 S. Warner  
 J. Weber  
 M. Williams  
 K. Woolfe

#### EXPERIMENTAL SYSTEMS

**H. Padmore**, Group Leader  
**A. Warwick**, Deputy Leader  
 W. Caldwell  
 R. Celestre  
 S.-B. Choe  
 S. Clark  
 A. Doran  
 S. Fakra  
 J. Feng  
 A. Franck  
 E. Glover  
 E. Harvey  
 H. He  
 P. Heimann  
 M. Howells  
 S. Irick  
 A. MacDowell  
 M. Marcus  
 W. McKinney  
 A. Scholl  
 P. Schmid  
 R. Sublett  
 N. Tamura

A. Thompson  
 A. Warwick  
 A. Young

#### MECHANICAL ENGINEERING

**A. Paterson**, Group Leader  
**R. Schlueter**, Deputy Leader  
 J. Akro  
 N. Andresen  
 R. Armstrong  
 W. Baldock  
 D. Baum  
 L. Bonifas  
 D. Calais  
 D. Cambie  
 K. Carter  
 M. Coleman  
 D. Colomb  
 J. Comins  
 C. Cummings  
 D. Davis  
 M. Decool  
 R. DeMarco  
 A. Demello  
 R. Duarte  
 D. Eastman  
 Z. Eisentraut  
 D. Ellis  
 K. Franck  
 D. Fritz  
 A. Gavidia  
 D. Gibson  
 C. Hopkins  
 D. Hull  
 D. Jones  
 J.-Y. Jung  
 N. Kelez

S. Klingler  
 C. Knopf  
 G. Koehler  
 M. Kritscher  
 K. Krueger  
 A. Lim  
 R. Low  
 S. Lundgren  
 B. Macdonell  
 D. MacGill  
 S. Marks  
 C. Matuk  
 P. McKean  
 H. Meyer  
 V. Moroz  
 G. Morrison  
 D. Munson  
 W. Oglesby  
 J. Osborne  
 R. Patton  
 J. Pepper  
 K. Peterman  
 P. Pipersky  
 D. Plate  
 S. Prestemon  
 K. Rex  
 N. Searls  
 K. Sihler  
 T. Stevens  
 H. Stewart  
 M. Thomas  
 W. Thur  
 A. Wandesforde  
 R. Weidenbach  
 M. Wingert  
 E. Wong  
 J. Zbasnik  
 F. Zucca

#### OPERATIONS

**B. Samuelson**, Group Leader  
**T. Byrne**, Deputy Leader  
 D. Bentsen  
 J. Bishop  
 D. Brothers  
 E. Diaz  
 O. Jones  
 K. Osborne  
 J. Pusina  
 D. Richardson  
 S. Stricklin  
 M. Wolfe

#### PROCEDURE CENTER

R. Jones

#### PROJECT MANAGEMENT

A. Catalano  
 J. Harkins  
 S. Rossi

#### QUALITY ASSURANCE

E. Lampo

#### SCIENTIFIC SUPPORT

**Z. Hussain**, Group Leader  
**J. Bozek**, Deputy Leader  
 G. Ackerman  
 E. Arenholz  
 W. Bates  
 K. Chesnel  
 Y.-D. Chuang  
 J. Denlinger  
 A. Fedorov  
 B. Freelon  
 J. Guo

A. Guy  
 N. Hamdan  
 C. Hauck  
 R. Kimmerling  
 G. Lebedev  
 M. Martin  
 S. Mun  
 E. Rotenberg  
 B. Rude  
 F. Schlachter

#### USER SERVICES

**Gary Krebs**, Group Leader

**A. Robinson**, Deputy

Leader

T. Anderson  
 J. Coyne  
 S. Fujimura  
 G. Giangrasso  
 A. Greiner

D. Hamamoto  
 A. Lobodovsky  
 Z. Lowry  
 A. Marquez  
 E. Moxon  
 J. Murray  
 B. Phillips  
 B. Srulovitz  
 J. Troutman  
 L. Tamura  
 G. Vierra  
 K. Winters

#### VISITORS AND STUDENTS

A. Aguilar\*  
 A. Augustsson\*  
 B. Batterman  
 P. Bogdanov\*  
 V. Brouet  
 S. Canton

Y. Chen\*  
 H. Chong\*  
 S. Chourou  
 J. Diaz  
 C. Dong  
 D. Edwards\*  
 J. Glossinger\*  
 J. Graf  
 G.-H. Gweon  
 Z. Hasan\*  
 S. Johnson\*  
 N. Khan  
 D. Kilcoyne  
 J. Kirz  
 A. Lanzara  
 S. Locklin\*  
 D. Lowney\*  
 A. Manceau  
 C. Morin\*  
 S. Mun

M. Paik\*  
 J. Patel  
 D. Rolles\*  
 M. Salim  
 E.J. Singley  
 C. Slim\*  
 J. Spence  
 Z. Sun\*  
 W. Stolte  
 J. Turner  
 G. Turri  
 M. Van Hove  
 K. Wilson\*  
 C. Won\*  
 W. Yang  
 H.-S. Youn  
 X. Zhou  
  
 \*Graduate Student  
 Research Assistant

# FACTS AND FIGURES

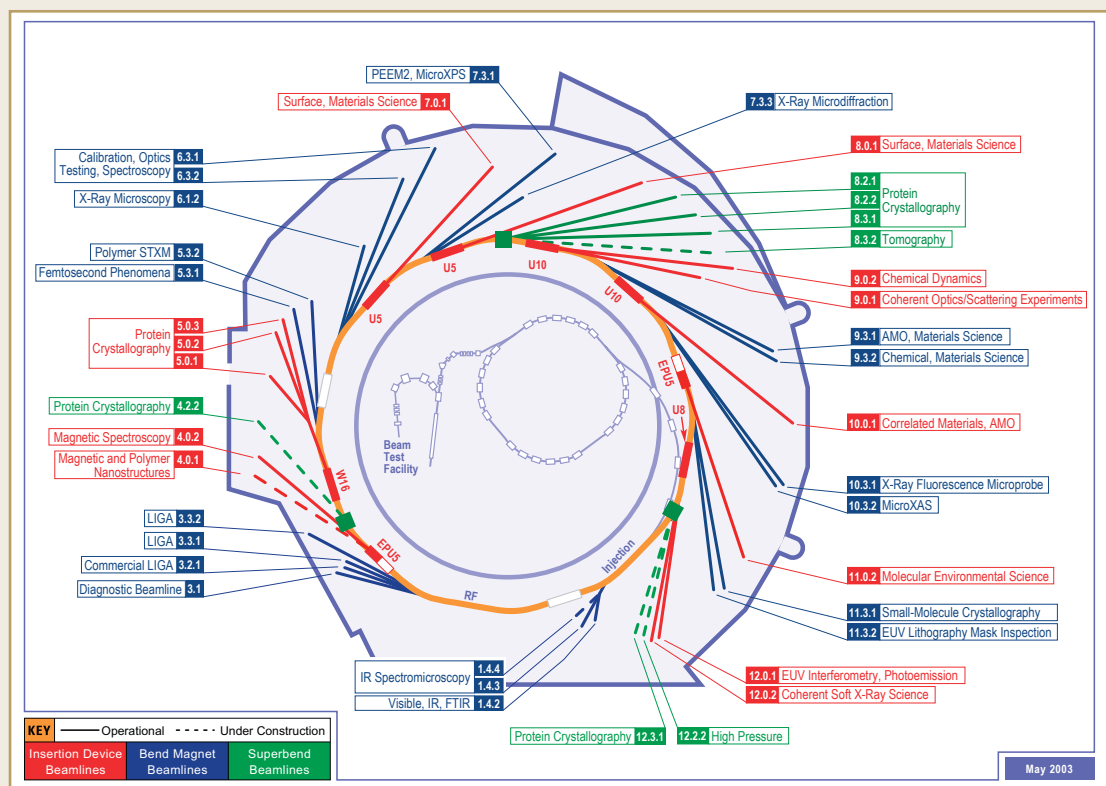
## USING THE ADVANCED LIGHT SOURCE

The ALS, a Department of Energy national user facility, welcomes researchers from universities, industry, and government laboratories. Qualified users have access either as members of a participating research team (PRT), as members of an approved program, or as general users. PRTs (groups of researchers with related interests from one or more institutions) construct and operate beamlines and have primary responsibility for experiment endstation equipment. They are entitled to a certain percentage of their beamline's operating time according to the resources contributed by the PRT. Through a peer-reviewed proposal process, the remaining beam time is granted to approved programs and general users, who may provide their own endstation or negotiate access to a privately owned endstation.

The ALS does not charge users for beam access if their research is nonproprietary. Users performing proprietary research are charged a fee based on full cost recovery for ALS usage. All users are responsible for the day-to-day costs of research (e.g., supplies, phone calls, technical support).

The nominal operating energy of the ALS storage ring is 1.9 GeV, although it can run from 1.0 to 1.9 GeV, allowing flexibility for user operations. At 1.9 GeV, the normal maximum operating current is 400 mA in multibunch operation. The spectral range of undulator and wiggler beamlines extends from photon energies of roughly 5 eV to 21 keV. On superbend beamlines, the range is between 2.4 and 60 keV. Bend magnets produce radiation from the infrared to about 20 keV.

The ALS is capable of accommodating approximately 50 beamlines and more than 100 endstations. The first user beamlines began operation in October 1993, and there were 32 operating beamlines, with several more under construction, by the end of 2002.



# ALS BEAMLINES\*

BEAMLINE	SOURCE**	AREAS OF RESEARCH/TECHNIQUES	MONOCHROMATOR	ENERGY RANGE	OPERATIONAL
1.4.2	Bend	Visible and infrared Fourier transform spectroscopy (FTIR)	Interferometer	0.002–3 eV (15–25,000 cm <sup>-1</sup> )	Now
1.4.3	Bend	Infrared spectromicroscopy	Interferometer	0.02–1 eV (200–10,000 cm <sup>-1</sup> )	Now
1.4.4	Bend	Infrared spectromicroscopy	Interferometer	0.05–1 eV (550–10,000 cm <sup>-1</sup> )	2003
3.1	Bend	Diagnostic beamline	Mirror/filter	1–2 keV	Now
3.2.1	Bend	Commercial deep-etch x-ray lithography (LIGA)	None	3–12 keV	Now
3.3.1	Bend	Deep-etch x-ray lithography (LIGA)	None	1–20 keV	Now
3.3.2	Bend	Deep-etch x-ray lithography (LIGA)	None	1–20 keV	Now
4.0.2	EPU5	Magnetic spectroscopy			
		XMCD chamber	Variable-included-angle PGM	52–1900 eV	Now
		X-ray absorption chamber	Variable-included-angle PGM	52–1900 eV	Now
		Advanced photoelectron spectrometer/diffractometer	Variable-included-angle PGM	52–1900 eV	Now
		Gas-phase absorption cell	Variable-included-angle PGM	52–1900 eV	Now
		Spin spectrometer	Variable-included-angle PGM	52–1900 eV	Now
		MXCD cryo-chamber	Variable-included-angle PGM	52–1900 eV	Now
		L-edge chamber with superconducting spectrometer	Variable-included-angle PGM	52–1900 eV	Now
		XMCD chamber (6 T, 2 K)	Variable-included-angle PGM	52–1900 eV	Now
		Photoemission electron microscope	Variable-included-angle PGM	52–1900 eV	Now
4.2.2	Superbend	Multiple-wavelength anomalous diffraction (MAD) and monochromatic protein crystallography	Double crystal	6–18 keV	2003
5.0.1	W16	Monochromatic protein crystallography	Curved crystal	12.4 keV	Now
5.0.2	W16	Multiple-wavelength anomalous diffraction (MAD) and monochromatic protein crystallography	Double crystal	3.5–14 keV	Now
5.0.3	W16	Monochromatic protein crystallography	Curved crystal	12.4 keV	Now
5.3.1	Bend	Femtosecond phenomena	Double crystal	1.8–12 keV	Now
5.3.2	Bend	Polymer scanning transmission x-ray microscopy	SGM	250–700 eV	Now
6.1.2	Bend	High-resolution zone-plate microscopy	Zone-plate linear	300–900 eV	Now
6.3.1	Bend	Calibration and standards, EUV/soft x-ray optics testing, solid-state chemistry	VLS-PGM	500–2000 eV	Now
6.3.2	Bend	Calibration and standards; EUV optics testing; atomic, molecular, and materials science	VLS-PGM	50–1300 eV	Now
7.0.1	U5	Surface and materials science, spectromicroscopy			
		Scanning photoemission microscope (SPEM)	SGM	100–800 eV	Now
		UltraESCA	SGM	60–1200 eV	Now
		Soft x-ray fluorescence spectrometer (SXF)	SGM	50–1200 eV	Now
7.3.1.1	Bend	Magnetic microscopy, spectromicroscopy	SGM	175–1500 eV	Now
7.3.1.2	Bend	Surface and materials science, micro x-ray photoelectron spectroscopy	SGM	175–1500 eV	Now
7.3.3	Bend	X-ray microdiffraction	White light, two or four crystal	6–12 keV	Now
8.0.1	U5	Surface and materials science, imaging photoelectron spectroscopy, soft x-ray fluorescence			
		Ellipsoidal-mirror electron energy analyzer (EMA)	SGM	65–1400 eV	Now
		Soft x-ray fluorescence spectrometer(SXF)	SGM	65–1400 eV	Now
8.2.1	Superbend	Multiple-wavelength anomalous diffraction (MAD) and monochromatic protein crystallography	Double crystal	5–17 keV	Now
8.2.2	Superbend	Multiple-wavelength anomalous diffraction (MAD) and monochromatic protein crystallography	Double crystal	5–17 keV	Now

BEAMLINE	SOURCE**	AREAS OF RESEARCH/TECHNIQUES	MONOCHROMATOR	ENERGY RANGE	OPERATIONAL
8.3.1	Superbend	Multiple-wavelength anomalous diffraction (MAD) and monochromatic protein crystallography	Double crystal	2.4–15 keV	Now
8.3.2	Superbend	Tomography	Double crystal	3–60 keV	2003
9.0.1	U10	Coherent optics/scattering experiments	None or off-axis zone plate	10–800 eV	Now
9.0.2	U10	Chemical reaction dynamics, photochemistry, high-resolution photoelectron and photoionization spectroscopy, photoelectron and photoionization imaging and spectroscopy			
		Crossed molecular beam	White light, Off-plane Eagle	5–30 eV	Now
		Molecular-beam photoelectron/photoion spectroscopy	White light, Off-plane Eagle	5–30 eV	Now
		Molecular-beam photoelectron/photoion imaging and spectroscopy	White light, Off-plane Eagle	5–30 eV	Now
		Flame chamber	White light, Off-plane Eagle	5–30 eV	Now
		Ablation chamber	White light, Off-plane Eagle	5–30 eV	Now
9.3.1	Bend	Atomic, molecular, and materials science			
		Angle-resolved time-of-flight electron spectrometer	Double crystal	2.2–6.0 keV	Now
		Ion time-of-flight spectrometer	Double crystal	2.2–6.0 keV	Now
		Magnetic mass analyzer	Double crystal	2.2–6.0 keV	Now
		Polarized-x-ray emission spectrometer	Double crystal	2.2–6.0 keV	2003
		X-ray absorption cell	Double crystal	2.2–6.0 keV	Now
9.3.2	Bend	Chemical and materials science, circular dichroism, spin resolution			
		Advanced materials chamber (AMC)	SGM	30–1400 eV	Now
		Ambient pressure photoemission	SGM	30–1400 eV	Now
10.0.1	U10	Photoemission of highly correlated materials; high-resolution atomic, molecular, and optical physics			
		High energy resolution spectrometer (HERS)	SGM	17–340 eV	Now
		Electron spin polarization (ESP)	SGM	17–340 eV	Now
		High-resolution atomic and molecular electron spectrometer (HIRAMES)	SGM	17–340 eV	Now
		Ion-photon beamline (IPB)	SGM	17–340 eV	Now
10.3.1	Bend	X-ray fluorescence microprobe	White light, multilayer mirrors	3–20 keV	Now
10.3.2	Bend	Environmental and materials science, micro x-ray absorption spectroscopy	White light, two crystal	2.5–17 keV	Now
11.0.2	EPU5	Molecular environmental science			
		Wet spectroscopy	Variable-included-angle PGM	75–2000 eV	Now
		High-pressure photoemission spectroscopy	Variable-included-angle PGM	75–2000 eV	Now
		Scanning transmission x-ray microscope (STXM)	Variable-included-angle PGM	180–1000 eV	Now
11.3.1	Bend	Small-molecule crystallography	Channel-cut Si(111)	6–17 keV	Now
11.3.2	Bend	Inspection of EUV lithography masks	VLS-PGM	50–1000 eV	Now
12.0.1	U8	EUV optics testing and interferometry, angle- and spin-resolved photoemission			
		EUV interferometer (two available)	VLS-PGM	60–320 eV	Now
		Angle- and spin-resolved photoemission	VLS-PGM	20–320 eV	2003
12.2.2	Superbend	California High-Pressure Science Observatory (CALIPSO)			
		Nanoscience/materials chemistry	Double crystal	6–40 keV	2003
		Solid-state physics/geoscience	Double crystal	6–40 keV	2003
12.3.1	Superbend	Multiple-wavelength anomalous diffraction (MAD) protein crystallography and small-angle x-ray scattering (SAXS)	Double crystal and double multilayer	6–18 keV	2003
BTF	Linac	Beam Test Facility	None	50-MeV electrons	Now

\*All listed beamlines except for Beamlines 1.4.2, 1.4.3, and 1.4.4 are capable of operating simultaneously. The information in this table is valid as of May 2003. The most current information on ALS beamlines is available on the Web at [http://www-als.lbl.gov/als/als\\_users\\_bl/bl\\_table.html](http://www-als.lbl.gov/als/als_users_bl/bl_table.html).

\*\*Bend = bend magnet; EPU5 = 5-cm-period elliptical polarization undulator; W16 = 16-cm-period wiggler; Ux = x-cm-period undulator; Superbend = superconducting bend magnet

## ALS INSERTION DEVICE PARAMETERS

DEVICE	BEAMLINE	STATUS	ENERGY RANGE (AT 1.5 GeV)	ENERGY RANGE (AT 1.9 GeV)	PERIOD LENGTH	NUMBER OF PERIODS	OPERATING GAP RANGE	PEAK EFFECTIVE FIELD RANGE
U5 Undulator	8.0	Operational	130–1900 eV	210–3000 eV	5.0 cm	89	1.4–4.5 cm	0.46–0.10 T
U5 Undulator	7.0	Operational	50–1900 eV	80–3000 eV	5.0 cm	89	1.4–4.5 cm	0.85–0.10 T
U8 Undulator	12.0	Operational	18–1200 eV	30–1900 eV	8.0 cm	55	2.5–8.3 cm	0.80–0.07 T
U10 Undulator	9.0	Operational	5–950 eV	8–1500 eV	10.0 cm	43	2.4–11.6 cm	0.98–0.05 T
U10 Undulator	10.0	Operational	8–950 eV	12–1500 eV	10.0 cm	43	2.4–11.6 cm	0.80–0.05 T
EPU5 Elliptical Undulator	4.0	Operational	60–1000 eV*	100–1500 eV*	5.0 cm	37	1.45–5.5 cm	0.79–0.10 T (vertical field) 0.54–0.10 T (horizontal field)
W16 Wiggler	5.0	Operational	5–13 keV	5–21 keV	16.0 cm	19	1.4–18.0 cm	2.1–0.03 T

\* Elliptical polarization mode

## ALS STORAGE RING PARAMETERS

PARAMETER	VALUE	PARAMETER	VALUE AT 1.5 GeV	VALUE AT 1.9 GeV
Beam particle	electron	Beam lifetime		
Beam energy	1.0–1.9 GeV	multibunch mode*	~3.5 hours at 400 mA	~8.0 hours at 400 mA
Injection energy	1.0–1.5 GeV	two-bunch mode	not used	~35 min. at 40 mA
Beam current		Horizontal emittance	4.2 nm-rad	6.75 nm-rad
multibunch mode	400 mA	Vertical emittance†	0.2 nm-rad	0.15 nm-rad
two-bunch mode	2 × 30 mA	Energy spread ( $\Delta E/E$ , rms)	$8 \times 10^{-4}$	$1 \times 10^{-3}$
Filling pattern (multibunch mode)	276 to 320 bunches possibility of 10-mA “camshaft” bunch in filling gap			
Bunch spacing				
multibunch mode	2 ns			
two-bunch mode	328 ns			
Circumference	196.8 m			
Number of straight sections	12			
Current number of insertion devices	7			
Radio frequency	500 MHz			
Beam size in straight sections, rms (multibunch mode)	310 microns horiz. × 23 microns vert. at 1.9 GeV			

\*In multibunch mode, the storage ring is typically filled every eight hours or as requested by our users.

†Vertical emittance is deliberately increased to improve beam lifetime.

# 2002 PUBLICATIONS

- Albrecht, M., M. Maret, A. Maier, F. Treuble, B. Riedlinger, U. Mazur, G. Schatz, and S. Anders, "Perpendicular magnetic anisotropy in CoPt<sub>3</sub>(111) films grown on a low energy surface at room temperature," *J. Appl. Phys.* **91**(10), 8153–8155 (May 2002).
- Allen, J.W., "Quasi-particles and their absence in photoemission spectroscopy," *Solid State Commun.* **123**(11), 469–487 (September 2002).
- Anders, S., M.F. Toney, T. Thomson, J.-U. Thiele, B.D. Terris, S. Sun, and C.B. Murray, "X-ray studies of magnetic nanoparticles," in *Proceedings of 47th Annual Conference on Magnetism and Magnetic Materials* (Tampa, Florida, November 11–15, 2002).
- Anders, S., S. Sun, C.B. Murray, C.T. Rettner, M.E. Best, T. Thomson, M. Albrecht, J.-U. Thiele, E.E. Fullerton, and B.D. Terris, "Lithography and self-assembly for nanometer scale magnetism," *Microelectron Eng.* **61–62**, 569–575 (July 2002).
- Axelrod, H., E.C. Abresch, M.Y. Okamura, A.P. Yeh, D.C. Rees, and G. Feher, "X-ray structure determination of the cytochrome *c*<sub>2</sub>: reaction center electron transfer complex from *Rhodobacter sphaeroides*," *J. Mol. Biol.* **319**(2), 501–515 (May 2002).
- Bajt, S., J.B. Alameda, T.W. Barbee, Jr., W.M. Clift, J.A. Folta, B. Kaufmann, and E.A. Spiller, "Improved reflectance and stability of Mo/Si multilayers," *Opt. Eng.* **41**(8), 1797–1804 (2002).
- Barry, W.C., K.M. Baptiste, R.J. Benjegerdes, A.K. Biocca, J.M. Byrd, W.E. Byrne, D. Cambie, M.J. Chin, J.P. Harkins, J.Y. Jung, S. Kwiatkowski, D. Li, S. Marks, M.C. Martin, W.R. McKinney, D.V. Munson, H. Nishimura, J.A. Paterson, D.W. Plate, K.R. Rex, D.S. Robin, S.L. Rossi, F. Sannibale, T. Scarvie, R.D. Schlueter, G.D. Stover, W.G. Thur, C. Steier, and J.P. Zbasnik, "A dedicated storage ring for far-IR coherent synchrotron radiation at the ALS," in *Proceedings of EPAC 2002* (Paris, France, June 3–7, 2002).
- Berrah, N., J.D. Bozek, G. Turri, G. Ackerman, B. Rude, H.L. Zhou, and S.T. Manson, "K-shell photodetachment of He<sup>-</sup>: Experiment and theory," *Phys. Rev. Lett.* **88**(9), Article 093001, 1–4 (2002).
- Birtalan, S.C., R.M. Phillips, and P. Ghosh, "Three-dimensional secretion signals in chaperone-effector complexes of bacterial pathogens," *Mol. Cell* **9**, 971–980 (May 2002).
- Bitto, E., and D.B. McKay, "Crystallographic structure of SurA, a molecular chaperone that facilitates folding of outer membrane porins," *Structure* **10**, 1489–1498 (November 2002).
- Bluhm, H., D.F. Ogletree, C.S. Fadley, Z. Hussain, and M. Salmeron, "The premelting of ice studied with photoelectron spectroscopy," *J. Phys: Condens. Matter* **14**(8), L227–L233 (March 2002).
- Bogdanov, P.V., A. Lanzara, X.J. Zhou, W.L. Yang, H. Eisaki, Z. Hussain, and Z.X. Shen, "Anomalous momentum dependence of the quasiparticle scattering rate in overdoped Bi<sub>2</sub>Sr<sub>2</sub>CaCu<sub>2</sub>O<sub>8</sub>," *Phys. Rev. Lett.* **89**(16), Article 167002, 1–4 (October 2002).
- Bonetta, D.T., M. Facette, T.K. Raab, and C.R. Somerville, "Genetic dissection of plant cell-wall biosynthesis," *Biochem. Soc. Trans.* **30**(2), 298–301 (2002).
- Bostedt, C., "Electronic structure of germanium nanocrystal films probed with synchrotron radiation," Ph.D. Thesis, Universität Hamburg, Germany, and Lawrence Livermore National Laboratory, 2002.
- Bostedt, C., T. van Buuren, T.M. Willey, N. Franco, T. Möller, and L.J. Terminello, "Photoemission spectroscopy of germanium nanocrystal films," *J. Electron Spectrosc.* **126**(1–3), 117–124 (October 2002).
- Bostedt, C.F.O., A. Van Buuren, T.M. Willey, A.J. Nelson, N. Franco, T. Moller, and L.J. Terminello, "Characterization of Ge-nanocrystal films with photoelectron spectroscopy," *Nucl. Instrum. Meth. B* **199**, 402–405 (January 2002); *Proceedings of the 3rd International Conference on Synchrotron Radiation in Materials Science*, Singapore, January 21–24, 2002.
- Braun, A., H. Wang, U. Bergmann, M.C. Tucker, W. Gu, S. Cramer, and E.J. Carins, "Origin of chemical shift of manganese in lithium battery electrode materials—A comparison of hard and soft x-ray techniques," *J. Power Sources* **112**(1), 231–235 (October 2002).
- Bressler, C., M. Saes, M. Chergui, D. Grolimund, and R. Abela, "Towards structural dynamics research with ultrashort pulse lasers and synchrotron radiation," in

- Femtochemistry and Femtobiology: Ultrafast Dynamics in Molecular Science*, Vol. I, edited by A. Douhal and J. Santamaria (World Scientific Publishing, Singapore, 2002), p. 49.
- Bressler, C., M. Saes, M. Chergui, D. Grolimund, R. Abela, and P. Pattison, "Towards structural dynamics in condensed chemical systems exploiting ultrafast time-resolved x-ray absorption spectroscopy," *J. Chem. Phys.* **116**(7), 2955–2966 (February 2002).
- Buonassisi, T., O.F. Vyvenko, A.A. Istratov, E.R. Weber, and R. Schindler, "Application of x-ray synchrotron techniques to the characterization of the chemical nature and recombination activity of grown-in and process-induced defects and impurities in solar cells," in *Materials Research Society Symposium Proceedings* (San Francisco, California, April 1–5, 2002).
- Buonassisi, T., O.F. Vyvenko, A.A. Istratov, E.R. Weber, R. Schindler, and G. Hahn, "Analysis of shunts in multicrystalline silicon solar cells using microprobe x-ray fluorescence technique," in *Proceedings of 12th Workshop on Crystalline Silicon Solar Cell Materials and Processes* (Breckenridge, Colorado, August 11–14, 2002).
- Butorin, S.M., C. Sathe, F. Saalem, J. Nordgren, and X.M. Zhu, "Probing the  $MN^{3+}$  sublattice in  $La_{0.5}Ca_{0.5}MnO_3$  by resonant inelastic soft x-ray scattering at the Mn  $L_{2,3}$  edge," *Surf. Rev. Lett.* **9**(2), 989–992 (2002).
- Byrd, J.M., W.C. Barry, H. Gang, and G.D. Stover, "Beam transfer function diagnostics for broadband multibunch feedback systems," in *Proceedings of EPAC 2002* (Paris, France, June 3–7, 2002).
- Byrd, J.M., A. Loftsdottir, W. Leemans, B. Marcellis, M. Martin, W. McKinney, F. Sannibale, T. Scarvie, and C. Steier, "Broadband self-amplified spontaneous coherent synchrotron radiation in a storage ring," in *Proceedings of EPAC 2002* (Paris, France, June 3–7, 2002).
- Byrd, J., S. De Santis, J. Jacob, and V. Serriere, "Transient beam loading effects in harmonic rf systems for light sources," *Phys. Rev. ST Accel. Beams* **5**(9), Article 092001, 1–11 (September 2002).
- Byrd, J.M., W.P. Leemans, A. Loftsdottir, B. Marcellis, M.C. Martin, W.R. McKinney, F. Sannibale, T. Scarvie, and C. Steier, "Observation of broadband self-amplified spontaneous coherent terahertz synchrotron radiation in a storage ring," *Phys. Rev. Lett.* **89**(22), Article 224801, 1–4 (2002).
- Canton, S.E., A.J. Yench, E. Kukk, J.D. Bozek, M.C.A. Lopes, G. Snell, and N. Berrah, "Experimental evidence of a dynamic Jahn–Teller effect in  $C_{60}^+$ ," *Phys. Rev. Lett.* **89**(4), Article 045502, 1–4 (2002).
- Carr, G.L., M.C. Martin, W.R. McKinney, K. Jordan, G.R. Neil, and G.P. Williams, "Very high power THz radiation at Jefferson Lab," *Phys. Med. Biol.* **47**, 3761–3764 (November 2002).
- Carr, G.L., M.C. Martin, W.R. McKinney, K. Jordan, G.R. Neil, and G.P. Williams, "High-power terahertz radiation from relativistic electrons," *Nature* **420**, 153–156 (November 2002).
- Carroll, T.X., K.J. Borve, L.J. Saethre, J.D. Bozek, E. Kukk, J.A. Hahne, and T.D. Thomas, "Carbon 1s photoelectron spectroscopy of  $CF_4$  and CO: Search for chemical effects on the carbon 1s hole-state lifetime," *J. Chem. Phys.* **116**(23), 10221–10228 (June 2002).
- Carroll, T.X., J.D. Bozek, E. Kukk, V. Myrseth, L.J. Saethre, T.D. Thomas, and K. Wiesner, "Xenon  $N_{4,5}OO$  Auger spectrum—A useful calibration source," *J. Electron Spectrosc.* **125**(2), 127–132 (2002).
- Cavalleri, M., H. Ogasawara, L.G.M. Pettersson, and A. Nilsson, "The interpretation of x-ray absorption spectra of water and ice," *Chem. Phys. Lett.* **364**(3–4), 363–370 (October 2002).
- Chambers, S.A., C.M. Wang, S. Thevuthasan, T. Droubay, D.E. McCready, A.S. Lea, V. Shutthanandan, and C.F. Windisch, Jr., "Epitaxial growth and properties of MBE-grown ferromagnetic Co-doped  $TiO_2$  anatase films on  $SrTiO_3(001)$  and  $LaAlO_3(001)$ ," *Thin Sol. Films* **418**(2), 197–210 (October 2002).
- Chang, C., P.P. Naulleau, E.H. Anderson, K.M. Rosfjord, and D.T. Attwood, "Diffractive optical elements based on Fourier optical techniques: A new class of optics for extreme ultraviolet and soft x-ray wavelengths," *Appl. Optics* **41**(35), 7384 (2002).
- Chang, G.S., T.A. Callcott, G.P. Zhang, G.T. Woods, S.H. Kim, S.W. Shin, K. Jeong, C.N. Whang, and A. Moewes, "Angular rotation of magnetic hysteresis of ion-irradiated ferromagnetic thin films," *Appl. Phys. Lett.* **81**(16), 3016–3018 (October 2002).
- Chen, W., M. Hochlaf, P. Rosmus, G.Z. He, and C.Y. Ng, "Vacuum ultraviolet pulsed field ionization-photoelectron study of OCS in the energy range of 15–19 eV," *J. Chem. Phys.* **116**(13), 5612–5621 (2002).
- Choi, W.J., T.Y. Lee, K.-N. Tu, N. Tamura, R.S. Celestre, A.A. MacDowell, Y.Y. Bong, L. Nguyen, and G.T. Sheng, "Structure and kinetics of Sn whisker growth on Pb-free

- solder finish," in *52nd Electronic Component & Technology Conference Proceedings* (San Diego, California, May 28–31, 2002).
- Choi, H.J., W.L. Ling, A. Scholl, J.H. Wolfe, U. Bovensiepen, F. Toyama, and Z.Q. Qiu, "Spin reorientation transition in magnetically coupled Fe/Cu/Ni/Cu(001)," *Phys. Rev. B* **66** (Article 014409), 1–5 (July 2002).
- Corlett, J.N., W. Barry, J.M. Byrd, R. Schoenlein, and A. Zholents, "Synchronization of x-ray pulses to the pump laser in an ultrafast x-ray facility," in *Proceedings of EPAC 2002* (Paris, France, June 3–7, 2002).
- Corlett, J.N., W. Barry, J.M. Byrd, S. DeSantis, P. Heimann, S. Lidia, D. Li, R. Rimmer, K. Robinson, R. Schoenlein, J. Tananbe, S. Wang, W. Wan, R. Wells, A. Zholents, M. Placidi, and W. Pirkel, "A recirculating linac based synchrotron light source for ultrafast x-ray science," in *Proceedings of EPAC 2002* (Paris, France, June 3–7, 2002).
- Covington, A.M., A. Aguilar, I.R. Covington, M.F. Gharaibeh, G. Hinojosa, C.A. Shirley, R.A. Phaneuf, I. Alvarez, C. Cisneros, I. Dominguez-Lopez, M.M. Sant'Anna, A.S. Schlacter, B.M. McLaughlin, and A. Dalgano, "Photoionization of Ne<sup>+</sup> using synchrotron radiation," *Phys. Rev. A* **66**(6, Article 062710), 1–10 (December 2002).
- Davies, D.R., H. Interthal, J.J. Champoux, and W.G. Hol, "The crystal structure of human Tyrosyl-DNA phosphodiesterase, Tdp1," *Structure* **10**(2), 237–248 (February 2002).
- Davies, D.R., H. Interthal, J.J. Champoux, and W.G. Hol, "Insights into substrate binding and catalytic mechanism of human tyrosyl-DNA phosphodiesterase (Tdp1) from vanadate and tungstate-inhibited structures," *J. Mol. Biol.* **324**(5), 917–932 (December 2002).
- Denecke, R., J. Morais, R.X. Ynzunza, G.H. Fecher, J.G. Menchero, J. Liesegang, J. Kortright, Z. Hussain, and C.S. Fadley, "Angular and temperature dependence of the magnetic circular dichroism in 4d core-level photoemission from Gd(0001)," *Phys. Rev. B* **65**(24, Article 245421), 1–18 (June 2002).
- Denlinger, J.D., G.-H. Gweon, J.W. Allen, and J.L. Sarrao, "Possibility of minimal surface contributions to low photon energy angle-resolved photoemission of CeRu<sub>2</sub>Si<sub>2</sub>," *Physica B* **312–313**, 670–672 (March 2002).
- Denlinger, J.D., G.-H. Gweon, J.W. Allen, and J.L. Sarrao, "Temperature dependent 5f-states in URu<sub>2</sub>Si<sub>2</sub>," *Physica B* **312–313**, 655–657 (March 2002).
- Denlinger, J.D., G.H. Gweon, J.W. Allen, A.D. Bianchi, and Z. Fisk, "Bulk band gaps in divalent hexaborides: A soft x-ray emission study," *Surf. Rev. Lett.* **9**(2), 1309–1330 (2002); *Proceedings of XIII International Conference on Vacuum Ultraviolet Radiation Physics, VUV-13, Trieste, Italy, July 23–27, 2001.*
- Denlinger, J.D., J.A. Clack, J.W. Allen, G.H. Gweon, D.M. Poirier, C.G. Olson, J.L. Sarrao, A.D. Bianchi, and Z. Fisk, "Bulk band gaps in divalent hexaborides," *Phys. Rev. Lett.* **89**(15, Article 157601), 1–4 (September 2002).
- Dessau, D., Z. Hussain, and Z.Q. Qiu, "Workshop on spectroscopies of electronic materials," *Synch. Rad. News* **15**(1), 13–14 (2002).
- Diaz, J., N.M. Hamdan, P. Jalil, Z. Hussain, S.M. Valvidares, and J.M. Alameda, "Understanding the magnetic anisotropy in Fe-Si amorphous alloys," *IEEE T. Magn.* **38**(5), 2811–2813 (2002).
- Díez Muiño, R., D. Rolles, F.J. García de Abajo, C.S. Fadley, and M.A. Van Hove, "Angular distributions of electrons photoemitted from core levels of oriented diatomic molecules: Multiple scattering theory in non-spherical potentials," *J. Phys. B-At. Mol. Opt.* **35**, L359–L365 (July 2002).
- Doukov, T.I., T.M. Iverson, J. Seravalli, S.W. Ragsdale, and C.L. Drennan, "A Ni-Fe-Cu center in a bifunctional carbon monoxide dehydrogenase/ acetyl-CoA synthase," *Science* **298**, 567–572 (October 2002).
- Duda, L.C., T. Schmitt, J. Nordgren, G. Dhalenne, and A. Revcolevschi, "Resonant inelastic soft x-ray scattering of insulating cuprates," *Surf. Rev. Lett.* **9**(2), 1103–1108 (2002).
- Eimueller, T., "Magnetic imaging of nanostructured systems with transmission x-ray microscopy," Ph.D. Thesis, University of Wuerzburg, Germany, 2002.
- Eimueller, T., M. Scholz, P. Guttmann, M. Koehler, G. Bayreuther, G. Schmahl, P. Fischer, and G. Schuetz, "Undulation instabilities in laterally structured magnetic multilayers," *J. Appl. Phys.* **91**(10), 7334–7336 (May 2002).
- Erzberger, J.P., M.M. Pirruccello, and J.M. Berger, "The structure of bacterial DnaA: Implications for general mechanisms underlying DNA replication initiation," *EMBO J.* **21**(18), 4763–4773 (September 2002).
- Feng, D.L., A. Damascelli, K. Shen, N. Motoyama, D.H. Lu, H. Eisaki, X.J. Zhou, Z.-X. Shen, et al., "Electronic structure of the trilayer cuprate superconductor Bi<sub>2</sub>Sr<sub>2</sub>Ca<sub>2</sub>Cu<sub>3</sub>O<sub>10+δ</sub>," *Phys. Rev. Lett.* **88**(10, Article 107001), 1–4 (March 2002).
- Feng, J., H. Padmore, D.H. Wei, S. Anders, Y. Wu, A. Scholl, and D. Robin, "Modeling the acceleration field and

- objective lens for an aberration corrected photoemission electron microscope," *Rev. Sci. Instrum.* **73**(3), 1514–1517 (March 2002).
- Finkelstein, L.D., E.I. Zabolotzky, M.A. Korotin, S.N. Shamin, S.M. Butorin, E.Z. Kurmaev, and J. Nordgren, "Vacant States of TiO<sub>2</sub> with rutile structure and their reflection in different-type x-ray absorption spectra," *X-Ray Spectrom.* **31**(6), 414–418 (2002).
- Fischer, P., G. Denbeaux, F. Nolting, D. Goll, T. Eimüller, Ch. Quitmann, and G. Schütz, "Imaging magnetic microstructures with soft x-ray microscopies," *IEEE T. Magn.* **2**(4), 234–237 (2002).
- Fischer, P., T. Eimueller, D. Goll, H. Stoll, A. Puzic, G. Schuetz, and G. Denbeaux, "Magnetic imaging with full-field soft x-ray microscopy," *Zeitschrift fuer Metall.* **93**(5), 372–376 (2002).
- Fischer, P., G. Denbeaux, T. Eimueller, D. Goll, and G. Schuetz, "Magnetic imaging with soft x-ray microscopy," *IEEE T. Magn.* **38**(5, Part 1), 2427–2431 (2002).
- Fischer, P., G. Denbeaux, T. Ono, T. Okuno, T. Eimueller, D. Goll, and G. Schuetz, "Study of magnetic domains with magnetic soft x-ray transmission microscopy," *J. Phys. D Appl. Phys.* **35**(19), 2391–2397 (October 2002).
- Föhlisch, A., O. Karis, M. Weinelt, J. Hasselström, A. Nilsson, and N. Mårtensson, "Auger resonant raman scattering in itinerant electron systems: Continuum excitations in Cu," *Phys. Rev. Lett.* **88**(2, Article 027601), 1–4 (January 2002).
- Fried, D., N. Ashouri, T. Breunig, and R. Shori, "Mechanism of water augmentation during IR laser irradiation of dental enamel," *Laser Surg. Med.* **31**(3), 186–193 (2002).
- Friedrich, S., T. Funk, O.B. Drury, S.E. Labov, and S.P. Cramer, "A multichannel superconducting soft x-ray spectrometer for high-resolution spectroscopy of dilute samples," *Rev. Sci. Instrum.* **73**(3), 1629–1631 (March 2002).
- Fullerton, E.E., O. Hellwig, Y. Ikeda, B. Lengsfeld, K. Takano, and J.B. Kortright, "Soft x-ray characterization of perpendicular recording media," *IEEE T. Magn.* **38**(4), 1693–1697 (2002).
- Funk, T., S. Friedrich, A. Young, E. Arenholz, and S. Cramer, "Requirements for x-ray magnetic circular dichroism on paramagnetic biological systems and model compounds," *Rev. Sci. Instrum.* **73**(3), 1649–1751 (March 2002).
- Goetz, D.H., M.A. Holmes, N. Borregaard, M.E. Bluhm, K.N. Raymond, and R.K. Strong, "The neutrophil lipocalin NGAL is a bacteriostatic agent that interferes with siderophore-mediated iron acquisition," *Mol. Cell* **10**, 1033–1043 (November 2002).
- Goldberg, K.A., "Graphical user interface for image acquisition and processing," January 1, 2002, Patent No. 6,341,183.
- Goldberg, K.A., P. Naulleau, and J. Bokor, "Fourier-transform interferometer alignment methods," *Appl. Optics* **41**(22), 4477–4783 (2002).
- Goldberg, K.A., P. Naulleau, J. Bokor, and H.N. Chapman, "Testing EUV optics with visible-light and EUV interferometry," *J. Vac. Sci. Technol. B* **20**(6), 2834–2839 (2002); Proceedings of the 46th International Conference on Electron, Ion and Photon Beam Technology and Nanofabrication, Anaheim, California, May 28–31, 2002.
- Goldberg, K.A., P. Naulleau, J. Bokor, and H.N. Chapman, "Honing the accuracy of extreme ultraviolet optical system testing: At-wavelength and visible-light measurements of the ETS Set-2 projection optic," in *Proceedings of SPIE Microlithography Conference 2002* (Santa Clara, California, March 5–7, 2002).
- Goldberg, K.A., P.P. Naulleau, J. Bokor, H.N. Chapman, A. Barty, D. Phillion, and G.E. Sommargren, "VNL research in interferometry for EUV optics," in *Proceedings of First International EUV Lithography Symposium* (Dallas, Texas, October 15–17, 2002).
- Goudeau, P., P. Villain, P.O. Renault, N. Tamura, R.S. Celestre, and H.A. Padmore, "Macro stress mapping on thin film buckling," *Mater. Sci. Forum* **404–407**, 709–714 (2002).
- Goudeau, P., P. Villain, N. Tamura, R.S. Celestre, and H.A. Padmore, "Residual stress mapping by micro x-ray diffraction: Application to the study of thin film buckling," *J. Physique IV France* **12**, 409–415 (2002).
- Gromko, A.D., Y.-D. Chuang, A.V. Fedorov, Y. Aiura, Y. Yamaguchi, K. Oka, Y. Ando, and D.S. Dessau, "ARPES studies of c-axis intracell coupling in Bi<sub>2</sub>Sr<sub>2</sub>CaCu<sub>2</sub>O<sub>8+δ</sub>," *J. Phys. Chem. Solids* **63**(12), 2299–2304 (December 2002).
- Guo, J., L. Vayssieres, C. Persson, R. Ahuja, B. Johansson, and J. Nordgren, "Polarization-dependent soft-x-ray absorption of highly oriented ZnO microrod arrays," *J. Phys: Condens. Matter* **14**(28), 6969–6974 (July 2002).
- Guo, J., Y. Luo, A. Augustsson, J.-E. Rubensson, C. Sathe, H. Agren, H. Siegbahn, and J. Nordgren, "X-ray emission spectroscopy of hydrogen bonding and electronic structure of liquid water," *Phys. Rev. Lett.* **89**(13, Article 137402), 1–4 (September 2002).

- Hamdan, N.M., P.V. Sastry, and J. Schwartz, "Magnetic properties of fluorinated HgPb-1223 high  $T_c$  superconductors," *IEEE T. Appl. Supercon.* **12**(1), 1132–1135 (2002).
- Hansen, D.L., W.C. Stolte, O. Hemmers, R. Guillemin, and D.W. Lindle, "Anion formation moderated by post-collision interaction following core-level photofragmentation of CO," *J. Phys. B-At. Mol. Opt.* **35**(17), L381–L386 (September 2002).
- Hansen, C.L., E. Skordalakes, J.M. Berger, and S.R. Quake, "A robust and scalable microfluidic metering method that allows protein crystal growth by free interface diffusion," *Proc. Natl. Acad. Sci. USA* **99**, 16531–16536 (October 2002).
- He, X., C. Radu, J. Sidney, A. Sette, E.S. Ward, and K.C. Garcia, "Structural snapshot of aberrant antigen presentation linked to autoimmunity: The immunodominant epitope of MBP complexed with I-Au," *Immunity* **17**(1), 83–94 (2002).
- He, X., M.E. Grigg, J.C. Boothroyd, and K.C. Garcia, "Structure of the immunodominant surface antigen from the *Toxoplasma gondii* SRS superfamily," *Nat. Struct. Biol.* **9**(8), 606–611 (2002).
- Head-Gordon, T.L., and G.L. Hura, "Water structure from scattering experiments and simulation," *Chem. Rev.* **102**(8), 2651–2670 (2002).
- Hellwig, O., D.T. Margulies, B. Lengsfeld, E.E. Fullerton, and J.B. Kortright, "Role of boron on grain sizes and magnetic correlation lengths in recording media as determined by soft x-ray scattering," *Appl. Phys. Lett.* **80**(7), 1234–1236 (February 2002).
- Hellwig, O., S. Maat, J.B. Kortright, and E. Fullerton, "Magnetic reversal of perpendicularly-biased Co/Pt multilayers," *Phys. Rev. B* **65** (14, Article 144418), 1–4 (March 2002).
- Hemmers, O.A., M. Blackburn, T.B. Goddard, P. Glans, H. Wang, S.B. Whitfield, R. Wehlitz, I.A. Sellin, and D.W. Lindle, "Dipole and nondipole angular-distribution effects in the valence photoemission of neon," *J. Electron Spectrosc.* **123**, 257–264 (January 2002).
- Hemphill, R., M.G. Pelizzo, and M. Hurwitz, "Extreme-ultraviolet calibration of thin-film Zr filters for the cosmic hot interstellar plasma spectrometer," *Appl. Optics* **41**(22), 4680–4685 (August 2002).
- Heske, C., O. Fuchs, D. Eich, A. Fleszar, L. Weinhardt, U. Groh, R. Fink, and E. Umbach, "Resonant soft x-ray Raman spectroscopy," in *XVIII Int. Conf. on Raman Spectroscopy* (Budapest, Hungary, August 25–30, 2002).
- Heske, C., U. Groh, L. Weinhardt, O. Fuchs, B. Holder, E. Umbach, C. Bostedt, L.J. Terminello, S. Zweigart, T.P. Niesen, and F. Karg, "Damp-heat induced sulfate formation in Cu(In,Ga)(S,Se)<sub>2</sub>-based thin film solar cells," *Appl. Phys. Lett.* **81**(24), 4550–4552 (December 2002).
- Hinojosa, G., A.M. Covington, R.A. Phaneuf, M.M. Sant'Anna, R. Hernandez, I.R. Covington, I. Dominguez, J.D. Bozek, A.S. Schlachter, I. Alvarez, and C. Cisneros, "Formation of long-lived CO<sup>2+</sup> via photoionization of CO<sup>+</sup>," *Phys. Rev. A* **66**(3, Article 032718), 1–5 (September 2002).
- Hitchcock, A.P., and J.J. Neville, "Photoionization dynamics from inner shell mass spectrometry," in *Chemical Applications of Synchrotron Radiation*, Vol. 12A, edited by T.K. Sham (World Scientific, Singapore, 2002), pp. 154–227.
- Hitchcock, A.P., C. Morin, T. Tyliczszak, I.N. Koprinarov, H. Ikeura-Sekiguchi, J.R. Lawrence, and G.G. Leppard, "Soft x-ray microscopy of soft matter—Hard information from two softs," *Surf. Rev. Lett.* **9**(1), 193–202 (February 2002).
- Hitchcock, A.P., C. Morin, Y.M. Heng, R.M. Cornelius, and J.L. Brash, "Towards practical soft x-ray spectromicroscopy of biomaterials," *Journal of Biomaterials Science, Polymer Edition* **13**(8), 919–938 (September 2002).
- Hlawatsch, S., C.D. Garbe-Schonberg, F.F. Lechtenberg, A. Manceau, N. Tamura, D.A. Kulik, and M. Kersten, "Trace metal fluxes to ferromanganese nodules from the western Baltic Sea as a record for long-term environmental changes," *Chem. Geol.* **182**(2–4), 697–709 (February 2002).
- Hochstrasser, M., J.G. Tobin, E. Rotenberg, and S.D. Kevan, "Spin-resolved photoemission of surface states of W(110)-(1×1)H," *Phys. Rev. Lett.* **89**(21, Article 216802), 1–4 (November 2002).
- Holm, A.P., S.M. Kauzlarich, S.A. Morton, G.D. Waddill, W.E. Pickett, and J.G. Tobin, "XMCD characterization of the ferromagnetic state of Yb<sub>14</sub>MnSb<sub>11</sub>," *J. Am. Chem. Soc.* **124**(33), 9894–9898 (2002).
- Holm, A.P., "Bulk and element-specific studies of some complex transition-metal zintl phases," Ph.D. Thesis, University of California, Davis, 2002.
- Holman, H.-Y., K. Nieman, D.L. Sorensen, C.D. Miller, M.C. Martin, T. Borch, W.R. McKinney, and R.C. Sims, "Catalysis of PAH biodegradation by humic acid shown in synchrotron infrared studies," *Environ. Sci. Technol.* **36**(6), 1276–1280 (2002).

- Holman, H.-Y., K.A. Bjornstad, M.P. McNamara, M.C. Martin, W.R. McKinney, and E.A. Blakely, "Synchrotron infrared spectromicroscopy as a novel bioanalytical microprobe for individual living cells: Cytotoxicity considerations," *J. Biomed. Opt.* **7**(3), 417–424 (2002).
- Holmes, M.A., P. Li, E.F. Petersdorf, and R.K. Strong, "Structural studies of allelic diversity of the MHC class I homolog MIC-B, a stress-inducible ligand for the activating immunoreceptor NKG2D," *J. Immunology* **169**(3), 1395–1400 (2002).
- Isaure, M.P., A. Laboudigue, A. Manceau, G. Sarret, C. Tiffreau, P. Trocellier, G. Lambelle, J.-L. Hazemann, and D. Chateigner, "Quantitative Zn speciation in a contaminated dredged sediment by  $\mu$ -PIXE,  $\mu$ -SXRF, EXAFS spectroscopy and principal component analysis," *Geochim. Cosmochim. Acta* **66**(9), 1549–1567 (May 2002).
- Istratov, A.A., H. Hieslmair, O.F. Vyvenko, E.R. Weber, and R. Schindler, "Defect recognition and impurity detection techniques in crystalline silicon for solar cells," *Sol. Energ. Mat. Sol. C.* **72**(1–4), 441–451 (April 2002).
- Jahnke, T., Th. Weber, A.L. Landers, A. Knapp, S. Schössler, J. Nickles, S. Kammer, O. Jagutzki, L. Schmidt, A. Czasch, T. Osipov, E. Arenholz, A. Young, R. Díez Muiño, D. Rolles, F.J. García de Abajo, C.S. Fadley, M.A. Van Hove, S.K. Semenov, N.A. Cherepkov, J. Rösch, M.H. Prior, H. Schmidt-Böcking, C.L. Cocke, and R. Dörner, "Circular dichroism in K-shell ionization from fixed-in-space CO and N<sub>2</sub> molecules," *Phys. Rev. Lett.* **88**(7, Article 073002), 1–4 (February 2002).
- Johnson, S.L., "Ultrafast x-ray absorption spectroscopy: Properties of liquid silicon and carbon," Ph.D. Thesis, University of California, Berkeley, 2002.
- Jung, C.U., J.Y. Kim, P. Chowdhury, K.H.P. Kim, S.-I. Lee, D.S. Koh, N. Tamura, W.A. Caldwell, and J.R. Patel, "Microstructure and pinning properties of hexagonal-disc shaped single crystalline MgB<sub>2</sub>," *Phys. Rev. B* **66**(18, Article 184519), 1–5 (November 2002).
- Kim, Y., S. Kim, T.N. Earnest, and W.G. Hol, "Precursor structure of cephalosporin acylase: Insights into auto-proteolytic activation in a new N-terminal hydrolase family," *J. Biol. Chem.* **277**(4), 2823–2829 (January 2002).
- Kittel, M., R. Terborg, M. Polcik, A.M. Bradshaw, R.L. Toomes, D.P. Woodruff, and E. Rotenberg, "The structure of the Pd(110)(2 $\times$ 1)-CO surface," *Surf. Sci.* **511**(1–3), 34–42 (2002).
- Kjornrattanawanich, B., "Reflectance, optical properties, and stability of molybdenum/strontium and molybdenum/yttrium multilayer mirrors," Ph. D. Thesis, University of California, Davis, and Lawrence Livermore National Laboratory, 2002.
- Klebanoff, L.E., W.M. Clift, N. Franco, C. Bostedt, and L.J. Terminello, "Assessment of extreme ultraviolet-induced charging of subtractive metal lithography masks," *J. Vac. Sci. Technol. B* **20**(6), 2367–2374 (2002).
- Knapp, A., M. Walter, Th. Weber, A.L. Landers, S. Schoessler, T. Jahnke, M. Schoeffler, J. Nickles, S. Kammer, O. Jagutzki, L.Ph.H. Schmidt, T. Osipov, J. Roesch, M.H. Prior, H. Schmidt-Boecking, C.L. Cocke, J. Feagin, and R. Doerner, "Energy sharing and asymmetry parameters for photo double ionization of helium 100 eV above threshold in single-particle and Jacobi coordinates," *J. Phys. B-At. Mol. Opt.* **35**(23), L521–L526 (December 2002).
- Knapp, A., A. Kheifets, I. Bray, Th. Weber, A.L. Landers, S. Schössler, T. Jahnke, J. Nickles, S. Kammer, O. Jagutzki, L.Ph.H. Schmidt, T. Osipov, J. Rösch, M.H. Prior, H. S. Schmidt-Böcking, C.L. Cocke, and R. Dörner, "Mechanisms of photo double ionization of helium by 530 eV photons," *Phys. Rev. Lett.* **89**(3, Article 033004), 1–4 (2002).
- Köhler, M., J. Zweck, G. Bayreuther, P. Fischer, G. Schütz, G. Denbeaux, and D. Attwood, "Micromagnetic investigation of sub-100-nm magnetic domains in atomically stacked Fe(001)/Au(001) multilayers," *J. Magn. Magn. Mater.* **240**(1–3), 79–82 (2002).
- Koprinarov, I.N., A.P. Hitchcock, C.T. McCrory, and R.F. Childs, "Quantitative mapping of structured polymeric systems using singular value decomposition analysis of soft x-ray images," *J. Phys. Chem. B* **106**(21), 5358–5364 (2002).
- Kortright, J.B., O. Hellwig, D.T. Margulies, and E. Fullerton, "Resolving magnetic and chemical correlations in CoPtCr films using soft x-ray resonant scattering," *J. Magn. Magn. Mater.* **240**(1–3), 325–330 (February 2002).
- Kukk, E., "Nuclear dynamics and electronic structure of molecules by resonant Auger spectroscopy," *J. Electron Spectrosc.* **127**(1–2), 43–51 (2002).
- Kurmaev, E.Z., I.I. Lyakhovskaya, J. Kortus, A. Moewes, N. Miyata, M. Demeter, M. Neumann, M. Yanagihara, M. Watanabe, T. Muranaka, J. Akimitsu, et al., "Electronic structure of MgB<sub>2</sub>: X-ray emission and absorption studies," *Phys. Rev. B* **65** (13, Article 134509), 1–4 (April 2002).
- Kurmaev, E.Z., K. Endo, T. Ida, T. Otsuka, S.Y. Kim, G.S. Chang, A. Moewes, N.Y. Kim, C.N. Whang, and D.L. Ederer, "The electronic structure of TPD films grown by different methods," *Orgel* **3**, 15–21 (Spring 2002).
- Kurmaev, E.Z., A. Moewes, R.P. Winarski, S.N. Shamin, D.L. Ederer, J.Y. Feng, and S.S. Turner, "Characterization

- of CN<sub>x</sub> films by x-ray emission measurements," *Thin Sol. Films* **402**(1–2), 60–64 (January 2002).
- Kurmaev, E.Z., A. Moewes, N.D. Zhigadlo, E. Takayama-Muromachi, I.A. Nekrasov, O.A. Bureev, G.T. Woods, T.A. Callcott, Y.M. Yarmoshenko, S.N. Shamin, D.L. Ederer, M. Yanagihari, et al., "Local electronic structure of doping atoms in MA<sub>2</sub>Ca<sub>n-1</sub>Cu<sub>n</sub>O<sub>2n+3</sub> high-T<sub>c</sub> superconductors with [M–12(n–1)n] type structures," *Surf. Rev. Lett.* **9**(2), 1345–1350 (April 2002).
- Kurmaev, E.Z., A. Moewes, and D.L. Ederer, "Soft x-ray fluorescence measurements in materials science," *X-Ray Spectrom.* **31**(3), 219–224 (2002).
- Kurmaev, E.Z., A. Moewes, S. Chiuzbaian, L.D. Finkelstein, M. Neumann, S.S. Turner, and P. Day, "Valence-band spectra of BEDT-TTF and TTF-based magnetic charge transfer salts," *Phys. Rev. B* **65**(Article 235106), 1–6 (June 2002).
- Kurmaev, E.Z., S. Shin, M. Watanabe, R. Eguchi, Y. Ishiwata, T. Takeuchi, A. Moewes, D.L. Ederer, Y. Gao, M. Iwami, M. Yanagihara, et al., "Probing oxygen and nitrogen bonding sites in chitosan by x-ray emission," *J. Electron Spectrosc.* **125**(2), 133–138 (August 2002).
- Kurmaev, E.Z., A. Moewes, J.-C. Pivin, M. Bach, K. Endo, T. Ida, S. Shimada, M. Neumann, S.N. Shamin, D.L. Ederer, M. Iwami, et al., "Polymer conversion into amorphous ceramics by ion irradiation," *J. Mater. Sci.* **37**(17), 3789–3793 (September 2002).
- Kurmaev, E.Z., A.V. Galakhov, A. Moewes, S. Moehlecke, and Y. Kopelevich, "Interlayer conduction band states in graphite-sulfur composite," *Phys. Rev. B* **66**(19, Article 193402), 1–3 (November 2002).
- Kurmaev, E.Z., A. Moewes, O.G. Bureev, I.A. Nekrasov, V.M. Cherkashenko, M.A. Korotin, and D.L. Ederer, "Electronic structure of niobium oxides," *J. Alloys Compd.* **347**(1–2), 213–218 (December 2002).
- Kurtis, K.E., C.L. Collins, and P.J.M. Monteiro, "The surface chemistry of the alkali-silica reaction: A critical evaluation and x-ray microscopy," *RILEM Concrete Sci. Eng.* **4**, 2–11 (March 2002).
- Kusinski, G.J., G. Thomas, G. Denbeaux, K.M. Krishnan, and B.D. Terris, "Temperature and ion irradiation dependence of magnetic domains and microstructure in Co/Pt multilayers," *J. Appl. Phys.* **91**(10), 7541–7543 (May 2002).
- Laidman, S., M. Pangilinan, R. Guillemin, S.W. Yu, G. Ohrwall, D.W. Lindle, and O. Hemmers, "Exploring the limits of the dipole approximation with angle-resolved electron time-of-flight spectrometry," *U.S. DOE J. Undergrad. Res.* **2**(2), 65–70 (2002).
- Lanzara, A., P.V. Bogdanov, X.J. Zhou, H. Eisaki, T. Yoshida, A. Fujimori, Z. Hussain, and Z.-X. Shen, "Coupling of quasiparticles to phonons in high temperature superconductors," *J. Electron Spectrosc.* **127**(1–2), 37–41 (November 2002).
- Lau, J.K., "A Gaussian-3 study of the photodissociation channels of propylene sulfide," *J. Phys. Chem. A* **106**(46), 11025–11028 (2002).
- Li, P., G. McDermott, and R.K. Strong, "Crystal structures of RAE-1β and its complex with the activating immunoreceptor NKG2D," *Immunity* **16**(1), 77–86 (January 2002).
- Li, D., and J.N. Corlett, "RF deflecting cavity design for Berkeley ultrafast x-ray source," in *Proceedings of EPAC 2002* (Paris, France, June 3–7, 2002).
- Ling, W.L., E. Rotenberg, H.J. Choi, J.H. Wolfe, F. Toyama, S. Paik, N.V. Smith, and Z.Q. Qiu, "Double quantum well states in Cu/Co/Cu grown on Co(001)," *Phys. Rev. B* **65**(11, Article 113406), 1–4 (March 2002).
- Lowther, W.T., H. Weissbach, F. Etienne, N. Brot, and B.W. Matthews, "The mirrored methionine sulfoxide reductases of *Neisseria gonorrhoeae* pilB," *Nat. Struct. Biol.* **9**(5), 348–352 (May 2002).
- Luebbert, D., J. Arthur, M. Sztucki, T.H. Metzger, P.B. Griffin, and J.R. Patel, "X-ray diffuse scattering study of the kinetics of stacking fault growth and annihilation in boron-implanted silicon," *Appl. Phys. Lett.* **81**(17), 3167–3169 (October 2002).
- Lunt, S., "Determining the indices of refraction of reactively sputtered uranium dioxide thin films from 46 to 584 angstroms," M.S. Thesis, Brigham Young University, Provo, Utah, 2002.
- Magnuson, M., S.M. Butorin, J.H. Guo, and J. Nordgren, "Electronic structure investigation of CoO by means of soft x-ray scattering," *Phys. Rev. B* **65**(20, Article 205106), 1–5 (May 2002).
- Malinowski, M., C. Steinhaus, M. Clift, L.E. Klefanoff, S. Mrowka, and R. Soufli, "Controlling contaminations in Mo/Si multilayer mirrors by Si surface-capping modifications," in *Emerging Lithographic Technologies VI* (Santa Clara, California, March 3–8, 2002).
- Manceau, A., M.A. Marcus, and N. Tamura, "Quantitative speciation of heavy metals in soils and sediments by synchrotron x-ray techniques," in *Applications of*

- Synchrotron Radiation in Low-Temperature Geochemistry and Environmental Science*, Vol. 49, edited by P. Fenter, M. Rivers, N.C. Sturchio, S. Sutton (Mineralogical Society of America, Washington, D.C., 2002), pp. 341–428.
- Manceau, A., N. Tamura, M.A. Marcus, A.A. MacDowell, R.S. Celestre, R.E. Sublett, G. Sposito, and H.A. Padmore, "Deciphering Ni sequestration in soil ferromanganese nodules by combining x-ray fluorescence, absorption and diffraction at micrometer scales of resolution," *Am. Mineral.* **87**, 1494–1499 (October 2002).
- Marchesini, S., N. Mannella, C.S. Fadley, M.A. Van Hove, J.J. Bucher, D.K. Shuh, L. Fabris, M.H. Press, M.W. West, W.C. Stolte, and Z. Hussain, "Holographic analysis of diffraction structure factors," *Phys. Rev. B* **66**(9), Article 094111, 1–4 (September 2002).
- Marks, S., J. Zbasnik, R.D. Schlueter, C. Steier, M. Chin, R. DeMarco, M. Fahmie, J.A. Paterson, J. Krupnick, D.S. Robin, et al., "ALS superbend magnet performance," *IEEE T. Appl. Supercon.* **12**(1), 149–152 (2002).
- Marks, S., R. Schlueter, D. Anderson, W. Gath, J.Y. Jung, D. Robin, C. Steier, and T. Stevens, "New chicane magnet design for insertion device straights at the Advanced Light Source," *IEEE T. Appl. Supercon.* **12**(1), 153–156 (2002).
- Martinez, S.E., A.Y. Wu, N.A. Glavas, X.-B. Tang, S. Turley, W.G.J. Hol, and J.A. Beavo, "The two GAF domains in phosphodiesterase 2A have distinct roles in dimerization and in cGMP binding," *Proc. Natl. Acad. Sci. USA* **99**(20), 13260–13265 (2002).
- McHugo, S.A., A. Mohammed, A.C. Thompson, B. Lai, and Z. Cai, "Copper precipitates in silicon: Precipitation, dissolution, and chemical state," *J. Appl. Phys.* **91**(10), 6396–6405 (May 2002).
- McLaughlin, K.W., O. Yenen, D.H. Jaecks, T.J. Gay, M.M. Sant'Anna, D. Calabrese, and B. Thaden-Jordan, "Effect of relativistic many-electron interactions on photoelectron partial wave probabilities," *Phys. Rev. Lett.* **88**(12), Article 123003, 1–4 (March 2002).
- Meng, W., L.L. Swenson, M.J. Fitzgibbon, K. Hayakawa, E. ter Haar, A.E. Behrens, J.R. Fulghum, and J.A. Lippke, "Structure of mitogen-activated protein kinase-activated protein (MAPKAP) kinase 2 suggests a bifunctional switch that couples kinase activation with nuclear export," *J. Biol. Chem.* **277**(40), 37401–37405 (October 2002).
- Miller, J.L., M.L. Morton, L.J. Butler, F. Qi, M.J. Krisch, and J. Shu, "Dissociation channels of the 1-propenyl radical and its photolytic precursor *cis*-1-bromopropene," *J. Phys. Chem. A* **106**(45), 10965–10967 (November 2002).
- Minko, S., M. Muller, D. Usov, A. Scholl, C. Froeck, and M. Stamm, "Lateral versus perpendicular segregation in mixed polymer brushes," *Phys. Rev. Lett.* **88**(3), Article 35502, 1–4 (January 2002).
- Mitchell, G.E., L.R. Wilson, M.T. Dineen, S.G. Urquhart, F. Hayes, E.G. Rightor, A.P. Hitchcock, and H. Ade, "Quantitative characterization of microscopic variations in the cross-link density of gels," *Macromol.* **35**(4), 1336–1341 (2002).
- Moewes, A., E.Z. Kurmaev, J. Tse, M. Geshi, M.J. Ferguson, V.A. Trofimova, and Y.M. Yarmoshenko, "Electronic structure of alkali-metal-doped  $M_8Si_{46}$  ( $M=Na, K$ ) clathrates," *Phys. Rev. B* **65**(15), Article 153106, 1–3 (April 2002).
- Morton, M.L., L.J. Butler, T.A. Stephenson, and F. Qi, "C–Cl bond fission, HCl elimination, and secondary radical decomposition in the 193 nm photodissociation of allyl chloride," *J. Chem. Phys.* **116**(7), 2763–2766 (February 2002).
- Morton, S.A., G.D. Waddill, S. Kim, I.K. Schuller, S.A. Chambers, and J.G. Tobin, "Spin-resolved photoelectron spectroscopy of  $Fe_3O_4$ ," *Surf. Sci.* **513**(3), 451–457 (August 2002).
- Morton, M.L., J.L. Miller, L.J. Butler, and F. Qi, "Dissociation channels of the 1-propenyl radical and its photolytic precursor *cis*-1-bromopropene," *J. Phys. Chem. A* **106**(45), 10831–10842 (2002).
- Mosavi, L.K., D.L. Minor, Jr., and Z.-Y. Peng, "Consensus-derived structural determinants of the ankyrin repeat motif," *Proc. Natl. Acad. Sci. USA* **99**(25), 16029–16034 (2002).
- Müller, A., R.A. Phaneuf, A. Aguilar, M.F. Gharaibeh, A.S. Schlachter, I. Alvarez, C. Ciscneros, G. Hinojosa, and B.M. McLaughlin, "Photoionization of  $C^{2+}$  ions: Time-reversed recombination of  $C^{3+}$  with electrons," *J. Phys. B-At. Mol. Opt.* **35**(7), L137–L143 (April 2002).
- Mura, C., "The structures, functions, and evolution of Sm-like archaeal proteins (SmAPs)," Ph.D. Thesis, University of California, Los Angeles, 2002.
- Muramatsu, Y., H. Takenaka, E.M. Gullikson, and R.C. Perera, "Evaluation methods of interlayer-structure-distribution in multilayers by total-electron-yield x-ray standing-wave measurements," *Adv. X-Ray Chem. Anal. Jpn.* **33**, 145–154 (2002).
- Muramatsu, Y., K. Kuramoto, E.M. Gullikson, and R.C. Perera, "Soft x-ray absorption spectra in the 0 K region of microporous carbon and some reference aromatic compounds," *Surf. Rev. Lett.* **9**(1), 267–270 (February 2002).

- Muramatsu, Y., H. Takenaka, E.M. Gullikson, and R.C. Perera, "Total-electron-yield x-ray standing-wave measurements of multilayer x-ray mirrors for the interface structure evaluation," *Jpn. J. Appl. Phys.* **1** **41**(6), 4250–4252 (2002).
- Myneni, S., Y. Luo, L.A. Naslund, L. Ojamae, H. Ogawawara, A. Pelmenchikov, P. Wernet, P. Vaterlain, C. Heske, Z. Hussain, L.G.M. Pettersson, and A. Nilsson, "Spectroscopic probing of local hydrogen-bonding structures in liquid water," *J. Phys: Condens. Matter* **14**(8), L213–L219 (March 2002).
- Myrseth, V., J.D. Bozek, E. Kukk, L.J. Saethre, and T.D. Thomas, "Adiabatic and vertical carbon 1s ionization energies in representative small molecules," *J. Electron Spectrosc.* **122**(1), 57–63 (2002).
- Nagar, B., W.G. Bornmann, P. Pellicena, T. Schindler, D.R. Veach, W.T. Miller, B. Clarkson, and J. Kuriyan, "Crystal structures of the kinase domain of c-Abl in complex with the small molecule inhibitors PD173955 and imatinib (STI-571)," *Cancer Res.* **62**, 4236–4243 (June 2002).
- Naulleau, P., K.A. Goldberg, E. Anderson, D. Attwood, P. Batson, J. Bokor, P. Denham, E.M. Gullikson, B. Hoef, K.H. Jackson, S. Rekawa, F. Salmassi, K.L. Blaedel, K.N. Chapman, L.C. Hale, R. Soufli, E.A. Spiller, D.W. Sweeney, J.S. Taylor, C.C. Walton, G.F. Cardinale, A.K. Ray-Chaudhuri, A. Fisher, D.J. O'Connell, R.H. Stulen, D.A. Tichenor, C.W. Gwyn, P. Yan, and G. Zhang, "Static microfield printing at the Advanced Light Source with the ETS set-2 optic," in *Emerging Lithographic Technologies VI* (Santa Clara California, March 3–8, 2002).
- Naulleau, P.P., E.H. Anderson, E.M. Gullikson, and J. Bokor, "Fabrication of high-efficiency multilayer-coated binary blazed gratings in the EUV regime," *Opt. Commun.* **200**(1–6), 27–34 (2001).
- Naulleau, P.P., P.J. Batson, P. Denham, D. Richardson, and J. Underwood, "An in situ scanning-slit alignment system for Kirkpatrick–Baez optics," *Opt. Commun.* **212**(4–6), 225–233 (2002).
- Naulleau, P.P., K.A. Goldberg, E.H. Anderson, D.T. Attwood, P.J. Batson, J. Bokor, P. Denham, E.M. Gullikson, B. Harteneck, B. Hoef, K. Jackson, D. Olynick, S. Rekawa, F. Salmassi, K. Blaedel, H. Chapman, H. Layton, P. Mirkarimi, S. Regina, E. Spiller, D. Sweeney, J. Taylor, C. Walton, A. Chaudhuri, D. O'Connell, R. Stulen, D. Tichenor, C. Gwyn, P. Yan, and G. Zhang, "Sub 70-nm EUV lithography at the Advanced Light Source static microfield exposure station using the ETS Set-2 optic," *J. Vac. Sci. Technol. B* **20**(6), 2829–2833 (2002).
- Naulleau, P.P., W.C. Sweatt, and D.A. Tichenor, "Theoretical efficiency analysis of a condenser-embedded grating-based spectral purity filter for EUV lithography," *Opt. Commun.* **214**(1–6), 31–38 (2002).
- Ng, C.Y., "Vacuum ultraviolet spectroscopy and chemistry by photoionization and photoelectron methods," *Ann. Rev. Phys. Chem.* **53**, 101–140 (February 2002).
- Ng, C.Y., "State-selected and state to state ion-molecule reaction dynamics," *J. Phys. Chem. A* **106**(25), 5953–5966 (2002).
- Nilsson, A., "Applications of core level spectroscopy to adsorbates," *J. Electron Spectrosc.* **126**(1–3), 3–42 (October 2002).
- Nolting, F., J. Luning, J. Rockenberger, J. Hu, and A.P. Alivisatos, "A PEEM study of small agglomerates of colloidal iron oxide nanocrystals," *Surf. Rev. Lett.* **9**(1), 437–440 (February 2002).
- Nordgren, E.J., S.M. Butorin, L.C. Duda, J.H. Guo, and J.E. Rubensson, "Soft x-ray fluorescence spectroscopy for materials science and chemical physics," in *Chemical Applications of Synchrotron Radiation*, Vol. 12, edited by T.K. Sham (World Scientific Publishing Co., River Edge, 2002), pp. 517–572.
- Nowakowski, J., C.N. Cronin, D.E. McRee, M.W. Knuth, C.G. Nelson, N.P. Pavletich, J. Rogers, B.-C. Sang, D.N. Scheibe, R.V. Swanson, and D.A. Thompson, "Structures of the cancer-related Aurora-A, FAK, and EphA2 protein kinases from nanovolume crystallography," *Structure* **10**(12), 1659–1667 (December 2002).
- Ogletree, D.F., H. Bluhm, G. Lebedev, C.S. Fadley, Z. Hussain, and M. Salmeron, "A differentially pumped electrostatic lens system for photoemission studies in the millibar range," *Rev. Sci. Instrum.* **73**(11), 3872–3877 (November 2002).
- Ohrwall, G., M.M. Sant'Anna, W.C. Stolte, I. Dominguez-Lopez, L.T.N. Dang, A.S. Schlachter, and D.W. Lindle, "Anion and cation formation following core-level photoexcitation of CO<sub>2</sub>," *J. Phys. B–At. Mol. Opt.* **35**(21), 4543–4552 (November 2002).
- Omori, S., L. Zhao, S. Marchesini, M.A. Van Hove, and C.S. Fadley, "Resonant x-ray fluorescence holography: Three-dimensional atomic imaging in true color," *Phys. Rev. B* **65**(1, Article 014101), 1–5 (2002).
- Omori, S., Y. Nihei, E. Rotenberg, J.D. Denlinger, S. Marchesini, S.E. Kevan, B.P. Tonner, M.A. Van Hove, and C.S. Fadley, "Differential photoelectron holography: A new approach for three-dimensional atomic imaging," *Phys. Rev. Lett.* **88**(5, Article 055504), 116–118 (February 2002).

- Ostheimer, G.J., A. Barkan, and B.W. Matthews, "Crystal structure of *E. coli* YhbY: A representative of a novel class of RNA binding proteins," *Structure* **10**(11), 1593–1601 (November 2002).
- Pan, H., S.C. Tsai, E.S. Meadows, L.J.M. Miercke, A.T. Keatinge-Clay, J. O'Connell, C. Khosla, and R.M. Stroud, "Crystal structure of the priming beta-ketosynthase from the R1128 polyketide biosynthetic pathway," *Struct. Fold. Des.* **10**(11), 1559–1568 (November 2002).
- Pederson, M.R., A.Y. Liu, T. Baruah, E.Z. Kurmaev, A. Moewes, S. Chiuzaian, M. Neumann, C.R. Kmety, K.L. Stevenson, and D. Ederer, "Electronic structure of the molecule-based magnet  $Mn[N(CN)_2]_2$  from theory and experiment," *Phys. Rev. B* **66**(1, Article 014446), 1–8 (July 2002).
- Piancastelli, M.N., W.C. Stolte, G. Öhrwall, S.-W. Yu, D. Bull, K. Lantz, A.S. Schlachter, and D.W. Lindle, "Fragmentation processes following core excitation in acetylene and ethylene by partial ion yield spectroscopy," *J. Chem. Phys.* **117**(18), 8264–8269 (November 2002).
- Preciado, J.A., B. Rubinsky, D. Otten, B. Nelson, M.C. Martin, and R. Greif, "Radiative properties of polar bear hair," in *Bio-engineering* **53**, Proceedings of ASME IMECE 2002 Conference (New Orleans, Louisiana, November 17–22, 2002).
- Qi, F., and A.G. Suits, "Photodissociation of propylene sulfide at 193 nm: A photofragment translational spectroscopy study with VUV synchrotron radiation," *J. Phys. Chem. A* **106**(46), 11017–11024 (2002).
- Qi, F., L. Sheng, M. Ahmed, D.S. Peterka, and T. Baer, "Exclusive production of excited state sulfur ( $^1D$ ) from 193 nm photolysis of thietane," *Chem. Phys. Lett.* **357**(3–4), 204–208 (May 2002).
- Qi, F., and A.G. Suits, "Photodissociation of propylene sulfide at 193 nm: A photofragment translational spectroscopy study with VUV synchrotron radiation," *J. Phys. Chem. A* **106**(46), 11017–11024 (November 2002).
- Qian, X.M., Y. Song, K.C. Lau, C.Y. Ng, J. Liu, W. Chen, and G.Z. He, "A pulsed field ionization photoelectron-photoion coincidence study of the dissociative photoionization process  $D_2O + hv \rightarrow OD^+ + D + e^-$ ," *Chem. Phys. Lett.* **353**(1–2), 19–26 (2002).
- Qin, B.Y., S.S. Lam, J.J. Correia, and K. Lin, "Smad3 allosteric links TGF-beta receptor kinase activation to transcriptional control," *Genes Dev.* **16**(15), 1950–1963 (August 2002).
- Qiu, Z.Q., and N.V. Smith, "Quantum well states and oscillatory magnetic interlayer coupling," *J. Phys: Condens. Matter* **14**(8), 169–193 (March 2002).
- Quillin, M.L., and B.W. Matthews, "Generation of noble-gas binding sites for crystallographic phasing using site-directed mutagenesis," *Acta Crystallogr. D.* **58**(1), 97–103 (January 2002).
- Radisky, E.S., and D.E. Koshland, Jr., "A clogged gutter mechanism for protease inhibitors," *Proc. Natl. Acad. Sci. USA* **99**(16), 10316–10321 (2002).
- Rahmim, A., S. Tixier, T. Tiedje, S. Eisebitt, M. Loergen, R. Scherer, W. Eberhardt, J. Luening, and A. Scholl, "Interference between magnetism and surface roughness in coherent soft x-ray scattering," *Phys. Rev. B.* **65**(23, Article 235421), 1–13 (June 2002).
- Rathbone, G.J., "Mode specific photoionization dynamics in polyatomic molecules," Ph.D. Thesis, Louisiana State University, Baton Rouge, 2002.
- Rehr, J.J., W. Schattke, F.J. García de Abajo, R. Díez Muiño, and M.A. Van Hove, "Development of the scattering theory of x-ray absorption and core level photoemission," *J. Electron Spectrosc.* **126**(1–3), 67–76 (October 2002).
- Rightor, E.G., S.G. Urquhart, A.P. Hitchcock, H. Ade, A.P. Smith, G.E. Mitchell, R.D. Priester, W.E. Lidy, G. Appel, G. Wilkes, et al., "Identification and quantitation of urea precipitates in flexible polyurethanes by x-ray spectromicroscopy," *Macromolecules* **35**(15), 5873–5882 (July 2002).
- Roberts, D.R., "Speciation and sorption mechanisms of metals in soils using bulk and micro-focused spectroscopic and microscopic techniques," Ph.D. Thesis, University of Delaware, Newark, 2002.
- Roberts, D.R., A.C. Scheinost, and D.L. Sparks, "Zn speciation in a smelter-contaminated soil profile using bulk and microspectroscopic techniques," *Environ. Sci. Technol.* **36**(8), 1742–1750 (2002).
- Robin, D.S., A.L. Robinson, and L.S. Tamura, "Superbends extend the scope of Berkeley's ALS," *CERN Courier* **42**(2), 28–31 (2002).
- Robin, D., R. Benjegerdes, A. Biocca, P. Bish, W. Brown, W. Byrne, D. Calais, M. Chin, C. Corradi, D. Coulomb, J. De Vries, R. DeMarco, M. Fahmie, A. Geyer, J. Harkins, T. Henderson, J. Hinkson, E. Hoyer, D. Hull, S. Jacobson, J. Krupnik, S. Marks, J. McDonald, P. Molinari, R. Mueller, L. Nadolski, K. Nishimura, F. Ottens, J.A. Paterson, P. Pipersky, A. Ritchie, S. Rossi, B. Salvant, R. Schlueter, A. Schwartz, J. Spring, C. Steier, C. Taylor, W. Thur, C. Timossi, A. Wandesforde, J. Jbasnik, J. Chen, B. Wang, and W. Decking, "Successful completion of the ALS Superbend Project," in *Proceedings of EPAC 2002* (Paris, France, June 3–7, 2002).

- Robinson, J.C., S.A. Harris, W. Sun, N.E. Sveum, and D.M. Neumark, "Photofragment translational spectroscopy of 1,3-butadiene and 1,3-butadiene-1,1,4,4- $d_4$  at 193 nm," *J. Am. Chem. Soc.* **124**(34), 10211–10224 (December 2002).
- Rockenberger, J., F. Nolting, J. Luning, J. Hu, and A.P. Alivisatos, "Soft x-ray imaging and spectroscopy of single nanocrystals," *J. Chem. Phys.* **116**(14), 6322–6328 (2002).
- Rotenberg, E., and S.D. Kevan, "Electron–phonon coupling in W(110)–(1×1)H," *J. Electron Spectrosc.* **126**(1–3), 125–132 (2002).
- Rotenberg, E., W. Theis, and K. Horn, "Model simulations of momentum-resolved photoemission from quasicrystals," *J. Alloys Compd.* **342**(1–2), 348–351 (2002).
- Rubin, S.M., S.-Y. Lee, E.J. Ruiz, A. Pines, and D.E. Wemmer, "Detection and characterization of xenon-binding sites in proteins by  $^{129}\text{Xe}$  NMR spectroscopy," *J. Mol. Biol.* **322**(2), 425–440 (September 2002).
- Rudenko, G., L. Henry, K. Henderson, K. Ichtchenko, M.S. Brown, J.L. Goldstein, and J. Deisenhofer, "Structure of the LDL receptor extracellular domain at endosomal pH," *Science* **298**(5602), 2353–2358 (2002).
- Rupert, P.B., A.P. Massey, S.T. Sigurdsson, and A.R. Ferre-D'Amare, "Transition state stabilization by a catalytic RNA," *Science* **298**(5597), 1421–1424 (2002).
- Ruscic, B., A.F. Wagner, L.B. Harding, R.L. Asher, D. Feller, D.A. Dixon, K.A. Peterson, Y. Song, X. Qian, C.Y. Ng, J. Liu, W. Chen, and D.W. Schwenke, "On the enthalpy of formation of hydroxyl radical and gas-phase dissociation energies of water and hydroxyl," *J. Phys. Chem. A* **106**(11), 2727–2747 (2002).
- Ryter, J.M., C.Q. Doe, and B.W. Matthews, "Structure of the DNA binding region of Prospero reveals a novel homeo-Prospero domain," *Structure* **10**, 1541–1549 (2002).
- Sacchi, M., and C.F. Hague, "Magnetic coupling in thin layers and superlattices investigated by resonant scattering of polarized soft x-ray," *Surf. Rev. Lett.* **9**, 811–820 (April 2002).
- Sae-Lao, B., S. Bajt, C. Montcalm, and J.F. Seely, "Performance of normal-incidence molybdenum/yttrium multilayer-coated diffraction grating at wavelength of 9 nm," *Appl. Optics* **41**(13), 2394–2400 (2002).
- Sae-Lao, B., and R. Soufli, "Measurements of the refractive index of yttrium in the 50–1300 eV energy region," *Appl. Optics* **41**(34), 7309–7316 (2002).
- Saiz, E., M. Goldman, J.M. Gomez-Vega, A.P. Tomsia, G.W. Marshall, and S.J. Marshall, "In vitro of silicate glass coatings in  $\text{Ti}_6\text{Al}_4\text{V}$ ," *Biomaterials* **23**(17), 3749–3756 (September 2002).
- Sarret, G., P. Saumitou-Laprade, V. Bert, O. Proux, J.L. Hazemann, A. Traverse, M.A. Marcus, and A. Manceau, "Forms of zinc accumulated in the hyperaccumulator *Arabidopsis halleri*," *Plant Physio.* **130**, 1815–1826 (December 2002).
- Schafer, J., R. Claessen, E. Rotenberg, S.D. Kevan, P. Blaha, and R.E. Thorne, "Peierls fluctuations in the electron system of a quasi-one-dimensional solid," *Surf. Rev. Lett.* **9**(2), 1029–1033 (2002).
- Schafer, J., E. Rotenberg, S.D. Kevan, P. Blaha, R. Claessen, and R.E. Thorne, "Electronic precursor states of the charge density wave in  $\text{NbSe}_3$ ," *Physica B* **312–313**, 650–652 (March 2002).
- Scheider, G., M.A. Meyer, G. Denbeaux, E. Anderson, B. Bates, A. Pearson, C. Knochel, D. Hambach, E.A. Stach, and E. Zschech, "Electromigration in passivated Cu interconnects studied by transmission x-ray microscopy," *J. Vac. Sci. Technol. B* **20**(6), 3089–3094 (2002).
- Schippers, S., S. Kieslich, A. Müller, G. Gwinner, M. Schnell, A. Wolf, A. Covington, M.E. Bannister, and L.-B. Zhao, "Interference effects in the photorecombination of argon-like  $\text{Sc}^{3+}$  ions: Storage-ring experiment and theory," *Phys. Rev. A* **65**(4, Article 042723), 1–10 (April 2002).
- Schippers, S., A. Müller, S. Ricz, M.E. Bannister, G.H. Dunn, J. Bozek, A.S. Schlachter, G. Hinojosa, C. Cisneros, A. Aguilar, A.M. Covington, M.F. Gharaibeh, R.A. Phaneuf, et al., "Experimental link of photoionization of  $\text{Sc}^{2+}$  to photorecombination of  $\text{Sc}^{3+}$ : An application of detailed balance in a unique atomic system," *Phys. Rev. Lett.* **89**(19, Article 193002), 1–10 (April 2002).
- Schmitt, T., L.-C. Duda, A. Augustsson, J. Guo, J. Nordgren, J.E. Downes, C. McGuinness, K.E. Smith, G. Dhalenne, A. Rewoleschi, K. Klemm, and S. Horn, "Resonant soft x-ray emission spectrometer of  $\text{V}_2\text{O}_3$ ,  $\text{VO}_2$  and  $\text{NaV}_2\text{O}_5$ ," *Surf. Rev. Lett.* **9**(2), 1369–1374 (2002).
- Schneider, G., G. Denbeaux, E.H. Anderson, B. Bates, A. Pearson, M.A. Meyer, E. Zschech, D. Hambach, and E.A. Stach, "Dynamical x-ray microscopy investigation of electromigration in passivated inlaid Cu interconnect structures," *Appl. Phys. Lett.* **81**(14), 2535–2537 (2002).
- Scholl, A., "Thin-film magnetism: PEEM studies," in *Encyclopedia of Materials: Science and Technology*, from [http://www.elsevier.com/homepage/sai/emsat\\_gateway/](http://www.elsevier.com/homepage/sai/emsat_gateway/), edited by K.H.J. Buschow, R.W. Cahn, M.C. Flemings, B. Ilshner, E.J. Kramer, S. Mahajan, Elsevier (Oxford, 2002).

- Scholl, A., H. Ohldag, F. Nolting, J. Stohr, and H.A. Padmore, "X-ray photoemission electron microscopy, a tool for the investigation of complex magnetic structures," *Rev. Sci. Instrum.* **73**(3), 1362–1366 (March 2002).
- Serriere, V., "Longitudinal beam dynamics in electron storage rings with a harmonic RF system for bunch lengthening," Ph.D. Thesis, University Paris XI, France, 2002.
- Shein, I.R., A.L. Ivanovskii, E.Z. Kurmaev, A. Moewes, S. Chiuzaibaian, L.D. Finkelstein, M. Neumann, Z.A. Ren, and G.C. Che, "Effect of Co doping on the electronic structure of MgCNi<sub>3</sub>," *Phys. Rev. B* **66**(2, Article 024520), 1–5 (July 2002).
- Shiau, A.K., D. Barstad, J.T. Radek, M.J. Meyers, K.W. Nettles, B.S. Katzenellenbogen, J.A. Katzenellenbogen, D.A. Agard, and G.L. Greene, "Structural characterization of a subtype-selective ligand reveals a novel mode of estrogen receptor antagonism," *Nat. Struct. Biol.* **9**(5), 359–364 (2002).
- Shin, D.H., H. Yokota, R. Kim, and S.H. Kim, "Crystal structure of conserved hypothetical protein Aq1575 from *Aquifex aeolicus*," *Proc. Natl. Acad. Sci. USA* **99**(12), 7980–7985 (2002).
- Sintchak, M.D., G. Arjara, B.A. Kellogg, J. Stubbe, and C.L. Drennan, "The crystal structure of class II ribonucleotide reductase reveals how an allosterically regulated monomer mimics a dimer," *Nat. Struct. Biol.* **9**(4), 293–300 (April 2002).
- Snell, G.P., B. Langer, A. Young, and N. Berrah, "Spin-polarization measurements of the krypton M<sub>4,5</sub>NN and xenon N<sub>4,5</sub>OO Auger electrons: Orientation and intrinsic parameters," *Phys. Rev. A* **66**(2, Article 022701), 1–13 (2002).
- Sorenson, T.A., S.A. Morton, G.D. Waddill, and J.A. Switzer, "Epitaxial electrodeposition of Fe<sub>3</sub>O<sub>4</sub> thin films on the low index planes of gold," *J. Am. Chem. Soc.* **124**(25), 7604–7609 (June 2002).
- Spence, J.C., U. Weierstall, and M. Howells, "Phase recovery and lensless imaging by iterative methods in optical, x-ray and electron diffraction," *Philos. Trans. Math. Phys. Eng. Sci.* **360**(1794), 875–895 (March 2002).
- Spezzani, C., P. Torelli, M. Sacchi, R. Delaunay, C.F. Hague, A. Mirone, F. Salmassi, E.M. Gullikson, and J.H. Underwood, "Magnetic coupling in Co/Cu multilayers: Field dependent antiferromagnetic ordering investigated by resonant x-ray scattering," *Surf. Rev. Lett.* **9**(2), 921–924 (2002).
- Spezzani, C., P. Torelli, M. Sacchi, R. Delaunay, C.F. Hague, F. Salmassi, and E.M. Gullikson, "Hysteresis curves of ferromagnetic and antiferromagnetic order in metallic multilayers by resonant x-ray scattering," *Phys. Rev. B* **66**(Article 052408), 1–4 (August 2002).
- Spezzani, C., P. Torelli, M. Sacchi, R. Delaunay, C.F. Hague, V. Cros, and F. Petroff, "Antiferromagnetic hysteresis in magneto-resistive multilayers viewed by x-ray resonant scattering," *Appl. Phys. Lett.* **81**(18), 3425–3427 (2002).
- Stamos, J., M.X. Sliwkowski, and C. Eigenbrot, "Structure of the epidermal growth factor receptor kinase domain alone and in complex with a 4-anilinoquinazoline inhibitor," *J. Biol. Chem.* **277**(48), 46265–46272 (2002).
- Staudte, A, C.L. Cocke, M.H. Prior, A. Belkacem, C. Ray, H. Chong, T.E. Glover, R.W. Schoenlein, and U. Saalman, "Observation of a nearly isotropic, high-energy Coulomb explosion group in the fragmentation of D<sub>2</sub> by short laser pulses," *Phys. Rev. A* **65**(2, Article 20703), 1–4 (February 2002).
- Steier, C., D. Robin, L. Nadolski, W. Decking, Y. Wu, and J. Laskar, "Measuring and optimizing the momentum aperture in a particle accelerator," *Phys. Rev. E* **65**(5, Article 056506), 1–17 (May 2002).
- Steier, C., A. Biocca, E. Domning, S. Jacobson, L. Nadolski, G. Portmann, T. Scarvie, and E. Williams, "Orbit feedback development at the ALS," in *Proceedings of EPAC 2002* (Paris, France, June 3–7, 2002).
- Steier, C., T. Byrne, L. Nadolski, D. Robin, B. Salvant, T. Scarvie, and W. Decking, "Commissioning of the ALS with superbends," in *Proceedings of EPAC 2002* (Paris, France, June 3–7, 2002).
- Stolte, W.C., G. Ohrwall, M.M. Sant'Anna, I. Dominguez Lopez, L.T. Dang, M.N. Piancastelli, and D.W. Lindle, "100% site-selective fragmentation in core-hole-photoexcited methanol by anion-yield spectroscopy," *J. Phys. B-At. Mol. Opt.* **35**(12), L253–L259 (June 2002).
- Strawn, D.G., H.E. Doner, and S. McHugo, "Microscale investigation into the geochemistry of arsenic, selenium, and iron in soil developed in pyritic shale materials," *Geoderma* **108**, 237–257 (May 2002).
- Sun, S., S. Anders, H.F. Hamann, J.-U. Thiele, J.E.E. Baglin, T. Thomson, E.E. Fullerton, C.B. Murray, and B.D. Terris, "Polymer mediated self-assembly of magnetic nanoparticles," *J. Am. Chem. Soc.* **124**(12), 2884–2885 (2002).
- Szpunar, D.E., M.L. Morton, L.J. Butler, and P.M. Regan, "Primary and secondary dissociation from allyl iodide excited at 193 nm: Centrifugal effects in the unimolecular dissociation of the allyl radical," *J. Phys. Chem. B* **106**(33), 8086–8095 (2002).

- Takenaka, H., K. Nagai, H. Ito, T. Sakuma, K. Namikawa, Y. Muramatsu, E.M. Gullikson, and R.C. Perera, "Soft x-ray reflectivity and thermal stability of CoCr/C multilayer x-ray mirrors," *Surf. Rev. Lett.* **9**(1), 593–596 (2002).
- Talley, J.W., U. Ghosh, S.G. Tucker, J.S. Furey, and R.G. Luthy, "Particle-scale understanding of the bioavailability of PAHs in sediment," *Environ. Sci. Technol.* **36**(3), 477–483 (2002).
- Tamura, N., R.S. Celestre, A.A. MacDowell, H.A. Padmore, R. Spolenak, B.C. Valek, N. Meier Chang, A. Manceau, and J.R. Patel, "Submicron x-ray diffraction and its applications to problems in materials and environmental science," *Rev. Sci. Instrum.* **73**(3), 1369–1372 (2002).
- Tamura, N., A.A. MacDowell, R.S. Celestre, H.A. Padmore, B. Valek, J.C. Brawman, R. Spolenak, W.L. Brown, T. Marieb, H. Fujimoto, B.W. Batterman, J.R. Patel, et al., "High spatial resolution grain orientation and strain mapping in thin films using polychromatic submicron x-ray diffraction," *Appl. Phys. Lett.* **80**(20), 3724–3727 (2002).
- Terry, J.H., R.K. Schulze, J.D. Farr, T.G. Zocco, K. Heinzelman, E. Rotenberg, D.K. Shuh, G. van der Laan, D.A. Arena, and J.G. Tobin, "5f resonant photoemission from plutonium," *Surf. Sci.* **499**(1), L141–L147 (February 2002).
- Tobin, J.G., D.A. Arena, B.W. Chung, P. Roussel, J.H. Terry, R.K. Schulze, J.D. Farr, T.G. Zocco, K. Heinzelman, E. Rotenberg, and D.K. Shuh, "Photoelectron spectroscopy of plutonium at the Advanced Light Source," *J. Nucl. Sci. Technol.* **33**, 98–101 (November 2002).
- Tsai, S.C., H. Lu, D.E. Cane, C. Khosla, and R.M. Stroud, "Insights into channel architecture and substrate specificity from crystal structures of two macrocycle-forming thioesterases of modular polyketide synthases," *Biochemistry-US* **41**(42), 12598–12606 (October 2002).
- Usov, D., M. Stamm, S. Minko, C. Froeck, A. Scholl, and M. Muller, "Nanostructured polymer brushes with reversibly changing properties," *MRS 2002 Proc. (Symp. R)* **727**, R2.2 (Spring 2002).
- Vajdos, F.F., C.W. Adams, T.N. Breece, L.G. Presta, A.M. de Vos, and S.S. Sidhu, "Comprehensive functional maps of the antigen-binding site of an anti-ErbB2 antibody obtained with shotgun scanning mutagenesis," *J. Mol. Biol.* **320**(2), 415–428 (July 2002).
- Valek, B.C., J.C. Brawman, N. Tamura, A.A. MacDowell, R.S. Celestre, H.A. Padmore, R. Spolenak, W.L. Brown, B.W. Batterman, and J.R. Patel, "Electromigration-induced plastic deformation in passivated metal lines," *Appl. Phys. Lett.* **81**(22), 4168–4170 (2002).
- Van Buuren, A., C.F.O. Bostedt, B.R. Taylor, T.M. Willey, L. Hope-Weeks, B. Weeks, and L.J. Terminello, "X-ray absorption study of colloidal Ge quantum dots," *Proc. SPIE* **4807**, 1–9 (September 2002); Proceedings of the SPIE Conference, Seattle, Washington, July 7–11, 2002.
- Vayssieres, L., J. Guo, and J. Nordgren, "3D highly oriented nanoparticulate and microparticulate array of metal oxide materials," *Mater. Res. Soc. Symp. Proc.* **704**, 341–351 (Winter 2002); Materials Research Society Symposium Proceedings, Boston, Massachusetts, December 2–6, 2002.
- Vogel, J.P., T.K. Raab, C.L. Schiff, and S.C. Somerville, "PMR6, a pectate lyase-like gene required for powdery mildew susceptibility in arabidopsis," *Plant Cell* **14**, 2095–2106 (September 2002).
- Vyvenko, O., A. Buonassisi, A.A. Istratov, H. Hieslmair, A.C. Thompson, R. Schindler, and E.R. Weber, "X-ray beam induced current—A synchrotron radiation based technique for the in situ analysis of recombination properties and chemical nature of metal clusters in silicon," *J. Appl. Phys.* **91**(6), 3614–3617 (March 2002).
- Vyvenko, O.F., T. Buonassisi, A.A. Istratov, and E.R. Weber, "Application of synchrotron radiation based x-ray microprobe techniques for the analysis of recombination activity of metals precipitated at Si/SiGe misfit dislocations," in *Proceedings of 12th Workshop on Crystalline Silicon Solar Cell Materials and Processes* (Breckenridge, Colorado, August 11–14, 2002).
- Vyvenko, O.F., T. Buonassisi, A.A. Istratov, and E.R. Weber, "Application of x-ray fluorescence technique to studies of aluminum gettering in silicon," in *Proceedings of 12th Workshop on Crystalline Silicon Solar Cell Materials and Processes* (Breckenridge, Colorado, August 11–14, 2002).
- Vyvenko, O.F., T. Buonassisi, A.A. Istratov, E.R. Weber, M. Kittler, and W. Seifert, "Application of synchrotron-radiation-based x-ray microprobe techniques for the analysis of recombination activity of metals precipitated at Si/SiGe misfit dislocations," *J. Phys. Condens. Matter* **14**(48), 13079–13086 (December 2002).
- Wardell, M., Z. Wang, J.X. Ho, J. Robert, F. Ruker, J.R. Ruble, and D.C. Carter, "The atomic structure of human methemalbumin at 1.9 Å," *Biochem. Biophys. Res. Comm.* **291**(4), 813–819 (2002).
- Warwick, T., H. Ade, D. Kilcoyne, M. Kritscher, T. Tyliczcak, S. Fakra, A. Hitchcock, P. Hitchcock, and H. Padmore, "A new bend-magnet beamline for scanning transmission x-ray microscopy at the Advanced Light Source," *J. Synchrotron Radiat.* **9**(4), 254–257 (July 2002).

- Weierstall, U., Q. Chen, J.C. Spence, M.R. Howells, M. Isaacson, and R.R. Panepucci, "Image reconstruction from electron and x-ray diffraction patterns using iterative algorithms: Experiment and simulation," *Ultramicroscopy* **90**(2–3), 171–195 (February 2002).
- Wilkinson, T.J., D.L. Perry, W.R. McKinney, and M.C. Martin, "Physics and forensics," *Phys. World* **15**(3), 43–46 (2002).
- Wilkinson, T.J., D.L. Perry, M.C. Martin, W.R. McKinney, and A.A. Cantu, "Use of synchrotron reflectance infrared spectromicroscopy as a rapid, direct, non-destructive method for the study of inks on paper," *Appl. Spectrosc.* **56**(6), 800–803 (2002).
- Wills, A.A., E.J. Sokell, T.W. Gorczyca, X. Feng, M.F. Wiedenhoef, S.E. Canton, and N. Berrah, "Importance of spin-orbit interactions for the He  $2lnl$  states revealed by a novel use of angle-resolved photoelectron spectroscopy," *J. Phys. B-At. Mol. Opt.* **35**(15), L367–L374 (August 2002).
- Wilson, K.R., M. Cavalleri, B.S. Rude, R.D. Schaller, A. Nilsson, L.G. Pettersson, N. Goldman, R. Catalano, J.D. Bozek, et al., "Characterization of hydrogen bond acceptor molecules at the water surface using near-edge x-ray absorption fine-structure spectroscopy and density functional theory," *J. Phys. Condens. Matter* **14**(8), L221–L226 (March 2002).
- Wilson, K.R., R.D. Schaller, D.T. Co, R.J. Saykally, B.S. Rude, T. Catalano, and J.D. Bozek, "Surface relaxation in liquid water and methanol studied by x-ray absorption spectroscopy," *J. Chem. Phys.* **117**(16), 7738–7744 (October 2002).
- Windt, D.L., E.M. Gulliksen, and C.C. Walton, "Normal-incidence reflectance of optimized W/B<sub>4</sub>C x-ray multilayers in the range 1.4 nm <  $\lambda$  < 2.4 nm," *Opt. Lett.* **27**(24), 2212–2214 (December 2002).
- Witty, M., C. Sanz, A. Shah, J.G. Grossmann, K. Mizuguchi, R.N. Perham, and B. Luisi, "Structure of the periplasmic domain of *Pseudomonas aeruginosa* TolA: Evidence for an evolutionary relationship with the TonB transporter protein," *EMBO J.* **21**(16), 4207–4218 (2002).
- Wood, Z.A., L.B. Poole, R.R. Hantgan, and P.A. Karplus, "Dimers to doughnuts: Redox-sensitive oligomerization of 2-cysteine peroxiredoxins," *Biochemistry-US* **41**(17), 5493–5504 (April 2002).
- Woods, G.T., G.P. Zhang, T.A. Callcott, L. Lin, G.S. Chang, B. Sales, D. Mandrus, and J. He, "Site-selected O 2p densities of states in NaV<sub>2</sub>O<sub>5</sub> determined from angular-dependent x-ray absorption and emission spectra," *Phys. Rev. B* **65**(16, Article 165108), 1–6 (April 2002).
- Wu, Y.Z., C. Won, and Z.Q. Qiu, "Magnetic uniaxial anisotropy of Fe films grown on vicinal Ag(001)," *Phys. Rev. B* **65**(18, Article 184419), 1–6 (May 2002).
- Wu, Y.Z., C.Y. Won, E. Rotenberg, H.W. Zhao, F. Toyoma, N.V. Smith, and Z.Q. Qiu, "Dispersion of quantum well states in Cu/Co/Cu(001)," *Phys. Rev. B* **66**, 245418–245423 (December 2002).
- Wu, Y.Z., C. Won, A. Scholl, A. Doran, F. Toyoma, X.F. Jin, N.V. Smith, and Z.Q. Qiu, "Interfacial magnetism of fcc Fe and the effect of the oscillatory interlayer coupling on the Ni magnetic properties in Ni/Fe/Co/Cu(100)," *Phys. Rev. B* **65**(21, Article 214417), 1–7 (June 2002).
- Yang, S., B.S. Mun, N. Mannella, S.-K. Kim, J.B. Kortright, J.H. Underwood, F. Salmassi, E. Arenholz, A. Young, Z. Hussain, M.A. Van Hove, and C.S. Fadley, "Probing buried interfaces with soft x-ray standing wave spectroscopy: Application to the Fe/Cr interface," *J. Phys. Condens. Matter* **14**(23), L407–L420 (June 2002).
- Yee, N., and L.G. Benning, "In situ FTIR study of the protonation reactions at the bacteria-water interface," *Geochim. Cosmochim. Acta* **66**(15A) (2002); Proceedings of Goldschmidt Conference, Devos, Switzerland, August 18–23, 2002.
- Young, A.T., E. Arenholz, J. Feng, H. Padmore, S. Marks, R. Schlueter, E. Hoyer, N. Kelez, and C. Steier, "A soft x-ray undulator beamline at the Advanced Light Source with circular and variable linear polarization for the spectroscopy and microscopy of magnetic materials," *Surf. Rev. Lett.* **9**(1), 549–554 (2002).
- Young, A.T., E. Arenholz, S. Marks, R. Schlueter, C. Steier, H.A. Padmore, A.P. Hitchcock, and D.G. Castner, "Variable linear polarization from an x-ray undulator," *J. Synchrotron Radiat.* **9**(4), 270–274 (2002).
- Zavarin, M., and H.E. Doner, "Interpretation of heterogeneity effects in synchrotron x-ray fluorescence microprobe data," *Geochem. Transact.* **3**(7), 51–55 (2002).
- Zhang, G.P., T.A. Callcott, G.T. Woods, L. Lin, B. Sales, D. Mandrus, and J. He, "Electron correlation effects in resonant inelastic x-ray scattering of NaV<sub>2</sub>O<sub>5</sub>," *Phys. Rev. Lett.* **88**(7, Article 077401), 279–282 (February 2002).
- Zhang, G.P., G.T. Woods, E.L. Shirley, T.A. Callcott, L. Lin, G.S. Chang, B.C. Sales, D. Mandrus, and J. He, "Orbital-resolved soft x-ray spectroscopy of NaV<sub>2</sub>O<sub>5</sub>," *Phys. Rev. B* **65** (16, Article 165107), 1–6 (April 2002).

Zhang, Y., J. Sesharnais, S.E. Greasley, G.P. Beardsley, D.L. Boger, and I.A. Wilson, "Crystal structures of human GAR Tfase at low and high pH and with substrate beta-GAR," *Biochemistry-US* **41**(48), 14206–14215 (2002).

Zhou, X.J., Z. Hussain, and Z.-X. Shen, "High resolution angle-resolved photoemission study of high temperature superconductors: Charge-ordering, bilayer splitting and electron–phonon coupling," *J. Electron Spectrosc.* **126**(1–3), 145–162 (2002).



# FOR MORE INFORMATION

## FOR INFORMATION ABOUT USING THE ALS, CONTACT

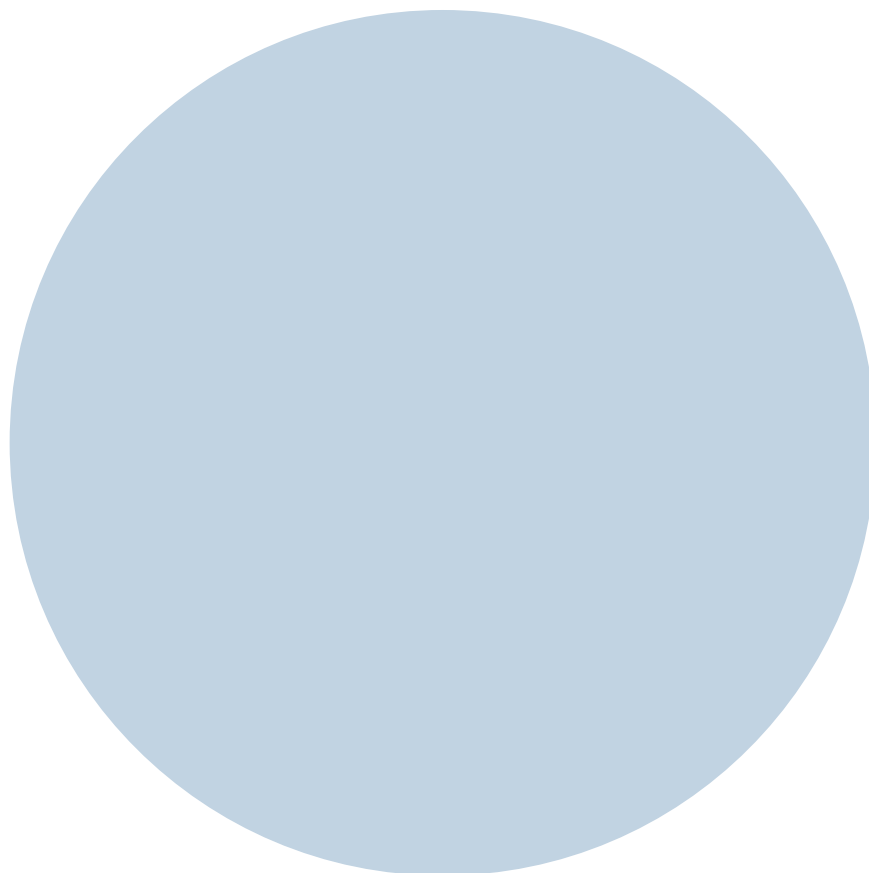
Gary Krebs  
User Services Group Leader  
Advanced Light Source  
Lawrence Berkeley National Laboratory  
MS 6R2100  
Berkeley, CA 94720-8235  
*Tel:* (510) 486-7727 *Fax:* (510) 486-4773  
*Email:* gfkrebs@lbl.gov

## FOR ALL OTHER INFORMATION CONCERNING THE ALS, CONTACT

Jeffrey Troutman  
User Services Administrator  
Advanced Light Source  
Lawrence Berkeley National Laboratory  
MS 6R2100  
Berkeley, CA 94720-8235  
*Tel:* (510) 495-2001 *Fax:* (510) 486-4773  
*Email:* alsuser@lbl.gov

## ALS HOME PAGE

[www-als.lbl.gov/](http://www-als.lbl.gov/)





Supported by the U.S. Department of Energy under Contract No. DE-AC03-76SF00098

Advanced Light Source | Ernest Orlando Lawrence Berkeley National Laboratory  
University of California Berkeley, California 94720-8235

